

Surrogate Safety Measures in Traffic Safety Analysis

Lead Guest Editor: Yanyong Guo

Guest Editors: Mohamed Hussein, Feng Chen, and Neng-Chao Lyu





Surrogate Safety Measures in Traffic Safety Analysis

Journal of Advanced Transportation

Surrogate Safety Measures in Traffic Safety Analysis

Lead Guest Editor: Yanyong Guo





Guest Editors: Mohamed Hussein, Feng Chen, and
Neng-Chao Lyu



Copyright © 2021 Hindawi Limited. All rights reserved.







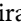



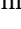
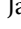

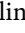









This is a special issue published in "Journal of Advanced Transportation." All articles are open access articles distributed under the Creative Commons Attribution License, which permits unrestricted use, distribution, and reproduction in any medium, provided the original work is properly cited.

Associate Editors

Juan C. Cano , Spain
Steven I. Chien , USA
Antonio Comi , Italy
Zhi-Chun Li, China
Jinjun Tang , China

Academic Editors

Kun An, China
Shriniwas Arkatkar, India
José M. Armingol , Spain
Socrates Basbas , Greece
Francesco Bella , Italy
Abdelaziz Bensrhair, France
Hui Bi, China
María Calderon, Spain
Tiziana Campisi , Italy
Giulio E. Cantarella , Italy
Maria Castro , Spain
Mei Chen , USA
Maria Vittoria Corazza , Italy
Andrea D'Ariano, Italy
Stefano De Luca , Italy
Rocío De Oña , Spain
Luigi Dell'Olio , Spain
Cédric Demonceaux , France
Sunder Lall Dhingra, India
Roberta Di Pace , Italy
Dilum Dissanayake , United Kingdom
Jing Dong , USA
Yuchuan Du , China
Juan-Antonio Escareno, France
Domokos Esztergár-Kiss , Hungary
Saber Fallah , United Kingdom
Gianfranco Fancello , Italy
Zhixiang Fang , China
Francesco Galante , Italy
Yuan Gao , China
Laura Garach, Spain
Indrajit Ghosh , India
Rosa G. González-Ramírez, Chile
Ren-Yong Guo , China

Yanyong Guo , China
Jérôme Ha#rri, France
Hocine Imine, France
Umar Iqbal , Canada
Rui Jiang , China
Peter J. Jin, USA
Sheng Jin , China
Victor L. Knoop , The Netherlands
Eduardo Lalla , The Netherlands
Michela Le Pira , Italy
Jaeyoung Lee , USA
Seungjae Lee, Republic of Korea
Ruimin Li , China
Zhenning Li , China
Christian Liebchen , Germany
Tao Liu, China
Chung-Cheng Lu , Taiwan
Filomena Mauriello , Italy
Luis Miranda-Moreno, Canada
Rakesh Mishra, United Kingdom
Tomio Miwa , Japan
Andrea Monteriù , Italy
Sara Moridpour , Australia
Giuseppe Musolino , Italy
Jose E. Naranjo , Spain
Mehdi Nourinejad , Canada
Eneko Osaba , Spain
Dongjoo Park , Republic of Korea
Luca Pugi , Italy
Alessandro Severino , Italy
Nirajan Shiwakoti , Australia
Michele D. Simoni, Sweden
Ziqi Song , USA
Amanda Stathopoulos , USA
Daxin Tian , China
Alejandro Tirachini, Chile
Long Truong , Australia
Avinash Unnikrishnan , USA
Pascal Vasseur , France
Antonino Vitetta , Italy
S. Travis Waller, Australia
Bohui Wang, China
Jianbin Xin , China






Hongtai Yang , China
Vincent F. Yu , Taiwan
Mustafa Zeybek, Turkey
Jing Zhao, China
Ming Zhong , China
Yajie Zou , China

Contents


Research of Surrogate Measure for Freeway Crashes Based on Tire Skid Marks

Yan Ma , Wenjing Huang, Zong Tian , Donghong Li, Hongzhou Cai, and Jie Su
Research Article (17 pages), Article ID 6673933, Volume 2021 (2021)





A Combined Simulation Approach to Evaluate Overtaking Behaviour on Two-Lane Two-Way Rural Roads

Valentina Branzi , Monica Meocci , Lorenzo Domenichini , and Margherita Calcinai
Research Article (18 pages), Article ID 9973138, Volume 2021 (2021)






Exploring Driver Injury Severity in Single-Vehicle Crashes under Foggy Weather and Clear Weather

Fulu Wei, Zhenggan Cai, Pan Liu, Yongqing Guo , Xin Li, and Qingyin Li
Research Article (12 pages), Article ID 9939800, Volume 2021 (2021)


Simulation Study of Rear-End Crash Evaluation considering Driver Experience Heterogeneity in the Framework of Three-Phase Traffic Theory

Haifei Yang , Yao Wu , Huihui Xiao , and Yi Zhao 
Research Article (13 pages), Article ID 5533722, Volume 2021 (2021)

Evaluating the Safety Impact of Connected and Autonomous Vehicles with Lane Management on Freeway Crash Hotspots Using the Surrogate Safety Assessment Model

Hui Zhang , Ninghao Hou , Jianhua Zhang , Xuyi Li , and Yan Huang 
Research Article (14 pages), Article ID 5565343, Volume 2021 (2021)


A Dynamic Bayesian Network-Based Real-Time Crash Prediction Model for Urban Elevated Expressway

Xian Liu, Jian Lu , Zeyang Cheng, and Xiaochi Ma
Research Article (12 pages), Article ID 5569143, Volume 2021 (2021)




Modeling and Analysis on Minimum Safe Distance for Platooning Vehicles Based on Field Test of Communication Delay

Mengyan Hu , Xiangmo Zhao, Fei Hui , Bin Tian , Zhigang Xu , and Xinrui Zhang
Research Article (15 pages), Article ID 5543114, Volume 2021 (2021)








Quantification of Rear-End Crash Risk and Analysis of Its Influencing Factors Based on a New Surrogate Safety Measure

Qiangqiang Shangguan, Ting Fu , Junhua Wang, Rui Jiang, and Shou'en Fang
Research Article (15 pages), Article ID 5551273, Volume 2021 (2021)

Pedestrian Crash Exposure Analysis Using Alternative Geographically Weighted Regression Models

Seyed Ahmad Almasi , Hamid Reza Behnood , and Ramin Arvin 
Research Article (13 pages), Article ID 6667688, Volume 2021 (2021)

Can I Trust You? Estimation Models for e-Bikers Stop-Go Decision before Amber Light at Urban Intersection

Jing Cai , Jianyou Zhao , Yusheng Xiang , Jing Liu , Gang Chen , Yueqi Hu , and Jianhua Chen 

Research Article (17 pages), Article ID 6678996, Volume 2020 (2020)

Analysis of Freeway Secondary Crashes in Different Traffic Flow States by Three-Phase Traffic Theory

Bo Yang , Yao Wu , and Weihua Zhang 

Research Article (10 pages), Article ID 8890351, Volume 2020 (2020)

A Framework for Intersection Traffic Safety Screening with the Implementation of Complex Network Theory

Xueyu Mi, Chunfu Shao, Chunjiao Dong , Chengxiang Zhuge, and Yan Zheng

Research Article (12 pages), Article ID 8824447, Volume 2020 (2020)

Research Article

Research of Surrogate Measure for Freeway Crashes Based on Tire Skid Marks

Yan Ma ¹, Wenjing Huang,¹ Zong Tian ², Donghong Li,¹ Hongzhou Cai,¹ and Jie Su¹

¹School of Civil Engineering, Tianjin Chengjian University, 26 Jinjing Road, Tianjin 300384, China

²Center for Advanced Transportation Education and Research, University of Nevada (Reno), 1664 N Virginia Street, Reno, NV 89557, USA

Correspondence should be addressed to Zong Tian; zongt@unr.edu

Received 13 November 2020; Revised 1 August 2021; Accepted 27 August 2021; Published 18 October 2021

Academic Editor: Neng-Chao Lyu

Copyright © 2021 Yan Ma et al. This is an open access article distributed under the Creative Commons Attribution License, which permits unrestricted use, distribution, and reproduction in any medium, provided the original work is properly cited.

Traditional approaches to evaluating and predicting safety issues in traffic systems are via crash records. However, considering the characteristics of scarcity, inconsistency, inaccuracy, and incompleteness of crash records, conclusions and recommendations drawn purely based on crashes have limitations. Tire skid marks are considered an indication of some safety hazards, and it could have good potential to be used as surrogates for crashes. By collecting and analyzing the data based on selected arterial and freeway segments in the Reno-Sparks area in northern Nevada, a methodology was developed to categorize different tire skid marks. Sliding window and linear regression techniques were applied to determine any correlation between tire skid marks and crashes. The analyses indicated that there was a relatively strong linear correlation between skid marks and crashes on freeway segments.

1. Introduction

The current practice of traffic safety programs primarily relies on crash data, such as crash frequency, crash rate, and crash severity, for making roadway safety improvement decisions. Such an approach is considered a passive or reactive approach because corrective action takes place only after crashes have occurred. Additionally, there are some limitations of using crash data, including randomness, underreporting, subjectivism, and long observation periods [1]. These limitations of crash data may hinder comprehensive assessment of safety performance and limit further developments of safety methodologies [2]. Due to these limitations, it is needed for researchers to explore other alternatives to crash data, which could be less time consuming and more informative. These alternatives to crashes are referred to as surrogate measures or crash surrogates, which are viewed as proactive measures of safety research.

As early as 1982, Datta et al. [3] suggested that a crash surrogate measure is defined as a quantifiable observation that can be used in place of, or as a supplement to, crash records. Surrogates should have a definite correlation with

crashes and thereby to safety-related improvements in roadways. Tarko et al. [4] mentioned that surrogate measures include critical events, such as aggressive lane changing, speeding and red-light turning, acceleration noise, postencroachment time, time-integrated time-to-collision, deceleration-to-safety-time, and even traffic characteristics like volume, speed, and delay. Wu and Jovanis [5] have critically deliberated on desirable criteria for crash surrogates, stating that a crash surrogate (a) should have a short observation period, (b) should be correlated with clinically meaningful outcomes, i.e., crashes, (c) should be statistically and causally related to crashes, (d) should be affected by a safety treatment similarly to how a safety treatment would affect crashes, and (e) should be “markers” of crashes with a time-scale underpinning, meaning that they should be part of the same sequence of events that produce crashes.

Based on the above definition and criteria, crash surrogates are substitute measures that are likely indicators of crash occurrences, but they occur more frequently than crashes on roadways. Similar to forecasting storms and earthquakes, surrogate measures might be used at a particular location to determine whether an increased

probability of higher-than-average crash rates is likely. Preventative actions could then be taken when the surrogate measures indicate a high likelihood of future crashes. The main advantage of using surrogates is that they occur more frequently than crashes; therefore, the data on surrogate measures can be collected over a shorter time frame than crashes but with similar statistically significant measures as crash data. In addition, a surrogate measure must have a valid statistical relationship with crashes and be sensitive to traffic safety-related improvements. In practice, data for surrogate measures must be comparatively easier to collect with less manpower, training, and equipment.

Because of the limitations of crash data and the merits of surrogate measures mentioned above, there has been steady progression in the use of surrogate measures in safety analysis [5–10]. Several studies used surrogate measures derived from vehicle trajectories extracted from traffic surveillance videos to assess risk among vehicles [11–13]. Saunier and Sayed [11] extracted vehicle trajectory data from videos recorded at intersections and quantified the probability of collision using traffic conflicts identified by time to collision (TTC). Oh et al. [12] proposed a novel methodology to monitor safety conditions on freeways by detecting hazardous traffic events from videos. Gao and Tian [6] focused on tire skid marks to find the linear correlation between skid marks and crashes collected from selected road segments. St-Aubin et al. [14] proposed a framework for automated vehicle tracking from large-scale traffic video data and showed the potential of using high-resolution vehicle trajectory data for safety analysis using TTC.

Statistically significant positive correlation was found between crash data and conflicts identified by various surrogate measures from various vehicle trajectory data sources in several previous studies [15–18]. Besides, correlating surrogate measures with crash data, many studies have attempted to reveal the relationships between surrogate measures and crash data by developing more advanced statistical modeling approaches. Tarko [19] and Zheng et al. [20] summarized common models of characterizing SSM-crash relationships. Wu and Jovanis [5] developed a conceptual structure.

Using surrogate measures as a means of evaluating safety performance has been sought by many researchers. However, the application of surrogate measures still faces many issues and challenges, for example, the lack of a consistent definition, their validity as an indicator of traffic safety performance, and the reliability of their data. Therefore, this study specifically focuses on documenting the development of surrogates for freeway crashes to provide an effective research method to improve freeway safety.

2. Methodologies of Studying Surrogate Measures

The Road Safety Audit program lunched by the FHWA has been implemented in most states. Road Safety Audit is a formal safety performance examination of existing or future roads or intersections by an independent, multidisciplinary team. The task of Road Safety Audit is to identify what

elements of the road may present a safety concern to what extent, to which road users, and under what circumstances. The task also includes identifying valid measures to eliminate or mitigate the identified safety problems.

Because a Road Safety Audit does not rely on crash records, the outcome of the Road Safety Audit evaluation is not biased by the crash data. Road Safety Audit also has the ability to observe physical evidence of past crashes, if any, and off-road excursions, such as damages to curbs, roadside barriers, trees, utility poles, delineator posts, and signs; scuff marks on curbs and concrete barriers; tire skid marks, broken auto parts, oil patches on the roads; and vehicle tracks or rutting in the ground adjacent to a roadway. When such evidence concentrates at a particular location, it may be an indication of some safety hazards, and adequate safety mitigation measures could be taken to prevent future crashes. As a result, these types of evidence could have good potential to be used as indicators or surrogates for crashes. Consequently, examination of these factors as potential surrogates will be a primary focus of this study.

The Road Safety Audit program provides new ways of approaching traffic safety issues and identifying promising surrogate measures, which have not received much attention up to now. These potential surrogates included citizen complaints and physical evidence of past crashes and off-road excursions, such as curb damage, tire skid marks, and evidence of broken auto parts.

Tire skid marks were identified as innovative factor in this research. The tire skid marks are usually made by vehicles accelerating/decelerating intensively or changing their motion courses abruptly, so that the vehicle would leave tire marks on the pavement. Because tire skid marks of different characteristics are caused by different situations, different types of skid marks were used to describe different incidents. All skid marks observed were categorized by their shape, intensity, impact, and direction by the authors. Similar work was not found in any previous study. Furthermore, to establish statistical correlation with crash records, the numbers of the skid marks and their locations were two main concerns in the study.

Statistical models are a prevalent tool in studying traffic safety. In this study, the approach was to construct linear regression models between skid marks on the pavement and crash records. If the statistical correlations between them were significant (under a certain confidence level), skid marks were regarded as a crash surrogate.

3. Correlation Analysis between Skid Marks and Crashes

The statistical relationship between skid marks and crashes was studied to identify if skid marks could be recognized as a crash surrogate. Two freeway sites were selected for the study.

3.1. Data Collection. Given that there are only two major freeways in the Reno-Sparks area, the freeway sites were selected on both facilities. The study boundaries were

determined such that each section began and ended at main boundaries of the urbanized area. Thus, the first study section included approximately 10.5 miles of Interstate 80 between Robb Drive (Exit 9) and Vista Boulevard (Exit 21) interchanges. The second section was US Highway 395 (Interstate 580) between Mount Rose Highway/SR 431 (Exit 56) and Panther Valley (Exit 72) interchanges, the distance of approximately 14.8 miles. Both directions of travel on each freeway were evaluated separately, resulting in four freeway sections analyzed in this study.

A map of the study sections is shown in Figure 1.

3.2. Crash Record. To capture the skid mark data, the videos of the pavement surface for each study section were recorded. When filming the videos, every effort was made to maintain a clear viewing angle to simplify the data extraction process. Majority of the videos were recorded early on weekend mornings, in order to encounter fewer vehicles on the roadways, which could block the camera's view of the pavement. Additionally, the research vehicle generally remained as close to the center of the directional roadway as practical. Also, an attempt was made to keep the research vehicle moving at a constant speed generally at or slightly below the posted speed limit (60 mph on freeways).

Once skid mark videos had been obtained and compiled, crash records for these areas were requested. So a correlation analysis between the skid marks and crashes could be made. Crash records for the study sections were obtained by courtesy of the NDOT Safety Division.

The crash records for the freeway sections were obtained for the one-year period. Table 1 shows the number of reported crashes by crash type for the freeway study sections. As can be seen in the table, the number of rear-end crashes was more than half of the total crashes occurring in all eight study sections. Because they comprised such a large proportion of the total crashes in each section, rear-end crashes were evaluated separately in addition to the total crash evaluation performed in this study.

The location of reported crashes would become a crucial element in the study. In the provided records, officers responding to crashes typically reported the crash location by its relative distance to a prominent reference point. Thus, it was necessary to ensure that the crash locations were all related to a common referencing system, in order to simplify the analysis. In the case of crashes along freeways, the relative distance and direction to a given point, such as a milepost, cross street, or ramp, were used. This position was then internally modified in NDOT's records to correspond with an actual milepost location referred to as the "Adjusted Mile Marker." Because freeway crash locations were normalized to milepost locations, which are continuous along entire freeway sections, no adjustments were needed by the research team.

3.3. Locating Skid Marks. Once the videotaping was completed, it became apparent that a method was needed to relate the relative location of skid marks found in the videos to the Adjusted Mile Marker or a zero intersection. This is

called "study" position. This was necessary for the correlation analysis because the crash records note crash locations relative to its study position. To accomplish this, a relationship between video time, driving speed, and study position was developed for each study section.

Along the freeway sections, the milepost markers were used to determine skid mark locations. The freeways were driven again in order to pinpoint all visible milepost markers erected alongside the highway. After the milepost locations were identified in the field, the video clips were then reviewed in order to determine the video time index where each milepost appeared. Both standard MUTCD mile markers (Figure 2(a)) and NDOT reference panels (found at bridges and other points, Figure 2(b)) were identified. By giving the time index and distance between successive mileposts, original driving speeds on the videos could be estimated. Each freeway section was divided into four or five smaller areas for the purposes of assigning an average travel speed. Based on these calculations, it was possible to assign an approximate milepost location to each skid mark seen in the videos.

In most instances, it was likely that most vehicles leaving a skid mark on the roadway were undergoing a sudden deceleration in a preventative or evasive action to avoid a suddenly stopped car or other obstacles. Thus, it would be reasonable to assume that a collision involving a vehicle that left a skid mark occurred towards the end of the mark. Therefore, when calculating the relative location of skid marks, the downstream end of each mark was used as a reference point for determining the location of a collision.

3.4. Skid Mark Cataloging. Once the logistics of determining skid mark locations was finalized, the videos were extensively reviewed. In reviewing the videos, many areas of the study sections had multiple marks and sometimes overlapping skid marks on the pavement; this was especially apparent along some freeway sections. Also, skid marks usually had distinct characteristics that varied widely. Thus, it was deemed necessary to document and categorize each skid mark individually. The research team identified ten parameters to document based upon the trends and observations made during the video reviews. The two most important parameters were as follows:

- (i) Time index: the "time index" parameter is defined as the time position of the video file at which the skid mark occurs. This parameter has two components: the start and the stop time. The starting time begins at the video time stamp in which the skid first appears, and the stop time is the timestamp where the mark disappears from the screen. For the sake of consistency, a uniform method of observing the time index was adopted. The skid mark's relation to the bottom of the video screen was the primary consideration point for recording the video time position. Thus, the start time recorded for each skid mark was the exact second that the leading edge of the skid passes out of view on the bottom edge of the screen, and the stop time was the second in which the trailing edge of the mark touched the bottom of the

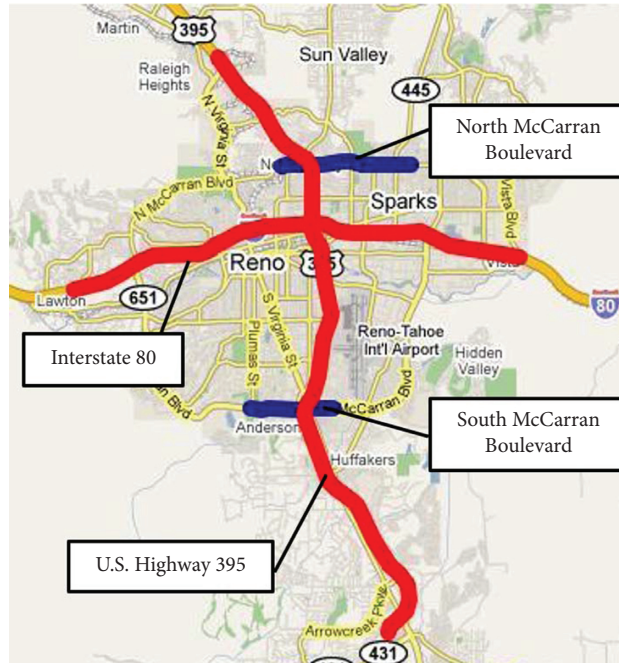


FIGURE 1: Map of freeway study sections.

TABLE 1: Reported crash types in study sections.

Study section	Direction	Angle	Crash type					Total crashes
			Noncollision	Rear-end	Sideswipe	Others	Unknown	
Interstate 80	EB	30	81	134	21	3	6	275
	WB	28	56	65	16	2	3	125
US Highway 395	NB	35	73	283	24	2	8	425
	SB	26	77	141	22	2	5	273



FIGURE 2: Milepost panels found along freeway study segments.

video window. In the event that a video skid mark did not touch the bottom of the screen, either the lower side edges of the video were used or the approximate location of the time point (based upon pavement markings or other identifiable features in

adjacent lanes) was used to determine the time index. Smaller skid marks that appeared on video for less than one second were recorded with the same start and stop indices.

- (ii) Location: the “location” parameter was used to calculate the cumulative distance from the beginning of the study section (on arterials) or the approximate milepost (on freeways), based on the methodology presented in the report. It should again be noted that these calculated locations are estimates only, based on time-space relationships derived from the study videos. Because crashes are more likely to occur at the end of a skid mark, the time index where the trailing end of the skid mark appeared was the point used as the basis for estimating the location of each mark.

Other parameters noted for each skid mark include lane position, whether caused by heavy vehicle, number of wheels on vehicle leaving a mark, direction of the mark, apparent impact to roadside barrier, intensity of the mark, skipping characteristic, and changes in mark width (a more detailed explanation of all the classification parameters can be found in Appendix). The skid marks of different characteristics may serve to predict different types of crashes. For example,

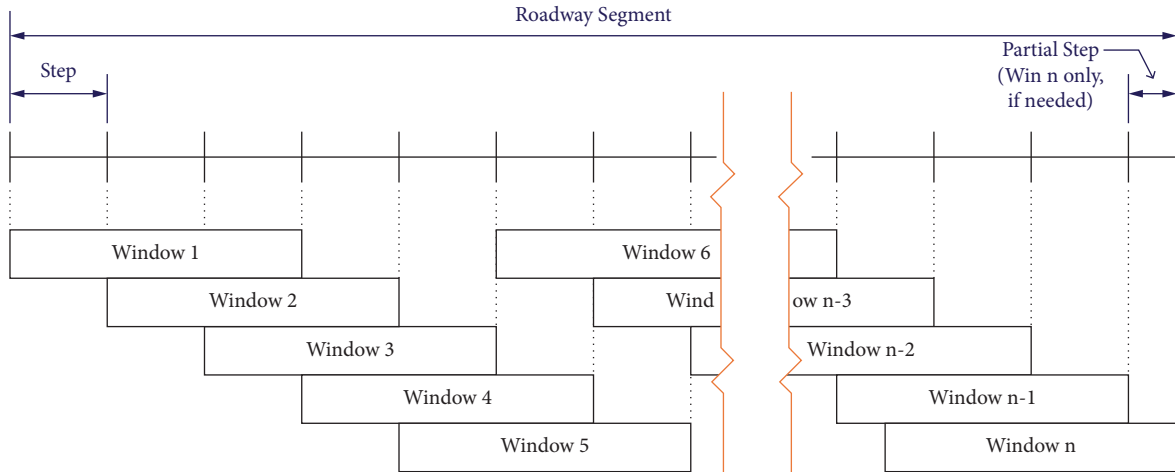


FIGURE 3: Sliding window searching method.

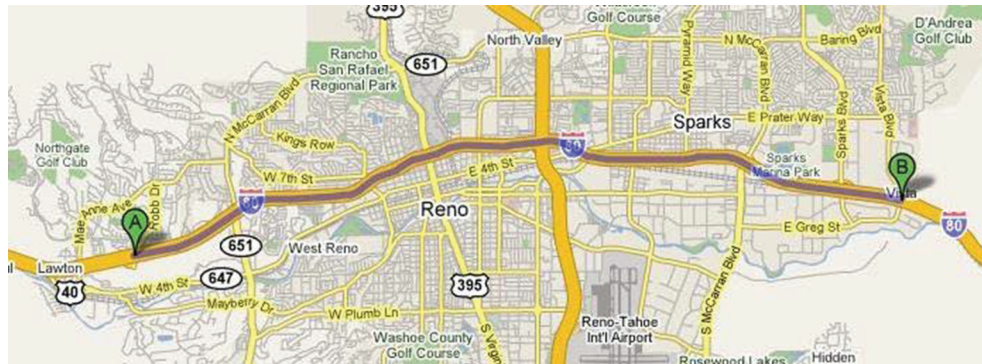


FIGURE 4: Map of Interstate 80 study sections.

TABLE 2: Segment crashes and skid marks on Interstate 80 eastbound.

EB segment #	Mileposts	# of crashes	# of rear-end crashes	# of skid marks
1	9-10	11	3	7
2	10-11	9	3	40
3	11-12	8	2	56
4	12-13	17	4	13
5	13-14	56	36	75
6	14-15	94	66	71
7	15-16	40	11	54
8	16-17	28	9	55
9	17-18	18	6	44
10	18-19	22	7	42
11	19-20	10	3	24

TABLE 3: Segment crashes and skid marks on Interstate 80 westbound.

WB segment #	Mileposts	# of crashes	# of rear-end crashes	# of skid marks
11	20-19	9	6	5
10	19-18	17	8	13
9	18-17	12	4	18
8	17-16	17	5	24
7	16-15	44	21	11
6	15-14	31	4	13
5	14-13	21	10	15
4	13-12	16	5	3
3	12-11	15	4	7
2	11-10	7	3	7
1	10-9	6	3	3

skid marks that veered off course might be indicative of sideswipe crashes, or darker skid marks might predict a higher likelihood of rear-end crashes. Ultimately, the analysis undertaken in this research focused on time and location only.

3.5. *Data Processing Program and Sliding Window.* An interactive program was developed utilizing the Visual Basic macro language within Microsoft Excel. First, the user

inserted a list of skid mark locations (ordered by cumulative distance or milepost) and the number of skid marks occurring at each location. Next, a corresponding list of crash locations was entered. Then, the user specified starting and ending points, a window, for the analysis. When these variables were entered, the software progressed through each list and calculated the number of skid marks and crashes that were documented within the specified limits of the “sliding window.” The window endpoints and the number of skids

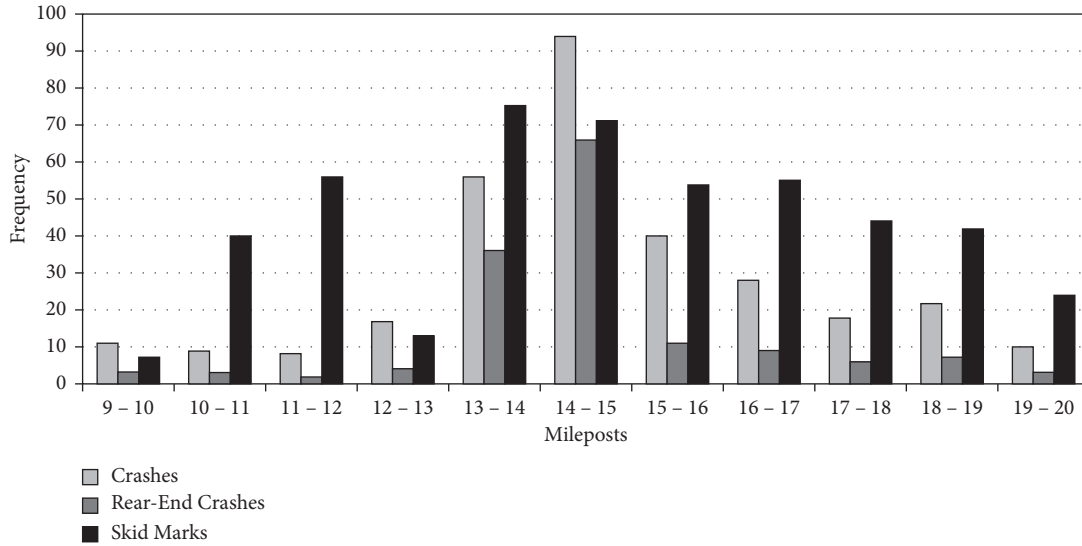


FIGURE 5: Number of crashes and skid marks on Interstate 80 eastbound.

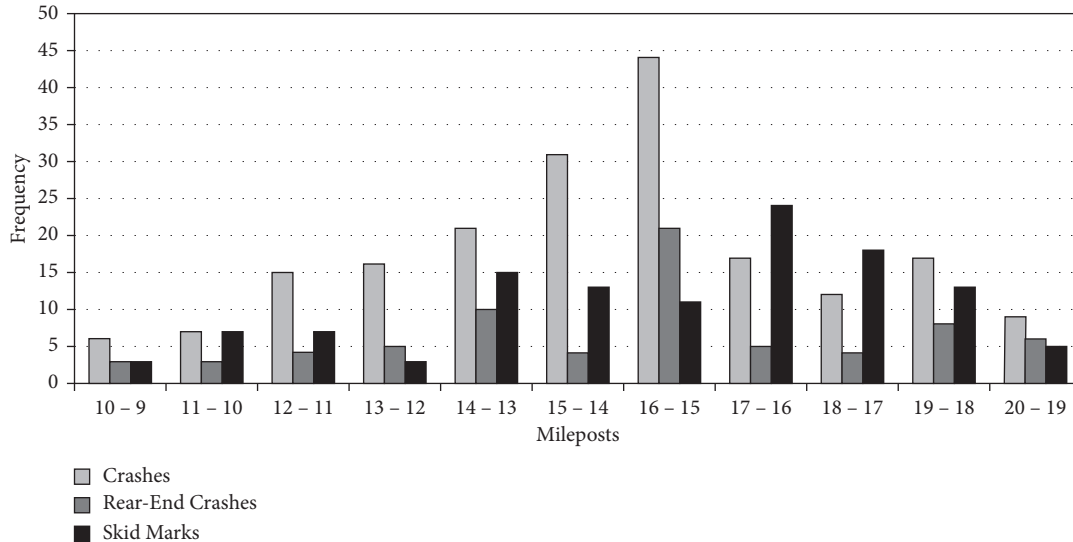


FIGURE 6: Number of crashes and skid marks on Interstate 80 westbound.

and crashes were outputted into the spreadsheet, which was easily transferred to another document for analysis.

Another function of this program is the capability to utilize the sliding window concept for data analysis as illustrated in Figure 3. For this concept, the window has a user-determined length and slides forward by a small interval specified by the user. The analysis begins with one window at the beginning of the study section. Once the data within the first window are reported, the window “slides” forward by the defined small interval and reports all relevant information in the second window. This process continues until the end of the section is reached. This sliding window method provides for considerable overlap, which is useful in determining where the crashes and skid marks are concentrated. Additionally, the process partitions the study sections into more divisions than intersections or mileposts, and, therefore, it provides a greater number of observations

for the regression analyses. This ultimately increases the accuracy of the analysis.

4. Freeway Analysis

The study discusses the examination of crash and skid mark correlations along the freeway study sections: Interstate 80 and US Highway 395. The analysis methods of the two freeways are the same, so Interstate 80 is selected as an example for freeway analysis.

Figure 4 shows a map of the study sections along Interstate 80. The study corridor contains 12 interchanges, with various entrance and exit ramps. The interchanges include the following:

- (i) Robb Drive
- (ii) McCarran Boulevard West

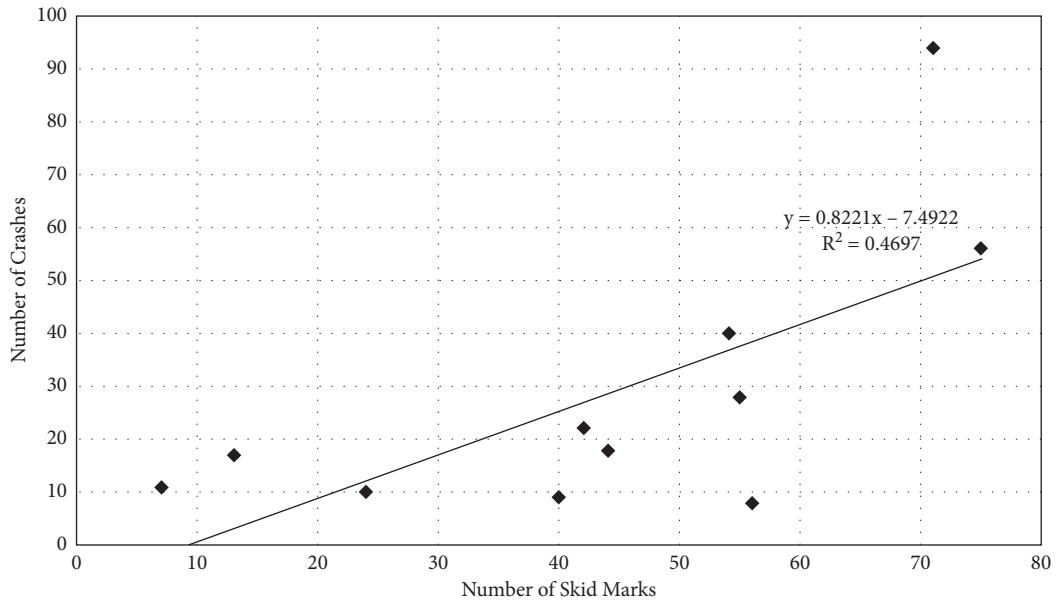


FIGURE 7: Crash vs. skid correlation by 1-mile segments on Interstate 80 eastbound.

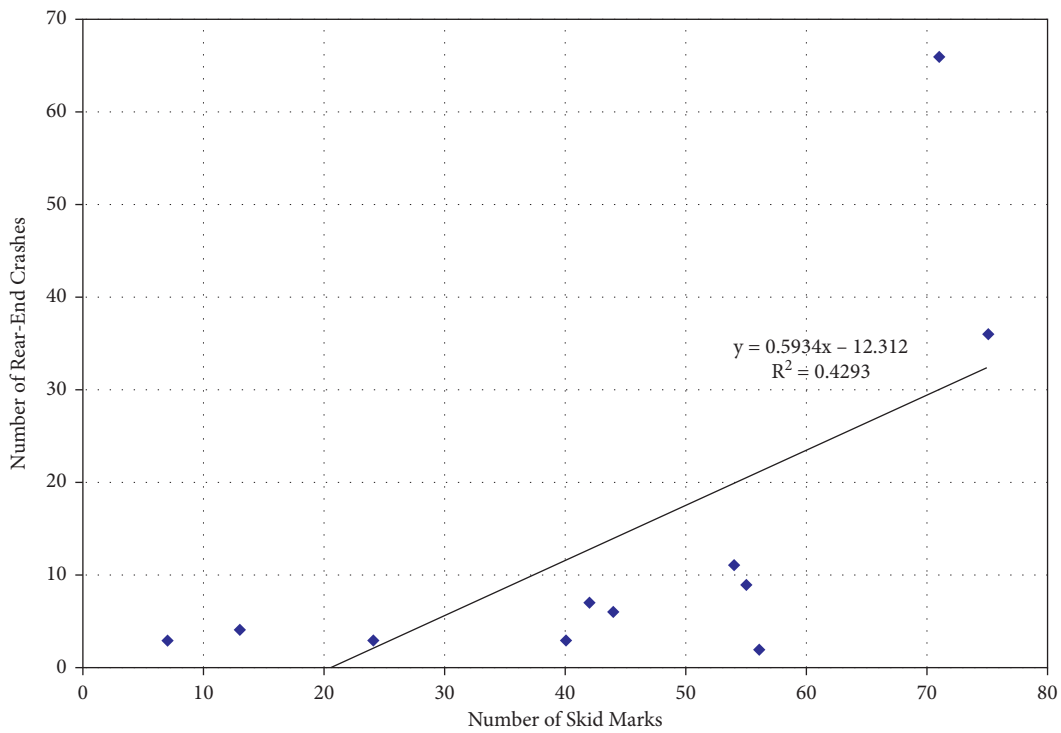


FIGURE 8: Rear-end crash vs. skid correlation by 1-mile segments on Interstate 80 eastbound.

- (iii) Keystone Avenue
- (iv) Virginia Street
- (v) Wells Avenue
- (vi) US Highway 395
- (vii) Victorian Avenue/4th Street
- (viii) Rock Boulevard
- (ix) Pyramid Way
- (x) McCarran Boulevard East

- (xi) Sparks Boulevard
- (xii) Vista Boulevard/Greg Street

The study position of all crashes and skid marks in these study sections were noted based on the methods discussed previously. Because locations along the free-ways were determined based on mileposts, each study section was easily divided into segments based on the mileposts for the analysis. Tables 2 and 3 show information relating to these segments and the number of

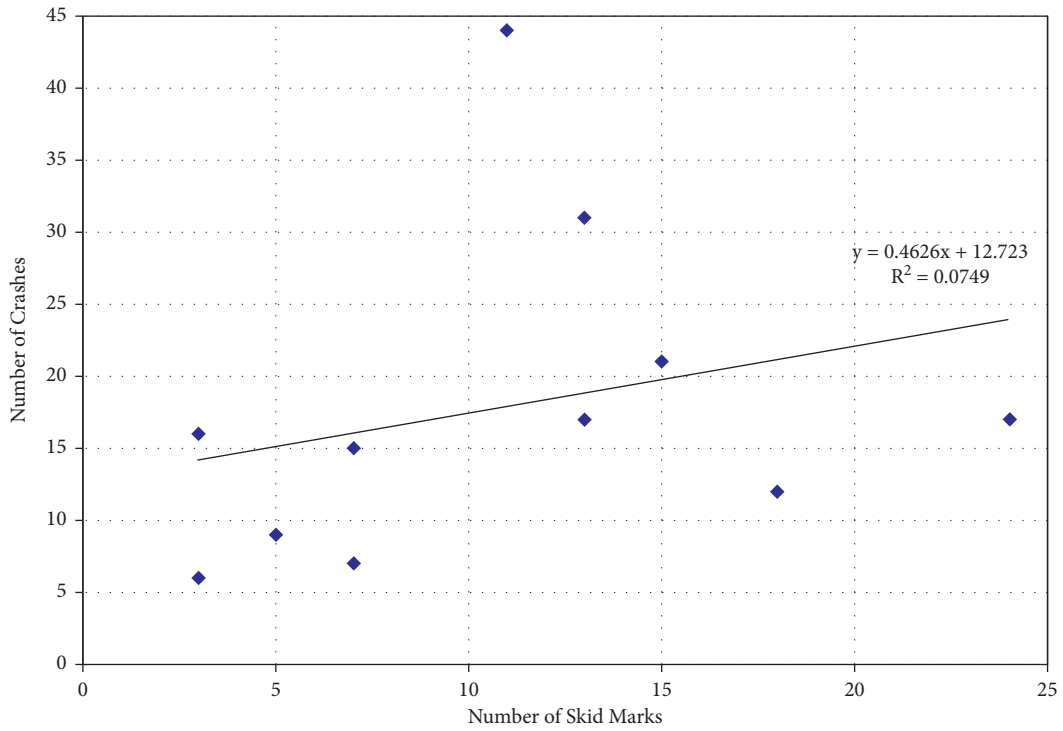


FIGURE 9: Crash vs. skid correlation by 1-mile segments on Interstate 80 westbound.

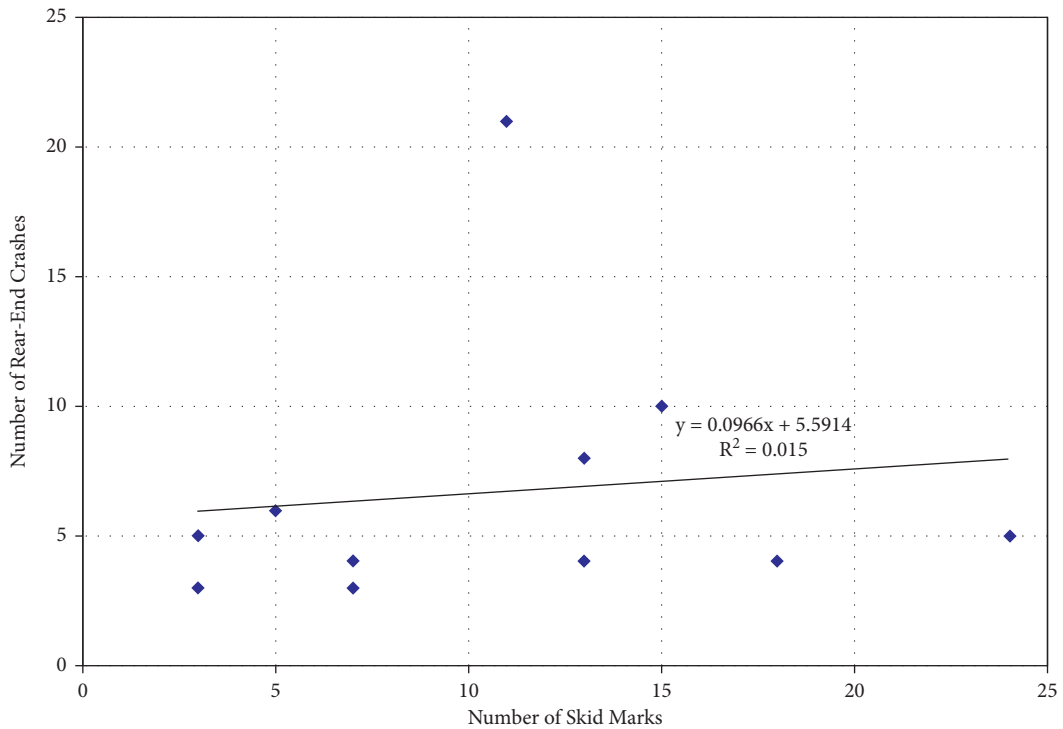


FIGURE 10: Rear-end crash vs. skid correlation by 1-mile segments on Interstate 80 westbound.

crashes and skid marks in each. The data in these tables are plotted in Figures 5 and 6. As can be seen in the figures, an increase in the number of skid marks is generally accompanied by an increase in the number of crashes. However, such increases are not always

proportional. Additionally, it appears that crashes and skid marks increase towards the center of the study sections. This makes sense intuitively because the center of the study sections is closer to the center of Reno-Sparks and the interchange with US 395 because there are higher

TABLE 4: R-squared values for different regression analyses on Interstate 80 based on various sliding window parameters.

Sliding window parameters			R-squared value			
Window length (mi)	Step increment (mi)	# of data points	Interstate 80 eastbound		Interstate 80 westbound	
			Skids vs. crashes	Skids vs. rear-end crashes	Skids vs. crashes	Skids vs. rear-end crashes
1	0.2	51	0.51	0.53	0.17	0.22
	0.1	101	0.51	0.53	0.15	0.21
	0.05	201	0.51	0.53	0.15	0.21
0.5	0.2	54	0.42	0.46	0.11	0.12
	0.1	106	0.41	0.47	0.09	0.11
	0.05	211	0.41	0.47	0.08	0.12
0.25	0.1	101	0.30	0.38	0.02	0.03
	0.05	201	0.30	0.38	0.04	0.04

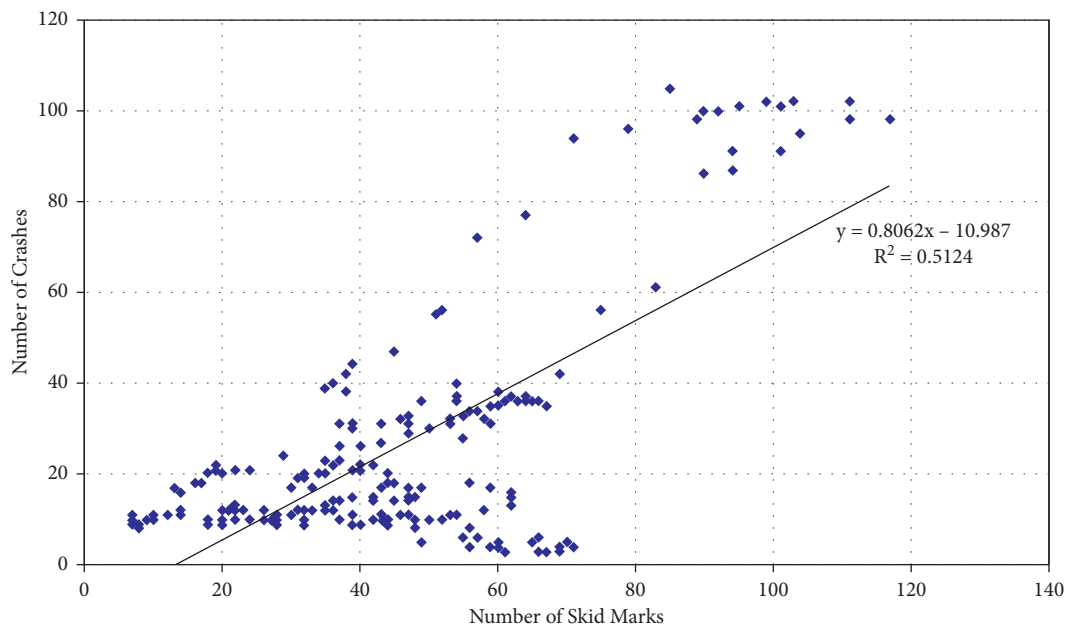


FIGURE 11: Sliding windows crash vs. skid correlation on Interstate 80 eastbound (1.0-mile windows, 0.05-mile step).

traffic volumes. One interesting note is that there are considerably more crashes and skid marks observed along the eastbound section than the westbound section as described next.

Utilizing the data in Tables 2 and 3, linear regression modeling was used to analyze the relationship between the frequency of skid marks and the frequency of crashes and also between skid mark frequency and rear-end crash frequency in each segment. Graphs depicting the results are given in Figures 7 through 10 .

For the eastbound direction, it can be seen in Figures 7 and 8 that both the skid vs. crash and skid vs. rear-end crash regressions produced good trend lines. The R-squared value of both correlations was above 0.4, which suggested average correlation between the skid marks and crashes. In Figures 9 and 10, the trend lines were positive for both the crash and rear-end crash scenarios, but the R-squared values for both analyses were lower than 0.1, indicating poor linear correlation.

Analyzing data based on 1-mile consecutive segments alone did not provide a comprehensive analysis. As an example, such examinations will not show a potential small segment with the highest frequencies of skid marks or crashes if it were to spread across any milepost. For this reason, the sliding window concept was also applied to the freeway sections. By shifting the analysis window gradually along the freeway, specific ranges of locations can be studied, thus providing additional data and insight into the analysis.

Multiple scenarios of window length and forward step increments were initially studied: 1-mile windows with 0.2-, 0.1-, and 0.05-mile steps; 0.5-mile windows with 0.2-, 0.1-, and 0.05-mile steps; and 0.25-mile windows with 0.1- and 0.05-mile step. Using the outputs of these scenarios, linear regression analysis was performed to again test the relationship between crashes and skid marks for each sliding window. Table 4 lists the R-squared value for each of these regressions.

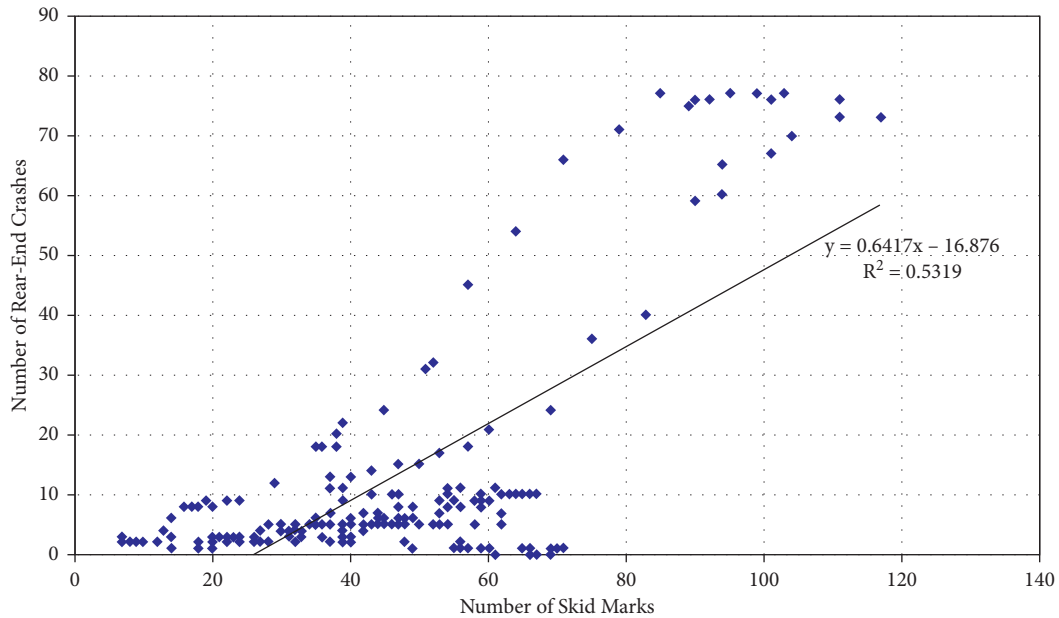


FIGURE 12: Sliding windows rear-end crash vs. skid correlation on Interstate 80 eastbound (1.0-mile windows, 0.05-mile step).

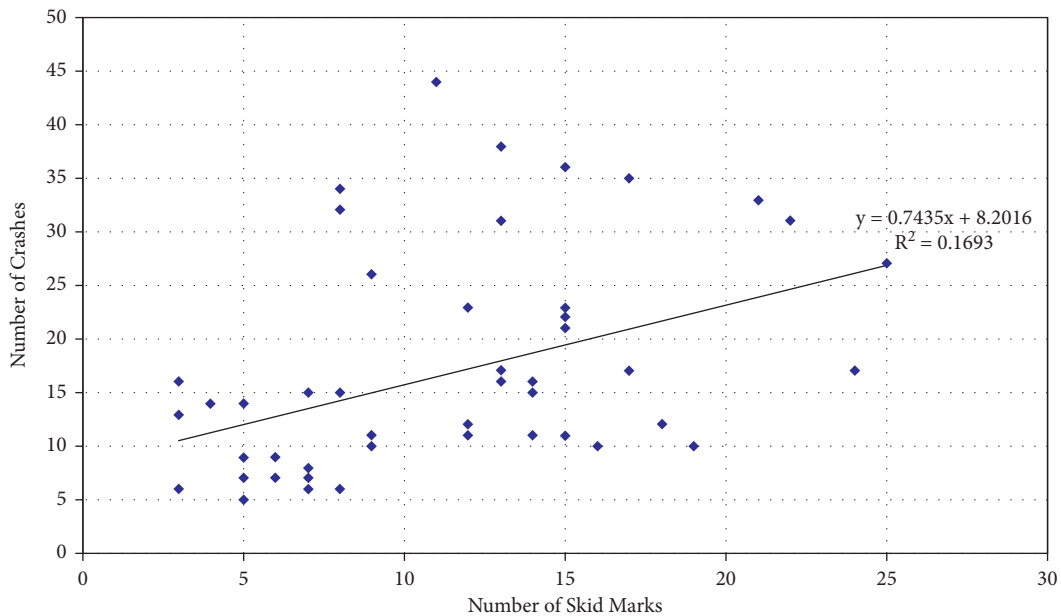


FIGURE 13: Sliding windows crash vs. skid correlation on Interstate 80 westbound (1.0-mile windows, 0.20-mile step).

As can be seen in Table 4, regressions using a 1-mile window produced the best correlations between skid marks and crashes, although the step increments varied between the best regressions. Additionally, regressions using rear-end crashes only achieved slightly better R -squared values along Interstate 80 eastbound and much higher values than the counterparts in the westbound direction.

The regressions from Table 4 obtaining the highest R -squared values were selected for further analysis. For Interstate 80 eastbound, however, the best regression on the skids versus crashes had a different sliding window step increment than the

skids versus rear-end crashes regression; both regressions using a 0.05-mile step increment were used in order to make similar comparisons. Figures 11 through 14 show the results of the regression using sliding windows. As can be seen, both directions of Interstate 80 have positive trends using the sliding window method. Eastbound sections have the better correlation, with the rear-end crash correlation being slightly superior.

Based on the sliding window outputs, frequencies of crashes and skid marks are plotted in Figures 15 and 16. In these graphs, the x -axis represents the milepost location of the starting point of each mile-long sliding widow. The frequency of crashes and skid marks of any 1-mile segment can be determined by

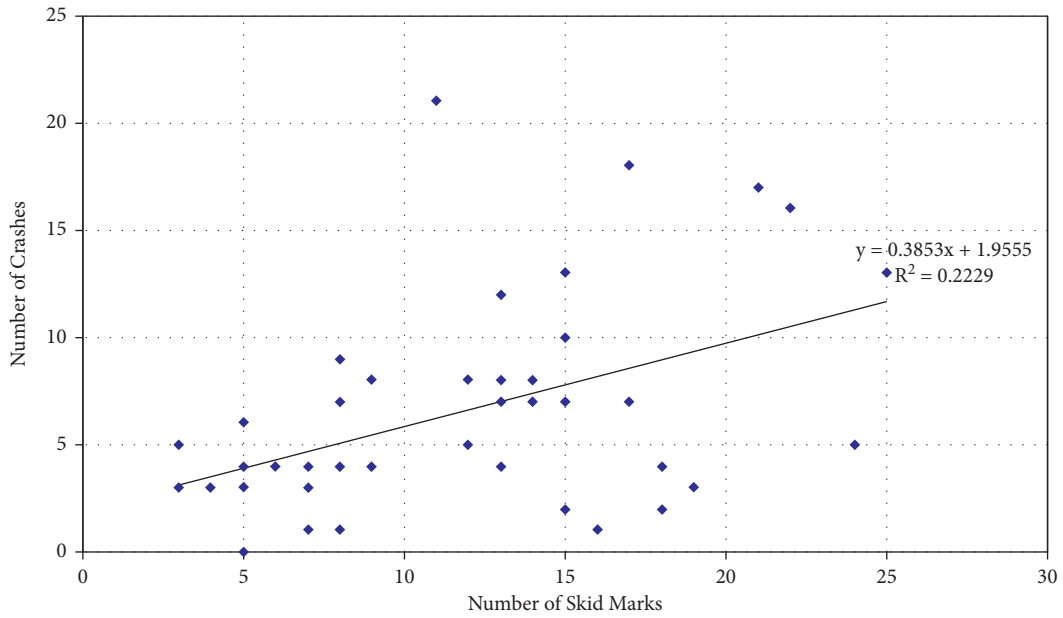


FIGURE 14: Sliding windows rear-end crash vs. skid correlation on Interstate 80 westbound (1.0-mile windows, 0.20-mile step).

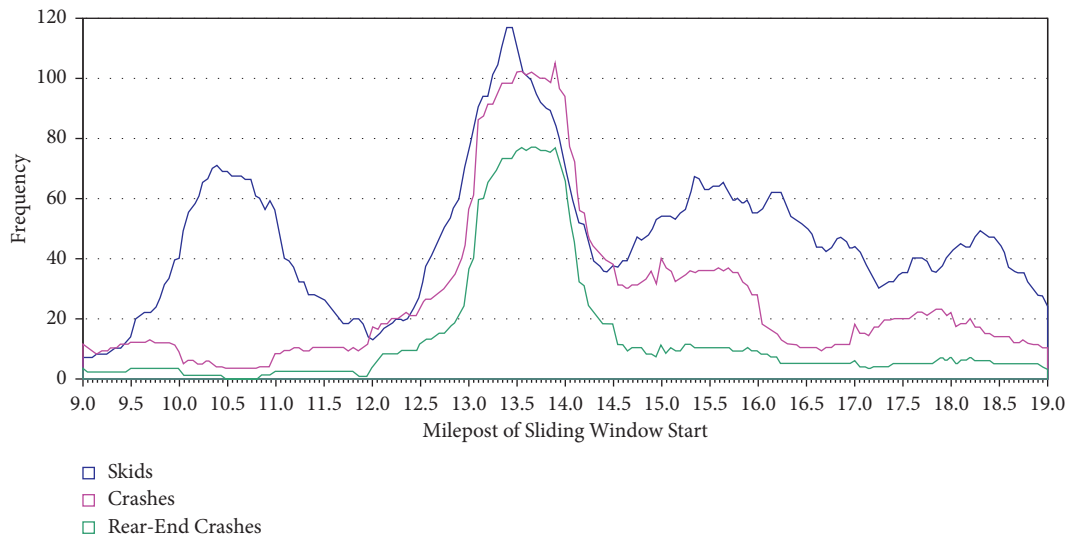


FIGURE 15: Sliding windows crash/skid frequency on Interstate 80 eastbound (1.0-mile windows, 0.05-mile step).

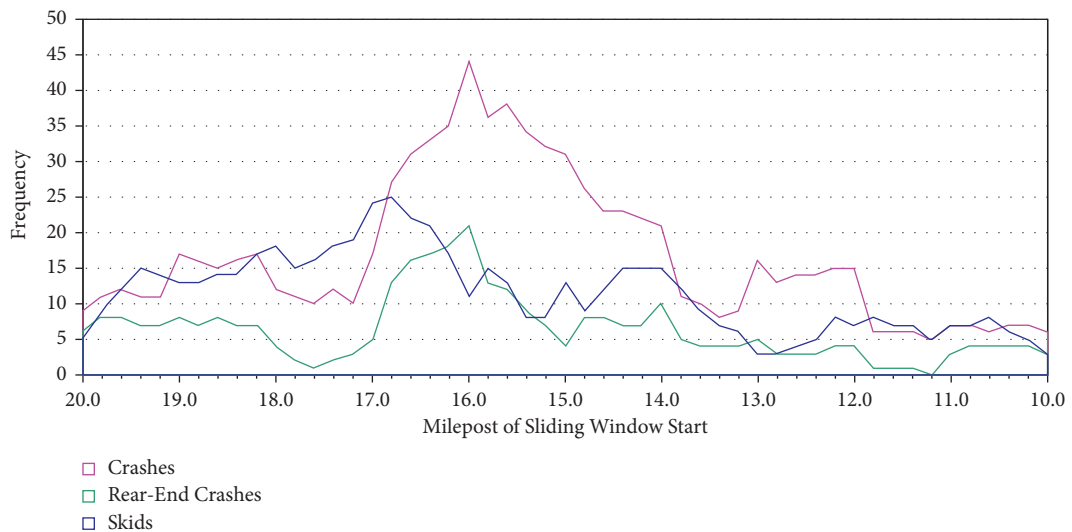


FIGURE 16: Sliding windows crash/skid frequency on interstate 80 westbound (1.0-mile windows, 0.20-mile step).

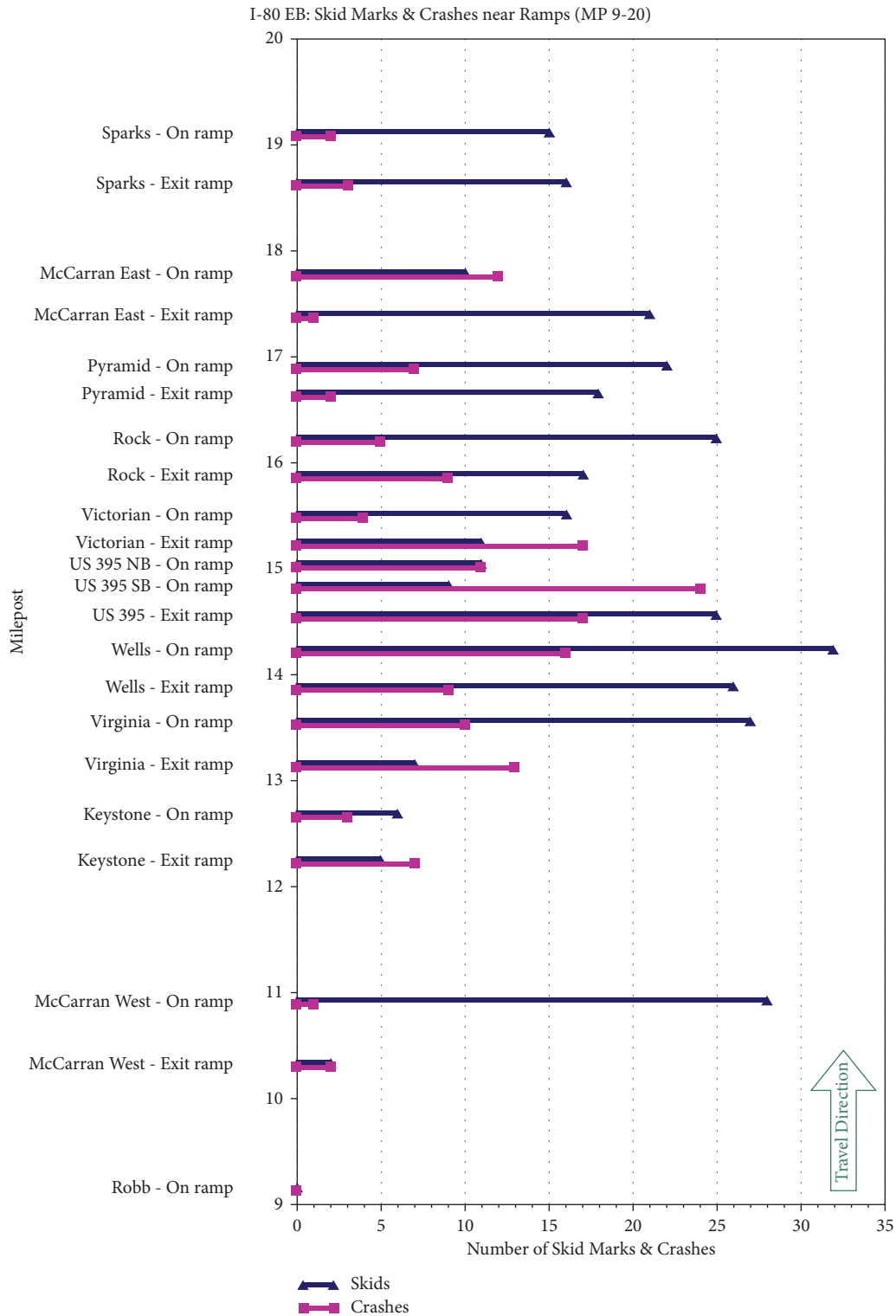


FIGURE 17: Crashes and skid marks at Interstate 80 eastbound ramps.

looking at the area under the graph for the beginning of the selected area.

Following the eastbound section of Interstate 80, one can notice several locations where the skid marks spike, namely, beginning near milepost 10, mileposts 13-14, and near mileposts 15.50–16.50. However, crashes and rear-end crashes

only seem to have similar spikes around milepost 13-14 and to a lesser extent near milepost 15.50. These might be plausible to consider as locations needing attention. In the westbound section, the only major spike seems to be the area beginning roughly near mileposts 16.6-15.6. For this case, the number of crashes outnumbers skid marks. It was

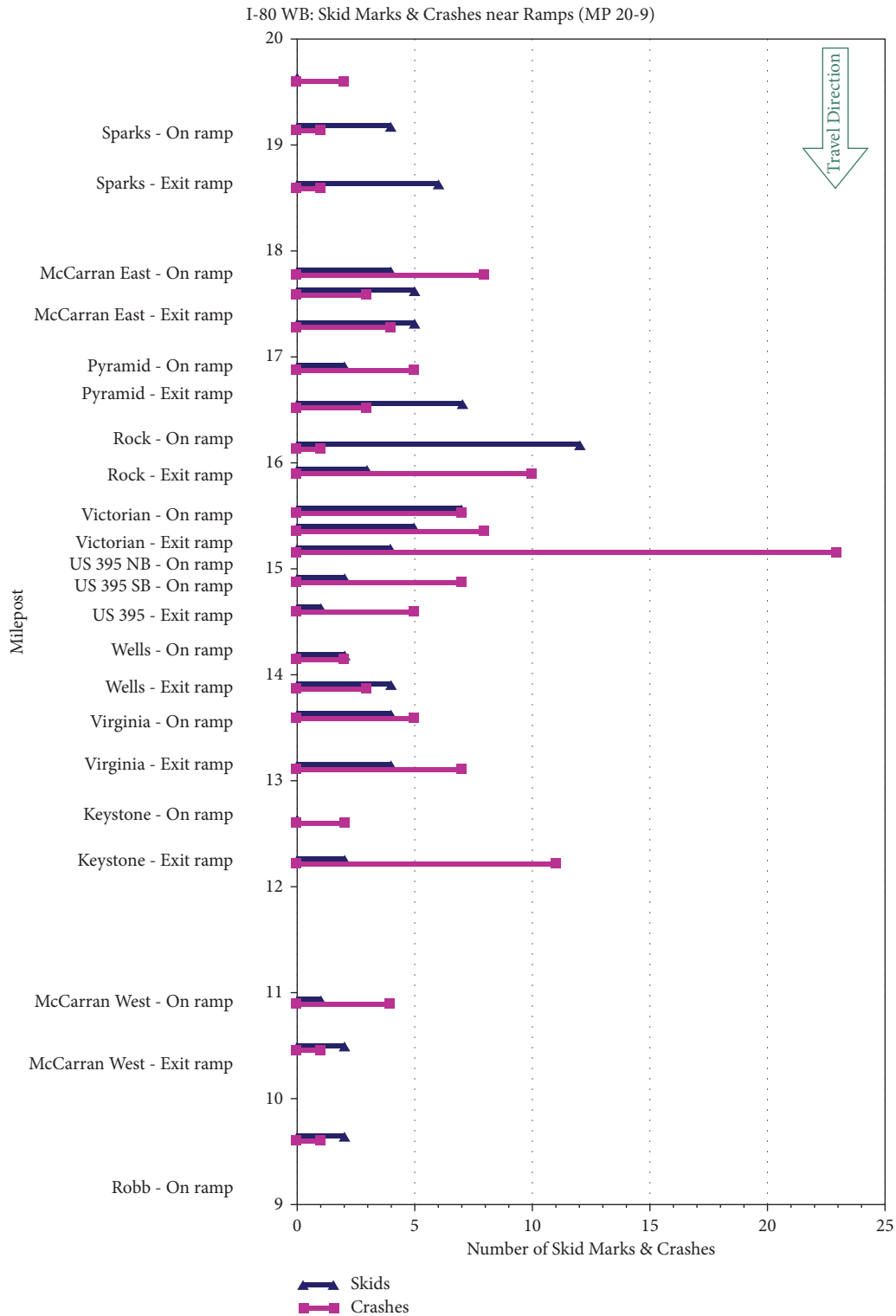


FIGURE 18: Crashes and skid marks at Interstate 80 westbound ramps.

noticed that all the locations mentioned above usually have high volumes coming from the freeway interchange at busy surface roadways, for example, North Virginia Street, North McCarran Boulevard, Rock Boulevard, and Pyramid Way.

In all the above analyses, it was recognized that examining these freeway sections with a given distance does not consider possible effects due to vehicles weaving near interchanges. Thus, additional analyses were performed pertaining solely to freeway entrance and exit ramps. For this examination, the exit ramp

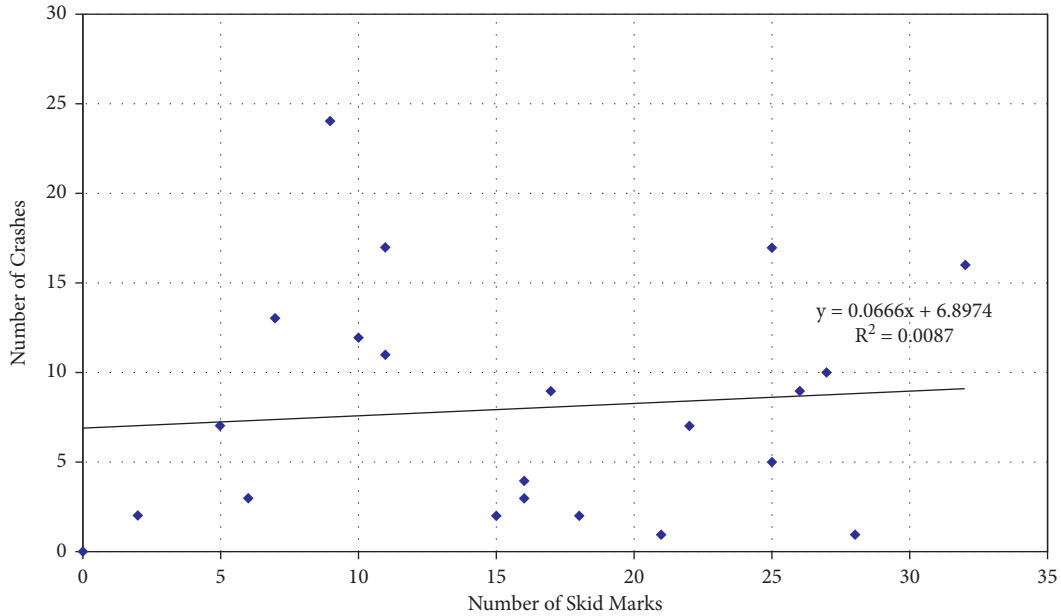


FIGURE 19: Crash vs. skid correlation at Interstate 80 eastbound ramps.

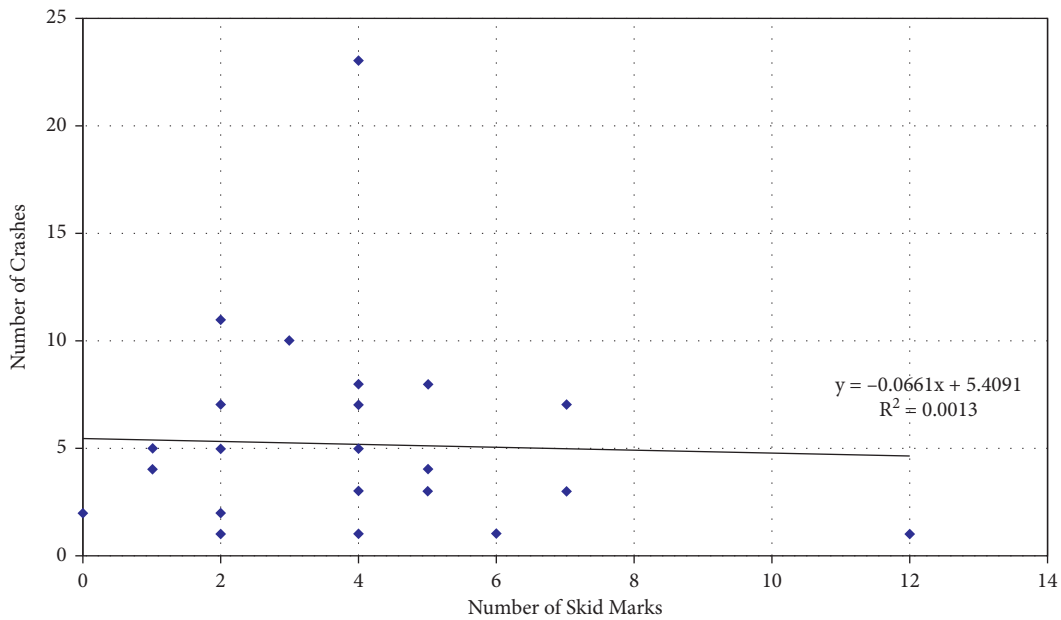


FIGURE 20: Crash vs. skid correlation at Interstate 80 westbound ramps.

areas studied consisted of the distance between the physical gore of the off ramp and 0.30-miles upstream, whereas the entrance ramps used the distance from physical gore to 0.30 miles downstream. The 0.30-mile distance was selected based on a definition used by Safety Analyst documentation as the boundary of the “interchange influence area” [21].

Figures 17 and 18 give a graphical representation of the number of skid marks and crashes for each freeway ramp within the eastbound and westbound study sections, respectively. As can be seen, the number of skids and crashes did not necessarily

correspond because the highest skid mark location is not the same as the highest crash location.

Figures 19 and 20 present the results of a regression given all the ramp data for a direction of freeway. As evidenced by the figures, it is unlikely that any correlation exists. Each section obtains from the regression an *R*-squared value below 0.01, and the westbound regression produces a negative trend. These facts indicate that a very poor correlation exists between crashes and skid marks when only ramps were considered.

TABLE 5: Regression outputs for freeways.

	Freeway stretch	Segmentation scale	Direction	Regression equation		<i>P</i> value of slope	<i>R</i> -square
				Slope	Intercept		
Crashes vs. skid marks	Interstate 80	Milepost	EB	0.82	-7.49	0.02	0.47
			WB	0.46	12.72	0.42	0.07
		Sliding window	EB	0.81	-10.99	≤0.001	0.51
	WB		0.74	8.20	≤0.001	0.17	
	US Highway 395	Milepost	NB	1.48	0.81	≤0.001	0.85
			SB	1.66	10.50	≤0.001	0.52
Sliding window		NB	1.30	0.00	≤0.001	0.88	
			SB	1.69	9.01	≤0.001	0.55
Rear-end crashes vs. skid marks	Interstate 80	Milepost	EB	0.59	-12.31	0.03	0.43
			WB	0.10	5.59	0.72	0.01
	US Highway 395	Milepost	NB	1.24	-4.91	≤0.001	0.84
			SB	1.01	4.24	≤0.001	0.50

5. Concluding Remarks

This study discussed a detailed analysis performed to ascertain whether tire skid marks on a pavement surface can be used to predict crashes or determine locations with possible safety concerns. Study sections on freeways in the Reno-Sparks urbanized area were identified to analyze and in order to make this determination. Video recordings documented positions of the skid marks along the roadways in the study. NDOT crash records provided locations where reported crashes had occurred. Based on these data, linear regression techniques were utilized to discover whether skid marks and crash data were indeed correlated. Considering rear-end crashes comprise a large proportion of all types of crashes (referred as crashes in this study), linear relationship between rear-end crashes and skid marks were also examined.

Table 5 presents the results from the linear regression analyses for the study freeway segments. Given that all slopes are consistently positive, it is reasonable to conclude that crashes/rear-end crashes generally increase as the skid marks increase in our cases. Additionally, except for the westbound direction of Interstate 80 under milepost scale, the *P* values for regression slopes are small (values italicized in Table 5), which provides strong evidence that skid mark frequency contains useful information in explaining and predicting crashes/rear-end crashes, given a confidence level of 95%. Also, the *R*-squared values of all scenarios were examined to evaluate the correlation between frequencies of skid marks and crashes/rear-end crashes, and the closer the value is to 1, the greater the degree of linear association between them. Thus, based on the regression results of crashes vs. skid marks, by comparing the outputs of the same freeway stretch of any direction under two division scales, it is found that regressions supported by sliding windows yield higher *R*-squared values than those supported by mileposts. This suggests that the linear association between skid marks and crashes is relatively stronger using sliding windows. In addition, given the fairly high *R*-

squared values on most of the stretches (except for Interstate 80 westbound for crashes vs. skid marks and Interstate 80 westbound for rear-end crashes vs. skid marks), linear correlation between skid marks and crashes might exist in these cases (values underlined in Table 5).

For the freeway sites, finding pertaining tire skid marks are summarized as follows:

- Crashes/rear-end crashes generally increased with increasing skid marks
- Skid-mark frequency is a suitable predictor of crash/rear-end crash frequency in most of the scenarios (87.5% for crash scenarios and 75% for rear-end crash scenarios) with a confidence level at 95%
- In most scenarios, skid marks and crashes showed good linear correlation as indicated by relatively high *R*-squared values

Due to strong correlation between tire skid marks and crashes on the selected freeway segments, more case studies need to be initiated on freeways in other urban areas. Also, additional work should be conducted to study how the tire skid marks could be used to help determine crash mitigation measures.

Appendix

Skid Mark Catalog Parameter Definitions

Lane: the “lane” parameter is defined as the lane of the roadway in which the skid mark occurs. In the event, a single skid mark follows a path through more than one lane, the lane in which the skid first appears was identified for the purposes of this parameter (with appropriate notation given in the notes column). The numbering of travel lanes and turn lanes followed the conventional road lane numbering schemes. The left-most lane (i.e., the lane closest to the median/center

line) was designated lane 1, with lane numbers increasing with each consecutive travel/turn lane to the right of the center line.

Heavy vehicle: the “HV” parameter indicates whether or not a skid mark appears to have been caused by the actions of a heavy vehicle. For the purposes of classifying this parameter, a heavy vehicle was defined as a truck, bus, trailer, or other commercial vehicle, which typically features four or more wheels on its rear axle. If two skid marks were closely spaced on one side of a lane, began and ended at approximately the same point, and follow one distinct path, then the marks were indicated to have been caused by a heavy vehicle.

Wheels: the “wheels” parameter indicates whether the actions of a single vehicle left behind skid marks on one or both sides of the vehicle. If a set of skid marks were on opposite sides of a lane, began and ended at approximately the same point, and followed a similar trajectory, then the marks were assumed to have been formed by both the left and right side tires of a single vehicle. Otherwise, if a skid mark appeared singularly and was aligned closer to the left or right side of the lane, then the mark was assumed to have been formed by either the left or right side tires of a single vehicle, respectively. For other singular skid marks aligned near the center of a lane, it was difficult to ascertain which side of the vehicle formed the mark (or whether the mark was made by a motorcycle) without additional information.

Direction: the “direction” parameter indicates the approximate direction the vehicle was heading when it formed the skid mark. This parameter was given three basic severity levels of straight, veered, or swerved, based on the apparent trajectory suggested by the skid mark. A skid mark in which the mark mostly paralleled the lane line markings was considered to be a straight mark. Any skid mark that shifted slightly to one side (but still remained mostly parallel to the lane line) and did not cross a lane line was also considered to be a straight mark. A skid mark was considered to veer when the mark gradually encroached upon an adjacent lane or lane line. Skid marks that followed a direct path into the adjacent lane and those that encroached upon the adjacent lane at the end of a predominantly straight path were also considered to be veering marks. Generally, a skid mark considered to veer had a long length and trajectory oriented primarily in the direction of travel. As a rule of thumb, skid marks deviating less than approximately 30° from the center line of the original lane were considered to veer. A skid mark was considered to swerve when the mark suddenly or drastically crossed into one or more adjacent lanes. Generally, a swerve was a skid mark that curved sharply away from the originating lane and took a trajectory oriented more perpendicular to the direction of travel. As a rule of thumb, skid marks appearing to deviate more than 30° from the center line of the original lane were considered to swerve. Some swerve marks first swerved one direction and then in another. In such

instances, the initial swerve direction was indicated under this parameter, with additional swerves mentioned in the Notes section.

Impact: the “impact” parameter indicates whether the vehicle that caused the skid mark appears likely to have impacted the roadside barrier (dividing wall, guardrail, median, etc.). Determination of this parameter is based on the location and trajectory of the skid mark in relation to the barrier, as well as the appearance of deformations or repairs on the barrier. Generally, a skid mark that indicates a barrier impact has also veered or swerved from its original trajectory.

Intensity: the “intensity” parameter is a relative measure of the darkness of the skid mark. This parameter was given three basic severity levels, based upon the contrast of the color of the skid mark versus the color of the pavement surface. A skid mark that was difficult to see was considered a faint mark. Over the surface area of a faint skid mark, the predominant visible color was that of the pavement surface. Most skid marks were considered average marks. The surface area of an average skid mark displayed a balance between the color of the pavement surface and the color of black tire rubber. For average skid marks, it was generally fairly easy to see the tire tread pattern on the pavement when viewing the video. A skid mark that appeared very black on the pavement was considered a dark mark. Over the surface area of a dark skid mark, the predominantly visible color was that of black tire rubber. For dark skid marks, the mark generally appeared to be a solid black line where tread marks could not be easily discerned.

Skip: the “skip” parameter indicates whether a skid mark appeared as a dotted line on the pavement. The individual dots of a skipping skid mark had to appear to follow the same trajectory (as if there were no dotted line at all) to be considered a single entity. Skipping was most likely to occur on marks that were also classified as heavy vehicles.

Thickness: the “thickness” parameter indicates the relative thickness of the skid mark. This parameter has no definitive parameters, but instead it indicates whether the mark got wider or narrower as the mark progressed longitudinally along the pavement.

Data Availability

The data used to support the findings of this study are available from the corresponding author upon request.

Conflicts of Interest

The authors declare that they have no conflicts of interest.

References

- [1] A. Arun, M. M. Haque, A. Bhaskar, S. Washington, and T. Sayed, “A systematic mapping review of surrogate safety assessment using traffic conflict techniques,” *Accident Analysis and Prevention*, vol. 153, pp. 1–20, 2021.

- [2] F. L. Mannering and C. R. Bhat, "Analytic methods in accident research: methodological frontier and future directions," *Analytic Methods in Accident Research*, vol. 1, pp. 1–22, 2014.
- [3] T. K. Datta, D. D. Perkins, J. I. Taylor, and H. T. Thompson, *Accident Surrogates for Use in Analyzing Highway Safety Hazards. Publication FHWA-RD-82-103*, FHWA, U.S. Department of Transportation, Washington, DC, USA, 1982.
- [4] A. Tarko, G. Davis, N. Saunier, T. Sayed, and S. Washington, "White paper: surrogate measures of safety," *Committee on Safety Data Evaluation and Analysis (ANB20)*, 2009.
- [5] K. F. Wu and P. P. Jovanis, "Crashes and crash-surrogate events: exploratory modeling with naturalistic driving data," *Accident Analysis & Prevention*, vol. 45, pp. 507–516, 2012.
- [6] H. Y. Gao and Z. Z. Tian, "Determination of crash surrogates using tire skid marks," in *Proceedings of the Seventh International Conference on Traffic and Transportation Studies*, pp. 1457–1468, ASCE, Kunming, China, August 2010.
- [7] A. P. Tarko, "Use of crash surrogates and exceedance statistics to estimate road safety," *Accident Analysis & Prevention*, vol. 45, pp. 230–240, 2012.
- [8] S. Jaehyun and D. George, "Development and evaluation of an enhanced surrogate safety assessment framework," *Transportation Research Part C*, vol. 50, no. 50, pp. 51–67, 2015.
- [9] K. Mattas, M. Makridis, G. Botzoris et al., "Fuzzy surrogate Safety Metrics for real-time assessment of rear-end collision risk. A study based on empirical observations," *Accident Analysis and Prevention*, vol. 148, pp. 1–10, 2020.
- [10] D. Yang, K. Xie, K. Ozbay, and H. Yang, "Fusing crash data and surrogate safety measures for safety assessment: development of a structural equation model with conditional autoregressive spatial effect and random parameters," *Accident Analysis and Prevention*, vol. 152, pp. 1–13, 2021.
- [11] N. Saunier and T. Sayed, "Probabilistic framework for automated analysis of exposure to road collisions," *Transportation Research Record*, vol. 2083, no. 1, pp. 96–104, 2008.
- [12] C. Oh, J. Oh, and J. Min, "Real-time detection of hazardous traffic events on freeways: methodology and prototypical implementation," *Transportation Research Record*, vol. 2129, no. 1, pp. 35–44, 2009.
- [13] A. Laureshyn, Å. Svensson, and C. Hydén, "Evaluation of traffic safety, based on micro-level behavioural data: theoretical framework and first implementation," *Accident Analysis & Prevention*, vol. 42, no. 6, pp. 1637–1646, 2010.
- [14] P. St-Aubin, N. Saunier, and L. Miranda-Moreno, "Large-scale automated proactive road safety analysis using video data," *Transportation Research Part C: Emerging Technologies*, vol. 58, pp. 363–379, 2015.
- [15] Y. Kuang, X. Qu, and S. Wang, "A tree-structured crash surrogate measure for freeways," *Accident Analysis & Prevention*, vol. 77, pp. 137–148, 2015.
- [16] K. Xie, C. Li, K. Ozbay et al., "Development of a comprehensive framework for video-based safety assessment," in *Proceedings of the 2016 IEEE 19th International Conference on Intelligent Transportation Systems (ITSC)*, pp. 2638–2643, Janeiro, Brazil, November 2016.
- [17] S. M. S. Mahmud, L. Ferreira, M. S. Hoque, and A. Tavassoli, "Using a surrogate safety approach to prioritize hazardous segments in a rural highway in a developing country," *IATSS Research*, vol. 44, no. 2, pp. 132–141, 2020.
- [18] Y. Kuang, Y. Yu, and X. Qu, "Novel crash surrogate measure for freeways," *Journal of Transportation Engineering, Part A: Systems*, vol. 146, no. 8, p. 04020085, 2020.
- [19] A. P. Tarko, "Surrogate measures of safety," in *Safe Mobility: Challenges, Methodology and Solutions*, pp. 383–405, Emerald Publishing Limited, Bingley, UK, 2018.
- [20] L. Zheng, T. Sayed, and F. Mannering, "Modeling traffic conflicts for use in road safety analysis: a review of analytic methods and future directions," *Analytic Methods Accident Research*, vol. 29, Article ID 100142, 2020.
- [21] D. J. Torbic, D. W. Harwood, D. K. Gilmore, and K. R. Richard, *Interchange Safety Analysis Tool (ISAT): User Manual. Publication FHWA-HRT-07-045*, FHWA, U.S. Department of Transportation, Washington, DC, USA, 2007.

Research Article

A Combined Simulation Approach to Evaluate Overtaking Behaviour on Two-Lane Two-Way Rural Roads

Valentina Branzi ¹, **Monica Meocci** ¹, **Lorenzo Domenichini** ¹
and **Margherita Calcinaï**²

¹Civil and Environmental Engineering Department, University of Florence, Via S. Marta 3, 50139 Firenze, Italy

²Tecne SPA-Gruppo Autostrade per l'Italia, Via dei Valtorta, 48, 2017 Milano, Italy

Correspondence should be addressed to Monica Meocci; monica.meocci@unifi.it

Received 17 March 2021; Accepted 12 August 2021; Published 21 August 2021

Academic Editor: Mohamed Hussein

Copyright © 2021 Valentina Branzi et al. This is an open access article distributed under the Creative Commons Attribution License, which permits unrestricted use, distribution, and reproduction in any medium, provided the original work is properly cited.

A significant percentage of road fatalities and injuries occur in the nonmotorway rural road network. One of the main causes of accidents on these roads is represented by overtaking, as, by its nature, it involves a risk of a head-on collision with oncoming traffic. The paper describes a combined simulation approach (driving simulator and traffic microsimulation) designed to examine the influence of different traffic conditions on passing manoeuvres on two-lane two-way rural roads. The main focus was the evaluation of the end of the passing manoeuvre because it reflects the risk of a head-on collision. In addition, the study aimed to assess the usefulness of the proposed combined approach in the ability to proactively and quickly diagnose traffic safety problems and consequently to evaluate appropriate solutions. The data collected with an interactive driving simulator on a sample of 54 participants have been used to adjust some input data of the traffic microsimulation software. A specific situation consisting of a stationary heavy vehicle obstructing the entire lane was repeated in both experiments. The analyses focused on time-to-collision (TTC), defined as the remaining gap between the passing vehicle and the oncoming vehicle at the end of the passing manoeuvre. The results showed that the type of manoeuvre performed is significantly influenced by the traffic condition. Furthermore, the manoeuvre is influenced by the gap between two successive vehicles in the opposite lanes. Focusing on the end of the manoeuvre, it was found how a traffic increase leads to a significant reduction of the TTC values. Furthermore, the comparative analysis conducted between the data recorded following the combined approach and those obtained using exclusively the input data of the microsimulation software supports the usefulness of the proposed methodology for conducting road safety analyses, especially in complex traffic environments where drivers' behaviour plays a decisive role.

1. Introduction

Most road accidents worldwide occur on rural roads. They are associated with the highest risk of fatalities and serious injuries in the 41 OECD (Organization for Economic Cooperation and Development) countries [1] and accident data from other countries as the United States of America (USA) [2] and Australia [3] show comparable figures. Focusing on the European road network, between 2006 and 2015, about 180,000 people were killed in accidents on roads outside urban areas, excluding motorways. This number represents 55% of all road fatalities in the EU [4]. In Italy, the situation is slightly less serious. In 2019, road accidents reported on rural roads amount to 36,107 (21% of

the total) with 1,532 people killed (48.3%) and people injured 57,581 (23.9%) [5].

Two-lane, two-way rural roads (i.e., road consisting of two opposing lanes of undivided traffic, in which lane changing and passing is possible only in oncoming traffic) constitute worldwide an important part of the rural road network. On these types of roads, overtaking plays an important role in influencing both road safety and mobility, in terms of capacity and level of service. While the lack of the ability to overtake may lead to the formation of large queues [6], the interaction with oncoming traffic flow from the opposite direction may significantly increase the risk of accidents, for example, due to the false temporal and distance estimations regarding the oncoming vehicles made by

drivers [7–10]. Overtaking represents one of the most serious causes of two-lane two-way rural roads injuries and fatalities; due to its nature, it involves a risk of a head-on collision with oncoming traffic, and therefore it has a direct impact on safety. Previous studies showed that the accident severity resulting from this type of manoeuvre is significantly higher than that of other accident types on two-lane two-way rural roads [11–13].

In general, overtaking manoeuvre is one of the most complex and difficult driving processes which requires complicate decisions, involves a series of sequential actions (such as lane-change manoeuvres, possible acceleration and deceleration actions, and estimation on the relative speed of the overtaking and overtaken vehicles) and can fail in several ways. All these issues are undoubtedly amplified on two-lane two-way roads, mainly due to the variety of influencing factors. The drivers who overtake have to go through certain decision-making processes to accept or reject gaps presented to them in the oncoming traffic stream and to determine whether passing is justified under the constantly changing road and traffic conditions [14, 15]. The overtaking manoeuvre, indeed, can be performed in different ways, mainly based on the speed of the vehicle to be overtaken and the oncoming traffic in the opposite direction.

The overtaking manoeuvre was examined focusing on two aspects: (a) the development of models capable of explaining the different factors that can influence this manoeuvre and (b) the analysis of driving behaviour during the overtaking conducted in different conditions. In both cases, the analysis data were collected through in-field and naturalistic driving studies and, recently, using simulation techniques, especially by means of driving simulators.

The first relevant data to develop the overtaking manoeuvres models were obtained by observation and field study by recording video from external fixed positions of passing zones using only one camera in each passing zone [16, 17] and, more recently, using six cameras installed at a fixed point, next to passing sections [18, 19]. In both cases, although data were recorded according to traffic volumes ranging between 300 and 1,000 vehicles per hour, results were not provided for different traffic volumes, as only in a few manoeuvres did an opposing vehicle occur approaching the vehicles passing and getting in the way.

Other researchers [20, 21] carried out naturalistic driving studies using instrumented vehicles to evaluate the driver's behaviour and performance (in terms of assessing collision risk with either the oncoming car) in real-time, by analysing surrogate safety measures.

Field and naturalistic data undoubtedly provide a rich source of data related to real-world experience; however, they require significant costs, involve safety problems for drivers and observers and difficulties in controlling experimental conditions, and may not provide satisfactory information for a full experimental design.

The interdisciplinary approach based on driving simulations represents a promising alternative method, which offers advantages in terms of cost reduction, ease of data collection, and completely safe and controlled experimental conditions. In addition, several studies have shown the

reliability of the acquired data (i.e., the correspondence between the driver behaviour in the simulator and in the real world) in different driving environments, traffic situations, etc. [22–27], enough to make this approach a valid and reliable alternative to study complex manoeuvres.

In this context, some studies have used driving simulators to analyse and identify factors that influence driving behaviour during this critical manoeuvre, such as speed [11], the influence of different traffic-flow conditions [28], the visual-motor control strategies, and cognitive decision-making of drivers [7, 29]. Other researchers, instead, used driving simulator data to develop models to estimate the passing sight distance [30], the passing gap acceptance [31], the passing duration and passing distance [32], and the probability of head-on collisions that result from unsuccessful passing manoeuvres [33].

Although the approach adopted in these studies seems to be very promising, there are some disadvantages, mainly concerning the number of participants for each trial. In fact, in general, the driving simulator studies are carried out on samples composed of a limited number of subjects and consequently, the collected and analysed data are also limited and may not provide a complete generalization of the phenomenon studied.

An innovative method could be to use a combined approach based on the driving simulator and the microscopic traffic simulator. Indeed, the integrated simulation approach can provide a more realistic simulation platform for modelling conflicts [34].

Microscopic traffic simulators are powerful tools that, through the implementation of behavioural models, allow reproducing and predicting the evolution of different traffic situations and obtaining a multitude of data by generating various simulations.

Traditionally, traffic simulation models have been used to evaluate traffic system performance, and just more recently, there has been a growing interest in developing traffic simulation models to study the impact of traffic on road safety. Initially, the simulation-based approach offers the ability to proactively and quickly diagnose traffic safety problems and evaluate appropriate initiatives [34]. The microscopic model allows the estimation of road safety performance through a series of indicators, which represent real-time interactions between different pairs of vehicles belonging to the traffic flow. This approach is mainly based on the Traffic Conflict Technique (TCT) [35]. The TCT consists of capturing the near-misses conflicts and assessing the frequency and severity of collisions objectively and qualitatively, through the use of the so-called surrogate safety measures [36]. The use of these measures, which are not based on the observation of actual crashes, but instead on the probability of crashes, is proving increasingly interesting and promising for modelling and estimating safety, and it has a clear advantage over using crash data. Indeed, the use of crash data is a reactive approach that takes longer as data is infrequent, as well as being often of poor quality and underestimated. According to Gettman et al. [37], the ratio between conflicts and actual crash frequencies is generally in the range of thousands to 1 (depending on the definition of conflict).

Some studies have integrated these two simulation tools (driving simulator and microscopic traffic simulator). However, the purpose of this integration was oriented to develop and implement a real-time running traffic simulation model capable of generating and simulating surrounding vehicles in a driving simulator. Focusing on the analysis of overtaking manoeuvres, only Jenkins and Rilett [38] developed a prototype that combined the microscopic traffic simulation program VISSIM with the driving simulator. The methodology of integrating simulations was applied to study the impact of both the length and the speed of the impeding vehicle on passing behaviour. By comparing the results from the passing experiments with field observations, the authors demonstrated some benefits of this approach, including the ability to generate specific vehicle volumes in the driving simulator and the ability to acquire comprehensive data.

Although the potential benefits of this approach have been recognized, the incorporation of the performance safety measures into traffic simulation models has been slow. Consequently, road safety simulation models are still being investigated [39]. In particular, there is still a significant obstacle in the development and application of the simulation model to assess traffic safety on rural roads [34]. Most studies concern intersections and most applications focus on modelling rear-end conflicts using car-following theory, but no studies appear to consider head-on collision on two-lane two-way roads [34].

All currently available microsimulation software packages are based on different submodels that explain how the drivers make decisions, in terms of route choice, car following, and lane selection, which are repeatable across the entire road network. All drivers' behaviour models consist of parameters, allowing users to enter input values within a specified range. These values may vary significantly based on driving conditions and geographical location (i.e., the local traffic characteristics and traffic conditions for a specific area). Thus, the default values for such variables must be adjusted for a realistic replication of local driving conditions [40].

The data recorded in virtual reality, which are representative of driving behaviour in specific, controlled, and safe driving conditions, could therefore be used for this purpose, that is, to "adjust" some of the default parameters characterizing the models of which the microscopic traffic simulators are composed. In this way, the advantages of both simulation tools could be fully used: the possibility of carrying out road safety analyses of complex situations on a considerable amount of data, using traffic microsimulator models whose parameters are representative of the drivers' behaviour in the geographic area and driving conditions analysed. However, this approach appears to be unexplored. This research opportunity motivates our study.

2. Research Objective and Motivation

The purpose of this study is to evaluate the influence of different traffic-flow conditions on the occurrence of potential risk situations, which could lead to a crash event,

during the passing manoeuvre on two-lane two-way rural roads, using a combined simulation approach. Specifically, this paper focused on the analysis of the end of the passing manoeuvre, since up till this moment, there is still a risk of collision, therefore, reflecting the risk of head-on collisions (i.e., a collision with the opposite vehicle) and also because not many studies focused on the detailed analysis of the link between passing manoeuvres and head-on collisions in relation to traffic flows in the opposite direction.

Several studies analysed the passing manoeuvres on this type of road, mainly based on field and driving simulation studies. All these studies showed that one of the most critical factors involved in passing behaviour is the drivers' ability to estimate the required gap for passing a lead vehicle in front of an oncoming one. Specifically, they revealed that drivers' accepted passing gaps are widely influenced by several factors (such as the type of overtaking manoeuvre that a driver intends to perform, the traffic conditions in the opposite direction, and/or the waiting time for an opportunity for overtaking) which clearly suggest that drivers adapt their accepted gaps to overtake, depending on the traffic situation [21]. However, in literature, there are a few contributions [28, 32, 41] that provide indications of the influence of different traffic volumes on the driver's behaviour during the overtaking manoeuvre. Overall, all three studies highlighted, as is conceivable, that the amount of oncoming traffic significantly affects the driving behaviour and the kind of manoeuvre adopted by the driver. While the studies conducted by [29, 32] were able to show this result only at the end of the passage manoeuvre (evaluating only this phase), the work in [28] extended this result, proving that traffic significantly influences the behaviour of drivers in all three phases of the passing manoeuvre analysed (beginning of the manoeuvre, occupation of the left lane, re-entry in the right lane). Specifically, it revealed that the manoeuvres carried out are all the riskier, the greater the traffic volume.

Compared to these previous studies, a novel and peculiar feature of our study is to use both driving simulation and microscopic traffic simulations. In particular, the present study used the LaSIS driving simulator to better understand the interaction between the overtaking driver and the oncoming traffic, in order to obtain more reliable behavioural data. The results of driving simulator experiments are then used to adjust some driving behaviour parameters of the microscopic passing manoeuvre model for two-lane rural roads specially developed for the Aimsun microsimulation software [42], in order to effectively represent the driving behaviour during the overtaking manoeuvre on these types of roads.

Finally, in order to be able to provide the first suggestions on the potential for using such an approach, the traffic simulations conducted by the Aimsun software were also run with the software default values (without any adjustments). The results of this simulation and those obtained from the one in which some parameters were set according to the data recorded in the simulator were compared by statistical analysis to assess whether there were significant differences.

3. Aimsun Microscopic Passing Manoeuvre Model for Two-Lane Rural Roads

The Aimsun (Advanced Interactive Microscopic Simulator for Urban and Non-Urban Networks, <http://www.aimsun.com>) microsimulation software [42] was used because of its ability to appropriately represent road network geometry and model in detail the behaviour of individual vehicles to reproduce explicitly traffic signal control plans, pretimed and actuated, and because it has an easy-to-use graphical user interface. Also, a particular feature of Aimsun is its ability to capture the empirical evidence that driver behaviour often depends on local circumstances (i.e., the acceptance of speed limits on-road sections, the influence of gradients, driver interaction whilst travelling in adjacent lanes).

Three main behavioural models are implemented on the base of the software operation, which allow describing the behaviour of the single vehicle reproducing the real traffic situations in the conditions of (a) car following, (b) lane changing, and (c) gap acceptance. In addition to these three main models, other models are implemented within the software for particular contexts and derivations from the main models themselves.

Recently, Llorca et al. [43] developed and calibrated a passing manoeuvre model in Aimsun [42]. In particular, it has been implemented in Aimsun 8.0.3. This model, used in the present work, covers the desire, decision, and execution processes of passing manoeuvres and relied on 14 parameters, defined specifically for the two-lane highways model. The 14 model parameters are associated with the experiment, the vehicle type, or the section Aimsun editors.

The parameters that affect the entire experiment are (1) delay time threshold for passing decision (delayTh) (s); (2) minimum speed difference threshold (mindV) (km/h); (3) maximum speed difference threshold (maxdV) (km/h); (4) maximum rank in the platoon to desire to pass (maxRank) (vehicles); (5) number of simultaneous passes allowed (maxSimul) (passes); (6) delay between simultaneous passes (delaySimul) (s); (7) sensitivity factor for reduced car-following (RCF); (8) passing vehicle speed enhancement (PVSE); (9) speed difference threshold for enhanced passing vehicle speed (PVSETh) (km/h); and (10) remaining time to the end of the highway segment threshold (remainingtimeTh) (s). Traffic demand in Aimsun may be divided into several vehicle types.

The parameter that affects a particular vehicle type is safety margin for passing manoeuvre (safetymargin), defined by its minimum, maximum, mean, and standard deviation values (values in s).

The parameters that affect a single section are (1) mirror section identification (MirrorID); (2) available sight distance at the end of the passing zone (ASD) (m); and (3) sight distance factor (SDfactor).

4. Methodology

4.1. Overall Framework. This study proposed an integrated methodology that combines virtual reality driving simulation with traffic microsimulation. Figure 1 illustrates the

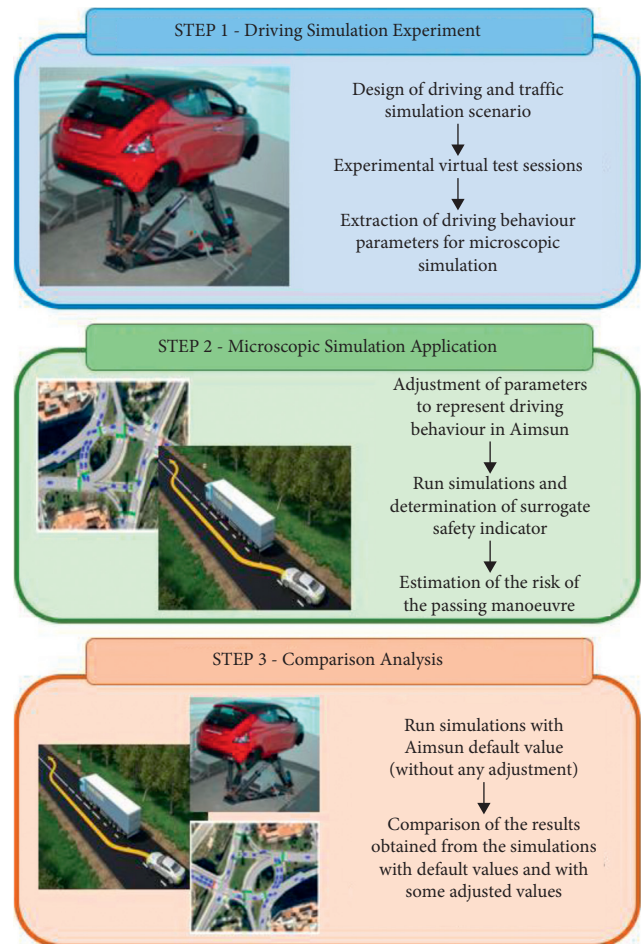


FIGURE 1: The overall framework of the proposed methodological approach.

overall design of the methodological approach proposed. It consists of three steps: (1) driving simulation experiments, (2) microscopic traffic simulation, and (3) comparison analysis. A driving simulation experiment is carried out to obtain information regarding driving behaviour during the overtaking manoeuvres under different traffic-flow conditions. The driving simulation environment allows capturing various driving behaviour patterns in a scientific and systematic manner. Therefore, the results help to gather different driving performances and behaviours that characterize different subjects belonging to a population. The results of this first step were further processed to adjust some parameters of microscopic traffic simulations. In the second step, Aimsun was used to assess the risk, in terms of safety, of the passing manoeuvres in different traffic-flow conditions. Some driving behaviour parameters of Aimsun were modified based on the results of the driving simulation experiment in step 1. In the traffic simulation, three different traffic-flows conditions were also set and the consequent change in vehicle manoeuvres was obtained and recorded. The change in driving performances due to traffic-flow conditions was assessed taking into account a surrogate safety measure. Finally, in the last stage (step 3), further microscopic traffic simulations were carried out with the

default values. The results obtained from these last simulations were processed and analysed according to phase two, to compare them with those obtained from the simulations in which some driving behavioural parameters were adjusted and to evaluate any statistically significant differences.

4.2. Driving Simulation Experiment

4.2.1. Apparatus. The LaSIS driving simulator used in this study is a motion-base simulator, equipped with a full-scale vehicle fitted on a 6° of freedom Stewart's platform, allowing roll, yaw, and pitch. The vehicle interior is identical to the commercial version and it includes all commands normally available in such kinds of cars, with the steering wheel with force feedback. The cabin is surrounded by a cylindrical screen about 200° wide, on which 4 projectors reproduce the driving environment. Sounds and noise of traffic in the environment and of the participant's car are generated by a multichannel audio system. The data acquisition frequency of the apparatus is 20 Hz. The apparatus was previously validated as a reliable tool to predict the driver's behaviour in the real world and used to evaluate the driver's performance in terms of speed, acceleration/deceleration, and lateral position under various road environments and driving conditions [22, 23, 44–46].

4.2.2. Simulated Road Scenario. About 50 km of a two-way two-lane rural road, with a posted speed limit of 80 km/h, was designed and implemented in the LaSIS driving simulator. It should be noted that although, according to the Italian Highway Code [47], the speed limit for the type of simulated roads is 90 km/h, it was cautiously chosen to set it equal to 80 km/h based on the analysis of the data collected on the main two-way two-lane rural road located in the province of Florence, where the maximum limit recorded was 70 km/h.

The cross section of the carriageway is composed of two lanes (one for each direction), each 3.75 m wide and 1.50 m wide shoulders according to [48].

The road section was designed without any longitudinal grade and with few curves and no intersections, in order to exclude any possible influences of the sight distance on the driver's behaviour during passing manoeuvres. The driving experiments were carried out during daylight conditions and with good weather conditions (dry pavement). The passing was permitted only in the straight sections. The sections where the passage was not allowed were marked.

During the simulated route, the participants drove through four different analysis configurations, depending on the gap in the traffic in the opposite direction. Each analysis configuration was preceded by approximately 7 km of the standard route, where the road layout and traffic did not require the driver to change the desired driving style. Four different scenarios were built. The sequence of the four analysis configurations was counterbalanced to avoid influences due to the repetition of the same order in the experimental conditions.

The virtual scenarios were characterized by autonomous traffic, made with different vehicles, organized as “swarm” around the interactive vehicle. For each configuration, in the preliminary section of virtual road (7 km of the standard route) the autonomous traffic was organized in both directions, while, in the examined section, it was only in the opposite direction to the subjective vehicle to avoid affecting the drivers' performance, in terms of speed, acceleration, deceleration, and so forth.

The situation that participants encountered in each of the four analysis configurations is shown in Figure 2. The subject vehicle was passing an impeding vehicle (front vehicle) while other vehicles were approaching from the opposite direction. The front vehicle was represented by a stopped heavy vehicle that simulated the situation of a vehicle in mechanical failure forced to obstruct the entire traffic lane due to the absence of a lay-by where you take refuge and wait for help. It was decided to obstruct the entire traffic lane (despite the possibility that the heavy vehicle occupied the shoulder) in order to reproduce the same situation that could be simulated in the Aimsun software. In fact, the Aimsun simulation does not allow the evaluation of the lateral movement of the vehicle, but it only identifies whether the vehicle is positioned in one or the other traffic lane, and it considers the obstruction of the entire lane.

The traffic approaching from the opposite direction consisted of the same platoon made up of six light vehicles; thus, the conditions to which the participants were subjected were the same in each configuration and there were no further variables (albeit of a minor entity, such as the type of vehicles and the colour of the vehicles) that, in some way, could affect the driver's performance and behaviour.

The passing gaps, which are the gap between the first and second vehicles of the platoon, were defined by the time spacing between these two vehicles at the time the subject encounters the lead opposite vehicle as illustrated in Figure 2. These passing gaps took on a different value in each analysis configuration, while the gap between the other vehicles of the platoon was set equal to 2 seconds in each configuration examined. The aim was to induce the driver to overtake by exploiting the first available gap; in fact, if the driver was unable to exploit this gap, he/she was forced to stop behind the stopped vehicle and wait for the whole platoon to pass, as a gap of 2 seconds did not allow overtaking.

An increase in passing gap was simulated for the four analysis configurations: a “critical” situation, a “precautionary” situation, and two other intermediate situations. The “critical” situation represented the space needed to physically perform the overtaking manoeuvre [49], while the “precautionary” situation represented the space needed to perform the overtaking manoeuvre in safety, according to Italian regulation on road design [48]. The “critical” and “precautionary” passing gaps were equal to 8 seconds and 20 seconds, respectively. They have been determined assuming that the driver maintains a speed corresponding to the imposed speed limit (equal to 80 km/h). Two passing gaps of 12 seconds and 16 seconds were chosen as intermediate situations. Table 1 summarizes the four different traffic conditions that the user has faced along the virtual road.

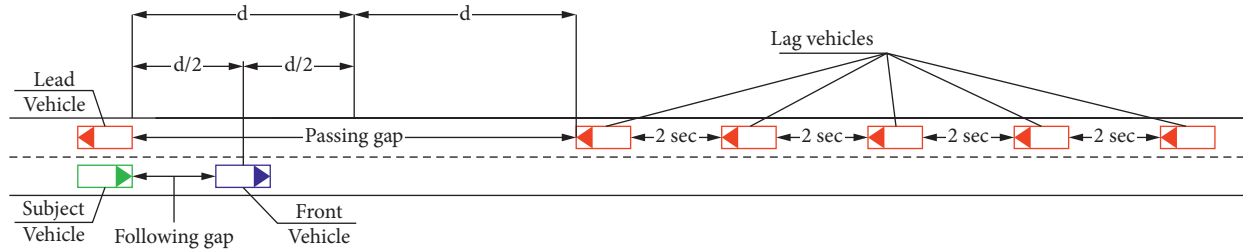


FIGURE 2: Passing gap configuration.

TABLE 1: Characteristics of the analysis configurations.

Configuration	Traffic condition	Passing gap (s)	Passing gap (m)
1	Critical	8	178
2	Intermediate low	12	267
3	Intermediate high	16	356
4	Precautionary	20	444

It is important to note that, except for the subject vehicle, the speeds of all vehicles and the route they followed in the scenarios were previously programmed to be constant to allow the correct size and distribution of the passing gaps analysed.

4.2.3. Participants and Test Protocol. The minimum sample size was determined according to Cohen's theory [50], given the desired probability level, the anticipated effect size, and the desired statistical power level. The anticipated effect size χ^2 was assumed equal to 0.6; the statistical power level and the P value were set, respectively, equal to 90% and 5% (according to the previous studies, [45, 51]). Using these parameters, the minimum sample size is sixty-five. Based on these results, sixty-five subjects (29 women and 36 men) were recruited voluntarily among students, staff of the University of Florence (Italy), and other volunteers from outside the University according to the following criteria: possession of a valid Italian driver's license, with at least five years of driving experience, an annual driven distance greater than 5000 km, and low susceptibility to motion sickness. In order to avoid any bias of the outcomes, eventually related to the inexperience (young drivers) and aging (elderly drivers), the subjects aged less than 25 years and the subjects aged more than 65 years were excluded from the experimental study.

Five selected participants (2 women and 3 men) subsequently withdrew from the study and six subjects (5 women and 1 man) exhibited simulator sickness and did not complete the experiment. Thus, fifty-four subjects (22 women and 32 men) participated in the research, whose main characteristics are indicated in Table 2.

The selected participants were all residents of Tuscany and they had a normal or corrected-to-normal vision.

A chi-square goodness-of-fit test was conducted to determine whether the participants recruited were representative of the driver population resident of Tuscany.

Specifically, it was analysed whether these had the same proportion, in terms of age (according to the 4 age groups indicated in Table 2) and sex. The test was performed at a level of significance of 5%. The results indicated that age and gender were similarly distributed among the participants recruited to the study as the Tuscan driver population ($\chi^2(7) = 9.348$, $P = 0.229$).

All participants followed the same test protocol, explained below. The driving simulation experiment consisted, after signing the informed consent form, of the following steps: (a) communicating to the participants some basic information on the use of the simulator, as well as advising them to drive and to behave like in real-life situations, warning about possible simulator sickness and saying that they could stop the test at any time; (b) training phase to familiarize with the interactive vehicle and its control instruments; (c) a rest of 5 min to restore psychophysical conditions similar to those at the beginning of the test; (d) experimental phase in which each participant drove the simulation scenario with a specific sequence of traffic condition configurations.

Each participant encountered each of the four traffic condition configurations in random order to reduce the biases within the data collection. The participants were tested individually and were not briefed about the objectives of the research. Their participation was voluntary and no monetary reward was given for their involvement, which lasted about 45 min.

4.2.4. Extraction and Processing of Driving Behaviour Data. Two of the 14 parameters that characterized the Aimsun passing manoeuvre were selected in the present study as those most influenced by the driver's behaviour when overtaking a stopped vehicle: "PSVE" and "safetymargin" parameters. The first is defined as the ratio between the maximum speed maintained by 5% of drivers at the end of the passing manoeuvre and the posted speed limit. It takes into account the possibility of travelling at a speed higher than the driver's free-flow desired speed. The second is defined as the safety margin for the passing manoeuvre and it is the parameter by which the risk of the manoeuvre is assessed. It represents the time to collision (TTC) between the passing vehicle and the opposite vehicle at the end of the overtaking process (i.e., the remaining gap between the two vehicles considered). When it reaches a value below a certain threshold (precisely considered "safety margin"), overtaking can be risky. Specifically, if the sum of the value of this

TABLE 2: Participant characterization according to the factors considered.

		25–34 years	35–44 years	45–54 years	55–64 years	Total
Sample consistency		14	17	15	8	54
Gender	F	7	6	5	4	22
	M	7	11	10	4	32
Age	MV	27.6	39.6	48.9	57.4	38.5
	SD	2.5	2.8	2.8	1.5	9.7
Driving experience (years)	MV	9.6	21.6	30.9	39.4	20.5
	DS	2.5	2.8	2.8	1.5	9.7

F = female; M = male; MV = mean value; SD = standard deviation.

parameter and the time required to complete the manoeuvre is less than the TTC assessed at the start of the manoeuvre, the overtaking is considered not to be at risk and can be completed safely. Otherwise, the opposite is true. The “safetymargin” parameter, during microscopic traffic simulations, takes on a different value for each vehicle.

To evaluate the first parameter considered, the PVSE, defined by a scalar factor, the speed reached by each driver at the end of the passing manoeuvre was extracted from the raw driving simulator data. For the determination of the “safety margin,” the TTC between the subject vehicle and the lead opposite vehicle was calculated at the end of each passing manoeuvre. The TTC is measured at the end of the passing manoeuvre (as there is still a risk of the collision up to this moment) and reflects the risk to collide with the opposite vehicle. The end of a passing manoeuvre was defined, for each driver, as the instant when the subject vehicle wholly turns back into his lane (in front of the impeding vehicle) corresponding to the instant in which the subject vehicle’s rear left wheel touches the centre line (Figure 3).

It is important to point out that these measures were available only for “accepted” passing gaps, that is the situation in which the driver has believed the first available gap (i.e., the one between the first and the second vehicle coming from the opposite direction, as shown in Figure 2) was sufficiently wide and he/she has completed the passing manoeuvres. In fact, due to how the analysis configurations in virtual reality were built, if the drivers did not exploit the first available gap, they were forced to wait for the complete passage of the entire platoon and overtake the stopped vehicle when there was no traffic in the opposite lane (this situation, in the rest of the text, will be indicated as the one in which the gap is rejected).

In addition, the speed held by each participant in free-flow driving conditions was also extracted from the raw driving simulator data. It is the speed recorded along a road section where there were no road geometrical characteristics and traffic conditions that forced the driver to change his driving style and to adopt a speed other than the desired one.

4.3. Traffic Microscopic Simulation

4.3.1. Network Model Coding and Run Simulation. The road network consists of a single straight segment of one kilometre in length, without intersections, with a single carriageway and two traffic lanes (one for each direction). Each

traffic lane is 3.75 meters wide. The posted speed limit is 80 km/h, and it is consistent with the scenario used in the virtual reality experiment.

The traffic demand was assigned through the use of the origin/destination (O/D) matrix, characterized by the following input data: centroids of origin and destination, vehicle types in the network and their attributes, vehicle classes, and the number of movements from each origin centroid to each destination centroid. For the experiment, two centroids were defined at the ends of the segment, and a single vehicle class consisting of light vehicles was defined. As regards the determination of the number of movements, three different matrices were defined, each associated with a different traffic flow to reproduce three different levels of service (LOS). In this way, it was possible to reproduce different traffic-flow conditions in the opposite direction to the subject vehicle and, thus, assess how the LOSs may affect the execution of the passing manoeuvre. Specifically, three traffic-flow values were considered corresponding to service levels A, B, and C for a road with a speed limit of 80 km/h, according to the Highway Capacity Manual [52].

Two different traffic distributions were selected for the two different directions of travel. In the traffic lane where the stationary heavy vehicle was located, a uniform distribution was selected with a number of arrivals such that it did not create the phenomenon of multiple queuing behind the stationary heavy vehicle, while in the opposite direction, an exponential distribution of arrivals was selected.

As regards the input data relating to vehicle classes, in addition to some behavioural parameters recorded through the driving simulator, it was decided to adjust other two input data of the microsimulation model in order to obtain results closer to reality: (a) the reaction time and (b) the maximum acceleration. Specifically, the value of 1 second has been assigned to the first parameter, according to Basak et al. [53] (the default value assumed by the software is 1.2 seconds), while, according to the acceleration/deceleration model defined by Bokare et al. [54], an average value of 1.2 m/s^2 and a standard deviation of 0.3 m/s^2 have been assigned for the second parameter (the default values are, respectively, 3 m/s^2 and 0.2 m/s^2).

Once the scenario described above was set up, it was decided to run the experiment using the Monte Carlo algorithm. Three different experiments were performed, each characterized by a different traffic demand, corresponding to the three LOS examined.

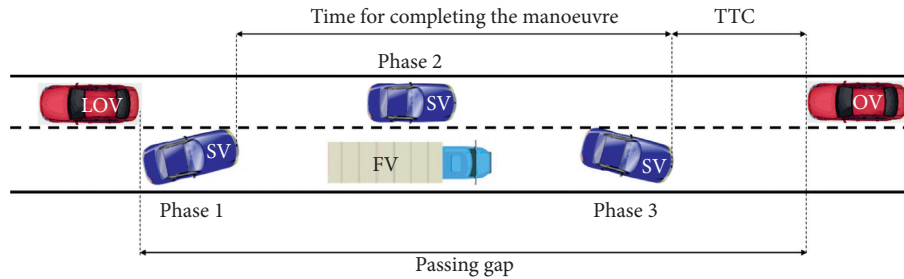


FIGURE 3: Passing manoeuvre phases (LOV = leading opposite vehicle; OV = opposite vehicle; SV = subject vehicle; FV = front vehicle).

A series of replicas were defined for each experiment to obtain a consistent data sample for subsequent analyses. Specifically, for each of the three experiments, the following replicas were carried out in order to obtain a comparable number of overtaking manoeuvres for the three different traffic conditions considered: (a) 12 replications for LOS A condition, (b) 36 replications for LOS B condition, and (c) 48 replications for LOS C condition. The different number of replicas for the different LOS conditions analysed is explained by the fact that it was necessary to generate a smaller number of vehicles in the lane where the stationary vehicle was in order not to create queuing phenomenon behind it.

4.3.2. Estimation of the Risk of Passing Manoeuvre. In order to assess the influence of different traffic-flow conditions on the risk of passing manoeuvre, the TTC was selected as a surrogate safety indicator. It is considered the most efficient and it is usually quantified using microscopic traffic simulations [55–57]. TTC is defined as the time remaining to the collision between two vehicles if they continue at their current speed and remain on their paths until the moment of the crash. Therefore, TTC is inversely related to accident risk: the smaller the value assumed by the TTC, the greater the probability that the conflict evolves into an accident (i.e., a null value of the TTC reflects a collision).

In this study, according to several similar types of research [8, 28, 33, 41, 58–60], the minimum TTC to the opposite vehicle at the end of the passing manoeuvre was used as a head-on collision proximity measure. Specifically, the minimum TTC was defined as the remaining gap (in seconds) between the passing vehicle and the opposite vehicle at the end of the overtaking process. Mathematically, the TTC was calculated by the division of the distance between the fronts of the subject vehicle and the opposite vehicle by the sum of their speeds. The minimum TTC was the TTC value at the end of a successful passing manoeuvre.

Several threshold values have been suggested for TTC in the literature. In the present study, according to the information provided by [52], passing with a final clearance time of less than 2 s was deemed risky.

The data sample recorded during the traffic microsimulations was analysed (as previously described) by dividing it into six subsets, according to the traffic condition (LOS A, LOS B, and LOS C) and the type of manoeuvre performed. Preliminarily, by analysing the driving

behaviour in the initial phase of the passing manoeuvres recorded during the traffic microsimulation (in particular by examining the speed), it was possible to distinguish them into two types: (a) flying passing manoeuvre (i.e., a pass in which the driver is not forced to slow down before making the pass, referred to as type “1” passing manoeuvre) and (b) passing manoeuvre after waiting for queues (i.e., when the user decides to stop behind the impeding front vehicle and wait for the first available gap to be able to pass it safely, referred to as type “2” passing manoeuvre).

Each subset was analysed in terms of both the gap accepted by the user to carry out the overtaking manoeuvre and TTC with respect to traffic coming in the opposite direction.

4.4. Comparative Analysis. To preliminarily evaluate the effectiveness of the proposed methodology in carrying out safety analysis, further microscopic traffic simulations were performed with only Aimsun default values. Specifically, the results, obtained from these latter microscopic traffic simulations, were processed and analysed in the same way adopted in the second step (Figure 1), in order to compare them with those obtained from the microsimulations, in which some driving behavioural parameters were adjusted to evaluate any statistically significant differences.

The most popular statistical approaches for group comparisons (such as parametric tests for unpaired samples: independent *t*-test and ANOVA test) are typically used to examine the level of confidence about the hypothesis that the data of two groups of different samples belong to the same population. Among them, in the comparative analysis of the two considered traffic microsimulation applications, bilateral independent-samples Student’s *t*-tests (*t*-test) were carried out to determine the statistical significance of the results achieved. Specifically, for both dependent variables (gap and TTC), six bilateral independent-samples *t*-tests were run: one for each LOS and type of manoeuvre considered (3 LOS x 2 types of manoeuvre). Preliminarily, it was verified that the data recorded can be analysed using this type of test, verifying the assumptions that must be considered (normality distribution and homogeneity of variances). In the null hypothesis (H_0), the indicators (gap and TTC values) in the two data sets were considered to belong to the same population. The threshold for statistical significance was set at 0.05.

5. Results and Discussion

5.1. Driving Simulator Results

5.1.1. General Statistics. The resulting data set included a total of 216 passing gap observations (54 participants * 4 configurations of passing gaps). In two cases, these passing manoeuvres ended in a collision; both crashes occurred in the “critical” configuration and at the end of the passing manoeuvre (during the reentry phase). The drivers collided with the stationary heavy vehicle to avoid a head-on collision with the oncoming vehicle in the opposite direction. These two observations were removed from the estimation data sets and, thus, 214 passing gap observations were examined. Of these passing gaps, 134 (62.6%) were accepted, while the rest were rejected.

Table 3 presents summary statistics of passing manoeuvres relating to the number of accepted and rejected gaps in the 4 different analysis configurations. The analysis of the type of behaviour approaching the heavy stopped vehicle (Table 3) understandably showed that, as the available gap increases, the number of gaps accepted by drivers also increases. Specifically, the results showed that, in the “critical” gap situation (8 s), most of the participants (52%) did not perform any manoeuvre and they preferred waiting behind the stationary vehicle. On the contrary, in presence of larger gaps, the percentage of the motorists who performed an overtaking manoeuvre increased considerably reaching 78% in the configuration “4” (available gap equal to 20 s).

The Chi-squared test results showed that there was a statistically significant association between configuration and the type of manoeuvre chosen by the driver (no passing/passing) ($\chi^2(3) = 11.928$ and $P = 0.008$). The association was moderately strong according to Cohen [50] (Cramer's $V = 0.235$). Therefore, the considered passing gaps significantly affected the driver's manoeuvre approaching the heavy stopped vehicle.

5.1.2. Driving Behaviour Parameters for Microscopic Simulation

(1) *PSVE.* To determine the PVSE parameter, the speed recorded at the end of the overtaking manoeuvre was extracted for each participant in each analysis configuration. The mean speed and the standard deviation of acquired data are summarized in Table 4.

The results revealed that the average value of all speeds recorded at the end of the overtaking manoeuvre (considering all configurations) was 71.58 km/h (DS = 12.55 km/h). Specifically, it was found that the speed at the end of the analysed manoeuvre increases as the gap available in the opposite traffic flow increases. The speed increase recorded is about 22 km/h (i.e., 38%) between configurations “1” and “4,” whose speed at the end of the manoeuvre reached a value close to the posted speed limit. This is probably due to the way the drivers are overtaken based on the available gaps. In fact, it was found that, in the smallest gap configurations (8 s and 12 s), after passing the stationary vehicle, drivers

were forced to turn sharply to reenter into their lane. This did not allow them to reaccelerate and to reach the desired speed. In the wider gap configurations (16 s and 20 s); on the contrary, drivers overtook less abruptly, using these spaces to accelerate again, regain the desired speed, and get back into their lane.

It should also be noted that, as the available gap increased, higher standard deviations were recorded, highlighting a reduction in the homogeneous behaviour of the driver where the gap available to overtake increased.

In order to understand if these differences were attributable to the analysed configuration and were not random, a one-way repeated measures ANOVA test was conducted. There were no outliers and the data were normally distributed, as assessed by Shapiro–Wilk's test ($P > 0.05$). The assumption of sphericity was violated, as assessed by Mauchly's test of sphericity ($\chi^2(5) = 15.683$, $P = 0.008$) and, therefore, a Greenhouse–Geisser correction was applied ($\epsilon = 0.720$). The findings of the statistical test revealed that the configuration (i.e., the gap available to perform the passing manoeuvre) made statistically significant speed changes recorded at the end of the passing manoeuvre ($F(2.159, 51.807) = 48.457$, $P < 0.001$, partial $\eta^2 = 0.669$). Post hoc analysis with a Bonferroni adjustment revealed that there are significant differences between all configurations ($P < 0.001$), except between the configuration “3” and the configuration “4” ($P = 0.065$).

Before determining the value of the PVSE parameter, the speed data observed at the end of the manoeuvre were organized into a histogram (Figure 4) and the Shapiro–Wilk's test was conducted to verify the goodness of fit of these data to the normal distribution. Specifically, it was assumed that the speed data are from a normally distributed population ($H_0 =$ null hypothesis) if the resulting P value was equal to or higher than 0.05. The results showed that the speed data can be considered as fitting a normal distribution ($P = 0.192$).

Subsequently, the speed value adopted by 5% of users (95th percentile-V95) was calculated and, consequently, the value of the PVSE factor, as the ratio between the obtained value of V95 and the posted speed limit. The two parameters were, respectively, 92.23 km/h (dashed red line in Figure 4) and 1.15.

The PVSE value obtained is higher than the Aimsun default value set at 1.10 determined based on the overtaking data recorded during the field observations [43], thus showing that the speed recorded in the virtual reality experimentation at the end of the manoeuvre analysed is greater than that observed in the field. This difference may be caused by some differences in the situation analysed, in terms of the type of passing manoeuvre faced by the driver and the type of vehicle to overtake. While in the field study [43] the overtaking manoeuvre of a moving vehicle was examined, in the present virtual reality experimentation, the overtaking manoeuvre of a stationary heavy vehicle was instead analysed. This can presumably lead you to believe that it has changed the user's behaviour. In fact, while the situation of overtaking a vehicle in motion is a situation frequently faced by the driver in the real world, the situation analysed in this study represents an unusual condition that occurs much less frequently on Italian

TABLE 3: Gaps accepted and rejected in the analysis configuration.

Configuration	Passing gap (s)	No. of gaps accepted	No. of gaps rejected
1	8	25 (48%)	27 (52%)
2	12	31 (57%)	23 (43%)
3	16	36 (67%)	18 (33%)
4	20	42 (78%)	12 (22%)

TABLE 4: Number of measurements, mean value, and standard deviation of speed in each analysis configuration.

Configuration	No. of measurements	Mean value (km/h)	St. deviation (km/h)
1 (gap: 8 s)	25	57.88	7.92
2 (gap: 12 s)	31	66.75	8.17
3 (gap: 16 s)	36	75.47	9.66
4 (gap: 20 s)	42	79.98	11.12
All configurations	134	71.58	12.55

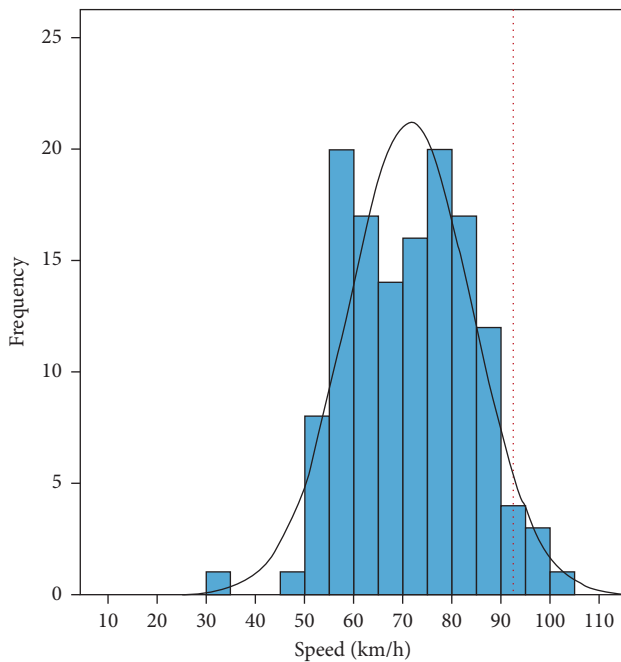


FIGURE 4: Histogram of speed data at the end of passing manoeuvre.

rural roads. Therefore, it is plausible that the driver, in this situation, has performed the manoeuvre in a less “quiet” and more sudden way due to the lack of habit in practising it. This hypothesis was confirmed by the results of the questionnaire filled out by the participants at the end of the virtual experiment; many of them declared that they had made a hasty decision on how to carry out the manoeuvre, as it was not clear to them whether the stopped vehicle was isolated or the last one in a queue.

Furthermore, since, in the experiment, the driver has to overtake a heavy vehicle (approximately twice the length of a light vehicle), he/she will presumably tend to assume a higher speed at the end of the manoeuvre, due to a longer acceleration phase held during the manoeuvre itself: the longer the vehicle to be overtaken, the greater the space in which the vehicle will have to accelerate.

(2) *Safetymargin*. As regards the evaluation of the “safetymargin” parameter, the value of TTC recorded for all the passing manoeuvres observed, for each analysis configuration, was determined. The descriptive statistics of observed data are summarized in Table 5.

The results highlighted a very different driver behaviour in the analysed configurations. A similar trend to that recorded for the speed values at the end of the passing manoeuvre can be observed. Specifically, it was found that the TTC value increases as the gap available in the opposite traffic flow increases. The maximum increase (corresponding to 2.47 seconds) was recorded between configurations “1” and “4.” It should also be noted that, as the available gap increased, higher standard deviations were recorded. It confirms the results described in the previous session, that is, a reduction of homogeneity in the driver behaviour where the gap available for overtaking has increased.

Only in low traffic conditions (configuration “4” characterized by the widest gap analysed), the driver turns back into the right lane with a mean value of TTC greater than 2 seconds, while in the other analysis situations the mean value of TTC is less than 2 seconds, resulting even below the second in the configurations characterized by the smallest available gaps (configurations “1” and “2”). Also, considering the four configurations, the average TTC at the end of the passing manoeuvre was less than 2 seconds (1.56 s). Furthermore, as can be seen from Table 5, approximately 69% of the observations (total observations 134) were less than 2 s. In particular, in all the analysis configurations except for configuration “4,” a TTC value less than 2 seconds was recorded for most of the observed manoeuvres, even reaching 100% in configuration “1.” Therefore, according to the AASHTO Manual [52] which recommends a minimum TTC value of 2 s, as well as other studies that have classified risky passing manoeuvres with clearance gaps of less than 2 s [61, 62], the manoeuvres recorded in all the analysis configurations (except in the “4” configuration) are, on average, to be considered risky.

A one-way repeated measures ANOVA was conducted to determine if the differences in recorded TTC values, between the configurations, were statistically significant.

TABLE 5: Number of measurements, mean value, and standard deviation of TTC in each analysis configuration.

Configuration	N	$N_{TTC < 2s}$	MV (s)	SD (s)	Min (s)	Max (s)
1 (gap = 8 s)	25	25 (100%)	0.39	0.20	0.02	0.78
2 (gap = 12 s)	31	29 (94%)	0.91	0.47	0.38	2.21
3 (gap = 16 s)	36	28 (78%)	1.43	0.60	0.40	2.75
4 (gap = 20 s)	42	11 (26%)	2.86	1.05	0.80	5.62
All configurations	134	93 (69%)	1.56	1.18	0.02	5.62

N = number of measurements; $N_{TTC < 2s}$ = number of measurements with TTC values less than 2 seconds; MV = mean value; SD = standard deviation.

There were no outliers and the data were normally distributed, as assessed by Shapiro–Wilk’s test ($P > 0.05$). The assumption of sphericity was violated, as assessed by Mauchly’s test of sphericity ($\chi^2(5) = 38.000$, $P < 0.001$) and, therefore, a Greenhouse–Geisser correction was applied ($\epsilon = 0.556$). The findings of the statistical test revealed that the configuration (i.e., the gap available to perform the passing manoeuvre) made statistically significant changes in TTC recorded ($F(1.669, 40.048) = 99.152$, $P < 0.001$, partial $\eta^2 = 0.805$), showing that drivers adopted very different behaviours in terms of risk at the end of the manoeuvre, according to the changes in the traffic configuration. Post hoc analysis with a Bonferroni adjustment revealed that there are significant differences between all configurations ($P < 0.001$).

Few driving simulation studies are available in the literature to compare the obtained TTC values. Specifically, the comparison with these studies shows a very similar value with the TTC mean value obtained by [28], in which a value equal to 1.30 s was recorded, as well as a fairly appreciable difference (approximately 1 second higher than the value recorded in this study) with the study by Farah et al. [41]. This difference is probably due to the different configurations of the driving simulators since Farah et al. [41] used a low-cost driving simulator (steering and pedals not installed on a real vehicle, only one screen in front of the driver with a usual field of view of only 60°). Therefore, bearing in mind differences in equipment and traffic conditions used in the different experiments, our results are consistent with those obtained in previous studies carried out using driving simulators.

Based on the data obtained from the driving simulations (Table 5), the safety margin parameter for passing manoeuvre, defined by its average, standard deviation, minimum, and maximum values, is characterized, respectively, by the following values (in seconds): 1.56, 1.18, 0.02, and 5.62. These values differ from the Aimsun default values, which instead assume the following values, respectively: 5, 5.8, 1, and 10. According to Llorca et al. [43], a minimum value of 1 s was chosen based on previous research [17, 61], while the maximum value was 10 s, as longer safety margins were not considered reasonable by them even with very conservative drivers. The mean and standard deviation values were selected (by adjusting simulated and observed critical gaps with a probability of acceptance equal to 0.5) to

be 5 s and 5.8 s, respectively. These differences are attributable (according to the results of the questionnaire filled out by the recruited subjects), to the differences in the situation analysed in terms of the overtaking type to be performed (vehicle stopped and not in motion) and of the type of vehicle to overcome (heavy vehicle, rather than a light vehicle).

(3) *Desired Speed.* The desired speeds adopted by the drivers while driving in a road section where they were able to adopt the desired driving style were calculated, in order to characterize the drivers’ behaviour while driving in “undisturbed” conditions.

Preliminary, the speed data observed were organized into a histogram (Figure 5).

The Shapiro–Wilk’s test was conducted to analyse the appropriateness of the normal distribution to the desired speed data. The test results showed that the null hypothesis (data are from the hypothesized normal distribution), cannot be rejected at the 95% confidence level ($P = 0.864$).

The means and standard deviation values of the free-flow speed are 92.70 km/h and 9.38 km/h, respectively. This result is consistent with the indications of the Highway Capacity Manual [6], which provides an approximate estimate of the speed desired by the driver corresponding to the posted speed limit plus 10 mph (approximately, 16 km/h) or corresponding to the design speed of the road. Due to the dependence of the desired speed to the posted speed limit equal to 100 km/h [42], the average desired speed value obtained in the virtual reality simulation (92.70 km/h with standard deviation equal to 9.38 km/h) and that defined by the Aimsun default values (equal to 110 km/h) is not comparable. However, regardless of the posted speed limit, the standard deviation obtained by driving simulator results is consistent with the Aimsun default values, equal to 10 km/h. Therefore, in this case, the findings show a similar distribution between the real behaviour and the lane-change model used in the Aimsun microsimulator [43].

5.2. Traffic Microscopic Simulation Results

5.2.1. *General Statistics.* The data set from the traffic microsimulations included a total of 1,114 passing gap observations. In 622 (56%) on these gaps, the passing manoeuvre type “1” was performed (i.e., the stationary vehicle was passed, without waiting behind it), while in the rest 492 cases (44%), a type “2” overtaking manoeuvre was observed. Table 6 shows summary statistics of observed passing manoeuvres based on the three LOS conditions considered. The results are consistent with those obtained from the experiments conducted in virtual reality. As traffic flow increases, the percentage of vehicles forced to queue behind the stopped vehicle and wait for the passing of the platoon coming in the opposite direction (before overtaking) increased; consequently, the percentage of flying pass manoeuvres observed decreased. Specifically, the results (Table 6) highlighted that, in LOS A traffic conditions, most of the vehicles (74.3%) performed the passing manoeuvre,

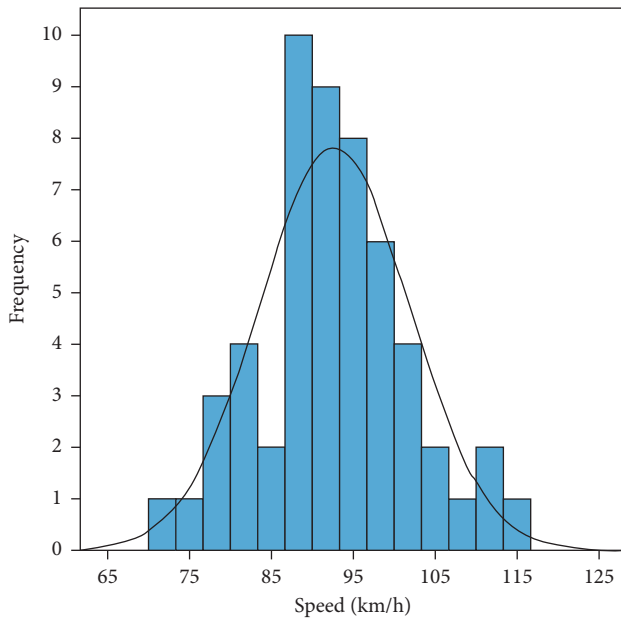


FIGURE 5: Histogram of free-flow speed data.

TABLE 6: Type of manoeuvres performed according to the different LOS analysed.

LOS	Type of passing manoeuvre				Total passing manoeuvre	
	1		2		N	%
	N	%	N	%		
A	373	74.3	129	25.7	502	100
B	159	46.4	184	53.6	343	100
C	90	33.2	181	66.8	271	100

1 = flying pass manoeuvre; 2 = overtaking manoeuvre, observed after waiting behind the stationary vehicle.

not performing any deceleration behaviour. This trend was completely reversed in the traffic condition represented by a LOS C (only 33.2% of the total passing manoeuvres observed were classified as flying pass manoeuvres), while an intermediate situation occurred in the LOS B traffic conditions. Although, in this situation, the percentage of overtaking carried out without stopping behind the stationary vehicle is still lower (46.4%) to the one in which the opposite behaviour was observed (53.6%).

The Chi-squared test results showed that there was a statistically significant association between traffic conditions and the type of passing manoeuvre performed (flying pass/pass after stopping behind the stopped vehicle) ($\chi^2(2) = 142.042$ and $P < 0.0001$). The association was quite strong, according to Cohen [50] (Cramer's $V = 0.355$). Therefore, the traffic-flow condition significantly affected the passing manoeuvre approaching the heavy stopped vehicle.

5.2.2. Risk Analysis of the Passing Manoeuvre. Data set recorded were preliminarily plotted into histograms in which the TTC frequency was correlated to the three different traffic-flow conditions, respectively, for the two types of passing manoeuvres analysed (Figure 6). It is possible to

note that, in both manoeuvres, as traffic increases (i.e., as LOS decreases) the frequency of lower TTC values increases. In particular, for the most intense traffic conditions (LOS C), no TTC values higher than 10 seconds for type "1" passing manoeuvre and exceeding 12 seconds for type "2" passing manoeuvre were recorded. This is because high time gaps do not occur as traffic increases, as shown by the histograms in Figure 7 which represent the accepted gap distributions in the three different traffic conditions, respectively, for the two manoeuvres analysed.

Figure 7 highlights how, as traffic increases, the width of the most accepted gap decreases. Specifically, for LOS A, there is a fairly uniform distribution of the gaps included in the interval (4 s–6 s) for the type A manoeuvre and in the widest interval (8 s–14 s) for the type "2" manoeuvre. For LOS B and LOS C, on the other hand, the histograms show peaks shifted to the left, in the interval (4 s–6 s) for the type "1" manoeuvre and in the interval (6 s–10 s) for the type "2."

Table 7 summarizes the gap and TTC values (mean and standard deviation), as well as the results relating to manoeuvres considered at risk, that is, those for which a risk threshold TTC value has been recorded (set equal to 2 s following the Highway Safety Manual [52]). The results showed that, as traffic increases, the number of manoeuvres considered at risk increases. In fact, as the traffic flow increases, there are fewer gaps of such width as to guarantee the possibility of carrying out the manoeuvre safely, and the users who have to overtake, after having waited for a certain time for the gap useful to carry out the manoeuvre, are willing to accept gaps of a smaller size than is deemed appropriate. As a result, the TTC values are significantly reduced and the percentage of manoeuvres considered at risk increases. Specifically, between the situation of LOS A and that of LOS B, there was an increase in manoeuvres considered at risk of around 10% for both types of passing manoeuvres. While between the situation of LOS B and LOS C, there was a greater increase for type "1" passing manoeuvre (8%) and a negligible increase in type "2" passing manoeuvre (2%).

It was also found that, for passing manoeuvre "1," greater manoeuvres at risk were recorded compared to those recorded for passing manoeuvre "2," in all traffic-flow conditions. This difference can be attributed to the different driver behaviour in the two different circumstances. In fact, in the first condition, the driver is now projected towards the manoeuvre and, therefore, accepts even smaller gaps. In the case of the second type of passing manoeuvre, however, the driver, stopping behind the heavy vehicle, must consider that the time necessary to carry out the manoeuvre corresponds to the sum of the latter and that necessary for its restart. Consequently, he/she is forced to carry out the manoeuvre only where there are larger gaps. In addition, for the first type of manoeuvre, it should be considered that being carried out entirely in the dynamic phase, the driver could also have greater difficulty in assessing the available gaps.

A two-way ANOVA was conducted to examine the effects of type of passing manoeuvre and LOS on the gap and TTC values. For the analysis of both dependent variables, outliers were assessed by inspection of a boxplot, normality

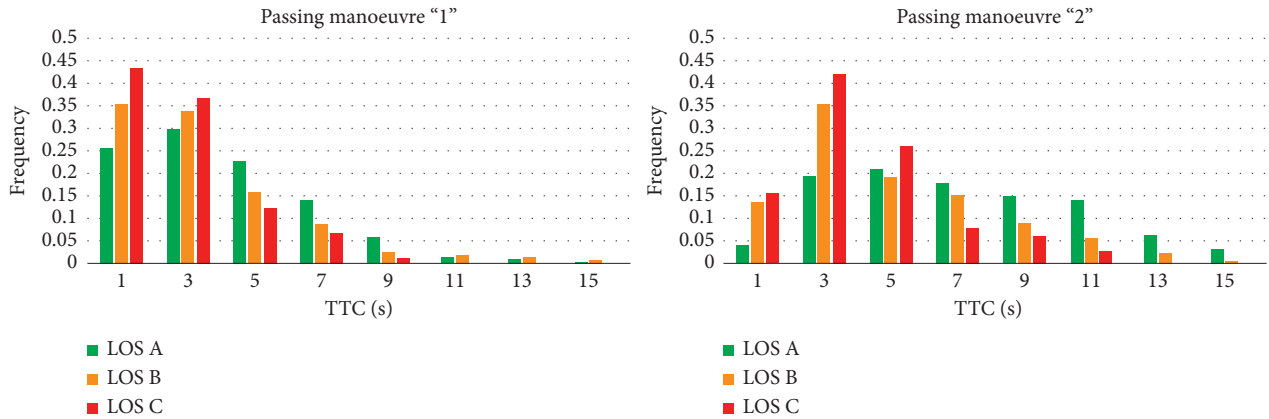


FIGURE 6: Histograms of TTC for recorded passing manoeuvre of types "1" and "2."

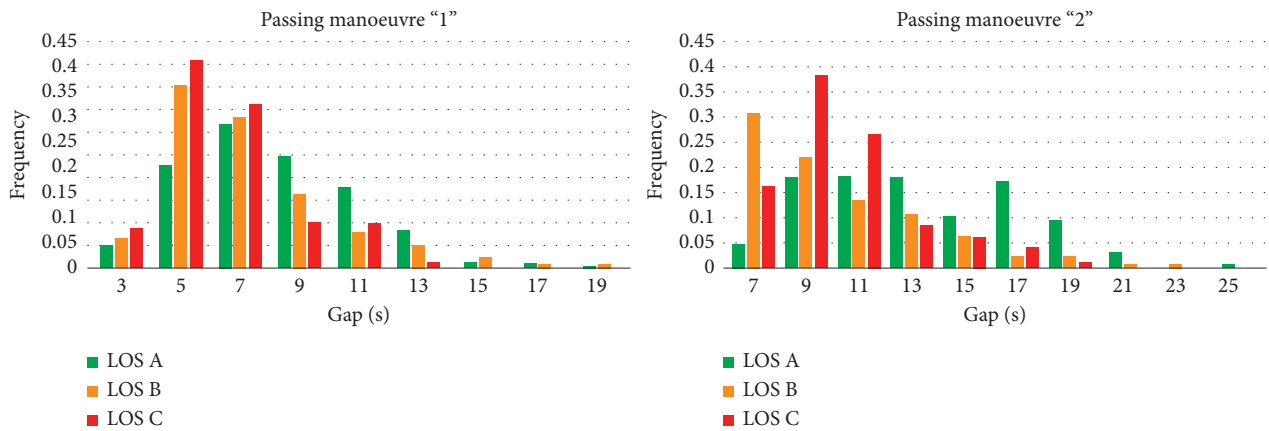


FIGURE 7: Histograms of gap distributions for recorded passing manoeuvre of types "1" and "2."

TABLE 7: Mean value and standard deviation of the gap, TTC, and risky manoeuvres.

Type of passing manoeuvre	LOS	Gap		TTC		TTC < 2 s		
		MV (s)	SD (s)	MV (s)	SD (s)	N (%)	MV (s)	SD (s)
1	A	8.12	2.79	4.08	2.68	95 (25.5)	1.10	0.58
	B	7.21	2.84	3.37	2.67	56 (35.2)	1.09	0.59
	C	6.47	2.02	2.64	1.92	39 (43.3)	1.07	0.53
2	A	13.63	3.98	6.98	3.47	5 (3.9)	1.56	0.25
	B	11.36	3.48	4.90	3.05	25 (13.6)	1.30	0.36
	C	10.42	2.65	4.02	2.34	28 (15.5)	1.19	0.50

1 = flying pass manoeuvre; 2 = overtaking manoeuvre, observed after queuing behind the stationary vehicle.

was assessed using Shapiro–Wilk’s normality test for each cell of the design, and homogeneity of variances was assessed by Levene’s test. There were no outliers, residuals were normally distributed ($P > 0.05$), and there was homogeneity of variances ($P > 0.05$). The findings of the statistical test revealed that the interaction effect between the type of passing manoeuvre and LOS on both the gap and TTC values was statistically significant, respectively ($F(2, 1120) = 6.787, P = 0.001$; partial $\eta^2 = 0.012$) and ($F(2, 1110) = 6.787, P \leq 0.001$; partial $\eta^2 = 0.014$). Therefore, an analysis of simple main effects for type of passing manoeuvre and LOS was performed. There was a statistical significance in mean “gap” values for both factors ($F(1, 1120) = 529.957, P < 0.0001$;

partial $\eta^2 = 0.321$) and ($F(2, 1120) = 53.631, P < 0.0001$; partial $\eta^2 = 0.087$) and there was a statistical significance in mean “TTC” values for both factor ($F(1, 1110) = 115.495, P < 0.0001$; partial $\eta^2 = 0.094$) and ($F(2, 1110) = 51.616, P < 0.0001$; partial $\eta^2 = 0.085$). For both dependent variables (gap and TTC) and factors, all pairwise comparisons were run, where the reported 95% confidence interval and P value are Bonferroni-adjusted. These analyses showed that, for the type of manoeuvre factor, a statistical difference was recorded for each LOS considered (Table 8).

Regarding the LOS factor, the results showed that there was a statistical difference within the type “2” manoeuvre between all LOS groups, while this was not recorded between

TABLE 8: Results of the pairwise comparison test (P value) for the type of passing manoeuvre factor.

LOS	Dependent variable		Gap		TTC	
	Type of passing manoeuvre	"1"	"2"	"1"	"2"	
LOS A	"1"	—	<0.0001	—	<0.0001	
	"2"	<0.0001	—	<0.0001	—	
LOS B	"1"	—	<0.0001	—	<0.0001	
	"2"	<0.0001	—	<0.0001	—	
LOS C	"1"	—	<0.0001	—	<0.0001	
	"2"	<0.0001	—	<0.0001	—	

Boldface indicates statistically significant values with a 5% level of significance.

LOS B and LOS C as regards the type "1" manoeuvre (Table 9). These results confirm that, on two-lane two-way rural roads, the passing manoeuvre is strongly affected by the gap between two successive vehicles on the opposing lane. Therefore, the probability of a safe manoeuvre, especially a flying pass manoeuvre, strongly depends on the LOS that the road infrastructure can offer.

5.2.3. Comparative Analysis. Before presenting the results of the comparative analysis, the main results, obtained using exclusively all the default values of the Aimsun, are reported below. The data set, from this traffic microsimulations, included a total of 831 passing gap observations. In 232 (28%) of these gaps, the passing manoeuvre type "1" was performed, while in the remaining 599 cases (72%), a type "2" overtaking manoeuvre was observed. In this case, a different trend was recorded from that observed in step 2, where some input values were adjusted with the data recorded during the experiments in virtual reality: the number of fly manoeuvres is lower than those carried out following a stop behind the stationary vehicle.

Table 10 shows summary statistics of passing manoeuvres observed on the basis of the three LOS considered. Overall, also, in this case, the results showed that, as traffic flow increases, the percentage of type "1" passing manoeuvres decreases. In this situation, however, it is observed that even in the presence of a free-flow traffic condition (LOS A), in which users are practically unaffected by the presence of other vehicles on the road section, the percentage of vehicles that performed a type "2" passing manoeuvre is higher than those that performed a type "1" passing manoeuvre.

The Chi-squared test results showed that there was a statistically significant association between traffic conditions and the type of passing manoeuvre performed (flying pass/pass after stopping behind the stopped vehicle) ($\chi^2(2) = 94.673$ and $P < 0.0001$), even when using only default software input data. The association was quite strong, according to Cohen [50] (Cramer's $V = 0.338$). Therefore, it can be said that the traffic-flow conditions significantly affect the passing manoeuvre approaching the heavy stopped vehicle.

Developing the same analysis performed in step 2, the results (in terms of gap and TTC values, as well as these relating to manoeuvres considered at risk) summarized in

Table 11 were obtained. In this case, also, it was found that, as traffic increases, the TTC values are considerably reduced, and the percentage of manoeuvres considered at risk increases. Moreover, as recorded during step 2 the results showed that, for passing manoeuvre "1," greater manoeuvres at risk were recorded compared to those recorded in passing manoeuvre "2," in all traffic-flow conditions.

Unlike what was obtained from the simulations carried out in step 2, a difference was recorded between the types "1" and "2" of manoeuvre in terms of manoeuvres considered at risk; for the first type, there is a greater increase in these manoeuvres from LOS A to LOS C compared to the second type of manoeuvre. Specifically, considering the type "1" manoeuvre, there was an increase of approximately 10% between the LOS A configuration and that of LOS B and between the LOS B configuration and LOS C of approximately 7%. While for the second type of manoeuvre, the increases recorded between the different LOS conditions considered are always negligible (about 2% between LOS A and LOS B and 1% between LOS B and LOS C). However, the value of the percentage of manoeuvres considered risky recorded using only the default data of the Aimsun was lower than that obtained using data adjusted according to what was recorded in the virtual reality experiments.

All this highlights that the results obtained with the software default input values differ, in a more precautionary way, compared to those recorded in which some input parameters were adjusted according to the driving behaviour recorded during experiments conducted with a driving simulator. Specifically, it appears that the use of the Aimsun software with its default input values produces a more precautionary situation in terms of safety (in this study quantified in terms of reducing the number of overtaking manoeuvres considered at risk), but more critical in terms of functionality, or the level of service offered (increase in type "2" overtaking and therefore increase in waiting times, queuing times, etc.). This could be a consequence of the fact that these tools are created primarily to simulate road traffic in detail (both in the city and on the motorway) to develop more efficient mobility management strategies, rather than to perform road safety analyses. Therefore, although they can potentially be very powerful tools for also performing road safety analyses, in these cases, it seems appropriate that since the variability of driving behaviour plays a determining role, some input parameters are set after their careful evaluation to provide reliable results.

TABLE 9: Results of the pairwise comparison test (P value) for the LOS factor.

Type of passing manoeuvre	Dependent variable			Gap			TTC	
	LOS	LOS A	LOS B	LOS C	LOS A	LOS B	LOS C	
"1"	LOS A	—	0.004	<0.0001	—	0.020	<0.0001	
	LOS B	0.004	—	0.190	0.020	—	0.132	
	LOS C	<0.0001	0.190	—	<0.0001	0.132	—	
"2"	LOS A	—	<0.0001	<0.0001	—	<0.0001	<0.0001	
	LOS B	<0.0001	—	0.009	<0.0001	—	0.007	
	LOS C	<0.0001	0.009	—	<0.0001	0.007	—	

Boldface indicates statistically significant values with a 5% level of significance.

TABLE 10: Type of manoeuvres performed according to the different LOS analysed.

LOS	Type of passing manoeuvre						Total passing manoeuvre	
	1		2					
	N	%	N	%	N	%	N	%
A	159	45.3	192	54.7	351	100		
B	51	18.5	225	81.5	276	100		
C	22	10.8	182	89.2	204	100		

1 = flying pass manoeuvre; 2 = overtaking manoeuvre, observed after waiting behind the stationary vehicle.

TABLE 11: Mean value and standard deviation of the gap, TTC, and risky manoeuvres.

Type of passing manoeuvre	LOS	Gap		TTC		TTC < 2 s		
		MV (s)	SD (s)	MV (s)	SD (s)	N (%)	MV (s)	SD (s)
1	A	10.16	2.52	5.89	2.50	9 (5.7)	1.44	0.34
	B	9.25	2.94	5.29	2.88	8 (15.7)	1.48	0.41
	C	7.72	2.65	4.03	2.59	5 (22.73)	1.68	0.24
2	A	14.54	3.15	8.99	2.64	0 (0.0)	—	—
	B	13.30	3.46	7.93	2.90	4 (1.8)	1.50	0.19
	C	12.76	3.32	7.42	2.79	5 (2.8)	1.25	0.39

1 = flying pass manoeuvre; 2 = overtaking manoeuvre, observed after waiting behind the stationary vehicle.

TABLE 12: Result of statistical test for the GAP and TTC values recorded in the two microscopic traffic simulations performed.

GAP	Passing manoeuvre type "1"			Passing manoeuvre type "2"		
	$ t $	P value	Result of test	$ t $	P value	Result of test
LOS A	7.975	<0.001	H0 reject	2.272	0.024	H0 reject
LOS B	4.429	<0.001	H0 reject	5.633	<0.001	H0 reject
LOS C	2.445	0.016	H0 reject	7.418	<0.001	H0 reject
TTC	Passing manoeuvre type "1"			Passing manoeuvre type "2"		
	$ t $	P value	Result of test	$ t $	P value	Result of test
LOS A	7.290	<0.001	H0 reject	5.887	<0.0001	H0 reject
LOS B	4.375	<0.001	H0 reject	10.251	<0.0001	H0 reject
LOS C	2.854	0.005	H0 reject	12.535	<0.001	H0 reject

The two data sets (the one related to all the default values and the other one obtained with some input values adjusted by driving simulation experiment) have been statistically analysed to determine if these differences were statistically significant. For both dependent variables (gap and TTC) 6 independent-samples t -test were run: one for each LOS and type of manoeuvre considered (3 LOS x 2 types of manoeuvre). There were no outliers in the data, as assessed by inspection of a boxplot. The gap and TTC values for each level of LOS and type of manoeuvre were normally distributed, as assessed by Shapiro–Wilk's test ($P > 0.05$), and

variances were homogeneous, as assessed by Levene's test for equality of variances ($P > 0.05$).

The results of statistical tests revealed that, at each level considered, the differences recorded in the two data sets (driving simulator input data and Aimsun default input data) were statistically significant (Table 12).

6. Conclusions

This study aimed to examine the influence of different traffic conditions on passing manoeuvres on rural two-lane two-

way rural roads, focusing on the end of the manoeuvre considered, using a combined simulation approach (driving simulator and traffic microsimulation).

The results showed that the passing manoeuvre is significantly conditioned on the gap between two successive vehicles on the opposing lane and, as presumably expected, the traffic condition significantly affects the type of manoeuvre performed. In fact, as traffic increases, the percentage of performed fly manoeuvres decreases (LOS A 74.3%, LOS B 46.4%, and LOS C 33.2%), a trend due to the occurrence of a smaller number of gaps of considerable width. This highlighted that a medium traffic-flow condition (LOS B) is sufficient to make a fly manoeuvre a less frequent event: compared to the condition of LOS A, a decrease of about 38% was recorded. The results obtained from traffic microsimulation confirm what had already emerged from the qualitative analysis of the data recorded through the driving simulator. It was found that over 50% of the participants in the experimentation in virtual reality did not take the risk of overtaking in the condition characterized by the minimum gap, which was strictly necessary to physically manoeuvre (corresponding to 8 s).

It was also found that at the end of the passing manoeuvre, the recorded behaviour is very different depending on the variations in the traffic conditions. Clearly, as vehicular flow increases, there are fewer gaps of sufficient width to ensure the possibility of performing the manoeuvre safely; therefore, it was recorded that after having waited for a certain time for the useful gap to carry out the manoeuvre, users are willing to accept gaps of a reduced width compared to that deemed appropriate. Consequently, the TTC values are significantly reduced and the percentage of manoeuvres considered at risk ($TTC < 2$ s) increases. From a traffic condition of LOS A to one of LOS B, there was an increase of about 10% for both types of manoeuvre, even if a higher percentage of risky overtaking was recorded, higher in the case when fly manoeuvre was carried out (about 25% compared to the other type): the user, already oriented to carry out the manoeuvre, tends to accept even smaller gaps. The results obtained confirmed the trend already observed in the data recorded in virtual reality, where even in that case, as the gap decreases, the overtaking considered at risky increased.

These results highlight that it would be advisable to reduce the interference caused by traffic to avoid unsafe behaviour during passing manoeuvres. Therefore, it might be appropriate to review some design requirements for the type of roads examined so that these also consider the performance of the road infrastructure under prevailing traffic conditions and these are not limited only to the use of design standards (such as passing sight distance) which are not correlated to the traffic condition. In this context, it could be useful to consider further design measures/solutions that meet the specific traffic demand of that specific road. For example, it would be appropriate to limit the longitudinal grade, add additional lanes for slow-moving vehicles, review the location on the road layout of emergency

lay-bays, especially where the amount of heavy vehicles is significant, and it might lead to not only a significant reduction in the level of service but also the probability that situations such as the one simulated in this study (stationary heavy vehicle obstructing the entire traffic lane) may arise.

Furthermore, the comparative analysis highlighted that there is a statistically significant difference between the results obtained from the traffic simulations, in which some input parameters of the microscopic passing manoeuvre model for two-lane rural roads were adjusted, with the data recorded in the virtual reality experiment and those that were instead collected from traffic microsimulations using all the software's default input data. Specifically, the results obtained from microsimulations (without adjustment) that have been adopted on the input data seem to differ from those, in which this was carried out more critically, in terms of the level of service offered by the road infrastructure (increase in waiting times, queuing times, etc.) and more precautionary in terms of road safety (in terms of reducing the number of overtaking manoeuvres considered at risk). This could be a consequence of the fact that these types of software were born and widely used and consequently validated to perform traffic management assessments, rather than road safety analyses. Therefore, since the variability of driving behaviour plays a decisive role, especially in complex driving environments such as rural roads, it seems appropriate that the input parameters that can be most influenced by the driver behaviour are set following a careful evaluation to the reality we want to represent.

Although the results obtained are promising and have allowed us to reach useful conclusions, this study presents some limitations that deserve further research in several directions and that it is worth mentioning.

The results obtained refer exclusively to the driving environments and situations considered: a road section in straight, flat, and excellent weather conditions. Therefore, further research efforts are necessary to generalize the results obtained by considering a wider range of driving environments and situations, including examining the impact of some geometric characteristics passing behaviour, such as vertical alignment, pavement quality, visual distances, and roadside characteristics.

The sample was one of convenience and representative only of the Tuscan driver population; as such, it may not be representative of the broader population of drivers. Therefore, further investigations will be performed to evaluate the impact of different driver groups (such as young and old drivers, drivers with different personality traits: anxious, aggressive, etc.) on the influence of traffic conditions on passing behaviour.

Finally, in order to develop predictive models which include traffic volumes, it may be appropriate to analyse other situations, such as overtaking of a moving vehicle.

Despite these limitations, the results obtained clearly show the effect of traffic on passing manoeuvre and promise to also guide the development of initiatives to improve the safety on two-lane two-way rural roads.

Data Availability

All data supporting the results are archived and kept by the Department of Civil and Environmental Engineering, Road Safety and Accident Reconstruct Laboratory (LaSIS).

Conflicts of Interest

The authors declare no conflicts of interest.

References

- [1] OECD, *Road Safety Annual Report 2019, IRTAD*, OECD/ITF, Paris, France, 2019.
- [2] National Center for Statistics and Analysis, *State Traffic Data: 2017 data, (Traffic Safety Facts. Report No. DOT HS 812 780)*, National Highway Traffic Safety Administration, Washington, DC, USA, 2019.
- [3] Bureau of Infrastructure Transport and Regional Economics (BITRE), *Road Trauma Australia 2015 Statistical Summary*, Commonwealth of Australia, Canberra, Australia, 2016.
- [4] European Commission, *Annual Accident Report 2018*, European Commission, Brussels, Belgium, 2018, https://ec.europa.eu/transport/road_safety/sites/roadsafety/files/pdf/statistics/dacota/asr2018.pdf.
- [5] ACI-ISTAT, *Incidenti Stradali in Italia-Anno 2019*, ACI-ISTAT, Rome, Italy, in Italian Language, 2019.
- [6] Highway Capacity Manual (HCM), *TRB*, National Research Council, Washington, DC, USA, 2010.
- [7] R. Gray and D. M. Regan, "Perceptual processes used by drivers during overtaking in a driving simulator," *Human Factors: The Journal of the Human Factors and Ergonomics Society*, vol. 47, no. 2, pp. 394–417, 2005.
- [8] G. Hegeman, A. Tapani, and S. Hoogendoorn, "Overtaking assistant assessment using traffic simulation," *Transportation Research Part C: Emerging Technologies*, vol. 17, no. 6, pp. 617–630, 2009.
- [9] S. Jamson, K. Chorlton, and O. Carsten, "Could intelligent speed adaptation make overtaking unsafe?" *Accident Analysis & Prevention*, vol. 48, pp. 29–36, 2012.
- [10] T. Richter, S. Ruhl, J. Ortlepp, and E. Bakaba, "Causes, consequences and countermeasures of overtaking accidents on two-lane rural roads," *Transportation research Procedia*, vol. 25, pp. 1989–2001, 2017.
- [11] H. Bar-Gera and D. Shinar, "The tendency of drivers to pass other vehicles," *Transportation Research Part F: Traffic Psychology and Behaviour*, vol. 8, no. 6, pp. 429–439, 2005.
- [12] M. M. Z. Á. Török, "Improving traffic flow characteristics by suppressing shared taxis maneuvers," *Periodica Polytechnica Transportation Engineering*, vol. 44, pp. 69–74, 2016.
- [13] A. T. Kashani, E. Ayaziand, and M. S. Ravasani, "Identifying significant variables influencing overtaking maneuvers on two-lane, two-way rural roads in Iran," *Periodica Polytechnica Transportation Engineering*, vol. 44, no. 3, pp. 155–163, 2016.
- [14] A. Polus and A. B. Tomecki, "Passing experiment on two-lane rural highways," *Transportation Research Record: Journal of the Transportation Research Board*, vol. 1112, pp. 115–123, 1987.
- [15] G. Asaithambi and G. Shrivani, "Overtaking behaviour of vehicles on undivided roads in non-lane based mixed traffic conditions," *Journal of Traffic and Transportation Engineering (English Edition)*, vol. 4, no. 3, pp. 252–261, 2017.
- [16] A. Polus, M. Livneh, and B. Frischer, "Evaluation of the passing process on two-lane rural highways," *Transportation Research Record: Journal of the Transportation Research Board*, vol. 1701, no. 1, pp. 53–60, 2000.
- [17] D. W. Harwood and D. K. G. K. R. Richard, "Criteria for passing sight distance for roadway design and marking," *Transportation Research Record: Journal of the Transportation Research Board*, vol. 2195, pp. 36–46, 2010.
- [18] C. Llorca and A. García, "Evaluation of passing process on two-lane rural highways in Spain with new methodology based on video data," *Transportation Research Record: Journal of the Transportation Research Board*, vol. 2262, no. 1, pp. 42–51, 2011.
- [19] A. Shariat-Mohaymany, A. T. Kashani, H. Nosrati, and S. Kazemzadehazad, "Development of head-on conflict model for overtaking maneuvers on two-lane rural roads using inductive loop detectors," *Journal of Transportation Safety & Security*, vol. 5, no. 4, pp. 273–284, 2013.
- [20] G. Hegeman, S. Hoogendoornand, and K. A. Brookhuis, "Observations overtaking manoeuvres on bi-directional roads," in *Advanced OR and AI Methods in Transportation*, A. Jaszkievicz, M. Kaczmarek, J. Zak et al., Eds., pp. 505–510, Publishing House of Poznan University of Technology, Poznan, Poland, 2005.
- [21] V. Papakostopoulos, D. Nathanael, E. Portouli, and N. Marmaras, "The effects of changes in the traffic scene during overtaking," *Accident Analysis & Prevention*, vol. 79, pp. 126–132, 2015.
- [22] V. Branzi, L. Domenichini, and F. La Torre, "Drivers' speed behaviour in real and simulated urban roads-a validation study," *Transportation Research Part F: Traffic Psychology and Behaviour*, vol. 49, pp. 1–17, 2017.
- [23] L. Domenichini, F. La Torre, V. Branzi, and A. Nocentini, "Speed behaviour in work zone crossovers. A driving simulator study," *Accident Analysis & Prevention*, vol. 98, pp. 10–24, 2017.
- [24] M. Klüver, C. Herrigel, C. Heinrich, H.-P. Schöner, and H. Hecht, "The behavioral validity of dual-task driving performance in fixed and moving base driving simulators," *Transportation Research Part F: Traffic Psychology and Behaviour*, vol. 37, pp. 78–96, 2016.
- [25] A. Knapper, M. Christoph, M. Hagenzieker, and K. Brookhuis, "Comparing a driving simulator to the real road regarding distracted driving speed," *European Journal of Transport and Infrastructure Research*, vol. 15, no. 2, pp. 205–225, 2015.
- [26] G. H. Bham, M. C. Leu, M. Vallati, and D. R. Mathur, "Driving simulator validation of driver behavior with limited safe vantage points for data collection in work zones," *Journal of Safety Research*, vol. 49, no. 6, pp. 53–60, 2014.
- [27] F. Bella, "Driving simulator for speed research on two-lane rural roads," *Accident Analysis & Prevention*, vol. 40, no. 3, pp. 1078–1087, 2008.
- [28] F. Bella, "How traffic conditions affect driver behavior in passing maneuver," *Advances in Transportation Studies*, pp. 113–126, 2011.
- [29] H. Farah, E. Yechiam, S. Bekhor, T. Toledo, and A. Polus, "Association of risk proneness in overtaking maneuvers with impaired decision making," *Transportation Research Part F: Traffic Psychology and Behaviour*, vol. 11, no. 5, pp. 313–323, 2008.
- [30] S. El-Bassiouniand and T. Sayed, "Design requirements for passing sight distance: a risk based approach," in *Proceedings of the 89th Annual Meeting Transportation Research Record*, Washington, DC, USA, 2010.

- [31] H. Farah and T. Toledo, "Passing behavior on two-lane highways," *Transportation Research Part F: Traffic Psychology and Behaviour*, vol. 13, no. 6, pp. 355–364, 2010.
- [32] H. Farah, "Modeling drivers' passing duration and distance in a virtual environment," *IATSS Research*, vol. 37, no. 1, pp. 61–67, 2013.
- [33] H. Farah and C. L. Azevedo, "Safety analysis of passing maneuvers using extreme value theory," *IATSS Research*, vol. 41, no. 1, pp. 12–21, 2016.
- [34] S. M. S. Mahmud, L. Ferreira, M. S. Hoque, A. Tavassoli, and A. Tavassoli, "Micro-simulation modelling for traffic safety: a review and potential application to heterogeneous traffic environment," *IATSS Research*, vol. 43, no. 1, pp. 27–36, 2019.
- [35] J. Archer, *Indicators for Traffic Safety Assessment and Prediction and Their Application in Micro-simulation Modelling: A Study of Urban and Suburban Intersections*, Royal Institute of Technology, Stockholm, Sweden, 2005.
- [36] FHWA, *Surrogate Measures of Safety from Traffic Simulation Models*, Federal Highway Administration, Washington, DC, USA, 2003.
- [37] D. Gettman, L. Pu, T. Sayed, and S. G. Shelby, "Surrogate safety assessment model and validation: final report," Turner-Fairbank Highway Research Center, McLean, VA, USA, FHWA-HRT-08-051, 2008.
- [38] J. J. L. Rilett, "Application of distributed traffic simulation for passing behavior study," *Transportation Research Record: Journal of the Transportation Research Board*, vol. 1899, pp. 11–18, 2005.
- [39] W. Young, A. Sobhani, M. G. Lenné, and M. Sarvi, "Simulation of safety: a review of the state of the art in road safety simulation modelling," *Accident Analysis & Prevention*, vol. 66, pp. 89–103, 2014.
- [40] H. M. Al-Ahmadi, A. Jamal, I. Reza, K. Assi, and S. A. Ahmed, "Using microscopic simulation-based analysis to model driving behavior: a case study of Khobar-Dammam in Saudi Arabia," *Sustainability*, vol. 11, no. 3018, 2019.
- [41] H. Farah, S. Bekhor, and A. Polus, "Risk evaluation by modeling of passing behaviour on two-lane rural highways," *Accident Analysis and Prevention*, vol. 41, no. 4, pp. 87–89, 2009.
- [42] TSS, *Aimsun Version 8.0.2 User Manual*, Transport Simulation Systems, Barcelona, Spain, 2013.
- [43] C. Llorca, A. T. Moreno, A. Lenorzer, J. Casas, and A. García, "Development of a new microscopic passing maneuver model for two-lane rural roads," *Transportation Research Part C: Emerging Technologies*, vol. 52, pp. 157–172, 2015.
- [44] L. Domenichini, F. La Torre, D. Vangi, A. Virga, and V. Branzi, "Influence of the lighting system on the driver's behavior in road tunnels. A driving simulator study," *Journal of Transportation Safety and Security*, vol. 9, no. 2, pp. 16–23, 2017.
- [45] L. Domenichini, V. Branzi, and M. Meocci, "Virtual testing of speed reduction schemes on urban collector roads," *Accident Analysis & Prevention*, vol. 110, pp. 38–51, 2018.
- [46] L. Domenichini, V. Branzi, and M. Smorti, "Influence of drivers' psychological risk profiles on the effectiveness of traffic calming measures," *Accident Analysis & Prevention*, vol. 123, pp. 243–255, 2019.
- [47] Ministry of Infrastructures and Transports, "Nuovo Codice Della Strada," D.L. 30 Aprile 1992 n.285 e Successive Modificazioni. Gazzetta Ufficiale della Repubblica Italiana, n. 114. MIT, Via G. Caraci 36, Roma, 1992, in Italian Language.
- [48] Ministry of Infrastructures and Transports, "Norme Funzionali e Geometriche Per La Costruzione Delle Strade," Decreto Ministeriale n.6792 del 05/11/2001. MIT, Via G. Caraci 36, Roma, 2001, in Italian Language.
- [49] D. Vangi, *Ricostruzione Della Dinamica Degli Incidenti Stradali-Principi e Applicazioni*, Firenze University Press, Nelson Mandela Bay, South Africa, 2008.
- [50] J. Cohen, *Statistical Power Analysis for the Behavioural Sciences*, Psychology Press, New York, NY, USA, 2nd edition, 1988.
- [51] M. Losa, F. Frenzo, A. Cofrancesco, and R. Bartolozzi, "Procedure for validating fixed base driving simulators," *Transport*, vol. 28, no. 2, pp. 420–430, 2013.
- [52] AASHTO, *Highway Safety Manual*, American Association of State and Highway Transportation Officials, Washington, DC, USA, 1st edition, 2010.
- [53] K. Basak, S. N. Hetu, Z. Li et al., "Modeling reaction time within a traffic simulation model," in *Proceedings of the 16th International IEEE Conference on Intelligent Transportation Systems (ITSC 2013)*, pp. 302–309, Hague, Netherlands, 2013.
- [54] P. S. Bokare and A. K. Murya, "Acceleration-deceleration behaviour of various vehicle types," *Transportation Research Procedia*, vol. 25, pp. 4733–4749, 2017.
- [55] Å. Svensson, *A Method for Analysing the Traffic Process in a Safety Perspective*, Lund University, Lund, Sweden, 1998.
- [56] Å. Svensson and C. Hydén, "Estimating the severity of safety related behaviour," *Accident Analysis & Prevention*, vol. 38, no. 2, pp. 379–385, 2006.
- [57] A. Dijkstra and J. Drolenga, "Safety effects of route choice in a road network: simulation of changing route choice," *Research in the Framework of the European Research Programme In-Safety*, SWOV Institute for Road Safety Research, Hague, The Netherlands, 2008.
- [58] R. J. Kiefer, C. A. Flannagan, C. Jerome, and C. J. Jerome, "Time-to-collision judgments under realistic driving conditions," *Human Factors: The Journal of the Human Factors and Ergonomics Society*, vol. 48, no. 2, pp. 334–345, 2006.
- [59] A. Shariat-Mohaymany, A. Tavakoli-Kashani, H. Nosrati, and A. Ranjbari, "Identifying significant predictors of head-on conflicts on two-lane rural roads using inductive loop detectors data," *Traffic Injury Prevention*, vol. 12, no. 6, pp. 636–641, 2011.
- [60] G. Hegeman, *Assisted Overtaking: An Assessment of Overtaking on Two-Lane Rural Roads*, Netherlands Research School for Transport, Delft, The Netherlands, 2008.
- [61] Y. Hassan, S. M. Easa, A. O. Abd El Halim, and A. O. A. El Halim, "Passing sight distance on two-lane highways: review and revision," *Transportation Research Part A: Policy and Practice*, vol. 30, no. 6, pp. 453–467, 1996.
- [62] J. Glennon, "New and improved model of passing sight distance," *Transportation Research Record: Journal of the Transportation Research Board*, vol. 1195, pp. 55–69, 1988.

Research Article

Exploring Driver Injury Severity in Single-Vehicle Crashes under Foggy Weather and Clear Weather

Fulu Wei,^{1,2} Zhenggan Cai,¹ Pan Liu,² Yongqing Guo ,¹ Xin Li,¹ and Qingyin Li¹

¹Department of Transportation Engineering, Shandong University of Technology, Zibo 255000, China

²Department of Transportation Planning and Management, Southeast University, Nanjing 210096, China

Correspondence should be addressed to Yongqing Guo; yongqing.guo@sdut.edu.cn

Received 11 March 2021; Accepted 19 July 2021; Published 11 August 2021

Academic Editor: Jinjun Tang

Copyright © 2021 Fulu Wei et al. This is an open access article distributed under the Creative Commons Attribution License, which permits unrestricted use, distribution, and reproduction in any medium, provided the original work is properly cited.

The purpose of this study is to investigate and compare the significant influencing factors of driver injury severity in single-vehicle (SV) crashes under foggy and clear weather conditions. Based on data for SV crashes in Shandong Province, China, the mixed logit model (MLM) was employed to interpret driver injury severity for SV crashes in clear and foggy weather. The results showed that there are significant differences in the influencing factors of the severity of SV crashes in foggy and clear weather. Specifically, 15 factors are significantly associated with the severity of SV crashes in clear weather, and 18 factors are significantly associated with the severity of SV crashes in foggy weather. In addition, young drivers (age < 30), non-dry road surfaces, and signal control significantly influence the severity of foggy weather crashes but not clear weather crashes. Self-employment and weekends have significant effects on the severity of crashes only in clear weather. Interestingly, drivers whose occupation is farming showed opposite trends in the effect of crash severity in foggy and clear weather. Based on the findings of this research, some potential countermeasures can be adopted to reduce crash severity in foggy and clear weather.

1. Introduction

The investigation of single-vehicle (SV) crash severity is of great interest to numerous transportation experts due to its high fatality rate. According to statistics from the National Highway Traffic Safety Administration (NHTSA) in 2017, SV crashes and fatal SV crashes accounted for 30% and 54% of total collisions and fatalities, respectively [1], and the fatality rate of drivers was higher than for other types of traffic collisions [2]. In Singapore, for example, the risk of fatality for drivers in SV crashes is 1.7 times compared to two-vehicle crashes [3]. Such information shows that extremely adverse effects are initiated by SV crashes; to better understand the impact of contributing factors on the severity of SV crashes, in-depth research is urgently needed.

Some differences in SV crashes between foggy and clear weather may exist [4, 5]. The low visibility caused by fog affects driver behavior and the driving environment, which can lead to contributing effects on traffic collisions that are different from those in clear weather. Foggy weather and

clear weather effects in terms of both crash risk and severity are developed [6]. To clarify the influencing factors of crash risk, Wu et al. [7] compared the variability of traffic patterns and crash risk between clear and foggy weather. The research showed that traffic volume and vehicle speed on foggy days tend to decrease compared to sunny days. In addition, the risk of crashes on foggy days is significantly increased near ramps or with large traffic flow. However, to date, the difference in contributing factors influencing the severity of SV crashes between foggy and clear days has not been studied. Li et al. [8] discussed the contributing factors of low visibility-related SV crash severity, but the exploration did not include the variability of influencing factors in foggy and clear weather. Considering the different characteristics of traffic flow in different regions, the research conclusion according to US collision data cannot be directly transferred to other countries. For example, Feng et al. [9] uses the crash data of Shanghai, China, and Florida, USA, to establish safety performance functions (SPFs), respectively, and investigate the transferability between the two SPFs. It was found that

the transferability of SPFs between Florida and the Chinese cities turned out to be unsatisfactory and this phenomenon was contributed by the difference in traffic flow.

Based on an in-depth literature review of the potential correlation between different collision models, the existing literature on weather-related crashes can provide reference for modeling clear and fog-related SV crashes. In the existing literature, foggy and clear weather are usually analyzed and modeled as categorical variables of weather factors. For example, Wen and Xue [10] classified weather factors into four variables—sunny, rainfall, snowfall, and foggy. The study found that compared with sunny weather, the probability of fatal accidents increased by 3.4%, 3.3%, and 15.7%, respectively, for rainfall, snowfall, and fog. Research on the influence of severe weather on SV crashes mainly focuses on rainfall or snowfall weather. For example, Li et al. [11] developed a mixed logit model (MLM) for SV crashes in rainy weather to identify the influence of different factors on crash severity. Yu et al. [12] studied SV crashes in snowy weather and found that male drivers had individual heterogeneity on the impact of crash severity. In research on fog-related collisions, Moore and Cooper [13] conducted a study of traffic collisions in foggy weather and found that fog increases the probability of traffic collisions by 16%, noting that fog is one of the most feared weather hazards for drivers. Abdel-Aty et al. [14] developed a multilevel ordered logit model using collision data from Florida to study fog-related crashes. Early winter mornings and nights without streetlights were found to be the highest crash periods. It was considered that fog would dilute color depth and further aggravate the severity of traffic collisions. Later, based on the fact that fog can affect a driver's correct judgment of driving distance, Tarel et al. [15] proposed an algorithm to improve the visibility of road images, which was used to improve existing advanced driver assistance systems (ADAS) and improve traffic safety in foggy weather.

Modeling approaches are recognized as an important part of traffic safety research, and many discrete choice models have been established to analyze SV crashes [16]. Among them, the multinomial logit model (MNL) has been widely used. However, MNL involves two limitations: (1) it is based on the assumption of independence of irrelevant alternatives (IIA); this hypothesis is not always accepted as the model can be influenced by unobserved factors [17]; and, (2) the parameter is treated as a fixed value, which cannot reflect the individual heterogeneity across observations; this may lead to bias in parameter estimation. (a comprehensive analysis of the heterogeneous effects of independent variables was conducted by Mannering et al. [18]).

To overcome the limitation of traditional econometric models, the method of using an MLM to analyze the severity of SV crashes was proposed. MLM allows parameters to vary randomly across observations, which obviates the limitations of MNL. The diversity of random distribution forms makes MLM highly flexible and adaptable. Ideally, MLM can fit all data samples with random effects. Currently, most studies have concluded that the fit performance of MLM for crash data is significantly better than that of traditional discrete choice models. For instance, Ye and Lord [19]

verified that the fit performance of MLM outperforms conventional models that do not account for heterogeneity by allowing the model parameters to vary across the observations according to a predefined distribution. Therefore, the MLM was established to identify the influence of contributing factors on SV crash severity in foggy and clear weather. The marginal effects of significant independent variables in MLM were calculated to further quantify the effect of each contributing factor on crash severity.

In addition, considering that traffic crashes may lead to multiple casualties, three methods are generally used to classify the severity of crashes: (1) based on the severity of the driver's injury; (2) based on the most seriously injured passengers; and, (3) based on the most serious injury in the crash [20–22]. It has been widely recognized that there are differences existing in safety precautions among passengers as well as between drivers and passengers. The probability of injury is often different. To reduce the influence of potential factors on crash severity, driver injury severity is used as the index to measure crash severity.

The main objective of this research was to investigate the contributing factors of SV crash severity in foggy and clear weather. More specifically, this study focused on answering the following two questions: (1) is the prediction effect of MLM on the severity of SV crashes in foggy weather and clear weather satisfactory? (2) What are the different effects of different factors on the severity of SV crashes in foggy and clear weather?

2. Data Collection

With support of the Shandong Department of Transportation (SDOT), data on SV crashes over the five-year period of 2015–2019 that occurred on the national highway in winter were collected as the sample database. Considering that weather and visibility information were by observation, data were estimated by traffic police at the scenes of accident, and some errors may exist. According to the time of crashes, these data were obtained from the Shandong Climatic Data Center (SCDC).

National highways in China are indispensable and carry most intercity traffic volumes. The grade of the national highway is very high, and the average speed is fast. As a result, vehicles operating on national highways are more prone to serious crashes. Furthermore, in Shandong, the alternate occurrence of foggy and clear days often occurs in winter; thus, it is more suitable to use winter for studying the difference of crashes between foggy and clear weather.

In this study, visibility below 200 m was treated as foggy weather. Therefore, fog-related SV crashes were extracted when the visibility was less than 200 m. Visibility above 200 m was considered as clear weather. It is noted that rainfall and snowfall may also lead to low visibility; therefore, this part of the data was eliminated.

Based on the above selection rules, raw data for 11,126 SV crashes were obtained by data extraction. Of these, out-of-control crashes and rollover crashes were excluded due to them accounting for less than 1%. An additional 407 (3.9%) crash records were excluded due to missing vital

information. Ultimately, a total of 10,137 crashes were employed for subsequent analysis, including 5,138 SV crashes in foggy weather (SVCF) and 4,999 SV crashes in clear weather (SVCC). Crash severity was based on the severity of driver injuries and was classified as no injury, slight injury, and serious or fatality injury (a driver passing away within seven days was regarded as a fatal event). In the dataset, there were 6,854 (67.6%) no-injury crashes, 2,051 (20.2%) slight-injury crashes, and 1,232 (12.2%) serious or fatality injury (SFI) crashes. Annual distribution statistics of crashes with different severities are shown in Figure 1. As shown, the number of crashes decreased with the increase of injury severity, which is in line with reality.

Fifteen factors were chosen as independent variables from driver characteristics, vehicle type, road characteristics, and other characteristics. All independent variables have been discredited for modeling. More specifically, snowy pavement and wet pavement were combined as the non-dry road surface; therefore, dry and non-dry road surfaces were contained in road condition. In addition, more than 20 crash types were contained in the original records, which were combined into four categories: collision with non-fixed object, collision with fixed object, collision with pedestrian, and other crashes. There were nearly 80 types of motor vehicles. In the preprocessing process, less than 1% of vehicle types (e.g., farm machinery and large buses) were classified into other vehicle types. Ultimately, vehicle types were categorized into five types: passenger car, motorcycle, pickup, truck, and other vehicle types. The specific variable classification and description are shown in Table 1. Considering that the actual distribution of factors in the sample was masked by the discrete variables, the number changes of the two archetypal continuously distributed variables, driver age, and time of crashes are shown in Figures 2 and 3.

From Table 1, we can see that the percentage of SVCF resulting in slight injuries and SFI are 22.0% and 14.7%, respectively, which are higher than the percentage of SVCC (18.3% and 9.7%). This indicates a significant difference in the driver injury severity between fog-related SV crashes and clear-related SV crashes. For different age groups, the number of crashes is roughly the same in both foggy weather and clear weather. Figure 2 shows the trend more clearly; the highest percentage is between ages 38 and 47 in both weather conditions. In addition, it can be seen from Figure 3 that a significant differences' trend is shown about time characteristics during clear and foggy weather. The number of crashes in clear weather shows a slow upward trend from 06:00 am–18:00 pm, and the peak value is at 1500 pm–1800 pm. The number of crashes in foggy weather shows an upward trend from 15:00 pm–21:00 pm, and the peak value is at 18:00 pm–21:00 pm. The peak value of crashes in foggy weather is significantly higher than that in clear weather. These data further exemplify the differences in traffic operating characteristics between foggy and clear conditions. It is necessary to study the differences between SVCC and SVCF.

3. Methodology

3.1. Mixed Logit Model. The mixed logit probability can be derived from utility-maximizing behavior. Assume that driver injury severities are divided into J categories (in this

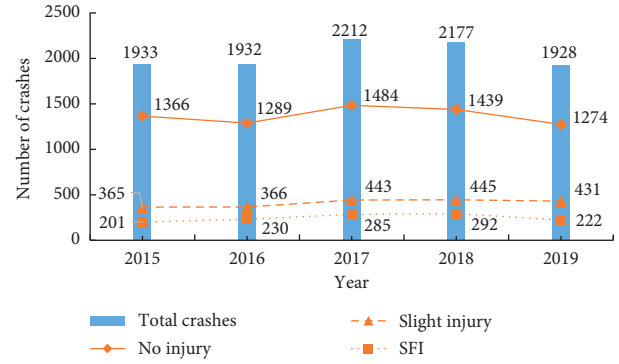


FIGURE 1: Annual distribution of number of crashes with different severities.

research, $J=3$). The utility function of the i th crash with the injury severity j can be specified as the following equation:

$$U_{ij} = x'_{ij}\beta_j + \varepsilon_{ij}, \quad (i = 1, \dots, n; j = 1, \dots, J), \quad (1)$$

where U_{ij} is the utility when the severity of the i th crash is j , x'_{ij} represents the independent variables, ε_{ij} is the observed disturbance term, β_j is the coefficient of the independent variable, and n indicates sample size.

When the injury severity of the i th crash is j , the utility is higher than that of other severe categories. Assuming that ε_{ij} obeys the generalized extreme value distribution, the probability of injury severity j for the i th crash can be expressed as equation (2), and it is also known as the MNL model:

$$P(y_i = j | x_{ij}) = P(U_{ij} \geq U_{ik}, \forall k \neq j) = \frac{\exp(x'_{ij}\beta_j)}{\sum_{j=1}^J \exp(x'_{ij}\beta_j)}. \quad (2)$$

Considering the random distribution of parameter across observations, the MLM can be expressed as the following equation:

$$P(y_i = j | \varphi) = \int \frac{\exp(x'_{ij}\beta_j)}{\sum_{j=1}^J \exp(x'_{ij}\beta_j)} f(\beta_j | \varphi) d\beta_j, \quad (3)$$

where $f(\beta_j | \varphi)$ represents the probability density function of parameter β_j , φ represents an unknown characteristic parameter of the probability density function, such as the mean value μ and the variance σ of normal distribution, which can be expressed as $\varphi = \{\mu, \sigma\}$, and parameter β_j varies across observations which may be random or fixed. MLM will degrade to MNL when all parameters in the model are fixed.

3.2. Marginal Effects. Given that the coefficient in MLM cannot measure the quantitative relationship between the independent variable and the dependent variable, the marginal effects of significant independent variables in the model were calculated. The mathematical meaning of the marginal effect refers to the probability change of a certain crash severity when a variable changes by one unit, while the

TABLE 1: Classification statistics of variables.

Variables	SVCF		SVCC		Total	
	Number	Rate (%)	Number	Rate (%)	Number	Rate (%)
Number of crashes	5138	50.7	4999	49.3	10137	100
Severity						
No injury*	3253	63.3	3601	72.0	6854	67.6
Slight injury	1135	22.0	916	18.3	2051	20.2
SFI	750	14.7	482	9.7	1232	12.2
Driver characteristics						
Driver gender						
Male	4860	94.5	4622	92.4	9482	93.5
Female*	278	5.5	377	7.6	655	6.5
Driver age						
<30	1195	23.3	1095	21.9	2290	22.6
30–60*	3658	71.2	3588	71.8	7246	71.5
>60	285	5.5	316	6.3	601	5.9
Seat belt used						
Not used	1211	23.6	875	17.6	2086	20.6
Used*	3927	76.4	4124	82.4	8051	79.4
Alcohol-impaired						
No*	4552	82.6	4264	85.3	8816	83.9
Yes	586	11.4	735	14.7	1321	13.1
Career						
Staff*	594	11.5	809	16.1	1403	13.8
Self-employed	768	14.9	1042	20.8	1810	17.8
Farmer	3296	64.1	2622	52.4	5918	58.3
Others	480	9.3	526	10.5	1006	9.9
Driving experience						
<4 years	983	19.1%	1031	20.6%	2048	20.2%
4–10 years*	2026	39.4%	1871	37.4%	3943	38.9%
>10 years	2125	41.4%	1977	39.5%	4146	40.9%
Driving license						
With license	4530	88.1%	4484	89.6%	9014	89.0%
Without license*	608	11.9%	515	10.3%	1123	11.0%
Vehicle characteristics						
Vehicle type						
Passenger car*	1859	36.1%	2019	40.3%	3878	38.2%
Motorcycle	1642	31.9%	1101	22.0%	2743	27.0%
Pickup	351	6.8%	439	8.7%	790	7.7%
Truck	1114	21.6%	1194	23.8%	2308	22.7%
Other	172	3.3%	246	4.9%	418	4.1%
Road characteristics						
Road surface						
Non-dry	526	10.2%	263	5.3%	789	7.8%
Dry*	4612	89.7%	4736	94.7%	9348	92.2%
Other characteristics						
Traffic controls						
No control*	1684	32.7%	1516	30.3%	3200	31.5%
Signal control	205	3.9%	292	5.8%	497	4.9%
Stop-yield sign	2899	56.4%	2964	59.2%	5863	57.8%
Other control methods	350	6.8%	227	4.5%	577	5.8%
Week						
Monday or Friday	2216	43.1%	1394	27.8%	2867	28.2%
Tuesday–Thursday*	1473	28.6%	2213	44.2%	4429	43.6%
Weekend	1449	28.2%	1392	27.8%	2841	28.0%
Intersection						
No*	3981	77.4%	3563	71.2%	7544	74.4%
Yes	1157	22.6%	1436	28.7%	2593	25.5
Time of accident						
00:00–07:00	1068	20.7%	442	8.8%	1510	14.8%
07:00–09:00	299	5.8%	1056	21.1%	1355	13.3%

TABLE 1: Continued.

Variables	SVCF		SVCC		Total	
	Number	Rate (%)	Number	Rate (%)	Number	Rate (%)
09:00–17:00*	802	15.6%	2613	52.2%	3415	33.6%
17:00–20:00	1587	30.8%	664	13.2%	2251	22.2%
20:00–24:00	1382	26.8%	224	4.4%	1606	15.8%
Area						
Urban*	3011	58.6%	3494	69.8%	6505	64.2%
Rural	2127	41.3%	1505	30.2%	3632	35.8%
Crash type						
Non-fixed object*	3670	71.4%	4234	84.6%	7904	77.9%
Fixed object	334	6.5%	195	3.9%	529	5.2%
Collision with pedestrian	1079	21.0%	500	10.0%	1579	15.5%
Other object	55	1.1%	70	1.4%	125	1.2%

Note: *indicates that that variable was a reference variable in the model.

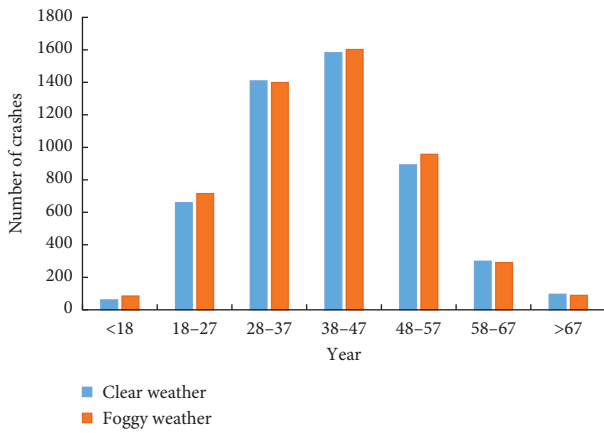


FIGURE 2: Driver age distribution characteristics of crashes.

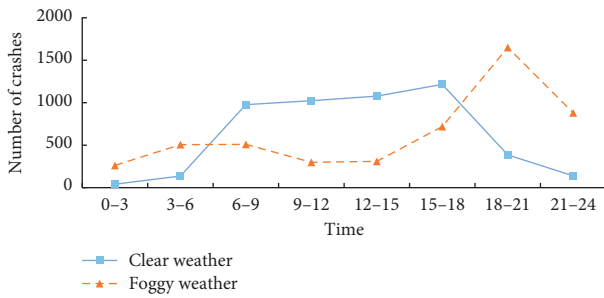


FIGURE 3: Time distribution characteristics of crashes.

value of other variables remains unchanged. Since the variables in the model have been transformed into discrete variables (the variables' value is 0 or 1), the marginal effects of the variables are shown in the following equation:

$$E_{x_{ijk}}^P(y_i=j) = P(y_i = j | x_{ijk} = 1) - P(y_i = j | x_{ijk} = 0), \quad (4)$$

where $E_{x_{ijk}}^P(y_i=j)$ denotes the marginal effect of the k th significant independent variable when the injury severity of the i th crash is j , it can measure the probability of the injury level j when the value of the binary variable x_k changes (from 0 to 1 or from 1 to 0), x_{ijk} represents the k th significant

independent variable, and $P(y_i = j | x_{ijk} = 1)$ denotes the probability when the severity of the i th crash is j given the value of independent variable x_{ijk} . For variables with random effects in the sample, the mean of the model coefficient is used to calculate the marginal effect of the variable.

3.3. *Model Diagnostics.* Model diagnostics mainly include tests for validity and goodness-of-fit. The validity test is achieved by checking the likelihood ratio (also known as the chi-square test). The likelihood ratio test is calculated, as shown in the following equation:

$$\chi^2 = -2(\text{LL}(0) - \text{LL}(\beta_j)) \sim \chi^2(k), \quad (5)$$

where the likelihood ratio test for the model is denoted by χ^2 , $\text{LL}(0)$ denotes log-likelihood at constants (the intercept model includes only the constant term), the log-likelihood at convergence is denoted by $\text{LL}(\beta_j)$, and k represents the number of model parameters (the full model with the constant term and all predicting variables). When the value of χ^2 is greater than the value of $\chi^2(k)$ on the given significance level α , the test is satisfied.

In terms of goodness-of-fit evaluation, the Akaike Information Criterion (AIC) avoids overfitting by introducing a penalty term for complexity. Thus, a criterion for weighing complexity and fit satisfaction was provided. However, the penalty factor for the parameters' number in AIC is not affected by the observation size (the penalty factor is always 2). The weakness of AIC will cause the estimated value to deviate from the real value, when the sample size is large enough. On the contrary, the Bayesian Information Criterion (BIC) compensates for the deficiency of AIC by introducing sample parameters, which makes the penalty term higher than AIC. Hence, the BIC can provide more reliable estimation.

Another evaluation index of model fitting is the McFadden pseudo R -squared. The ratio of the log-likelihood at convergence and the log-likelihood at constants measures the level of improvements over the constant term model offered by the full model. Satisfactory fit will be reflected by the larger McFadden pseudo R -squared value. Therefore, the MLM was diagnosed by AIC, BIC, as well as McFadden

pseudo R -squared. The formulas for AIC, BIC, and McFadden pseudo R -squared are shown in the following equations:

$$\text{AIC} = 2k - 2\text{LL}(\beta_j), \quad (6)$$

$$\text{BIC} = k \ln(n) - 2\text{LL}(\beta_j), \quad (7)$$

$$\text{McFadden Pseudo } R^2 = 1 - \frac{\text{LL}(\beta_j)}{\text{LL}(0)}, \quad (8)$$

where k is the number of parameters and n is the number of samples in the dataset. In general, the smaller the value of AIC and BIC, the better the fitting of the model to the dataset.

3.4. Model Transferability. The crash severity models may be different between clear weather and foggy weather conditions. It is necessary to investigate the transferability of the crash model under different scenarios. The transferability assessment of the crash model can be achieved by calculating the transfer index (TI), which is calculated as follows:

$$\text{TI}_b(\beta_a) = \frac{\text{LL}_b(\beta_a) - \text{LL}_b(\beta_{\text{reference},b})}{\text{LL}_b(\beta_b) - \text{LL}_b(\beta_{\text{reference},b})}, \quad (9)$$

where $\text{TI}_b(\beta_a)$ means the TI value, when the weather condition is a , the accident model with parameter of β_a is applied to the case of weather condition b and the corresponding TI value, $\text{LL}_b(\beta_a)$ denotes the log-likelihood of the model, established by the crash data of weather condition a and being applied to crash data of weather condition b , $\text{LL}_b(\beta_{\text{reference},b})$ is the log-likelihood of the intercept-only model for weather condition b , and $\text{LL}_b(\beta_b)$ is the full model built from the crash data of weather condition b .

TI criteria have an upper limit of 1, and no lower limit. The larger the TI value is, the better the transferability of the model. A negative TI value suggests that the transferability of the model is not satisfactory. The intercept-only model which is established under the weather condition b outperforms the full model which is established under the weather condition a in fitting the crash data of weather condition b .

4. Discussion

Since the probability function in MLM is nonclosed, the analytical solution cannot be achieved by calculating the integral. Therefore, the simulation-based maximum likelihood method was adopted for model estimation. By weighing computational efficiency against the goodness-of-fit, 1,000 iterations and Halton sequences in simulations were used to ensure effective estimation of parameters [12]. To select the most appropriate form of parameter distribution, it was necessary to test the four commonly-used distributions of the density function (log-normal, uniform, normal, and triangular).

Log-normal distribution requires all parameters to keep the same sign (all positive or all negative). However, the influence of different factors on driver injury severity may be either positively or negatively correlated. Thus, a log-normal distribution was not suitable for this research. Subsequently, the MLM with random coefficients following a log-normal distribution was ignored. When the SVCF model and the SVCC model obey normal distribution, triangular distribution, and uniform distribution, respectively, the fitting results of the models are shown in Table 2. It can be seen from Table 2 that the AIC and BIC of the SVCF model and the SVCC model with normal distribution are slightly better than those of triangular distribution and uniform distribution. The normal distribution provides a more straightforward description about the effect of random variables on injury severity than the triangular and uniform distribution. In this study, all random parameters in MLM were assumed to obey normal distribution to identify the variables that had random influence on injury severity. Normal distribution is also widely used in the existing research.

The MLM was employed to analyze the SVCF and the SVCC. The dependent variables include no injury, slight injury, and SFI. No injury was used as a reference variable during the modeling process. The parameter estimates are shown in Tables 3 and 4, and all parameters given in the model were significant at 90% confidence level. Average marginal effects are shown in Table 5. In evaluating the fit performance of the crash model, Mujalli and de Oña [23] concluded that a McFadden pseudo R -squared value of 0.2 to 0.4 would be sufficient. As can be seen from Tables 3 and 4, the McFadden pseudo R^2 values for the SVCC and SVCF models were 0.434 and 0.348, respectively, and the p value for the likelihood ratio test was less than 0.001. This indicates that the MLM fits the SVCF and SVCC data satisfactorily. Meanwhile, both models contain fixed parameters and random parameters, and the distribution of parameters in different injury severities is different. The results show that the MLM can effectively capture the unobserved heterogeneous across observations. The contributing factors that had a significant impact on injury severity of SVCC and SVCF (especially SFI) are discussed in detail. It should be pointed out that, in the follow-up discussion, the marginal effects were mainly used to quantify the influence of risk factors on the severity of crashes.

4.1. Driver Characteristics. Gender has a significant influence on driver injury severity of both SVCF and SVCC crashes. The marginal effect shows that compared with female drivers, the probability of SFI injury of male drivers in SVCF and SVCC accidents decreased by 4.5% and 0.3%, respectively [24, 25]. Moreover, the influence of male drivers on the occurrence of SFI crashes in both weather conditions shows a random effect. It can be seen that although the effect of gender on SVCF and SVCC injury severity levels is in the same direction, the proportion of SFI crashes in foggy weather is significantly lower than in clear weather. This finding is very meaningful, which not only can further

TABLE 2: Fitting index statistics of MLMs under different distributions.

Fitting test	SVCC model			SVCF model		
	Normal	Triangular	Uniform	Normal	Triangular	Uniform
LL(β_j)	-2187.58	-2188.19	-2187.90	-3029.94	-3030.51	-3030.42
AIC	4491.17	4492.39	4491.79	6159.88	6162.15	6161.54
BIC	4869.15	4870.34	4869.78	6487.10	6488.41	6487.82

TABLE 3: Model estimation results of SVCC.

Variable	Description	Slight injury			SFI		
		Mean	S.E.	z-value	Mean	S.E.	z-value
Driver characteristics							
Gender	Male	-0.702**	0.162	-4.33	-0.491*	0.267	-1.84
	Std. dev.	-	-	-	1.241	0.108	-
Age	>60	1.192**	0.194	6.14	2.151**	0.244	36.13
Seat belt used	Not used	0.370**	0.132	2.80	2.004**	0.170	11.79
Alcohol-impaired	Yes	0.950**	0.183	5.19	3.580**	0.194	18.45
	Self-employed	-	-	-	-0.624*	0.265	-2.35
Career	Farmer	-	-	-	-0.450*	0.207	-2.17
	With license	-0.681**	0.161	-4.23	-0.826**	0.227	-3.64
Vehicle characteristics							
Vehicle type	Motorcycle	2.594**	0.143	18.14	2.442**	0.226	10.81
	Pickup	-0.638**	0.167	-3.82	-0.692*	0.318	-2.18
	Truck	-	-	-	-0.776**	0.253	-3.07
Other characteristics							
Area	Rural	0.278*	0.109	2.55	0.403*	0.166	2.43
	Std. dev.	1.015	0.074	-	-	-	-
Week	Weekend	-	-	-	0.540**	0.176	3.07
	07:00-09:00	-0.268*	0.127	-2.111	-	-	-
Time of accident	20:00-24:00	1.056**	0.209	5.05	1.412**	0.299	4.72
	00:00-07:00	-	-	-	0.981**	0.254	3.86
	Fixed object	1.791**	0.253	7.08	3.440**	0.285	12.07
Crash type	Pedestrian	-1.997**	0.216	-9.25	-2.800**	0.454	-6.17
	Intercept	-1.994**	0.228	-8.75	-4.917**	0.401	-12.26
Likelihood ratio	$\chi^2(56) = 3350.98; p < 0.001$						
McFadden pseudo R^2	0.434						
Sample size	4999						

Note: ** and * indicate that variables are significant at 1% and 5% significance levels, respectively; S.E. means the standard error; - means this variable is not significant in the model.

validate and enrich existing findings but also clarify the impact of driver gender difference on SV crash severity under foggy and clear weather.

In terms of age, the marginal effect indicated that compared with middle-age drivers, the probability of SFI injury of young drivers (age < 30) in SVCF is reduced by 3.2%. The parameter corresponding to the SFI obeys a normal distribution with a mean of -0.476 (0.158) and a standard deviation of 1.10 (0.106). However, the effect of young drivers on SVCC injury severity is not significant. This discrepancy finding is of great interest and can be used to develop management measures such as increased supervision of middle-age drivers in foggy weather.

In SVCF and SVCC, older drivers (age > 60) lead to a significant increase in the probability of both slight and SFI injuries. The marginal effect indicated that the probability of SFI injury increased by 11.9% and 8.7%, respectively. Abdel-Aty [26] reached the same conclusion that older drivers are most vulnerable to serious injuries among different age

groups, as they need more reaction time in case of emergency and are more likely to sustain serious injury in case of a crash.

As can be seen from the model, no seatbelt use has a significant impact on the severity of both SVCF and SVCC crashes. Drivers not using a seat belt are 7.1% and 7.6% more likely to suffer SFI injuries in SVCF and SVCC, respectively, which is consistent with the findings of previous studies [11, 27]. Seatbelts, as an important part of passive safety defense measures, can restrain occupant displacement and absorb impact energy in a vehicle collision or emergency braking effectively. Especially when driving in foggy weather, it is difficult for drivers to maintain a satisfactory driving condition because they cannot distinguish obstacles ahead. Seatbelt use becomes even more important to protect drivers from fatal crashes. However, 20.6% of drivers still did not use seat belts in the total sample. It is necessary for traffic managers to take measure for this phenomenon, such as more publicity and education.

TABLE 4: Model estimation results of SVCF.

Variable	Description	Slight injury			SFI		
		Mean	S.E.	z-value	Mean	S.E.	z-value
Driver characteristics							
Gender	Male	-0.948**	0.176	-5.39	-1.132**	0.255	-4.44
	Std. dev.	-	-	-	0.881	0.120	-
Age	<30	-	-	-	-0.476**	0.158	-3.01
	Std. dev.	-	-	-	1.10	0.106	-
Seat belt used	>60	1.100**	0.195	5.64	1.834**	0.225	8.15
Alcohol-impaired	Not used	0.262*	0.109	2.40	1.017**	0.134	7.59
Career	Yes	0.619**	0.129	4.80	2.407**	0.140	17.19
Driving license	Farmer	-	-	-	0.487*	0.230	2.12
	With license	-	-	-	-0.538**	0.183	-2.94
Vehicle characteristics							
Vehicle type	Motorcycle	2.884**	0.115	25.08	3.289**	0.179	18.37
	Pickup	-0.721**	0.167	-4.32	-0.983**	0.277	-3.55
	Truck	-	-	-	-0.619**	0.194	-3.19
	Std. dev.	-	-	-	0.650	0.116	-
Road characteristics							
Road surface	Non-dry	-	-	-	-0.593**	0.187	-3.17
Traffic controls	Signal control	0.543**	0.206	2.64	0.603*	0.289	2.09
Other characteristics							
Area	Rural	-	-	-	0.234*	0.108	2.17
Time of accident	07:00–09:00	-0.593**	0.210	-2.82	-	-	-
	20:00–24:00	0.388**	0.137	2.83	0.581**	0.186	3.12
	00:00–07:00	0.292*	0.145	2.01	1.075**	0.187	5.75
Crash type	Fixed object	1.609**	0.197	8.17	3.053**	0.206	14.82
	Pedestrian	-1.718**	0.129	13.32	-2.358**	0.218	-10.82
Intercept		-1.831**	0.266	-6.89	-3.480**	0.346	-10.06
Likelihood ratio				$\chi^2(48) = 3228.21; p < 0.001$			
McFadden pseudo R^2				0.348			
Sample size				5138			

Note: ** and * indicate that variables are significant at 1% and 5% significance levels, respectively; S.E. means the standard error; - means this variable is not significant in the model.

Driver alcohol-impaired has a significant effect on the severity of SVCF and SVCC, and the probability of SFI increases by 15.5% and 12.9%, respectively. This finding can be confirmed in the existing literature. For example, it was found that the probability of fatal crashes caused by drunk driving increased by 150% [28]. This finding makes sense because alcohol can affect a driver's psychological and physiological functions (such as reaction time, vision, and agility). Also, it is difficult to maintain a normal driving state in case of emergency, which leads to an increased probability of serious crashes. Increasing driver education and enforcement intensity are effective measures to reduce driving under the influence (DUI). In addition, advanced vehicle identification systems can be developed to automatically monitor a driver's driving status and alcohol concentration in real time. If national standards are not met, mandatory measures could be implemented.

Significant differences are shown in the effect of occupation factors on the severity of SVCF and SVCC. Compared with company employment, the probability of SFI caused by self-employment decreases by 2.1% in SVCC, but this variable has no significant impact on injury severity of SVCF. On the contrary, the coefficient of farmers corresponding to SFI injury is the opposite in the SVCC and SVCF models

(the marginal effects of SVCC and SVCF are -0.015 and 0.036, respectively). All valuable findings suggest that there are significant differences in the influencing factors and effects of the severity of SVCC and SVCF. The influence of driver occupation on the severity of SV crashes in foggy weather is well revealed.

Model results indicate that with/without driver license is significant at a 90% confidence level ($p < 0.01$). The probability of SFI in SVCF and SVCC with driving license is 3% and 4.9% lower than that without driving license, respectively [29]. This finding suggests that traffic managers should strengthen management of driver licensing.

4.2. Vehicle Characteristics. Compared with passenger cars, the probability of SFI of motorcycles in SVCF and SVCC accidents increased by 14.4% and 4.7%, respectively, which is consistent with the existing literature [22]. Motorcycles are limited by their own characteristics and cannot provide adequate protection for a driver in a crash, which makes the driver exposed and easy to cause SFI. The rollover phenomenon tends to occur in motorcycle SV crashes, which increases the probability of SFI. In detail, it can be seen from the marginal effect that the probability of motorcycle drivers

TABLE 5: Average marginal effects of significant variables.

Variable	Description	SVCC		SVCF	
		Slight injury	SFI	Slight injury	SFI
Driver characteristics					
Gender	Male	-0.061	-0.003	-0.081	-0.045
Age	<30	-	-	-	-0.032
	>60	0.083	0.087	0.067	0.119
Seat belt used	Not used	-0.012	0.076	-0.010	0.071
Alcohol-impaired	Yes	0.008	0.129	-0.016	0.155
Career	Self-employed	-	-0.021	-	-
	Farmer	-	-0.015	-	0.036
Driving license	With license	-0.049	-0.018	-	-0.030
Vehicle characteristics					
Vehicle type	Motorcycle	0.341	0.047	0.356	0.144
	Pickup	-0.054	-0.015	-0.067	-0.043
	Truck	-	-0.029	-	-0.037
Road characteristics					
Road surface	Non-dry	-	-	-	-0.032
Traffic controls	Signal control	-	-	0.048	0.026
Other characteristics					
Area	Rural	0.023	0.011	-	0.014
Week	Weekend	-	0.023	-	-
	07:00-09:00	-0.031	-	-0.054	-
Time of accident	20:00-24:00	0.091	0.036	0.031	0.024
	00:00-07:00	-	0.041	-0.008	0.074
Crash type	Fixed object	0.107	0.201	0.061	0.266
	Pedestrian	-0.114	-0.052	-0.133	-0.085

Note: - means this variable is not significant in the model.

suffering from SFI in SVCF is significantly higher than that in SVCC (in the SVCF and SVCC models, the marginal effects of motorcycle drivers corresponding to SFI were 0.144 and 0.047, respectively). This may be due to low visibility in foggy weather, which affects a driver's correct judgment of headway distance.

In the SVCF and SVCC models, pickup and a driver's probability of slight injury and SFI injury are significantly negatively correlated (using passenger car as the reference). The reason is that the driving vision of a pickup is better than that of a passenger car and it can absorb more energy in crashes so as to reduce the risk of SFI. Furthermore, Desapriya et al. [30] found that when a passenger car collided with a pickup, the injury to the pickup driver was significantly lower than that of the passenger car driver. This finding confirms the validity of the conclusions drawn in this study.

Compared to passenger cars, the probability of SFI in truck-related SVCF and SVCC crashes are reduced by 3.7% and 2.9%, respectively. A similar conclusion was reached by Bédard et al. [31]. More specifically, the parameters of a truck corresponding to SFI in the SVCF model obey the normal distribution, with mean value of -0.619 and standard deviation of 0.650. However, there is no heterogeneity for this variable in the SVCC model. By constructing the MLMs under the conditions of SVCF and SVCC, respectively, the heterogeneity of influencing factors in the subset can be effectively identified. It is valuable for understanding the source of heterogeneity in the whole dataset.

4.3. Road Characteristics. In the SVCF model, road surface condition has a significant impact on SFI. The average marginal effect indicates that the probability of SFI caused by non-dry pavement decreases by 3.2% with a dry road surface as the reference. In foggy weather, drivers are more cautious when driving on non-dry road surface and usually keep a low speed. Thus, the probability of SFI will be reduced when an SV crash occur, but road surface condition has no significant effect on the severity of SVCC. This finding is equally contributory and can further improve the conclusions of Li et al. [8], who found a significant effect of the non-dry road surface on the severity of low visibility-related SV crashes and did not investigate clear weather scenarios.

The influence of signal control on the severity of SV crashes is significant on foggy days but not on sunny days. Specifically, the probability of slight injury and SFI injury caused by signal control increases by 4.8% and 2.6%, respectively, compared with uncontrolled roads in the SVCF model. This may be due to low visibility in foggy weather, and fog will dilute the color depth of the signal light [15]. Drivers cannot judge the color of the signal lamp in time. Thus, it is easier to hit roadside fixed facilities such as curb and guardrail.

4.4. Other Characteristics. Compared with the urban area, the probability of SFI injury increased by 1.1% and 1.4%, respectively, when SVCC and SVCF occurred in rural areas [32]. This is justified because traffic management in rural areas is unsatisfactory and speed on national highways is

high. Thus, the probability of serious crashes in rural areas is higher than that in urban areas.

In addition, the probability of SFI injury caused by a weekend day is significantly higher than that of a working day (marginal effect is 0.023) in the SVCC model. This is in agreement with the findings of previous studies. For example, Abrari Vajari et al. [33] conducted modeling and analysis on motorcycle crashes and found that the probability of fatal crashes on weekend days was 1.14 times that of working days. Salum et al. [34] noted that drivers with less driving experience are more likely to drive on weekends, which further supports our findings. However, there is not statistically significant relationship between weekend and SFI crashes in the SVCF model. This discovery is interesting and meaningful. It can verify the necessity of modeling clear and foggy days separately. More importantly, the traffic management department can formulate scientific management measures based on this discovery. For example, the management of weekend under clear weather should be strengthened.

For different time periods, 7:00–9:00 (morning peak), 20:00–24:00, and 00:00–7:00 have a significant effect on the severity of SVCF and SVCC, but the effect varies with time. The average marginal effects indicate that compared with 9:00–17:00 in SVCF and SVCC accidents, the probability of slight injury in the morning peak is reduced by 5.4% and 3.1%, respectively. This is because traffic is congested in the morning peak hours and driving speed is low. Thus, a driver is less likely to be injured in a collision. In addition, the probability of causing SFI injuries increased by 2.4% and 3.6% in SVCF and SVCC crashes from 20:00–24:00, respectively. There is also a significant positive correlation between 0:00–7:00 and injury severity (marginal effects of SVCF and SVCC are 0.074 and 0.041, respectively), which is consistent with the findings of previous studies [33]. The reason for this phenomenon may be that traffic control during the evening hours is weak, and drivers are more likely to drive fatigued or under the influence of alcohol. Increasing the monitoring of driving behavior during evening hours is considered a necessary measure to reduce the probability of severe crashes.

In the SVCF and SVCC models, the probability of SFI injury caused by collision with a fixed object increased by 26.6% and 20.1%, respectively. Other literature on this factor has reached consistent conclusions [35]. This may be due to the fact that when motor vehicles collide with roadside concrete facilities or other fixed obstacles, the collision energy cannot be absorbed by the fixed objects. Therefore, energy-absorbing devices should be installed on the surface of fixed obstacles (such as concrete facilities) to reduce the injury severity of SV crashes.

SV crashes with pedestrians are significantly and negatively correlated with driver injury severity. The marginal effects of the SVCF and SVCC models showed that drivers are 8.5% and 5.2% less likely to have a serious injury, respectively. It is reasonable to draw this conclusion because compared with motor vehicles, pedestrians are vulnerable. Collision with pedestrians will not cause serious injury to drivers but will have a serious impact on pedestrians.

TABLE 6: Model transferability test.

Crash model	Application data	
	SVCC	SVCF
SVCC	1	-0.172
SVCF	-0.306	1

4.5. Verify Model Transferability. To evaluate the model transferability under clear and foggy weather conditions, the TI values of the crash model under the two weather conditions were calculated. The specific calculation results are shown in Table 6. It is necessary to point out that the TI value of the crash severity analysis model for its local dataset is 1 because the model represents the local situation of the crash dataset. In addition, the remaining TI values in Table 6 are less than 0. This shows that the fitting performance of the intercept-only model established by local data is better than the transferred model. Hence, the model transferability test shows that the crash model established by SVCF and SVCC cannot be directly transferred. In the process of assessing the risk factors of crash severity, it is recommended to build the SVCC model and SVCF model, respectively.

5. Conclusion

This study used 10,137 SV crashes in Shandong Province, China, as sample data (from 2015 to 2019) and divided the dataset into two parts for modeling: single-vehicle crashes in foggy weather (SVCF) and single-vehicle crashes in clear weather (SVCC). On this basis, the MLM was employed to analyze the factors that have significant impact on the severity of SVCF and SVCC crashes. By examining the McFadden pseudo R -squared and random coefficient distributions of the model, it is concluded that the goodness-of-fit is satisfactory and could effectively capture unobserved heterogeneity across observations. In addition, the results of the model transferability test showed that the crash models established by SVCC and SVCF cannot be directly transferred to each other. It is recommended to build the SVCC model and SVCF model separately.

The findings in this study are as follows:

- (1) There are significant differences in the factors affecting injury severity of SV crashes in foggy and clear weather. In foggy weather crashes, both young drivers and non-dry road surfaces resulted in a 3.2% reduction in the probability of SFI. Signal control resulted in a 2.6% increase in the probability of SFI in SVCF. However, none of these variables have a significant effect on clear weather crashes. The probability of self-employment leading to SFI in clear weather crashes is reduced by 2.1%. Weekends resulted in a 2.3% increase in the probability of SFI in SVCC. However, two variables of foggy crashes are not significant. Interestingly, the effect of the farmer variable on the severity of foggy and clear weather crashes showed an opposite trend, i.e., the variable resulted in a 1.5% decrease in the probability of SFI

injuries in clear weather crashes and a 3.6% increase in the probability of SFI injuries in foggy weather crashes.

- (2) There is a commonality in the factors influencing the severity of SV crashes in foggy and clear weather. For instance, male drivers, having a license and using a pickup or a truck, resulted in significantly lower severity of both foggy and clear weather crashes. Older drivers, seat belts not used, drunk driving, motorcycles, rural areas, night time (20:00–07:00), and collisions with fixed objects resulted in significantly higher crash severity in both foggy and clear weather.

Targeted policies based on the conclusions are more cost-effective in reducing the severity of crashes. For example, in both foggy and clear weather, driving violations resulted in a significant increase in crash severity. Hence, advance traffic crash warning systems should be installed to detect dangerous driving behaviors (such as drunk driving and seat belts not used). Vehicle-to-road communication (V2I) technology can be used to provide road information in real time [36].

Collisions with fixed objects increase driver injury severity significantly. Thus, the focus should be on improvement of hard guardrails or other road surface fixtures on both sides of the road. The Department of Transportation should consider replacing hard guardrails with soft guardrails that can absorb collision energy; an energy-absorbing buffer device is installed on the fixed surface to reduce the severity of collision.

In the future, clustering techniques will be used to classify the data and reduce the heterogeneity of the data.

Data Availability

The traffic crash data used to support the findings of this study have not been made available because traffic accident data are required to be confidential by Shandong Department of Transportation.

Conflicts of Interest

The authors declare that there are no conflicts of interest regarding the publication of this paper.

Acknowledgments

The authors would like to thank the support of the Shandong Department of Transportation (SDOT) and Zibo Department of Transportation (ZDOT). This research was jointly supported by the National Natural Science Foundation of China (Grant nos. 71901134 and 71871057), National Science Foundation for Distinguished Young Scholars (Grant no. 51925801), Natural Science Foundation of Shandong (Grant no. ZR2018BF024), and Postdoctoral Research Assistance Program of Jianguo (Grant no. 2018K118C).

References

- [1] National Highway Traffic Safety Administration (NHTSA), *Traffic Safety Facts Annual Report Tables*, National Highway Traffic Safety Administration, Washington, DC, USA, 2018.
- [2] M. Zhou and H. C. Chin, "Factors affecting the injury severity of out-of-control single-vehicle crashes in Singapore," *Accident Analysis & Prevention*, vol. 124, pp. 104–112, 2019.
- [3] S. M. Rifaat and H. C. Chin, "Accident severity analysis using ordered probit model," *Journal of Advanced Transportation*, vol. 41, no. 1, pp. 91–114, 2007.
- [4] D. Ma, X. Luo, S. Jin, D. Wang, W. Guo, and F. Wang, "Lane-based saturation degree estimation for signalized intersections using travel time data," *IEEE Intelligent Transportation Systems Magazine*, vol. 9, no. 3, pp. 136–148, 2017.
- [5] D. Ma, X. Luo, W. Li, S. Jin, W. Guo, and D. Wang, "Traffic demand estimation for lane groups at signal-controlled intersections using travel times from video-imaging detectors," *IET Intelligent Transport Systems*, vol. 11, no. 4, pp. 222–229, 2017.
- [6] C. Xu, W. Wang, and P. Liu, "Identifying crash-prone traffic conditions under different weather on freeways," *Journal of Safety Research*, vol. 46, pp. 135–144, 2013.
- [7] Y. Wu, M. Abdel-Aty, and J. Lee, "Crash risk analysis during fog conditions using real-time traffic data," *Accident Analysis & Prevention*, vol. 114, pp. 4–11, 2018.
- [8] Z. Li, C. Chen, Q. Wu et al., "Exploring driver injury severity patterns and causes in low visibility related single-vehicle crashes using a finite mixture random parameters model," *Analytic Methods in Accident Research*, vol. 20, pp. 1–14, 2018.
- [9] M. Feng, X. Wang, J. Lee et al., "Transferability of safety performance functions and hotspot identification for freeways of the United States and China," *Accident Analysis & Prevention*, vol. 139, p. 105493, 2020.
- [10] H. Wen and G. Xue, "Injury severity analysis of familiar drivers and unfamiliar drivers in single-vehicle crashes on the mountainous highways," *Accident Analysis & Prevention*, vol. 144, p. 105667, 2020.
- [11] Z. Li, Y. Ci, C. Chen et al., "Investigation of driver injury severities in rural single-vehicle crashes under rain conditions using mixed logit and latent class models," *Accident Analysis & Prevention*, vol. 124, pp. 219–229, 2019.
- [12] H. Yu, R. Yuan, Z. Li et al., "Identifying heterogeneous factors for driver injury severity variations in snow-related rural single-vehicle crashes," *Accident Analysis & Prevention*, vol. 144, p. 105587, 2020.
- [13] R. L. Moore and L. Cooper, "Fog and road traffic," TRRL Report, Transport and Road Research Laboratory, Wokingham, UK, 1972.
- [14] M. Abdel-Aty, A.-A. Ekram, H. Huang, and K. Choi, "A study on crashes related to visibility obstruction due to fog and smoke," *Accident Analysis & Prevention*, vol. 43, no. 5, pp. 1730–1737, 2011.
- [15] J.-P. Tarel, N. Hautiere, L. Caraffa, A. Cord, H. Halmaoui, and D. Gruyer, "Vision enhancement in homogeneous and heterogeneous fog," *IEEE Intelligent Transportation Systems Magazine*, vol. 4, no. 2, pp. 6–20, 2012.
- [16] Y. Guo, Z. Li, P. Liu, and Y. Wu, "Modeling correlation and heterogeneity in crash rates by collision types using full Bayesian random parameters multivariate tobit model," *Accident Analysis & Prevention*, vol. 128, pp. 164–174, 2019.
- [17] J. Lee and F. Mannering, "Impact of roadside features on the frequency and severity of run-off-roadway accidents: an

- empirical analysis," *Accident Analysis & Prevention*, vol. 34, no. 2, pp. 149–161, 2002.
- [18] F. L. Mannering, V. Shankar, C. R. Bhat et al., "Unobserved heterogeneity and the statistical analysis of highway accident data," *Analytic Methods in Accident Research*, vol. 11, pp. 1–16, 2016.
- [19] F. Ye and D. Lord, "Comparing three commonly used crash severity models on sample size requirements: multinomial logit, ordered probit and mixed logit models," *Analytic Methods in Accident Research*, vol. 1, pp. 72–85, 2014.
- [20] H. Xiong, X. Zhu, and R. Zhang, "Energy recovery strategy numerical simulation for dual axle drive pure electric vehicle based on motor loss model and big data calculation," *Complexity*, vol. 2018, Article ID 4071743, 14 pages, 2018.
- [21] Y. Guo, T. Sayed, L. Zheng et al., "A hierarchical Bayesian peak over threshold approach for conflict-based before-after safety evaluation of leading pedestrian intervals," *Accident Analysis & Prevention*, vol. 147, p. 105772, 2020.
- [22] Z. Li, P. Liu, W. Wang, and C. Xu, "Using support vector machine models for crash injury severity analysis," *Accident Analysis & Prevention*, vol. 45, pp. 478–486, 2012.
- [23] R. O. Mujalli and J. de Oña, "Injury severity models for motor vehicle accidents: a review," *Proceedings of the Institution of Civil Engineers-Transport*, vol. 166, no. 5, pp. 255–270, 2013.
- [24] D. Ma, X. Luo, S. Jin, W. Guo, and D. Wang, "Estimating maximum queue length for traffic lane groups using travel times from video-imaging data," *IEEE Intelligent Transportation Systems Magazine*, vol. 10, no. 3, pp. 123–134, 2018.
- [25] Y. Guo, Z. Li, Y. Wu, and C. Xu, "Exploring unobserved heterogeneity in bicyclists' red-light running behaviors at different crossing facilities," *Accident Analysis & Prevention*, vol. 115, pp. 118–127, 2018.
- [26] M. Abdel-Aty, "Analysis of driver injury severity levels at multiple locations using ordered probit models," *Journal of Safety Research*, vol. 34, no. 5, pp. 597–603, 2003.
- [27] D. Ma, X. Song, and P. Li, "Daily traffic flow forecasting through a contextual convolutional recurrent neural network modeling inter- and intra-day traffic patterns," *IEEE Transactions on Intelligent Transportation Systems*, vol. 99, pp. 2627–2636, 2020.
- [28] J.-K. Kim, G. F. Ulfarsson, S. Kim, and V. N. Shankar, "Driver-injury severity in single-vehicle crashes in California: a mixed logit analysis of heterogeneity due to age and gender," *Accident Analysis & Prevention*, vol. 50, pp. 1073–1081, 2013.
- [29] Y. Guo, Z. Li, P. Liu, and Y. Wu, "Exploring risk factors with crashes by collision type at freeway diverge areas: accounting for unobserved heterogeneity," *IEEE Access*, vol. 7, pp. 11809–11819, 2019.
- [30] E. Desapriya, I. Pike, and J. Kinney, "The risk of injury and vehicle damage severity in vehicle mismatched side impact crashes in British Columbia," *IATSS Research*, vol. 29, no. 2, pp. 60–66, 2005.
- [31] M. Bédard, G. H. Guyatt, M. J. Stones, and J. P. Hirdes, "The independent contribution of driver, crash, and vehicle characteristics to driver fatalities," *Accident Analysis & Prevention*, vol. 34, no. 6, pp. 717–727, 2002.
- [32] S. Yasmin, N. Eluru, C. R. Bhat, and R. Tay, "A latent segmentation based generalized ordered logit model to examine factors influencing driver injury severity," *Analytic Methods in Accident Research*, vol. 1, pp. 23–38, 2014.
- [33] M. Abrari Vajari, K. Aghabayk, M. Sadeghian, and N. Shiwakoti, "A multinomial logit model of motorcycle crash severity at Australian intersections," *Journal of Safety Research*, vol. 73, pp. 17–24, 2020.
- [34] J. H. Salum, A. E. Kitali, H. Bwire, T. Sando, and P. Alluri, "Severity of motorcycle crashes in Dares Salaam, Tanzania," *Traffic Injury Prevention*, vol. 20, no. 2, pp. 189–195, 2019.
- [35] X. Zhu and S. Srinivasan, "A comprehensive analysis of factors influencing the injury severity of large-truck crashes," *Accident Analysis & Prevention*, vol. 43, no. 1, pp. 49–57, 2011.
- [36] R.-H. Zhang, Z.-C. He, H.-W. Wang, F. You, and K.-N. Li, "Study on self-tuning tyre friction control for developing main-servo loop integrated chassis control system," *IEEE Access*, vol. 5, pp. 6649–6660, 2017.

Research Article

Simulation Study of Rear-End Crash Evaluation considering Driver Experience Heterogeneity in the Framework of Three-Phase Traffic Theory

Haifei Yang ¹, Yao Wu ², Huihui Xiao ³, and Yi Zhao ⁴

¹College of Civil and Transportation Engineering, Hohai University, Nanjing 210098, China

²School of Modern Posts and Institute of Modern Posts, Nanjing University of Posts and Telecommunications, Nanjing 210003, China

³School of Air Transportation, Shanghai University of Engineering Science, Shanghai 201620, China

⁴College of Automobile and Traffic Engineering, Nanjing Forestry University, Nanjing 210037, China

Correspondence should be addressed to Haifei Yang; yanghaifei@hhu.edu.cn

Received 20 February 2021; Accepted 15 July 2021; Published 27 July 2021

Academic Editor: Jinjun Tang

Copyright © 2021 Haifei Yang et al. This is an open access article distributed under the Creative Commons Attribution License, which permits unrestricted use, distribution, and reproduction in any medium, provided the original work is properly cited.

Driving safety is considered to have a strong relationship with traffic flow characteristics. However, very few studies have addressed the safety impacts in the three-phase traffic theory that has been demonstrated to be an advancement in explaining the empirical features of traffic flow. Another important issue affecting safety is driver experience heterogeneity, especially in developing countries experiencing a dramatic growth in the number of novice drivers. Thus, the primary objective of the current study is to develop a microsimulation environment for evaluating safety performance considering the presence of novice drivers in the framework of three-phase theory. First, a car-following model is developed by incorporating human physiological factors into the classical Intelligent Driver Model (IDM). Moreover, a surrogate safety measure based on the integration concept is modified to evaluate rear-end crashes in terms of probability and severity simultaneously. Based on a vehicle-mounted experiment, the field data of car-following behavior are collected by dividing the subjects into a novice group and an experienced group. These data are used to calibrate the proposed car-following model to explain driver experience heterogeneity. The results indicate that our simulation environment is capable of reproducing the three-phase theory, and the changes in the modified surrogate safety measure are highly correlated with traffic phases. We also discover that the presence of novice drivers leads to different safety performance outcomes across various traffic phases. The effect of driver experience heterogeneity is found to increase the probability of the rear-end crashes as well as the corresponding severity. The results of this study are expected to provide a scientific understanding of the mechanisms of crash occurrences and to provide application suggestions for improving traffic safety performance.

1. Introduction

The understanding of traffic flow characteristics contributes to the investigation of various applications of transportation engineering [1–3]. It has been demonstrated that driving safety has a strong relationship with traffic states [4,5] and can be identified by the significant variance of dynamic features in terms of aggregated indicators, such as occupancy, speed, and speed difference [6–8]. Previous studies generally evaluated safety performance in the framework of

fundamental diagram that divides traffic into free flow and congestion [9–11]. However, this classical method has drawbacks in capturing empirical findings, especially for complicated congestion patterns [12]. Recently, some safety analyses were carried out based on finer classifications of traffic states. For example, Xu [13] evaluated the safety performance under different levels of service (LOS). Furthermore, a crash likelihood indicator was proposed by dividing traffic into five states in accordance with measured occupancies [14]. As expected, these refined considerations

on traffic flow states bring about positive impacts on crash evaluations.

Note that the aforementioned works do not have a universal and concrete theoretical framework to explain space-temporal traffic flow features, which may lead to problems in the transferability of the results throughout the world. In recent decades, Kerner proposed the three-phase traffic theory based on systematic empirical investigations [15–17] and theoretical studies [18,19]. According to Kerner's concept, a macroscopic traffic flow can be classified into three phases, including free flow (F), synchronized flow (S), and wide moving jam (J) phases. The typical phase transition $F \rightarrow S$ indicates the occurrence of a traffic breakdown, and wide moving jams emerge only within the synchronized flow. Both the synchronized flow and wide moving jams correspond to traffic congestion operating with significantly lower speeds. This theory has been tested and reproduced by notable numbers of studies, ranging from empirical investigations [20] to theoretical models [21], and provides instructions on traffic management [22]. Combined with proper crash evaluation method, it has the potential to explore safety performance that is associated with complicated spatiotemporal patterns. For example, driver's overdeceleration under congested phase usually implies dangerous situation which has higher probability of rear-end crash occurrence. Recently, Xu developed an approach to predict crash likelihoods by introducing the three-phase theory [23]. The results suggested that this theory helps to better understand the occurrence of crashes. Kerner's work on traffic flow is expected to have a more widespread application in safety analysis, and it could undergo rapid development by expanding the study with modern methodologies.

Simulation-based approach was originally developed for traffic efficiency studies, and now it has been regarded as a powerful tool for safety evaluation. The simulation-based approach is able to proactively provide deep insight into the details of the interactions among vehicles and has the power to collect and store the data in real time. These advantages bring about ongoing progress in the field of simulation-based safety evaluation. A large number of studies [24,25] were carried out by integrating simulations with surrogate safety measures, which present the sequence of events with the causative factors of crashes. However, most of the previous simulations focused on a homogeneous driver experience environment, which assumes that all drivers traveling on roads have similar driving experience with respect to safety. It is worth noting that novice drivers do not have adequate driving skills and have problems in recognizing traffic environments [26]. Their significant presence in traffic may have a noticeable impact on safety, especially in developing countries, as a rapidly growing number of people obtain their own vehicles and licenses. Based on this consideration, research is needed to incorporate driver experience heterogeneity into simulation-based safety evaluations.

Rear-end crashes have been found to be a major collision type as frequent decelerations and accelerations occur especially in congested traffic conditions [27]. Then, the

primary objective of the current study is to develop a microsimulation environment for rear-end crash evaluation in the framework of three-phase traffic theory. The study focuses on car-following scenarios and takes into account the impacts of driver experience heterogeneity. The remainder of the paper proceeds as follows. In the next section, previous studies related to safety analysis across traffic flow states, simulation-based safety evaluation, and driver experience heterogeneity are reviewed. In Section 3, a microsimulation environment consisting of a car-following model and a modified surrogate safety measure is developed. In Section 4, a vehicle-mounted experiment is carried out to provide data for model calibration. Section 5 reports the simulation results with a detailed discussion. Finally, the conclusions of the study are discussed in Section 6.

2. Review of Related Works

2.1. Safety and Traffic Flow Characteristics. Traffic characteristics have been found to have a significant correlation with crash occurrences. The core concept of previous studies was to evaluate the probability of crash occurrences by relating traffic flow factors to safety performance measures. Based on this concept, a notable number of statistical models have been carried out. For example, matched case-control logistic regression is a widely used statistical method to identify factors associated with crashes [28]. Moreover, some studies have suggested log linear models and Bayesian statistics to evaluate the likelihood of crashes in response to various traffic flow parameters [29,30]. In recent decades, with vigorous progress in the field of data science, artificial intelligent (AI) methods have been proposed to promote the accuracy of crash risk analysis. AI methods mainly include neural networks [8], random forests [31], support vector machines [32], and deep learning [33]. In comparison, these models aimed to improve prediction accuracy, while the statistical models had better interpretations.

The models developed in previous studies generally focused on identifying the relationship between crash and traffic flow parameters. Note that a certain value of a parameter can correspond to various traffic flow states in which drivers have significantly different psychological characteristics and driving behaviors. Such factors have been demonstrated to have great impacts on crash occurrence [14]. Based on this consideration, some studies have investigated the crash mechanism according to the fundamental diagram method, which divides traffic states into free flow and congested flow [9–11]. However, this traditional methodology ignores the fact that different dynamic features can exist within the same traffic flow states. Some recent studies have carried out safety evaluations by considering the finer classification of traffic states [13,14,23,34,35]. However, most of the classifications do not have a generally accepted theoretical framework. Recently, the results of several studies showed that the three-phase theory has positive impacts on fitting safety performance to empirical traffic states. For example, Xu et al. developed a crash prediction model by using statistical methods, which link safety to the phases and the phase transitions categorized by three-phase theory [23].

Hu et al. evaluated the safety performance when bikes and buses are present on a motorway based on a cellular automata model that can reproduce the empirical findings of the three-phase theory [34,35]. Drawing from the conclusions of these studies, it can be expected that such a predominant theory has great potential to explore safety performance in a manner considering more details with respect to driving safety.

2.2. Safety Evaluation with Microscopic Simulations. In recent decades, traffic simulation technology has achieved significant advancements in behavior modeling, data processing, and system optimization. Compared with statistical models and AI models, the simulation-based method for safety research has the ability to scan and repeat the process of a crash occurrence and provide scientifically based suggestions regarding how to reduce the likelihood of a crash. To date, commercial software packages have been proposed to evaluate various types of crashes. One of the most frequently used packages was VISSIM. Other packages, such as PARAMICS, AIMSUN, and CORSIM, also have notable applications [36]. By a systematic comparison, a review study concluded that none of the current commercial packages have noticeable superiority to the others in terms of safety evaluations [37]. Moreover, these tools have several weaknesses due to specific issues. First, complicated software operations cannot be started up quickly due to the numerous input settings. Second, there are insufficient options for modeling crash-related factors, as the simulation packages are not specially designed for traffic safety. Third, much coding time is needed for integration with surrogate safety measures and for processing output data.

Given that commercial simulation packages are still not targeted for safety evaluations, some recent studies began to develop original simulation frameworks regarding the specific factors of crash occurrences. Some of these simulation models were concerned about the “less-than-perfect” driving strategy associated with human drivers [38,39]. More specifically, factors regarding unsafe driving behavior, such as the inattention interval, variable reaction times, and perception limitations, were incorporated into the behavioral modeling of the simulations. On the other hand, some simulation models have addressed reproducing various crash-prone situations and have provided detailed insight into the mechanism of crash occurrences [34,35,40]. For example, Hou. et al. [40] proposed a holistic framework for safety evaluations based on cellular automata. The simulation model took into account several safety-related factors, including lane configurations and road surfaces in the work zone, adverse weather, and the effect of speed limits. The results suggested that the proposed framework was particularly suitable for a comprehensive evaluation of safety performance under specific driving situations.

2.3. Driver Experience Heterogeneity and Safety. Another key issue with respect to traffic safety is driver experience heterogeneity, which is especially prevalent in developing countries due to the notable growth in the number of novice

drivers [41]. There has been increased interest in the study of driver experience with respect to safety. It was found that the major causes of crashes for novice drivers included inadequate speed control, overreaction delay, and inappropriate attention allocation, all of which could be attributed to the lack of driving experience [42]. Some previous studies carried out experiments to record crash-relevant driving parameter data and compared the difference in safety performance between novice drivers and experienced drivers with statistical methods [43–45]. However, these results were drawn by relating crash occurrences to several driving parameters without considering their differences across various compositions of driver experience. In other words, the studies ignored the fact that drivers behave differently when interacting with various driver populations, and this difference could have unequal impacts under different traffic flow states.

2.4. Summary of the Review. According to our review of previous works, very few studies have focused on applying the simulation-based method to evaluate safety performance in the three-phase traffic theory, and even fewer have also focused on the impacts of driver experience. To this end, it is necessary to develop a systematic simulation framework for evaluating crashes considering driver experience heterogeneity under various traffic flow phases and that is able to benefit safety improvements in terms of both theoretical research and practical applications.

3. Model Development

3.1. Car-Following Model. Notable number of studies carried out car-following models to explain empirical findings in the three-phase theory. The modeling methodology generally includes spatially continuous model and cellular automata model. However, these models did not consider human driving characteristics or suffered from over-rigid modeling framework to avoid crash risk. For example, a classic car-following model named Kerner-Klenov model [18] has complicated update rule of vehicle motion to reproduce the theory from the view of traffic physics rather than human factors. Most cellular automata models [46,47] intend to avoid crash by incorporating rigid safety conditions into the models, which deviates from real driving behavior especially for safety evaluation. Then, this study proposes a new model by introducing typical human factors that are able to explore the relationship between rear-end crash and driver behavior. Moreover, the parameters in the model are expected to have significant meaning in explaining driver experience heterogeneity, and they can be estimated by our experimental data.

Previous studies have demonstrated that when an “indifference zone” is incorporated into a modeling framework for car-following behavior, the resulting model is capable of reproducing empirical findings in the three-phase theory [48]. More specifically, this zone reflects human driver’s psychological characteristics, suggesting that while driving vehicle in car-following scenarios, a driver tends to maintain

spacing or time headway within a satisfactory range instead of achieving an optimal value. The nonoptimal driving strategy has the potential to capture near accident scenarios as it reproduces unsafe driving associated with misjudgment and over reaction delay especially in complicated traffic conditions. Based on this consideration, we propose an improved car-following model by incorporating humans' unconscious reaction feature into the classical Intelligent Driver Model (IDM), which can lead to the occurrence of the "indifference zone."

The proposed unconscious reaction originates from Wiedemann's action point paradigm [49]. Wiedemann suggested that car-following has four reaction regimes identified by action point thresholds. As shown in Figure 1, AX is the desired distance between two successive stationary vehicles, which consists of the length of the leading vehicle and the front-to-rear distance. ABX defines the threshold of the minimum desired spacing with respect to traveling speed. This indicates that the driver realizes the following distance too small and consequently reacts with deceleration. SDX is the threshold of the maximum accepted spacing, which is 1.25–3.0 times ABX. This indicates that a driver perceives themselves to be too far away from the leading vehicle and hence decides to accelerate. CLDV or SDV is the threshold for recognizing the speed difference when approaching the leading vehicle, whereas OPDV is the threshold for recognizing the speed difference during an opening process. These thresholds indicate the action points where drivers react to changes in driving conditions and make the corresponding changes in acceleration.

As seen in Figure 1, within the unconscious regime enclosed by ABX, SDX, CLDV, and OPDV, drivers tend to unconsciously maintain a speed difference and spacing within a satisfactory range rather than maintaining the optimum value. Car-following spirals can be identified due to these nonoptimal expectations [39], resulting in the speed difference and spacing oscillating around the "optimal" state represented by a desired spacing and null speed difference. In this study, we propose an acceleration model to reproduce the car-following spirals based on the dynamic features of vehicle motion.

Figure 2 shows a typical car-following spiral drawn from our empirical data. Two subprocesses can be identified while undergoing a complete car-following spiral. It includes a deceleration subprocess (A-B-C) and an acceleration subprocess (C-D-A). During subprocess A-B-C, for example,

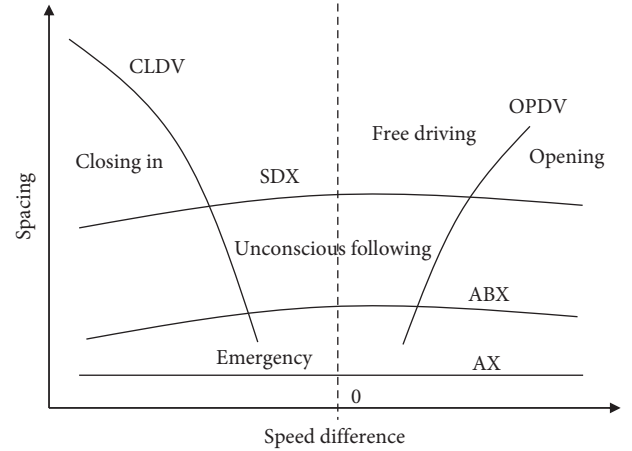


FIGURE 1: Action point thresholds and reaction states of Wiedemann's concept.

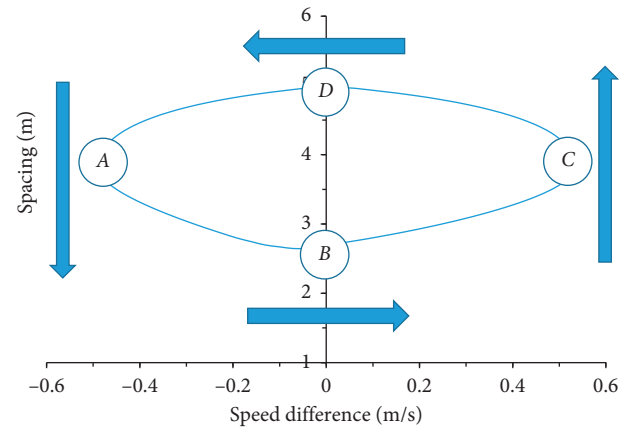


FIGURE 2: A typical spiral extracted from the unconscious reaction regime.

follower driver n starts to decelerate at point A with random deceleration a_n as the driver perceives slower leader $n-1$. Then, the distance between them gradually drops down and reaches an identified ABX value at point B associated with a null speed difference. However, the follower continues to keep decelerating until the speed distance reaches an OPDV value at point C. According to the basic principle of dynamics, the acceleration rates can be determined as follows.

For the subprocess A-B,

$$s_{n-1} + d_n = s_n + ABX, \quad (1)$$

$$\Rightarrow \frac{v_{n-1}(v_{n-1} - v_n)}{a_n} + \frac{1}{2} A_{n-1} \frac{(v_{n-1} - v_n)^2}{a_n^2} + d_n = \frac{v_{n-1}^2 - v_n^2}{2a_n} + ABX, \quad (2)$$

$$\Rightarrow a_n = \frac{\Delta v_n^2 + \sqrt{\Delta v_n^4 - 8(d_n - ABX)A_{n-1}\Delta v_n^2}}{4(ABX - d_n)}, \quad (3)$$

where $\Delta v_n = v_{n-1} - v_n$ is the speed difference between vehicle n and its leading vehicle and d_n is the net distance (gap) between the two vehicles. s_n is the distance traveled by vehicle n during subprocess A-B, and A_{n-1} is the initial acceleration rate of the leader at A. ABX is the identified action point at point A. A previous study found that the acceleration rate within the unconscious regime did not exceed the range of -0.6 m/s^2 and 0.6 m/s^2 and varied according to a certain probability [50,51]. Then, the acceleration rate is modified as follows:

$$a_n = \max \left\{ \frac{\Delta v_n^2 + \sqrt{\Delta v_n^4 - 8(d_n - \text{ABX})A_{n-1}\Delta v_n^2}}{4(\text{ABX} - d_n)} \times \text{NRND}, -0.6 \right\}, \quad (4)$$

where NRND is a normally distributed random parameter [51]. The acceleration rates during other subprocesses can be determined as above. They are presented in (5)–(7).

For the subprocess B-C,

$$a_n = \max \left\{ \frac{\text{OPDV}^2}{2(d_n - \text{SDX})} \times \text{NRND}, -0.6 \right\}. \quad (5)$$

For the subprocess C-D,

$$a_n = \min \left\{ \frac{\Delta v_n^2 + \sqrt{\Delta v_n^4 - 8(d_n - \text{SDX})A_{n-1}\Delta v_n^2}}{4(\text{SDX} - d_n)} \times \text{NRND}, 0.6 \right\}. \quad (6)$$

For the subprocess D-A,

$$a_n = \min \left\{ \frac{\text{CLDV}^2}{2(d_n - \text{ABX})} \times \text{NRND}, 0.6 \right\}, \quad (7)$$

where OPDV, SDX, and CLDV are the identified action points at points B, C, and D. The other variables have the same meaning as in (1)–(4).

When a vehicle passes any of the action point thresholds enclosing the unconscious regime, drivers consciously make changes in acceleration in response to variations in the driving environment. In this study, the IDM is proposed to

capture the dynamic features within conscious reaction regimes. The model is calculated by the following equations:

$$a_n(t + \tau) = a \left[1 - \left(\frac{v(t)}{v_0} \right)^4 - \left(\frac{S_{\text{des}}(t)}{d_n(t)} \right)^2 \right], \quad (8)$$

where a is the maximum acceleration, τ is the driver's reaction time, and S_{des} is the desired safety gap, which is written as follows:

$$S_{\text{des}}(t) = S_0 + v_n(t)T + \frac{v_n(t)\Delta v_n(t)}{2\sqrt{ab}}, \quad (9)$$

where S_0 is the jam distance when the vehicle stops, T is the desired safety time gap, and b is the desired deceleration.

3.2. Surrogate Safety Measure. Surrogate safety measures can be divided into two categories, including time-related indicator and energy-related indicator. For example, the time to collision (TTC) has been considered a major surrogate safety measure in crash evaluations. Previous studies have demonstrated that the TTC is able to indicate the probability of a crash but cannot describe the severity of a crash as speed is not involved in the measure [52]. In comparison, the energy-related indicator is developed by taking into account the kinetics (usually represented by speed or speed difference) to describe the severity of a crash. The estimation of such indicators usually needs to identify accurate trajectories with respect to conflicting vehicles. However, it lacks the associated data considering driver experience heterogeneity across various traffic phases. The simulation-based approach has advantages for studies using surrogate safety measures, as it is much less dependent on actual crash data, and intravehicle interactions of high resolution are allowed to be reproduced and collected. Therefore, this study developed a modified surrogate safety measure to evaluate rear-end crashes by integrating it with the proposed simulation model. More specifically, the measure comprehensively considers the probability of a rear-end crash and the associated severity based on the deceleration rate to avoid crash (DRAC). The DRAC is calculated as follows:

$$\text{DRAC}_n(t) = \frac{[v_n(t) - v_{n-1}(t)]^2}{2[x_n(t) - x_{n-1}(t) - L_{n-1}]}, \quad (10)$$

$$= \frac{[v_n(t) - v_{n-1}(t)]}{2[x_n(t) - x_{n-1}(t) - L_{n-1}]/[v_n(t) - v_{n-1}(t)]} = \frac{[v_n(t) - v_{n-1}(t)]}{2\text{TTC}_n(t)}, \quad (11)$$

where $\text{DRAC}_n(t)$ and $\text{TTC}_n(t)$ are the DRAC and the time to collision (TTC) of a following vehicle n at time t . $v_n(t)$ and $v_{n-1}(t)$ correspond to the speeds of vehicle n and leader $n-1$, respectively. $x_n(t)$ and $x_{n-1}(t)$ show the positions of vehicle n and leader $n-1$, respectively.

It is worth mentioning that, as shown in (11), the denominator (TTC) implies the crash likelihood, while the numerator (speed difference) indicates the severity of

the rear-end crash. According to previous studies, the smaller the TTC value, the higher the probability of a collision occurrence. Moreover, the greater the speed difference, the greater the energy generated by a vehicle collision, and the higher the severity of the crash. Thus, it is encouraging that DRAC has the ability to simultaneously evaluate traffic safety performance in terms of probability and severity.

A representative previous study [53] suggested that the integration of surrogate safety measure over space and time is able to fully utilize the advantages of simulation-based method. Driven by this consideration, we propose an integrated DRAC (IDRAC) through a generalization of the concept of time integrated time to collision (TIT) [53]. This

$$\text{IDRAC} = \sum_{n=1}^N \int_0^T [\text{DRAC}_n(t) - \text{DRAC}^*] dt, \quad \forall \text{DRAC}_n(t) > \text{DRAC}^*, \quad (12)$$

where N is the sample size of drivers and T is the time duration of observation or simulation. Furthermore, considering the fact that a simulation time is discretely driven,

$$\text{IDRAC} = \sum_{n=1}^N \sum_0^T [\text{DRAC}_n(t) - \text{DRAC}^*] \Delta t, \quad \forall \text{DRAC}_n(t) > \text{DRAC}^*. \quad (13)$$

To make the simulation results comparable with different sample sizes and time durations, IDRAC needs to be standardized to obtain the average IDRAC per vehicle per unit time:

$$\overline{\text{IDRAC}} = \frac{\text{IDRAC}}{N \cdot T}. \quad (14)$$

The combination of $\overline{\text{IDRAC}}$ and traffic simulation models hold promise for the safety evaluation as a DRAC value is standardized over a specific time horizon T for a certain roadway segment on which N vehicles run. Moreover, the probability of crashes as well as the associated severity can be evaluated by the modified indicator, simultaneously. Note that the critical safety threshold DRAC^* is related to factors such as driver characteristics, vehicle performance, traffic flow conditions, and road conditions. DRAC^* usually ranges from 1 m/s^2 to 3.5 m/s^2 . Because the proposed car-following does not consider some factors that may cause traffic accidents, such as driver distractions, operation errors, and illegal driving, a smaller value of 1.5 m/s^2 for the critical safety threshold is selected in the current study as a criterion for judging whether a traffic conflict incident is occurring.

4. Field Data Collection

4.1. Data Collection Environment. In this study, car-following data were measured on an eight-lane highway section over a length of 3.8 km in the city of Nanjing, China. The highway plays an important role in serving major traffic demand in the eastern area of Nanjing. More specifically, an average of more than 35,000 vehicles traveled through the experimental section every day in 2018. The speed limit is set at 80 km/h. Furthermore, the experimental section has the following characteristics with respect to geometric design, traffic states and environmental conditions: (1) the traffic in

surrogate safety measure focuses on general performance, which is calculated by the sum of the DRAC values that are higher than the critical safety threshold DRAC^* within the range of the investigation road section over time. The indicator can be determined as follows:

the time-discrete version of IDRAC is modified by the following equation:

both directions is separated by a physical central median, (2) the road pavement of the section is in good condition, (3) the traffic is mainly composed of passenger vehicles, and (4) the intensity of land-use development on either side of the section is limited.

4.2. Device System. To capture drivers' car-following characteristics in a natural traffic environment, a dedicated data collection system that uses an instrumented vehicle mounted with a GPS device, a laser rangefinder, and a microcomputer is developed. Figure 3 provides an overview of the data collection system and the instrumented vehicle. More specifically, GPS is used to track the instrumented vehicle's latitude and longitude coordinates, which can be converted to trajectory data. The laser rangefinder aims to determine the distance by measuring from the rear of the leading vehicle to the head of the instrumented vehicle. The laser rangefinder covers a range of approximately 100 m. The microcomputer can synchronize the GPS data and spacing data and store them in a format that can be read by the dedicated software. For the data validity test, the experimental scenario is recorded with a digital camera.

To ensure that the laser rangefinder's emission beam can reach the rear plate of the leading vehicle, it is mounted on the platform behind the windshield. The GPS device is fixed inside the vehicle. The microcomputer lies on the passenger seat and always maintains wired connections to the laser rangefinder and the GPS device. The digital camera is placed on the backrest of the rear seat to monitor the driver's behavior and the forward roadway. The instrumented vehicle (Figure 3(b)) equipped with the data collection system is a Hyundai Sonata, which has an engine displacement of 2.0 liters. This vehicle type has a dynamic performance similar to that of most vehicles traveling on the experimental section.



FIGURE 3: The device system and the instrumented vehicle. (a) The device system includes a laser rangefinder, a GPS device, and a microcomputer. (b) The instrumented vehicle is a Hyundai Sonata with an engine displacement of 2.0.

4.3. Participants. A total of 41 participants, including 20 experienced drivers and 21 novice drivers, were recruited in this study. They mainly differed in, first, driving experience (years) and, second, cumulative mileage (km). Drivers with less than 2 years of driving experience and no more than 12,000 km of cumulative mileage were categorized as novice drivers and otherwise categorized as experienced drivers. The results of the t -test indicated that there was no significant difference in gender between the two driver population groups. Male participants accounted for 71.1% and 69.1% of the drivers in the two groups. The average ages of the experienced and novice participants were 38.7 years old and 28.5 years old, respectively.

4.4. Procedure. The car-following data used in this study were collected under good weather conditions to avoid the impact of weather factors on the driving environment. The duration of the experiment spanned typical time periods, including morning rush hours, off-rush hours, and evening rush hours on various weekdays. During an experiment tour, the participants drove the instrumented vehicle in a natural driving environment without any interference from our research team. More specifically, every participants were employed to complete 2 tours which covered rush peak and off-rush peak. Each tour experienced a duration of 1 hour consisted of 15 minutes to get familiar with the instrumented vehicle and 45 minutes to drive as usual for data collection. Both the laser rangefinder and the GPS worked at a frequency of 1 Hz.

It should be noted that the measured following distance sometimes missed as the leading vehicle steered or when some random factors interrupted the emission beam. Locally weighted regression (LWR) is a statistical learning method that has been used for capturing missing data [54]. In this study, LWR is then used to yield the leading vehicles' trajectory profiles. The following distance is calculated by identifying the distance between the trajectory of the instrumented vehicle and that of the leading vehicle.

5. Results

5.1. Model Calibration. Empirical car-following spirals are taken from the collected data, and candidate action points are identified according to Brackstone's concept [55]. Furthermore, the perpetual thresholds including ABX, SDX, CLDV, and OPDV are fitted to the identified 95% values of the candidate action points by relating them to the speed or spacing. In this study, a linear relationship was used, which has been demonstrated by previous works to show good consistency with the data [56]. More specifically, the fitted thresholds for experienced drivers and novice drivers are shown as follows. For the experienced drivers,

$$\begin{aligned} \ln(\text{OPDV}) &= -1.029 + 0.043 \times v, \\ \ln(\text{CLDV}) &= -0.725 + 0.055 \times v, \\ \text{ABX} &= 1.914 + 1.767 \times \sqrt{v}, \\ \text{SDX} &= 1.83 \times \text{ABX}. \end{aligned} \quad (15)$$

For the novice drivers,

$$\begin{aligned} \ln(\text{OPDV}) &= -0.876 + 0.045 \times v, \\ \ln(\text{CLDV}) &= -0.547 + 0.040 \times v, \\ \text{ABX} &= 2.103 + 2.022 \times \sqrt{v}, \\ \text{SDX} &= 2.40 \times \text{ABX}, \end{aligned} \quad (16)$$

where v is the travel speed.

The R-square values for all of the fitted functions above are over 0.8, indicating good performance for determining the relationship between action points and driving parameters. It is worth noting that the fitted results imply that the "indifference zone" for experienced drivers has a smaller area, which may lead to improvements in safety performance, especially in the traffic oscillation under congested phases. The detailed discussion about the safety impacts of driver experience heterogeneity will be presented in Section 5.4.

By means of the genetic algorithm, the best parameter settings of the proposed car-following model for the

collected data are found, as shown in Table 1. As seen, experienced drivers prefer a larger desired speed and maximum acceleration and keep a smaller desired time gap and stop distance. In general, they tended to implement relatively aggressive driving manners compared with novice drivers. This may originate from their skillful driving experience in terms of perceiving and reacting to variations in the traffic environment. Theoretically, these differences in driving parameters indicate that driver experience heterogeneity could have significant impacts on traffic characteristics and safety performance.

In the next sections, periodic boundary conditions are selected for numerical simulations. The length of the road section is 2000 m, the vehicle length is 5 m, and the simulation step is 0.1 s. The default initial traffic consists of all novice drivers. A simulation first runs with a warm-up duration of 3600 s to eliminate the transient effects, and then the relevant traffic data are collected after the warm-up period.

5.2. Basic Traffic Flow Characteristics. The following two initial conditions are implemented to explore the basic traffic characteristics of the proposed model: (1) vehicles are homogeneously distributed on the test road and (2) vehicles are distributed a mega-jam form. Moreover, the simulated traffic consisted 100% novice drivers as their safety performance constitutes a major concern of this study. The fundamental diagram is presented in Figure 4, where the data points are the aggregations over 5 min flow rate data collected from the virtual detectors.

Three various traffic phases can be identified, which is consistent with the three-phase traffic theory. When the occupancy rate is low, the traffic operates under free flow phase in which drivers drive steadily at their own desired speed. The flow rate increases approximately linearly with the increase in the density. When the density reaches $k_1 < k < k_c$, the free flow is in a metastable state, indicating that the phase transition $F \rightarrow S$ may occur with probability as the internal disturbance of the traffic may exceed a certain extent. The critical occupancy k_c corresponds to the maximum flow rate that the free flow can reach.

When the density reaches $k_c < k < k_2$, synchronized flow emerges. Due to the decrease in the distance between vehicles, vehicle motion is restricted by the associated leading vehicle, and the traveling speed is significantly lower than drivers' expectation. The flow rate decreases with the increasing occupancy. In this phase, car-following spirals can be identified within the corresponding "indifference zone." Such unconscious driving stabilizes traffic because of the absence of overreaction to small speed difference between successive vehicles. Then, local fluctuations will not be enhanced, and no traffic jams occur within the traffic flow. However, if the vehicles are initially distributed in a mega-jam form, the jam does not dissipate over time.

When the density further exceeds k_2 , jams spontaneously occur within the synchronized flow. Within this density range, fluctuations caused by a vehicle can trigger the followers to take overdeceleration, which causes the

TABLE 1: The calibrated parameter sets.

Driver population	Model parameters					
	v_0 (m/s)	S_0 (m)	T (s)	A (m/s ²)	b (m/s ²)	τ (s)
The novice	21.94	2.35	1.65	0.81	-1.92	1.35
The experienced	25.27	1.75	1.12	0.88	-1.56	1.05

amplitude of the fluctuation to intensify while propagating upstream of the traffic. The internal density of a jam is extremely high, and the speed nearly decreases to a null value. The downstream boundary of a jam propagates upstream of the traffic with a rough constant speed, and there coexists free flow and synchronized flow between jams.

5.3. Evaluating Safety Performance in the Three-Phase Theory.

The simulation environment developed in the current study is used to evaluate the safety performance with respect to each traffic phase in the framework of three-phase theory. The occupancy is taken as the measure to indicate the traffic phase, and it varies between 0.0 and 0.6, which covers the entire phase spectrum. Fifteen independent simulations are carried out, and the corresponding variation trends of $\overline{\text{IDRAC}}$ are shown in Figure 5.

As seen in the simulation results, when the occupancy of traffic flow keeps in low range (< 0.16), the $\overline{\text{IDRAC}}$ value is close to 0, suggesting that the crash probability and severity are very small. As the occupancy continues to increase, the $\overline{\text{IDRAC}}$ increases sharply and reaches a peak near the critical occupancy (an occupancy at which the capacity occurs). This can be explained by the fact that small spacing with relatively high speed can lead to crashes with high uncertainty. When the occupancy further increases, $\overline{\text{IDRAC}}$ significantly decreases and fluctuates within a certain range, indicating an improvement in the safety performance. As the occupancy increases beyond a certain threshold (approximately 0.36), $\overline{\text{IDRAC}}$ increases again and then gradually decreases.

Figure 6 is a scatter plot of the average $\overline{\text{IDRAC}}$ values associated with different occupancies. According to the three-phase traffic flow theory, we propose the following statements:

- (i) When the average occupancy is low, the traffic state corresponds to the free flow phase, in which vehicles can run at their own desired speed and the distances between pairs of successive vehicles are large. The relaxed driving environment leads to small $\overline{\text{IDRAC}}$ values. The result indicates that the probability of the occurrence of a rear-end crash as well as the potential severity is low.
- (ii) As the occupancy gradually increases to the vicinity of the critical occupancy, the traffic flow is in the metastable state in which the transition from free flow to synchronized flow occurs with probability. Aggressive behaviors such as abrupt acceleration and overdeceleration would cause fluctuation, which can be intensified when propagating along a vehicle platoon. Compared with the free flow phase,

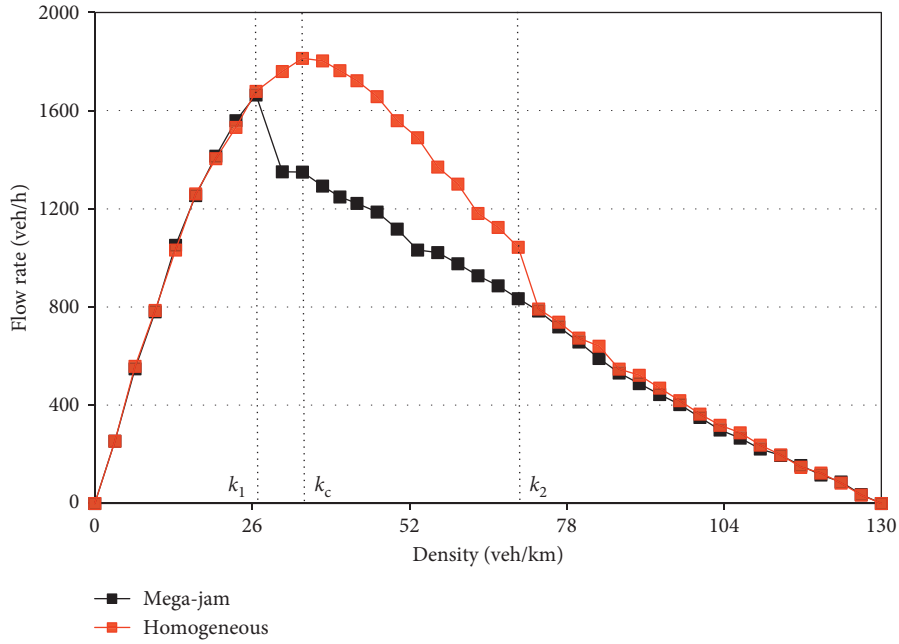


FIGURE 4: Fundamental diagram of the proposed model. Each data point is the average of 10 individual simulation runs that last 3600 time steps.

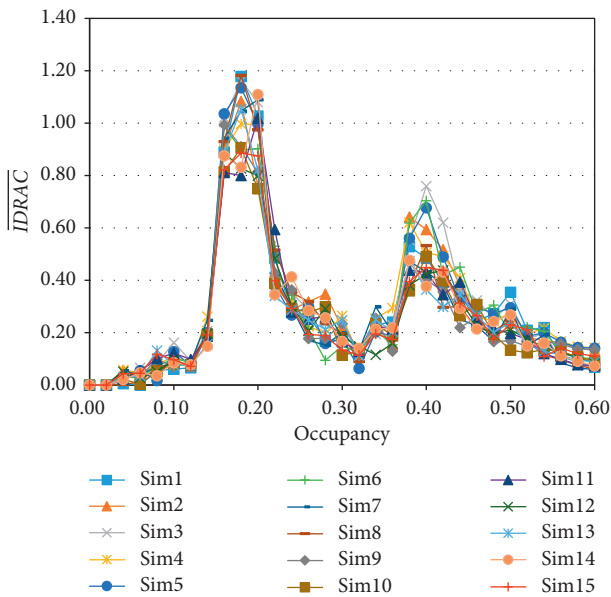


FIGURE 5: The variation trends of \overline{IDRAC} associated with the occupancy for 15 independent simulations.

\overline{IDRAC} dramatically increases, suggesting that the safety performance under this traffic state significantly deteriorates.

- (iii) When the occupancy exceeds the critical value, synchronized flow inevitably emerges. In this phase, as spacing and travel speed significantly decrease, drivers tend to take more cautious driving decisions in terms of driving with stable accelerations. Then, \overline{IDRAC} decreases and keeps within a relatively small range. The result indicates that the probability of a

crash as well as the potential severity are substantially reduced.

- (iv) As the formation of wide moving jams is usually accompanied by stop-and-go traffic, the speed difference between pairs of successive vehicles sharply increases, which contributes to an increase in \overline{IDRAC} , suggesting a higher crash probability and severity.

5.4. Evaluating the Impacts of Driver-Experienced Heterogeneity.

The proposed car-following model is calibrated to fit the measured data associated with novice drivers and experienced drivers. Thus, our simulation is capable of capturing driver experience heterogeneity for rear-end crash evaluation. The results in the above sections are achieved by assuming that traffic is consisted of 100% novice drivers. However, in real situations, both the novice and the experienced occupy significant proportions in traffic. In this section, the scenario of 100% novice drivers is set to be the base condition, and different proportions of experienced drivers are considered to study the impacts of driver experience heterogeneity on traffic safety performance. More specifically, the simulations are performed by increasing the proportion of experienced drivers from 0% to 100% with a step size of 10%, and a range of traffic occupancies between 0.0 and 0.6 is also applied as previously mentioned. The results are shown in Figure 7.

With the increase in the proportion of experienced drivers in the traffic flow, the values of \overline{IDRAC} in the free flow state do not change significantly. In the metastable state, the difference in \overline{IDRAC} values from the base condition gradually increases until the experienced drivers account for 60% of the drivers on the road, and then it decreases. When

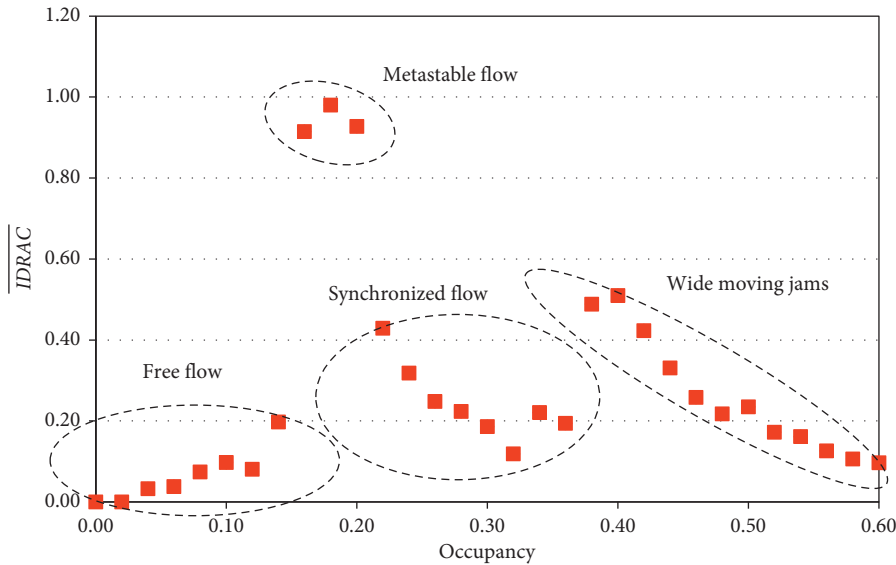


FIGURE 6: Scatter plot of the average \overline{IDRAC} values under different traffic phases.

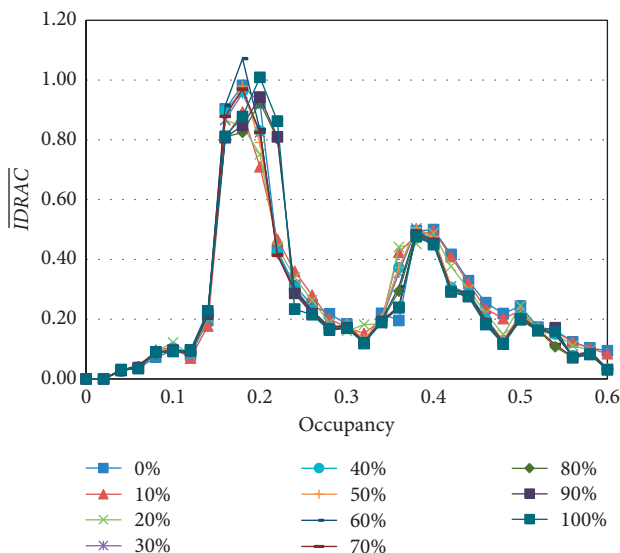


FIGURE 7: The variation trends of \overline{IDRAC} associated with different proportions of experienced drivers.

the occupancy reaches the levels of the congested phases (i.e., including synchronized flow and wide moving jam phases), this difference has a further downward trend. According to these simulated results, the following can be concluded .

- (i) Due to the large spacing between successive vehicles in free flow, there is ample driving space, and the crash is not sensitive to the change in the compositions of driver experience.
- (ii) In the metastable free flow, traffic breakdown can be triggered by small disturbance such as over-deceleration. The ever-increasing traffic occupancy leads to a significant shrink of the spacing between vehicles, whereas the traveling speed is still closed to the free flow speed. According to the

calibration results of the simulation model parameters, experienced drivers tend to drive with a more aggressive style in terms of smaller spacings and faster speeds, consequently resulting in rear-end crashes with higher probability and severity. The result is also consistent with some previous studies [57,58] which argued that aggressive driving had negative impacts on driving safety. It is worth mentioning that the maximum value of \overline{IDRAC} occurs when the percentage of experienced drivers reaches 60% (see Table 2). This implies that the higher the heterogeneity of the traffic composition, the worse the safety performance.

- (iii) In the congested phases, the traveling speed drops dramatically, indicating that a driver’s sensitivity to changes in the surrounding environment plays a major role in safety performance. This sensitivity is represented by the area of the “indifference zone” enclosed by the perpetual thresholds, as a follower in the zone is not sensitive to the speed difference of the leader. Then, the larger the area is, the less sensitive the follower is to the stimulus in terms of speed difference. Therefore, according to the fitted parameters, the presence of novice drivers brings about negative impacts on driving safety, as they have a larger “indifference zone” area and higher response delays.
- (iv) As can be drawn from the results above, the occurrence of rear-end crash is explained by a competition between headway and sensitivity to speed difference. Smaller headway is more likely to bring about a tendency towards a rear-end crash in the metastable flow, whereas less sensitivity to speed variation plays a more important role in such tendency when driving under the congested phases.

TABLE 2: The impact of driver experience heterogeneity on $\overline{\text{IDRAC}}$ under metastable flow.

Proportion of experienced drivers (%)	Traffic occupancy related with the metastable flow			
	0.16	0.18	0.2	0.22
0	0.915	0.980	0.927	0.429
10	0.807	0.893	0.709	0.467
20	0.865	0.847	0.751	0.440
30	0.866	0.955	0.825	0.425
40	0.899	0.962	0.829	0.424
50	0.876	0.980	0.791	0.417
60	0.914	1.072	0.833	0.416
70	0.878	0.970	0.825	0.414
80	0.810	0.825	0.926	0.803
90	0.808	0.847	0.943	0.810
100	0.812	0.877	1.009	0.862

6. Conclusion

The current study evaluates rear-end crash risk by developing a microsimulation in the framework of three-phase theory. The safety impact of driver experience heterogeneity is also considered as a major reason in the crash evaluation. A car-following model is developed by incorporating the classical action point paradigm and the IDM. This modeling methodology can explain human drivers' psychological factors for safety assessments. Field data collection is carried out to collect car-following data with respect to novice drivers and experienced drivers, respectively. The data is used to calibrate the proposed car-following model. A surrogate safety measure is proposed by the concept of integrating an individual's DRAC over spacing and time, which is suitable for simulation analysis. Moreover, the measure can simultaneously quantify the probability of a rear-end crash as well as the potential severity.

The simulation results show that the proposed car-following model is capable of simulating typical traffic dynamics in the framework of three-phase theory. More specifically, the model reproduces the three phases, including free flow (F), synchronized flow (S), and wide moving jams (J). These complicated empirical findings are captured by introducing the "indifference zone" into the modeling of car-following behavior. It is worth mentioning that the "indifference zone" has correlation with human drivers' nonoptimal driving strategies, which can provide better performance in catching near accident scenarios.

In the safety assessment, traffic phase transitions lead to changes in driving behavior and interactions among vehicles, which causes the proposed $\overline{\text{IDRAC}}$ value to change with the corresponding traffic phase. This implies that the probability of a crash and the potential severity are related to the traffic flow phase. More specifically, safety performance achieves the highest level in free flow. Nevertheless, the probability and severity of crashes sharply increase in the metastable state, where the transition from free flow to synchronous flow has a probability of occurring, and decrease when traffic completely evolves into a synchronized

flow. However, stop-and-go traffic in wide moving jams again brings about negative impacts on safety performance.

Driver experience heterogeneity has a profound impact on rear-end crashes. The presence of novice drivers affects the safety performance in two ways. On the one hand, novice drivers have drawbacks in responding to risk situations in terms of a larger "indifference zone" and reaction time, and this brings about a higher value of $\overline{\text{IDRAC}}$ under the synchronized phase and the jam phase. On the other hand, novice drivers tend to maintain a larger gap and slower speeds. In the face of metastable flow, such drivers can stabilize traffic due to larger safety margins, reducing the crash probability and the potential severity. Moreover, the simulation results indicate that as the composition of driver experience becomes more heterogeneous, the safety performance deteriorates associated with a higher value of $\overline{\text{IDRAC}}$.

The current study makes efforts to advance a comprehensive methodology for traffic safety evaluation through simulation. However, some problems need to be considered in future works. First, lane-changing behavior could be introduced into the simulation to analyze broader and more complicated situations, such as merging and diverging bottlenecks. Second, it is expected that the simulation performance would be improved by expanding the amount of driving behavior data with a naturalistic collection method. Finally, traffic control measures such as variable speed limits have correlation with crash risk and then their safety impacts in the three-phase theory could be evaluated by an integration with the proposed simulation environment. We recommend that future studies address these issues.

Data Availability

The data used to support the findings of this study are available from the corresponding author upon request.

Conflicts of Interest

The authors declare that they have no conflicts of interest.

Acknowledgments

This research was funded by the National Natural Science Foundation of China (71801080), Fundamental Research Funds for the Central Universities (B200202068), and Jiangsu Postdoctoral Research Funding Program (2018K043B).

References

- [1] R. Yu and M. Abdel-Aty, "An optimal variable speed limits system to ameliorate traffic safety risk," *Transportation Research Part C: Emerging Technologies*, vol. 46, pp. 235–246, 2014.
- [2] X. Luo, D. Li, Y. Yang, and S. Zhang, "Spatiotemporal traffic flow prediction with KNN and LSTM," *Journal of Advanced Transportation*, vol. 2019, Article ID 4145353, 10 pages, 2019.

- [3] S. Gokhale, "Impacts of traffic-flows on vehicular-exhaust emissions at traffic junctions," *Transportation Research Part D: Transport and Environment*, vol. 17, no. 1, pp. 21–27, 2012.
- [4] T. F. Golob and W. W. Recker, "A method for relating type of crash to traffic flow characteristics on urban freeways," *Transportation Research Part A: Policy and Practice*, vol. 38, no. 1, pp. 53–80, 2004.
- [5] T. F. Golob, W. W. Recker, and V. M. Alvarez, "Freeway safety as a function of traffic flow," *Accident Analysis & Prevention*, vol. 36, no. 6, pp. 933–946, 2004.
- [6] M. A. Abdel-Aty and R. Pemmanaboina, "Calibrating a real-time traffic crash-prediction model using archived weather and ITS traffic data," *IEEE Transactions on Intelligent Transportation Systems*, vol. 7, no. 2, pp. 167–174, 2006.
- [7] M. Hossain and Y. Muromachi, "Understanding crash mechanism and selecting appropriate interventions for real-time hazard mitigation on urban expressways," *Transportation Research Record: Journal of the Transportation Research Board*, vol. 2213, no. 1, pp. 53–62, 2011.
- [8] A. Pande, A. Das, M. Abdel-Aty, and H. Hassan, "Real-time crash risk estimation are all freeways created equal?" *Transportation Research Record: Journal of the Transportation Research Board*, vol. 2237, no. 1, pp. 60–66, 2011.
- [9] D. A. Hennessy and D. L. Wiesenthal, "Traffic congestion, driver stress, and driver aggression," *Aggressive Behavior*, vol. 25, no. 6, pp. 409–423, 1999.
- [10] G. Chang and H. Xiang, "The relationship between congestion levels and accidents," *Report*, 2005.
- [11] F. G. Habtemichael and L. de Picado Santos, "Crash risk evaluation of aggressive driving on motorways: microscopic traffic simulation approach," *Transportation Research Part F: Traffic Psychology and Behaviour*, vol. 23, pp. 101–112, 2014.
- [12] B. S. Kerner, "Empirical macroscopic features of spatial-temporal traffic patterns at highway bottlenecks," *Physical Review E, Statistical, Nonlinear, and Soft Matter Physics*, vol. 65, Article ID 046138, 2002.
- [13] C. Xu, P. Liu, W. Wang, and Z. Li, "Identification of freeway crash-prone traffic conditions for traffic flow at different levels of service," *Transportation Research Part A: Policy and Practice*, vol. 69, pp. 58–70, 2014.
- [14] C. Xu, P. Liu, W. Wang, and Z. Li, "Evaluation of the impacts of traffic states on crash risks on freeways," *Accident Analysis & Prevention*, vol. 47, pp. 162–171, 2012.
- [15] B. S. Kerner and H. Rehborn, "Experimental properties of complexity in traffic flow," *Physical Review E, Statistical Physics, Plasmas, Fluids, and Related Interdisciplinary Topics*, vol. 53, no. 5, pp. R4275–R4278, 1996.
- [16] B. S. Kerner and H. Rehborn, "Experimental features and characteristics of traffic jams," *Physical Review E*, vol. 53, no. 2, pp. R1297–R1300, 1996.
- [17] B. S. Kerner and H. Rehborn, "Experimental properties of phase transitions in traffic flow," *Physical Review Letters*, vol. 79, no. 20, pp. 4030–4033, 1997.
- [18] B. S. Kerner and S. L. Klenov, "A microscopic model for phase transitions in traffic flow," *Journal of Physics A: Mathematical and General*, vol. 35, no. 3, pp. 31–43, 2002.
- [19] B. S. Kerner and S. L. Klenov, "Microscopic theory of spatial-temporal congested traffic patterns at highway bottlenecks," *Physical Review E, Statistical, Nonlinear, and Soft Matter Physics*, vol. 68, no. 2, Article ID 036130, 2003.
- [20] R. Kouhi Esfahani, F. Shahbazi, and M. Akbarzadeh, "Three-phase classification of an uninterrupted traffic flow: a k-means clustering study," *Transportmetrica B: Transport Dynamics*, vol. 7, no. 1, pp. 546–558, 2019.
- [21] J. Tian, R. Jiang, G. Li, M. Treiber, B. Jia, and C. Zhu, "Improved 2D intelligent driver model in the framework of three-phase traffic theory simulating synchronized flow and concave growth pattern of traffic oscillations," *Transportation Research Part F: Traffic Psychology and Behaviour*, vol. 41, pp. 55–65, 2016.
- [22] S. Lee, B. Heydecker, Y. H. Kim, and E. Y. Shon, "Dynamic OD estimation using three phase traffic flow theory," *Journal of Advanced Transportation*, vol. 45, no. 2, pp. 143–158, 2011.
- [23] C. Xu, P. Liu, W. Wang, and Z. Li, "Safety performance of traffic phases and phase transitions in three phase traffic theory," *Accident Analysis & Prevention*, vol. 85, pp. 45–57, 2015.
- [24] J. Zhang, K. R. Wu, M. Cheng, M. Yang, Y. Cheng, and S. Li, "Safety evaluation for connected and autonomous vehicles' exclusive lanes considering penetrate ratios and impact of trucks using surrogate safety measures," *Journal of Advanced Transportation*, vol. 2020, Article ID 5847814, 17 pages, 2020.
- [25] U. Shandah, F. Saccomanno, and B. persaud, "Application of traffic microsimulation for evaluating safety performance of urban signalized intersections," *Transportation Research Part C: Emerging Technologies*, vol. 60, pp. 96–104, 2015.
- [26] S. Klauer, E. Olsen, B. Simons-Morton, and T. A. Dingus, "Detection of road hazards by novice teen and experienced adult drivers," *Transportation Research Record: Journal of the Transportation Research*, vol. 2078, pp. 26–32, 2008.
- [27] C. Oh and T. Kim, "Estimation of rear-end crash potential using vehicle trajectory data," *Accident Analysis & Prevention*, vol. 42, no. 6, pp. 1888–1893, 2010.
- [28] M. Abdel-Aty, N. Uddin, A. Pande, M. F. Abdalla, and L. Hsia, "Predicting freeway crashes from loop detector data by matched case-control logistic regression," *Transportation Research Record: Journal of the Transportation Research*, vol. 1897, no. 1, pp. 88–95, 2004.
- [29] M. M. Haque, H. C. Chin, and A. K. Debnath, "An investigation on multi-vehicle motorcycle crashes using log-linear models," *Safety Science*, vol. 50, no. 2, pp. 352–362, 2012.
- [30] J. Yuan, M. Abdel-Aty, L. Wang, J. Lee, R. Yu, and X. Wang, "Utilizing bluetooth and adaptive signal control data for real-time safety analysis on urban arterials," *Transportation Research Part C: Emerging Technologies*, vol. 97, pp. 114–127, 2018.
- [31] L. Lin, Q. Wang, and A. W. Sadek, "A novel variable selection method based on frequent pattern tree for real-time traffic accident risk prediction," *Transportation Research Part C: Emerging Technologies*, vol. 55, pp. 444–459, 2015.
- [32] L. Wang, M. Abdel-Aty, J. Lee, and Q. Shi, "Analysis of real-time crash risk for expressway ramps using traffic, geometric, trip generation, and socio-demographic predictors," *Accident Analysis & Prevention*, vol. 122, pp. 378–384, 2019.
- [33] T. Huang, S. Wang, and A. Sharma, "Highway crash detection and risk estimation using deep learning," *Accident Analysis & Prevention*, vol. 135, Article ID 105392, 2020.
- [34] X. Hu, W. Wang, and H. Yang, "Mixed traffic flow model considering illegal lane-changing behavior: simulations in the framework of kerner's three-phase theory," *Physica A: Statistical Mechanics and Its Applications*, vol. 391, no. 21, pp. 5102–5111, 2012.
- [35] Y. Li, Z. Yang, J. Lu, and L. Zhang, "A mixed-flow cellular automaton model for vehicle nonstrict priority give-way behavior at crosswalks," *Journal of Advanced Transportation*, vol. 2020, Article ID 5847814, 11 pages, 2020.
- [36] W. Young, A. Sobhani, M. G. Lenné, and M. Sarvi, "Simulation of safety: a review of the state of the art in road safety

- simulation modelling,” *Accident Analysis & Prevention*, vol. 66, pp. 89–103, 2014.
- [37] S. M. S. Mahmud, L. Ferreira, M. S. Hoque, and A. Tavassoli, “Micro-simulation modelling for traffic safety: a review and potential application to heterogeneous traffic environment,” *IATSS Research*, vol. 43, no. 1, pp. 27–36, 2019.
- [38] W. Xin, J. Hourdos, P. Michalopoulos, and G. Davis, “The less-than-perfect driver: a model of collision-inclusive car-following Behavior,” *Transportation Research Record: Journal of the Transportation Research*, vol. 2088, no. 1, pp. 126–137, 2008.
- [39] M. Treiber, A. Kesting, and D. Helbing, “Delays, inaccuracies and anticipation in microscopic traffic models,” *Physica A: Statistical Mechanics and Its Applications*, vol. 360, no. 1, pp. 71–88, 2006.
- [40] G. Hou and S. Chen, “Study of work zone traffic safety under adverse driving conditions with a microscopic traffic simulation approach,” *Accident Analysis & Prevention*, vol. 145, Article ID 105698, 2020.
- [41] H. Yang and Z. Wu, “Effect of novice driver’s car-following characteristic on roadway segment capacity,” *Advances in Mechanical Engineering*, vol. 9, no. 5, pp. 1–11, 2017.
- [42] S. Peer, A. Muermann, and K. Sallinger, “App-based feedback on safety to novice drivers: learning and monetary incentives,” *Transportation Research Part F: Traffic Psychology and Behaviour*, vol. 71, pp. 198–219, 2020.
- [43] Z. Yang, Q. Yu, W. Zhang, and H. Shen, “A comparison of experienced and novice drivers’ rear-end collision avoidance maneuvers under urgent decelerating events,” *Transportation Research Part F: Traffic Psychology and Behaviour*, vol. 76, pp. 353–368, 2021.
- [44] J. P. Ehsani, K. E. Seymour, T. Chirles, and N. Kinnear, “Developing and testing a hazard prediction task for novice drivers: a novel application of naturalistic driving videos,” *Journal of Safety Research*, vol. 73, pp. 303–309, 2020.
- [45] E. Chan, A. K. Pradhan, A. Pollatsek, M. A. Knodler, and D. L. Fisher, “Are driving simulators effective tools for evaluating novice drivers’ hazard anticipation, speed management, and attention maintenance skills?” *Transportation Research Part F: Traffic Psychology and Behaviour*, vol. 13, no. 5, pp. 343–353, 2010.
- [46] H. Yang, J. Lu, X. Hu, and J. Jiang, “A cellular automaton model based on empirical observations of a driver’s oscillation behavior reproducing the findings from kerner’s three-phase traffic theory,” *Physica A: Statistical Mechanics and Its Applications*, vol. 392, no. 18, pp. 4009–4018, 2013.
- [47] Y. S. Qian, X. Feng, and J. W. Zeng, “A cellular automata traffic flow model for three-phase theory,” *Physica A: Statistical Mechanics and Its Applications*, vol. 479, pp. 509–526, 2017.
- [48] M. Treiber and A. Kesting, “The intelligent driver model with stochasticity-new insights into traffic flow oscillations,” *Transportation Research Part B: Methodological*, vol. 117, pp. 613–623, 2018.
- [49] R. Wiedemann and U. Reiter, *Microscopic Traffic Simulation: The Simulation System MISSION*, CEC, Brussels, Belgium, 1992.
- [50] B. Sultan, “The study of motorway operation using a microscopic simulation model,” Ph.D. dissertation, Soton University, Soton, UK, 2000.
- [51] G. Song, L. Yu, and Z. Geng, “Optimization of wiedemann and fritzsche car-following models for emission estimation,” *Transportation Research Part D: Transport and Environment*, vol. 34, pp. 318–329, 2015.
- [52] H. W. Kraysse, “The subjective evaluation of traffic conflicts based on an internal concept of dangerousness,” *Accident Analysis & Prevention*, vol. 23, no. 1, pp. 53–65, 1991.
- [53] M. M. Minderhoud and P. H. L. Bovy, “Extended time-to-collision measures for road traffic safety assessment,” *Accident Analysis & Prevention*, vol. 33, no. 1, pp. 89–97, 2001.
- [54] T. Toledo, H. N. Koutsopoulos, and K. I. Ahmed, “Estimation of vehicle trajectories with locally weighted regression,” *Transportation Research Record: Journal of the Transportation Research Board*, no. 1999, pp. 161–169, 2007.
- [55] M. Brackstone, B. Sultan, and M. McDonald, “Motorway driver behaviour: studies on car following,” *Transportation Research Part F: Traffic Psychology and Behaviour*, vol. 5, no. 1, pp. 31–46, 2002.
- [56] W. Leutzbach and R. Wiedemann, “Development and applications of traffic simulation models at the karlsruhe institut Fur verkehrswesen,” *Traffic Engineering and Control*, vol. 27, no. 25, pp. 270–278, 1986.
- [57] K. H. Beck, M. Q. Wang, and M. M. Mitchell, “Concerns, dispositions and behaviors of aggressive drivers: what do self-identified aggressive drivers believe about traffic safety?” *Journal of Safety Research*, vol. 37, no. 2, 2006.
- [58] S. Park, C. Oh, Y. Kim, S. Choi, and S. Park, “Understanding impacts of aggressive driving on freeway safety and mobility: a multi-agent driving simulation approach,” *Transportation Research Part F: Traffic Psychology and Behaviour*, vol. 64, pp. 377–387, 2019.

Research Article

Evaluating the Safety Impact of Connected and Autonomous Vehicles with Lane Management on Freeway Crash Hotspots Using the Surrogate Safety Assessment Model

Hui Zhang ^{1,2}, Ninghao Hou ^{1,2}, Jianhua Zhang ^{1,2,3}, Xuyi Li ^{1,2} and Yan Huang ^{1,2}

¹Intelligent Transportation Systems Research Center, Wuhan University of Technology, Wuhan 430063, China

²Engineering Research Center of Transportation Safety, Wuhan 430063, China

³Wuhan Traffic Management Bureau, Wuhan 430030, China

Correspondence should be addressed to Jianhua Zhang; zjhls@whut.edu.cn

Received 7 February 2021; Accepted 25 June 2021; Published 7 July 2021

Academic Editor: Yanyong Guo

Copyright © 2021 Hui Zhang et al. This is an open access article distributed under the Creative Commons Attribution License, which permits unrestricted use, distribution, and reproduction in any medium, provided the original work is properly cited.

One goal for large-scale deployment of connected and autonomous vehicles is to achieve the traffic safety benefit since connected and autonomous vehicles (CAVs) could reduce the collision risk by enhancing the driver's situation perception ability. Previous studies have analyzed the safety impact of CAVs involved in traffic, but only few studies examined the safety benefits brought by CAVs when approaching high-collision-risk road segments such as the freeway crash hotspots. This study chooses one freeway crash hotspot in Wuhan, China, as an instance and attempts to estimate the safety benefits for differential penetration rates (PRs) of CAVs using the surrogate safety assessment model (SSAM). First, the freeway crash hotspot is identified with kernel density estimation and simulated by VISSIM. Then, the intelligent driver model (IDM) and Wiedemann 99 (a car-following model) are adopted and calibrated to control the driving behaviors of CAVs and human-driven vehicles (HVs) in this study, respectively. The impact that rather CAVs are constrained with or without managed lanes on traffic safety is also discussed, and the PR of CAVs is set from 10% to 90%. The results of this study show that when the PR of CAVs is lower than 50%, there is no significant improvement on the safety measures such as conflicts, acceleration, and velocity difference, which are extracted from the vehicle trajectory data using SSAM. When the penetration rate is over 70%, the experiment results demonstrate that the traffic flow passing the freeway hotspot is with fewer conflicts, smaller acceleration, and smaller velocity difference in the scenario where CAVs are constrained with managed lane compared with the scenario without managed lane control. The safety benefit that CAVs bring needs to be discussed. The lane management of CAVs will also lead to distinct safety impact.

1. Introduction

As vehicle-to-everything (V2X), vehicle sensors, on-board computers, and calculating efficiency develop, more connected and autonomous vehicles (CAVs) will be involved in traffic flow on road [1]. The development and application of technology need time; a mixed condition of CAVs and human-driven vehicles (HVs) will exist for several years [2].

For the benefit of situation perception technology and quick-response driving behavior, the involvement of CAVs would help improve traffic safety levels [3]. But due to the driving behavior difference and decision-making difference between CAV and HVs, CAVs and HVs may disturb each

other in the mixed condition, which may lead to hidden troubles on traffic safety [4]. The impact of the involving of CAVs on traffic remains unclear [5–7].

On the one hand, some research studies indicated that the involvement of CAVs might be of benefit to traffic safety. CAVs can improve string stability by preventing shockwaves [8]. CAVs equipped with beyond-line-of-sight ability can significantly improve safety by preventing the cascading of braking events [9]. The increase of penetration rate (PR) of CAVs would greatly improve traffic safety in the mixed flow in the way of keeping time to collision (TTC) an appropriate range [10]. In the mixed condition of CAVs and HVs, as the PR of CAVs increases, the potential conflicts decline both in

intersections and highways [11]. A CAV control algorithm improves road safety significantly by reducing conflicts even at low PRs of CAVs [12]. Based on crash data of 6 countries from 2012 to 2016, the reduction of the average number of crashes by 47.48% was revealed if all vehicles were equipped with connected vehicle (CV) or autonomous vehicle (AV) technologies [13]. These research studies demonstrated the advantages of CAVs in traffic safety. On the other hand, some researchers demonstrated that the mixed condition would cause interference between CAVs and HVs and negatively affect traffic safety under certain conditions [4, 14]. The involvement of CAVs may lead to an increase in potential collisions with low PRs of CAVs [11].

Considering the feature of CAVs, a road without lateral interference would make full use of CAVs' capability and improve traffic efficiency and safety with the formation of the fleet. To better investigate the influence of mixed conditions of CAVs and HVs on traffic safety, considering the characteristics of crash hotspots, urban freeway crash hotspots are chosen as the experiment conditions. Research on CAV traffic safety mainly used microsimulation to experiment and obtain data [10, 15–18]. To investigate the impact of CAVs and lane management strategy on traffic safety, microsimulation is used [19, 20].

Vehicle trajectory data are often used for the analysis of traffic flow characteristics [21]. Conflicts can be measured with trajectory data through the surrogate safety assessment model (SSAM) [22–26]. Combined with microscopic traffic simulation, precise trajectory data can be obtained.

In summary, to investigate the impact of CAVs on traffic safety on urban freeway, a simulation platform is necessary. With a simulation platform, the adjustment of PRs of CAVs is accessible, which could contribute to the further research into the traffic safety impact.

This study advances the understanding of the traffic safety impacts of CAVs on urban freeway crash hotspots with microscopic traffic simulation and explores the proper lane management under different PRs of CAVs. This paper is organized as follows: Section 2 introduces the experiment framework used in this research, which includes the selection of experiment road section, simulation scenarios design, the detail of the simulation and vehicle control algorithms for CAVs and HVs, surrogate safety assessment model for potential conflict detection, and the methods for traffic safety assessment. Section 3 contains the results obtained from the microsimulation and the analysis of the impact of CAVs on traffic safety through the calculation of 3 parameters. Section 4 discusses the limitation of this study and proposes improvement for the future traffic safety research involving CAVs. Section 5 includes the conclusion obtained from the research results.

2. Methods

2.1. Experimental Road Segment: Crash Hotspot Site. Crash data used for hotspots identification and analysis are extracted from the Crash Report System developed by the Ministry of Public Security. For each traffic crash case, its

detailed crash information was recorded, as shown in Table 1. The crashes that occurred from January 2016 to November 2019 and along the 3rd Ring Road of Wuhan city were used in this study. In summary, 11,498 crashes occurred in this six-lane two-way separated freeway in the period of 47 months.

A kernel density estimation method [27] is used to determine the hotspots in this study, and four crash hotspots are identified and indicated in Table 2 and Figure 1. The fourth hotspot is with the highest kernel density and chosen as the test site, which is located in the section of Luoshi South Road to Qingling Highway Interchange.

Then, a microscopic simulated road is built using VISSIM based on the fourth accident hotspot. This section of the road is 4.6 kilometers long, and it goes east–west with 3 lanes on each direction. The satellite imagery with accident stamps is shown in Figure 2.

In addition to the crash data, the traffic flow data recorded by microwave detectors could be used to represent the traffic condition and as an input of the simulation, as listed in Table 3.

2.2. Scenarios of CAVs Controlled by Lane Management.

Based on the real road condition of the section of Luoshi South Road to Qingling Highway Interchange on the Wuhan 3rd Ring Road, two scenarios are set. The purpose of these two different microscopic traffic simulation scenarios is to test how lane change management would affect traffic safety with different PRs of CAVs involved. With the setting of various penetration rates, the impact of CAVs on traffic safety could be reflected by conflicts [28, 29].

In scenario 1, no limits are set to the CAVs that CAVs could change lanes as they want. In scenario 2, a managed lane is set for CAVs where CAVs could only run on this managed lane.

The 4.6-kilometer road is divided into 2 parts: the first 500 meters of it is set to be the preparing part which helps make the traffic flow stable, and the rest part is set as the test part where the data are collected, presented in Figure 3.

For the decision-making mechanisms of CAVs and HVs are different, the response of two different types of vehicles under the same traffic condition would be different.

As time goes by, with the development of technology, the PR of CAVs would keep rising. A proper traffic management strategy of CAVs would be necessary to avoid the mutual interference of driving behaviors that CAVs and HVs would have on each other.

2.2.1. Scenario 1: CAVs Allowed to Change Lanes. As no lane-changing limits are set for the CAVs in scenario 1, a mixed condition of CAVs and HVs is shown as in Figure 4.

2.2.2. Scenario 2: CAVs Constrained to Managed Lanes. CAVs are only allowed to operate on the managed lane, while HVs could operate anywhere on the road at will. Scenario 2 is shown in Figure 5.

TABLE 1: Crash information recorded in the Crash Report System.

Parameter	Notes	Sample
Time	The time that crash occurred	2018/9/3 20:07:00
Description	The situation description of the crash	Two buses side impact
Location	The road name where crash occurred	Wuhan 3 rd Ring Road
Mileage	The mileage where crash occurred	K1 + 200 meter
Direction	The direction where crash occurred (downstream, upstream)	Downstream

TABLE 2: The location of 4 crash hotspots.

Crash hotspots	Location (all four hotspots are on Wuhan 3 rd Ring Road)
1	The section south of Changfeng Bridge
2	The section of Wangjiazui Highway Interchange
3	The section of Yingwu Highway Interchange
4	The section of Luoshi South Road to Qingling Highway Interchange

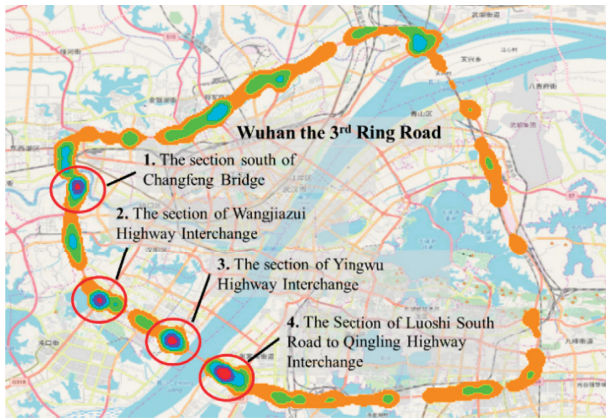


FIGURE 1: Visualization of the spatial distribution of accident density by kernel density estimation.

FIGURE 2: The location of accidents on the section of Wuhan 3rd Ring Road from Luoshi South Road to Qingling Highway Interchange.

2.3. Microsimulation and Vehicle Control Algorithm. The simulation test is conducted using the microsimulation software VISSIM. The trajectory file is generated from the simulation for surrogate safety measures. Control algorithms for CAVs and HVs shall be calibrated before the simulation.

Two scenarios are built for the simulation. The traffic vehicle composition settings, vehicle input, expected speed, traffic flow, and vehicle proportions are all based on the actual collected traffic flow data collected by microwave detectors as input.

2.3.1. Microsimulation. As for the simulation, to ensure the reliability of the simulation results of 2 scenarios, 5 different random seeds are set for each group of simulations in each scenario. For each scenario, simulations are set 5 times at each PR of CAVs with different random seeds, and the PR of CAVs is in the range of 10% to 90% at 10% interval. Overall, for each scenario, the total number of simulations is 45.

A single complete simulation consists of two phases, which are warm-up phase and data-recording phase. The set of warm-up phase is to make sure the traffic flow stabilizes during the simulation. Only the data recorded during the data-recording phase are used in data processing. The length of warm-up phase is 3600 s, the length of data-recording phase is 7200 s, and the total time of a complete simulation is 10800 s. All the trajectory files are imported into SSAM to analyze traffic conflicts.

2.3.2. Car-Following Behavior. In our study, with regard to the HV, the Wiedemann 99 model [30] is used to simulate the driving behavior of vehicles on the freeway. And the intelligent driving model (IDM) is adopted for CAV simulation.

For Wiedemann 99 model, the driving behavior is based on the following algorithm, as illustrated in equation (1). And the parameters involved in Wiedemann 99 are listed in Table 4.

$$dx_{\text{safe}} = CC_0 + CC_1 \cdot v, \quad (1)$$

where dx_{safe} denotes the safety distance between the leading vehicle and the following vehicle, CC_0 is the average distance when the vehicle is stopped, CC_1 denotes the desired headway, and v is the velocity.

The IDM was proposed by Treiber [31] in 2000 and has been used in many pieces of research on the control algorithm of CAVs [28, 32].

TABLE 3: Example of the traffic flow data recorded by microwave detectors.

Vehicle type (1—car, 2—truck)	Time	Checkpoint	Direction (south to north)	Velocity (km/h)	Lane
2	20190302230647300	1	South to north	37	3
2	20190303074851300	1	South to north	46	2
2	20190303095717700	1	South to north	50	3
2	20190304005344800	1	South to north	53	3
2	20190304181204800	1	South to north	53	2
2	20190306041031900	1	South to north	36	2
2	20190306132039000	1	South to north	38	2
2	20190306220631700	1	South to north	32	2
2	20190307010854000	1	South to north	62	3
2	20190307024558500	1	South to north	56	2
2	20190307050453600	1	South to north	67	2
2	20190307114304200	1	South to north	54	3

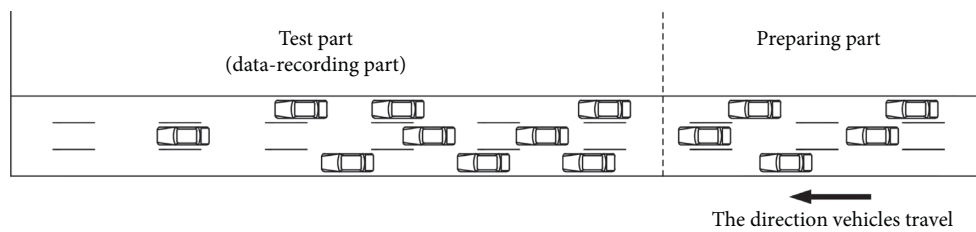


FIGURE 3: Schematic diagram of the experiment road section.

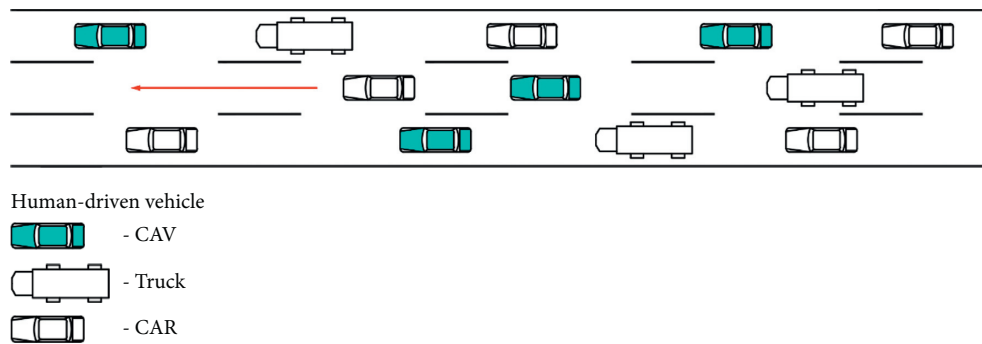


FIGURE 4: No lane-changing limits are set for CAVs.

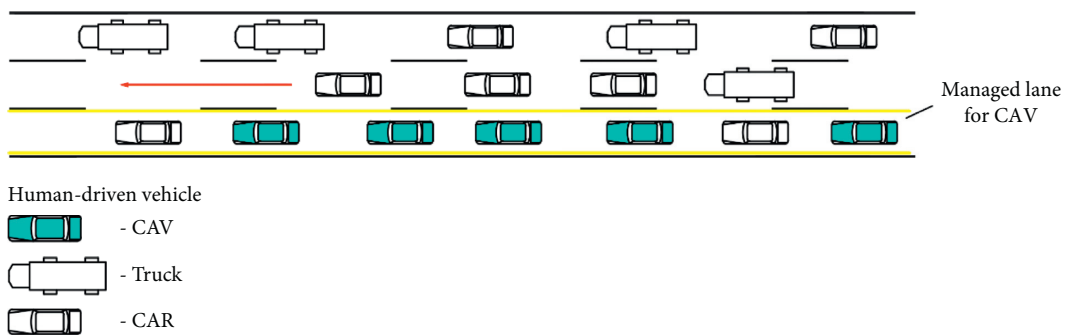


FIGURE 5: A managed lane is set for CAVs.

The basis of this theoretical car-following model is that assumes the IDM would fit well under both free flow and congested flow. Vehicles controlled by IDM could adjust the head spacing and their velocity to the vehicles ahead. With

better stability of vehicle control, the IDM is now wildly used.

As parameters of IDM have clear physical meanings, which could influence driving behaviors of controlled

TABLE 4: Wiedemann 99 parameters.

Parameter (unit)	Short description
CC ₀ (m)	Standstill gap
CC ₁ (m)	Headway time
CC ₂ (m)	“Following” variation
CC ₃ (s)	Threshold for entering “following”
CC ₄ (m/s)	Negative “following” threshold
CC ₅ (m/s)	Positive “following” threshold
CC ₆ (10 ⁻⁴ rad/s)	Speed dependency of oscillation
CC ₇ (m/s ²)	Oscillation acceleration
CC ₈ (m/s ²)	Standstill acceleration
CC ₉ (m/s ²)	Acceleration at 80 km/h
VDES	Desired speed of vehicles

vehicles. Moreover, the model could simultaneously describe the car-following behavior of vehicles on a single lane in the state of both free flow and congested flow. In the state of congested flow, when the velocity difference of two vehicles one after another is small, a slight change of space ahead would not cause rapid deceleration of vehicles. A relatively stable vehicle operating state helps provide a comfortable driving experience and improve traffic safety. The function of IDM is expressed as equations (2) and (3):

$$a = a_0 \left(1 - \left(\frac{v}{v_0} \right)^\delta - \left(\frac{s^*(v, \Delta v)^2}{s} \right)^2 \right), \quad (2)$$

$$s^*(v, \Delta v) = s_0 + vT + \frac{v\Delta v}{2\sqrt{a_0b}}, \quad (3)$$

where a is the acceleration of vehicle n , v is the velocity of vehicle n , Δv is the velocity difference of the following vehicle and the vehicle ahead, v_0 is the expected velocity of the vehicle in the free flow, a_0 is the acceleration, b is the deceleration, s_0 is the minimum space headway of the following vehicle when the vehicle stops, T is the expected time headway, and δ is the parameter which is normally 4.

For an accurate simulation of CAVs, an operation strategy is made. In the free flow, CAVs are expected to pass through the road section at a high speed. In a congested flow, CAVs could keep a shorter space headway. According to previous research [33], there is a reduction coefficient under each traffic condition, as shown in Table 5.

Combining previous research results and traffic characteristics of freeways in China, the parameters and value ranges of the selected IDM are shown in Table 6.

2.3.3. Lane-Changing Behavior. In this research, the lateral movement behaviors of all vehicles in the microsimulation are set to VISSIM default lane-changing control strategy.

2.4. Surrogate Safety Assessment Model. The surrogate safety assessment model is a model developed by the Federal Highway Administration (FHWA), U.S. Department of

TABLE 5: Reduction coefficient of IDM under different traffic conditions.

Reduction coefficient	η_T	η_{v_0}	η_{a_0}	η_b
Smooth traffic flow	1.0	1.0	1.0	1.0
Congestion	0.5	0.9	1.0	1.0

TABLE 6: The range of parameters of IDM.

Parameter	v_0	a_0	b	T	s_0
Upper bound	80	0.1	0.1	0.1	0.1
Lower bound	100	5	5	5	10
Value	86	1.2628	2.6907	1.5295	7.8893

Transportation, to automatically identify, classify, and evaluate potential vehicle-to-vehicle conflicts with trajectory files. A trajectory file could be output after running the microsimulation on VISSIM, which contains data about the positions, velocities, and other data of vehicles. SSAM uses several algorithms to identify potential conflicts based on vehicle trajectory files. Software with SSAM built in is developed by the FHWA on Windows.

Several parameters can be adjusted to determine the criterion of identifying conflicts. The criterion of conflicts detecting could be affected by the change of several parameters.

TTC is the minimum time-to-collision value during the conflict [34]. A TTC is the time step between the identification moment to the collision moment. As TTC is set larger, more potential conflicts will be detected.

To classify different types of conflicts, the conflict angle is set. A conflict angle is the approximate angle of the conflicting vehicles in a potential collision.

According to the conflict angle, vehicle-to-vehicle conflicts are divided into 3 types, presented in Figure 6. If θ is smaller than θ_1 , the conflict is of rear-end conflict. If θ is bigger than θ_2 , the conflict is of crossing conflict. If θ is bigger than θ_1 and smaller than θ_1 , the conflict is of lane-change conflict.

2.5. Assessment of Traffic Safety. To assess the impact of CAVs on traffic safety, three methods are used, which are the number of conflicts, acceleration distribution, and velocity. All these analyzing data are based on the data output from simulation.

2.5.1. Number of Conflicts. Conflicts between vehicles could result in crash; therefore, the number of conflicts could represent the performance of traffic safety [35]. The greater the number of conflicts, the lower the level of traffic safety.

2.5.2. Acceleration Distribution. Acceleration distribution of vehicles could represent the stability of traffic flows of the road section [36]. As crash occurs, the distance between vehicles is zero. In the process vehicles getting close to each other, a rapid acceleration or deceleration would occur. The

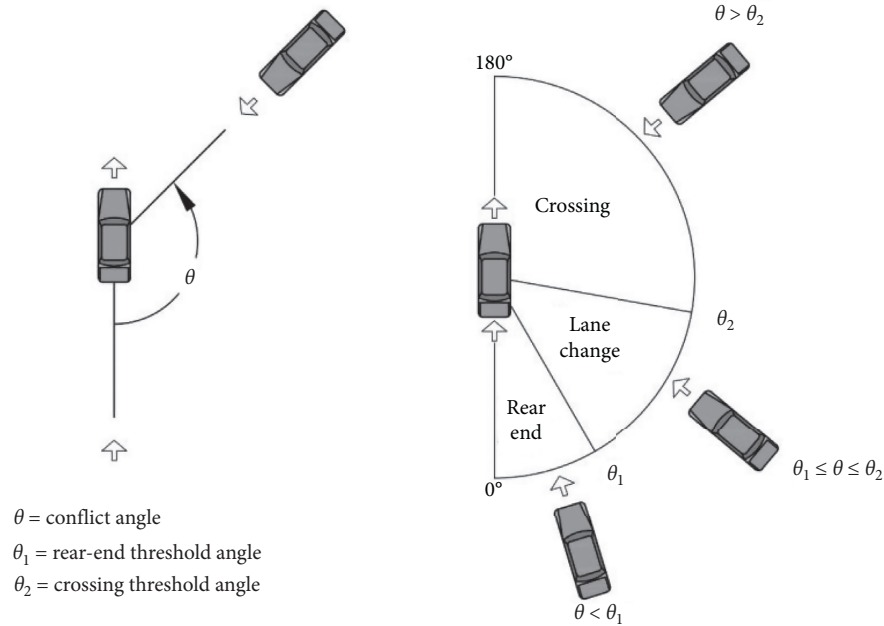


FIGURE 6: Diagrammatic sketch of conflict angle (source: [34]).

occurrence of a crash must be accompanied by intense acceleration or deceleration. Acceleration can indicate road safety [10]. As the acceleration closes to zero, the state of vehicles in traffic flow tends to keep stable, which represents a high level of traffic safety.

2.5.3. Velocity Difference. The distribution of velocity difference can represent the fluctuation of traffic flow. The velocity difference is the difference value between the velocity of front vehicle and the velocity of rear vehicle. As the absolute value of velocity difference gets higher, the distance between vehicles gets further or closer, which declares an unstable state of traffic flow.

The velocity difference is expressed as follows:

$$v_{\text{diff}} = v_{\text{front}} - v_{\text{rear}}, \quad (4)$$

where v_{diff} is the velocity difference, v_{front} is the velocity of front vehicle, and v_{rear} is the velocity of rear vehicle.

3. Results

The results obtained from the microsimulation are divided into 3 parts. Two different scenarios were tested in the microsimulation, and these results are measured as the mean value of the simulation output of all 5 random seeds. These results are the parts after the simulation has been started at 3600 s when the vehicle flows tended to remain relatively stable. The conflicts are exported from trajectory files analyzed through SSAM. With the existence of medial divider, considering only traffic flows in the same direction, no crossing conflict would exist, conflicts between vehicles are in the type of rear end and lane change regarding the conflict angle of two cars. All the parameters are set to default in SSAM.

3.1. Conflicts on Urban Freeway. Two scenarios are set for the microscopic simulation experiment.

In the simulation, the only parameter that has been changed is the PR of CAVs. The conclusion obtained in the simulation test is that while all the vehicles on road are CAVs, there would not be potential conflicts.

In scenario 1, no managed lane is set for CAVs; all the vehicles could change lanes or overtake other vehicles. The trend of changes in the number of potential conflicts is shown in Figure 7. The number of potential conflicts with various PRs of CAVs is listed in Table 7. As the PR of CAVs increases from 10% to 50%, the number of potential conflicts increases from 179 to 724, an increase of 304.47% on the number of conflicts at a PR of 10%. This indicates that the involvement of CAVs interferes with the running status of traffic flow and lowers the traffic safety level. From 50% to 80% of PR of CAVs, the number of potential conflicts barely changes. The mixed condition of CAVs and HVs tends to be stable. When the PR of CAV changes from 80% to 90%, the number of potential conflicts decreases from 726 to 584, a decrease of 19.56% on the number of conflicts at a PR of 80%. As CAVs take a large proportion of traffic flow, the advantage of CAVs starts to reveal.

In scenario 2, managed lanes are set to constrain lane-change behaviors of CAVs. Figure 8 provides a visual representation of the trend of the number of potential conflicts with the increase of PRs of CAVs. As the PR of CAVs increases from 10% to 90%, the number of potential conflicts decreases from 63 to 0, a decrease of 100% on the number of conflicts at a PR of 10%. The results indicate that setting managed lanes and constraining lane-change behaviors help CAVs avoid lateral interference and form fleet. CAV fleet could operate fast and smoothly. In the CAV fleet, CAVs could keep a short head spacing between each other.

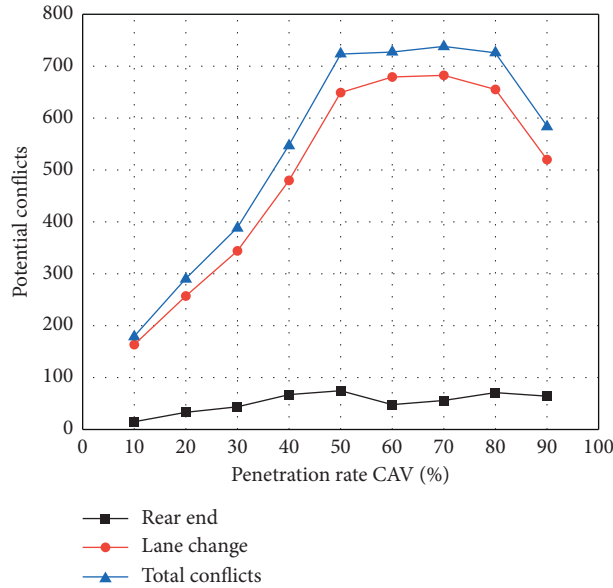


FIGURE 7: Number of potential conflicts in scenario 1 in 10% increments of CAV penetration rate.

TABLE 7: Tabular representation of the number of potential conflicts in two scenarios.

CAV penetration rate (%)	Scenario 1			Scenario 2		
	Rear end	Lane change	Total conflicts	Rear end	Lane change	Total conflicts
10	15	164	179	8	55	63
20	33	257	290	12	45	57
30	44	344	388	21	24	45
40	67	480	547	6	7	13
50	75	649	724	3	4	7
60	48	679	727	0	4	4
70	56	682	738	0	2	2
80	71	655	726	0	0	0
90	64	520	584	0	0	0

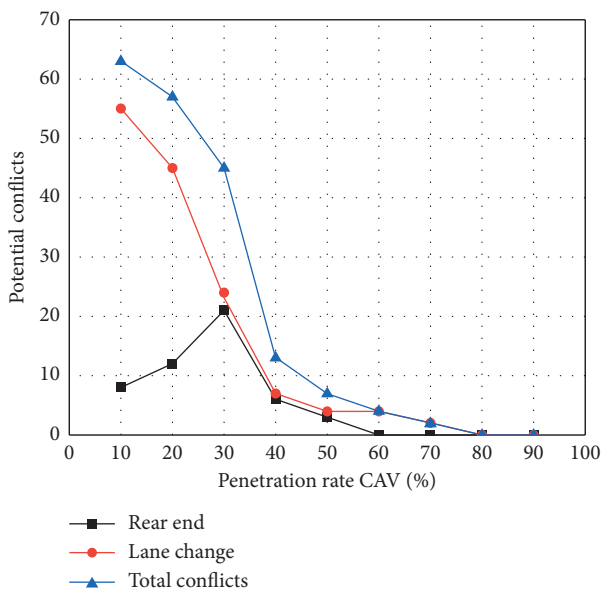


FIGURE 8: Number of potential conflicts in scenario 2 in 10% increments of CAV penetration rate.

3.2. *Acceleration Distribution on Urban Freeway.* Figure 9 presents acceleration distributions of two scenarios with the PR of CAVs increases from 10% to 90%. Figure 10 provides a visual representation of the change in standard deviation (SD) of acceleration as the PR of CAVs changes. The SD of acceleration and PR are listed in Table 8.

As Figure 9 shows, under both scenarios, a gradual increase in the ratio of the acceleration at 0 m/s^2 can be easily found, which indicates that the involvement of CAVs would boost the portion of smooth driving in the mixed traffic flow. With the increase in the PR of CAVs, the ratio of high deceleration rate is also decreased, which indicates that a smoother traffic flow can be attained.

3.3. *Velocity Difference on Urban Freeway.* According to the data of the microwave detector, traffic conditions on road can be analyzed. Comparing data recorded by the microwave detector and data exported through the simulation, the impact that CAVs made can be detected. Figure 11 demonstrates the velocity difference of vehicles in real situations and human-driven vehicles (PR of CAVs = 0) in simulation. The distribution of velocity difference is close to a normal

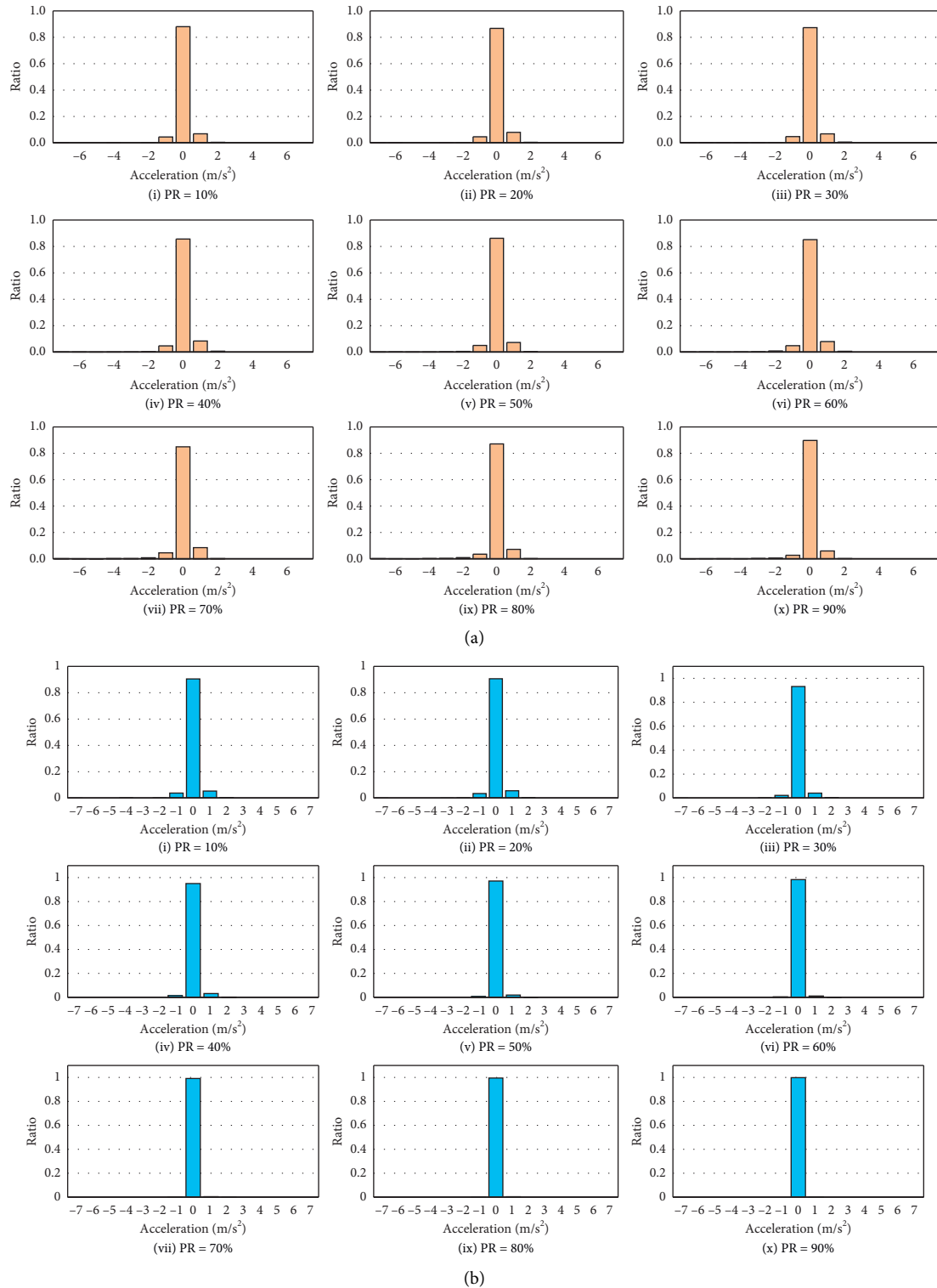


FIGURE 9: Acceleration of vehicles on the road of 2 scenarios at different PRs. (a) Scenario 1. (b) Scenario 2.

distribution. The SD of velocity difference on road is 10.504, and the SD of velocity difference in simulation is 8.653. Despite little difference, the close SD indicates the accuracy of simulation is high.

Previous studies showed that CAVs can affect traffic safety by affecting the speed of the front and rear cars [10]. In

this research, vehicle velocity differences have been calculated under various PRs of CAVs from 10% to 90%. Figure 12 presents the distribution of velocity differences of vehicles on the road of 2 scenarios. As shown in Figure 12, the velocity difference distribution is like normal distribution. In the mixed traffic flow, as the PR of CAVs increases,

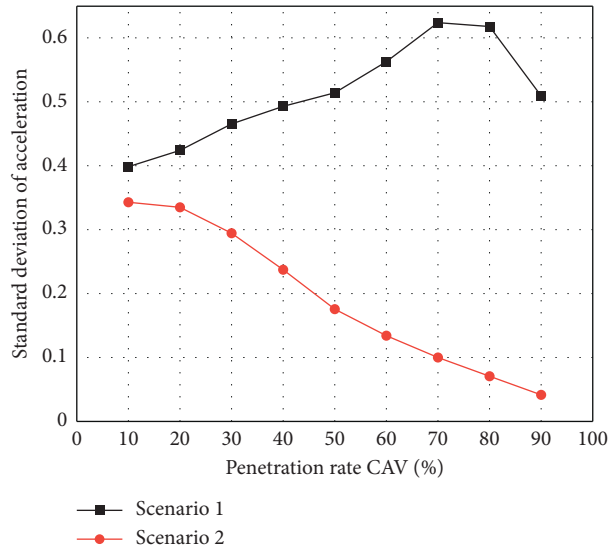


FIGURE 10: Standard deviation distribution of acceleration of vehicles in simulation.

TABLE 8: Tabular representation of the standard deviation of acceleration in two scenarios.

PR of CAVs (%)	SD of acceleration	
	Scenario 1	Scenario 2
10	0.39832	0.34323
20	0.42410	0.33488
30	0.46552	0.29471
40	0.49242	0.23735
50	0.51403	0.17574
60	0.56258	0.13405
70	0.62391	0.09934
80	0.61760	0.07070
90	0.50907	0.04140

velocity differences tend to close to 0, which represents that vehicles on road keep a relatively stable flow. These results show that CAVs can promote the stability of traffic flow. In scenario 2, the velocity differences converge to 0 faster than those in scenario 1, indicating that CAVs could help improve traffic safety on freeway crash hotspots.

As shown in Table 9, as the PR of CAVs increases, the SD of velocity difference in scenario 1 rises and then decreases. The trend of SD of velocity difference in scenario 2 falls, follows with rise, and then falls. But the range of SD of velocity difference is smaller in scenario 2 than in scenario 1.

Standard deviation is a good indicator to describe the degree of dispersion in a normal distribution. As shown in Figure 13, on the whole, the SD of velocity difference decreases as the PR of CAVs increases.

The velocity difference between the vehicles and the following vehicles can reflect the traffic safety level at the microscope level. Vehicles driving smoothly not only make drivers and passengers feel comfortable but also help increase the volume of traffic flow. In general, CAVs can promote the tendency of the velocity difference between the vehicles and the following vehicles to converge toward 0. As the PR of CAVs increases, the trend of aggregation of velocity difference is getting more obvious, which could

represent that CAVs could help the traffic flow operate smoothly. Constraining CAVs on the managed lane could help improve traffic safety with high PR of CAVs at the freeway crash hotspots. In the condition that CAVs can change lanes freely, velocity difference with different PRs of CAVs is not the same, but on the whole view, there is an aggregate trend that velocity difference gets close to 0. The reason why there is a trend is that, compared with HVs, CAVs can better perceive traffic conditions ahead and adjust their operation in time to keep a relative safe distance to the vehicle ahead in time. With a more sensitive response in the car-following flow, vehicles (include CAVs) can travel more smoothly and avoid nonsense deceleration and congestion. In this way, setting lane-change constrain to CAVs could better use the strengths of CAVs without the interference of HVs. The biggest feature of driver behaviors is random and unpredictable. With random deceleration, lane changing, and over-passing behaviors, the balance of traffic flow on road can be easily broken. That is one of the reasons why traffic jams would occasionally happen on road. In summary, as the PR of CAVs getting higher, the stability of the overall traffic flow tends to get better, where setting constraints to CAVs' lane-change behavior helps improve traffic safety.

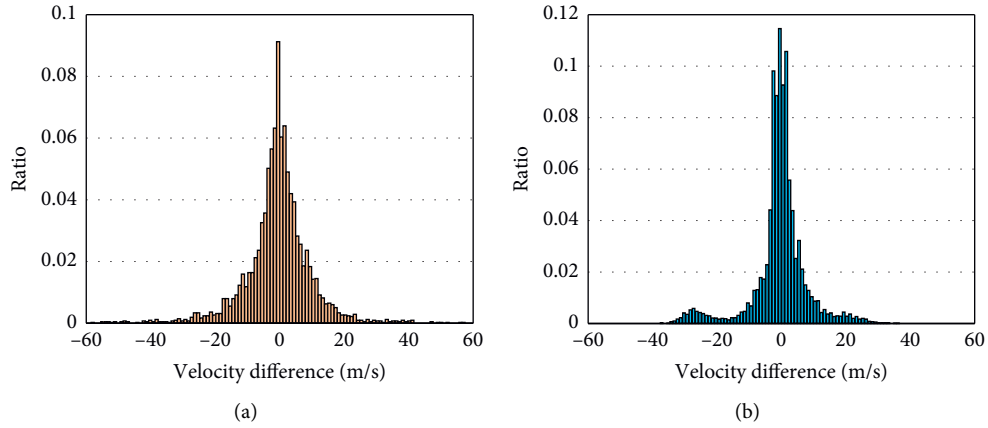


FIGURE 11: Velocity difference of vehicles from 7:00 to 9:00 on the selected road section. (a) Velocity difference of vehicles on the road. (b) Velocity difference of HVs in simulation.

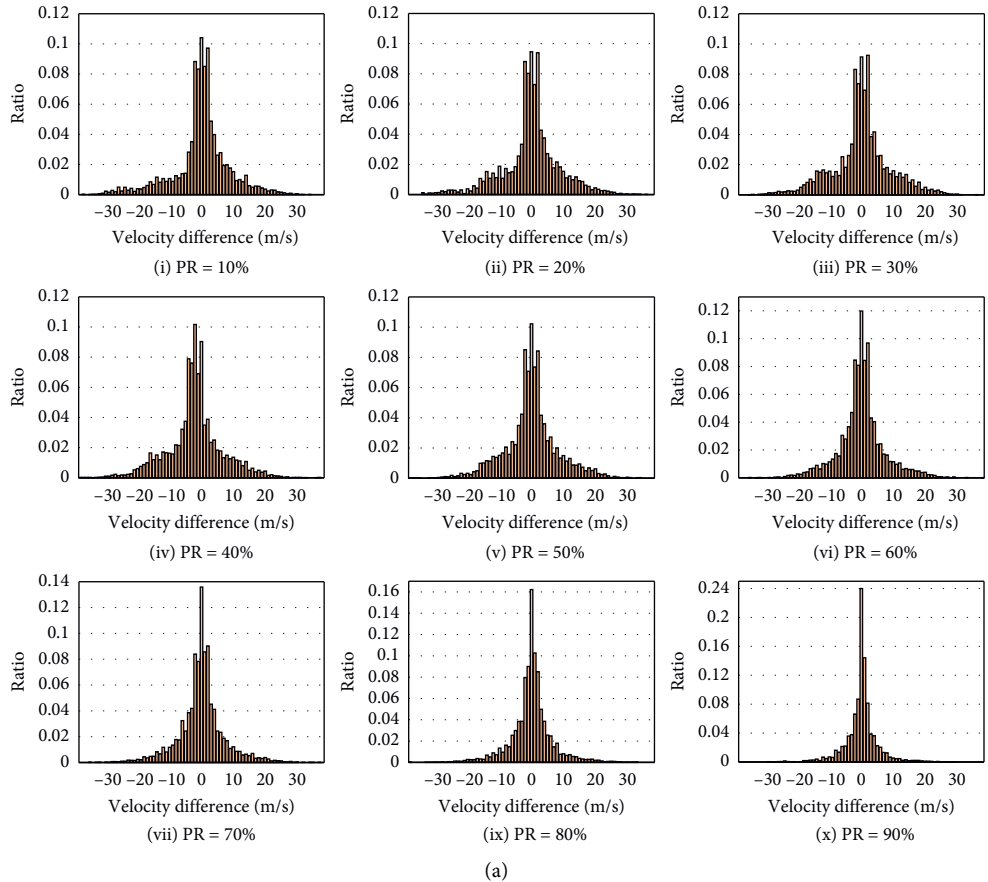


FIGURE 12: Continued.

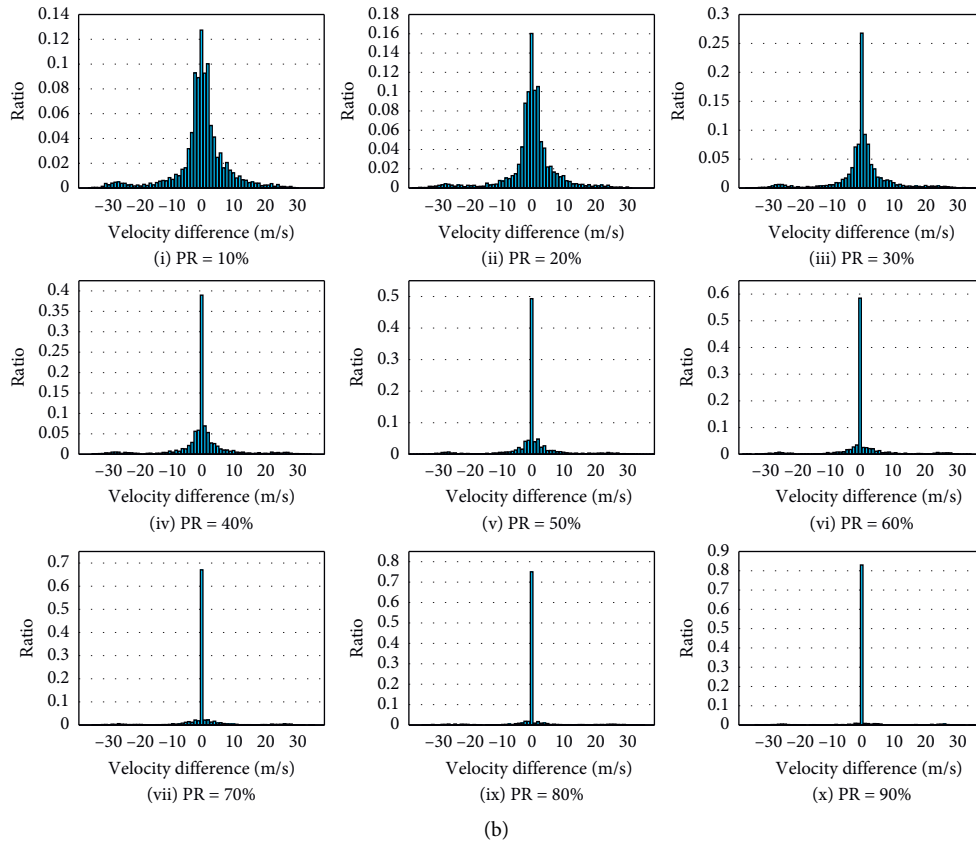


FIGURE 12: Velocity difference of vehicles on the road of 2 scenarios. (a) Scenario 1. (b) Scenario 2.

TABLE 9: Tabular representation of the standard deviation of velocity difference in two scenarios.

SD of velocity difference	0%	10%	20%	30%	40%	50%	60%	70%	80%	90%
Scenario 1	8.653	8.752	8.914	8.918	8.688	8.335	7.269	7.226	6.449	5.287
Scenario 2	8.653	8.497	8.156	8.337	8.711	8.857	8.522	8.542	7.956	7.112

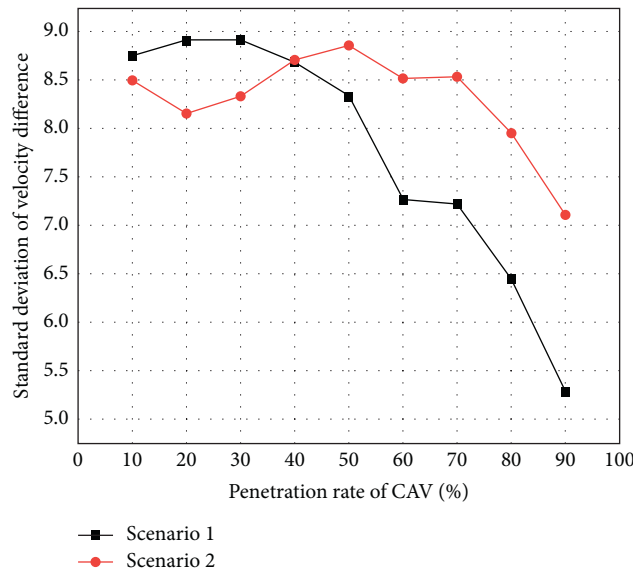


FIGURE 13: The standard deviation of velocity difference of vehicles in simulation.

4. Conclusions

In this research, the impact of CAVs on traffic safety with various PRs of CAVs is investigated by simulation, and two experiment scenarios are set to study the traffic safety improvement of two traffic management strategies.

The authors built a mixed traffic scene with CAVs and HVs using microscopic simulation software. During the experiment, the PR of CAVs has been changed from 10% to 90%, two traffic management strategies were designed by setting managed lanes for CAVs or not. Evaluation data were generated from the simulation, and potential conflict detection was completed through the surrogate safety assessment model using vehicle trajectory files.

Though that the situation perception advantages seem to provide CAVs with significant improvement in traffic safety, the results indicate that the involvement of CAVs in the mixed traffic flow on urban freeway would cause an increase of more than 300% in the number of conflicts and a decline in traffic safety levels as the PR of CAVs increases from 10% to 50%. The results indicate that the arrangement of managed lanes for CAVs rises in traffic safety as the PR of CAVs is in the range of 10% to 50% compared with allowing CAVs lane-changing. As the PR of CAVs rises above 70%, the safety level rises up again without lane management of CAVs. The reason for the traffic safety level decline may be the driving behavior difference between HVs and CAVs, and the difference may cause interference in vehicle operating and lead to conflicts. The results also indicate that setting managed lanes for CAVs could help improve traffic safety at the freeway crash hotspot. With a better perception of the surrounding conditions and information sharing, CAVs running at the same lane could keep a short head spacing and form a fleet.

Because only one set of traffic flow data was used in this study, the impact of CAVs on traffic safety may not be completely revealed. In the further study, more road situations with different traffic flow shall be considered, and the function of more detailed lane management shall be discussed.

5. Discussion

The impact of CAVs on traffic safety would change along with the change of PR of CAVs [11]. The number of potential conflicts increases with the increase of PR of CAVs, with the PR under 50%. The SD of acceleration also increases, which indicates the decline of traffic safety levels. When the PR of CAVs is between 50% and 80%, the number of potential conflicts, acceleration distribution, and velocity difference distribution barely change with PRs increasing. CAVs and HVs form a stable traffic flow state. As the PR of CAVs is beyond 80%, the number of potential conflicts and standard deviation of acceleration decrease with an increase in the PR of CAVs. This indicates the improvement of traffic level compared with the situation when the penetration is 50%. But the number of potential conflicts is still higher with the PR of CAVs at 90% compared with 10%.

After constraining CAVs not to change lanes, the number of potential conflicts and SD of acceleration decrease with an increase in the PR of CAVs, which indicates the improvement of traffic safety level.

Though simulation is relatively cheap and easy to conduct, the reliability and precision of simulation cannot fully reveal the actual rule of CAV field-driving behavior. For further investigation of the influence of CAVs on traffic safety, a real-road CAV test is essential. Two traffic management strategies were proposed in this research, which were no managed lane and managed lane for CAVs. A more specific and customized management strategy could improve traffic safety levels better. The PR mentioned in this research is the proportion rate of CAVs in the process of vehicle input before the simulation. The input proportion rate cannot reflect the PR in the traffic operating process accurately. For a more accurate investigation of the impact of the mixed condition of CAVs and HVs on traffic safety, controlling the PR during the simulation is essential.

For further research, calibrating the CAV control algorithms is necessary, which could help improve the accuracy of microsimulation and improve the reliability of the research. Experiments with real CAVs could reflect the driving behaviors directly, and traffic safety levels could be evaluated by analyzing the data collected in the experiment. More experiment scenarios could be designed, and a more concrete traffic management strategy should help the traffic flow operating more smoothly.

Data Availability

The data indicated in the findings have not been made available due to data privacy.

Conflicts of Interest

The authors declare that there are no conflicts of interest regarding the publication of this paper.

Acknowledgments

This research was supported by the National Key Research and Development Program of China (2019YFB1600800), National Natural Science Foundation of China (52072289 and 51775396), and Independent Innovation Foundation of Wuhan University of Technology: Risk Assessment and Prediction System of New Energy Vehicle Operation Safety Based on Terminal-Network-Cloud Integration (2020-zy-092).

References

- [1] A. D. Tibljas, T. Giuffre, S. Surdonja, and S. Trubia, "Introduction of autonomous vehicles: roundabouts design and safety performance evaluation," *Sustainability*, vol. 10, no. 4, p. 1060, 2018.
- [2] J. Rios-Torres and A. A. Malikopoulos, "A survey on the coordination of connected and automated vehicles at intersections and merging at highway on-ramps," *IEEE*

- Transactions on Intelligent Transportation Systems*, vol. 18, no. 5, pp. 1066–1077, 2017.
- [3] L. Wang, M. Abdel-Aty, W. Ma, J. Hu, and H. Zhong, “Quasi-vehicle-trajectory-based real-time safety analysis for expressways,” *Transportation Research Part C: Emerging Technologies*, vol. 103, pp. 30–38, 2019.
 - [4] S. C. Calvert, W. J. Schakel, and J. W. C. van Lint, “Will automated vehicles negatively impact traffic flow?,” *Journal of Advanced Transportation*, vol. 2017, Article ID 3082781, 17 pages, 2017.
 - [5] A. Mirheli, L. Hajibabai, and A. Hajbabaie, “Development of a signal-head-free intersection control logic in a fully connected and autonomous vehicle environment,” *Transportation Research Part C: Emerging Technologies*, vol. 92, pp. 412–425, 2018.
 - [6] A. Mirheli, M. Tajalli, L. Hajibabai, and A. Hajbabaie, “A consensus-based distributed trajectory control in a signal-free intersection,” *Transportation Research Part C: Emerging Technologies*, vol. 100, pp. 161–176, 2019.
 - [7] M. Karimi, C. Roncoli, C. Alecsandru, and M. Papageorgiou, “Cooperative merging control via trajectory optimization in mixed vehicular traffic,” *Transportation Research Part C-Emerging Technologies*, vol. 116, Article ID 102663, 2020.
 - [8] A. Talebpour and H. S. Mahmassani, “Influence of connected and autonomous vehicles on traffic flow stability and throughput,” *Transportation Research Part C: Emerging Technologies*, vol. 71, pp. 143–163, 2016.
 - [9] J. I. Ge, S. S. Avedisov, C. R. He, W. B. Qin, M. Sadeghpour, and G. Orosz, “Experimental validation of connected automated vehicle design among human-driven vehicles,” *Transportation Research Part C: Emerging Technologies*, vol. 91, pp. 335–352, 2018.
 - [10] L. Ye and T. Yamamoto, “Evaluating the impact of connected and autonomous vehicles on traffic safety,” *Physica A: Statistical Mechanics and Its Applications*, vol. 526, Article ID 121009, 2019.
 - [11] N. Virdi, H. Grzybowska, S. T. Waller, and V. Dixit, “A safety assessment of mixed fleets with connected and autonomous vehicles using the surrogate safety assessment module,” *Accident Analysis & Prevention*, vol. 131, pp. 95–111, 2019.
 - [12] A. Papadoulis, M. Quddus, and M. Imprialou, “Evaluating the safety impact of connected and autonomous vehicles on motorways,” *Accident Analysis & Prevention*, vol. 124, pp. 12–22, 2019.
 - [13] L. Wang, H. Zhong, W. J. Ma, M. Abdel-Aty, and J. Park, “How many crashes can connected vehicle and automated vehicle technologies prevent: a meta-analysis,” *Accident Analysis and Prevention*, vol. 136, Article ID 105299, 2020.
 - [14] A. Sinha, S. Chand, K. P. Wijayaratra, N. Virdi, and V. Dixit, “Crash severity and rate evaluation of conventional vehicles in mixed fleets with connected and automated vehicles,” *Procedia Computer Science*, vol. 170, pp. 688–695, 2020.
 - [15] A. Sinha, S. Chand, K. P. Wijayaratra, N. Virdi, and V. Dixit, “Comprehensive safety assessment in mixed fleets with connected and automated vehicles: a crash severity and rate evaluation of conventional vehicles,” *Accident Analysis and Prevention*, vol. 142, Article ID 105567, 2020.
 - [16] L. Cui, J. Hu, B. B. Park, and P. Bujanovic, “Development of a simulation platform for safety impact analysis considering vehicle dynamics, sensor errors, and communication latencies: assessing cooperative adaptive cruise control under cyber attack,” *Transportation Research Part C: Emerging Technologies*, vol. 97, pp. 1–22, 2018.
 - [17] C. Wang, C. Xu, J. Xia, Z. Qian, and L. Lu, “A combined use of microscopic traffic simulation and extreme value methods for traffic safety evaluation,” *Transportation Research Part C: Emerging Technologies*, vol. 90, pp. 281–291, 2018.
 - [18] M. Seraj, J. Li, and Z. Qiu, “Modeling microscopic car-following strategy of mixed traffic to identify optimal platoon configurations for multiobjective decision-making,” *Journal of Advanced Transportation*, vol. 2018, Article ID 7835010, 15 pages, 2018.
 - [19] S. Gong, J. Shen, and L. Du, “Constrained optimization and distributed computation based car following control of a connected and autonomous vehicle platoon,” *Transportation Research Part B: Methodological*, vol. 94, pp. 314–334, 2016.
 - [20] Z. H. Khattak, B. L. Smith, H. Park, and M. D. Fontaine, “Cooperative lane control application for fully connected and automated vehicles at multilane freeways,” *Transportation Research Part C: Emerging Technologies*, vol. 111, pp. 294–317, 2020.
 - [21] Z. Zhong, E. E. Lee, M. Nejad, and J. Lee, “Influence of CAV clustering strategies on mixed traffic flow characteristics: an analysis of vehicle trajectory data,” *Transportation Research Part C: Emerging Technologies*, vol. 115, Article ID 102611, 2020.
 - [22] R. Niroumand, M. Tajalli, L. Hajibabai, and A. Hajbabaie, “Joint optimization of vehicle-group trajectory and signal timing: introducing the white phase for mixed-autonomy traffic stream,” *Transportation Research Part C: Emerging Technologies*, vol. 116, Article ID 102659, 2020.
 - [23] Y. Guo, M. Essa, T. Sayed, M. M. Haque, and S. Washington, “A comparison between simulated and field-measured conflicts for safety assessment of signalized intersections in Australia,” *Transportation Research Part C: Emerging Technologies*, vol. 101, pp. 96–110, 2019.
 - [24] J. So, G. Dedes, B. B. Park, S. HosseinyAlamdary, and D. Grejner-Brzezinski, “Development and evaluation of an enhanced surrogate safety assessment framework,” *Transportation Research Part C: Emerging Technologies*, vol. 50, pp. 51–67, 2015.
 - [25] J. Lee, B. Park, K. Malakorn, and J. So, “Sustainability assessments of cooperative vehicle intersection control at an urban corridor,” *Transportation Research Part C: Emerging Technologies*, vol. 32, pp. 193–206, 2013.
 - [26] O. Giuffrè, A. Granà, M. L. Tumminello et al., “Evaluation of roundabout safety performance through surrogate safety measures from microsimulation,” *Journal of Advanced Transportation*, vol. 2018, Article ID 4915970, 14 pages, 2018.
 - [27] A. Okabe, T. Satoh, and K. Sugihara, “A kernel density estimation method for networks, its computational method and a GIS-based tool,” *International Journal of Geographical Information Science*, vol. 23, no. 1, pp. 7–32, 2009.
 - [28] M. S. Rahman, M. Abdel-Aty, J. Lee, and M. H. Rahman, “Safety benefits of arterials’ crash risk under connected and automated vehicles,” *Transportation Research Part C: Emerging Technologies*, vol. 100, pp. 354–371, 2019.
 - [29] H. Jiang, J. Hu, S. An, M. Wang, and B. B. Park, “Eco approaching at an isolated signalized intersection under partially connected and automated vehicles environment,” *Transportation Research Part C: Emerging Technologies*, vol. 79, pp. 290–307, 2017.
 - [30] M. Zhu, X. Wang, A. Tarko, and S. E. Fang, “Modeling car-following behavior on urban expressways in Shanghai: a naturalistic driving study,” *Transportation Research Part C: Emerging Technologies*, vol. 93, pp. 425–445, 2018.

- [31] M. Treiber, A. Hennecke, and D. Helbing, "Congested traffic states in empirical observations and microscopic simulations," *Physical Review E*, vol. 62, no. 2, pp. 1805–1824, 2000.
- [32] M. S. Rahman, M. Abdel-Aty, L. Wang, and J. Lee, "Understanding the highway safety benefits of different approaches of connected vehicles in reduced visibility conditions," *Transportation Research Record: Journal of the Transportation Research Board*, vol. 2672, no. 19, pp. 91–101, 2018.
- [33] A. Talebpour, H. S. Mahmassani, and F. E. Bustamante, "Modeling driver behavior in a connected environment: integrated microscopic simulation of traffic and mobile wireless telecommunication systems," *Transportation Research Record: Journal of the Transportation Research Board*, vol. 2560, no. 1, pp. 75–86, 2016.
- [34] D. Gettman, L. Pu, T. Sayed, and S. G. Shelby, "Surrogate safety assessment model and validation," *Final Report, Turner-Fairbank Highway Research Center, McLean, VA, USA*, 2008.
- [35] M. M. Morando, Q. Y. Tian, L. T. Truong, and H. L. Vu, "Studying the safety impact of autonomous vehicles using simulation-based surrogate safety measures," *Journal of Advanced Transportation*, vol. 2018, Article ID 6135183, 11 pages, 2018.
- [36] X. Y. Cai, C. L. Lei, B. Peng, X. Y. Tang, and Z. G. Gao, "Road traffic safety risk estimation method based on vehicle onboard diagnostic data," *Journal of Advanced Transportation*, vol. 2020, Article ID 3024101, 13 pages, 2020.

Research Article

A Dynamic Bayesian Network-Based Real-Time Crash Prediction Model for Urban Elevated Expressway

Xian Liu,^{1,2,3} Jian Lu ,^{1,2,3} Zeyang Cheng,^{1,2,3} and Xiaochi Ma^{1,2,3}

¹Jiangsu Key Laboratory of Urban ITS, Southeast University, Nanjing 211189, China

²Jiangsu Province Collaborative Innovation Center of Modern Urban Traffic Technologies, Southeast University, Nanjing 211189, China

³School of Transportation, Southeast University, Nanjing 211189, China

Correspondence should be addressed to Jian Lu; lujian_1972@seu.edu.cn

Received 24 January 2021; Revised 8 March 2021; Accepted 6 May 2021; Published 15 May 2021

Academic Editor: Eneko Osaba

Copyright © 2021 Xian Liu et al. This is an open access article distributed under the Creative Commons Attribution License, which permits unrestricted use, distribution, and reproduction in any medium, provided the original work is properly cited.

Traffic crash is a complex phenomenon that involves coupling interdependency among multiple influencing factors. Considering that interdependency is critical for predicting crash risk accurately and contributes to revealing the underlying mechanism of crash occurrence as well, the present study attempts to build a Real-Time Crash Prediction Model (RTCPM) for urban elevated expressway accounting for the dynamicity and coupling interdependency among traffic flow characteristics before crash occurrence and identify the most probable risk propagation path and the most significant contributors to crash risk. In this study, Dynamic Bayesian Network (DBN) was the framework of the RTCPM. Random Forest (RF) method was employed to identify the most important variables, which were used to build DBN-based RTCPMs. The PC algorithm combined with expert experience was further applied to investigate the coupling interdependency among traffic flow characteristics in the DBN model. A comparative analysis among the improved DBN-based RTCPM considering the interdependency, the original DBN-based RTCPM without considering the interdependency, and Multilayer Perceptron (MLP) was conducted. Besides, the sensitivity and strength of influences analyses were utilized to identify the most probable risk propagation path and the most significant contributors to crash risk. The results showed that the improved DBN-based RTCPM had better prediction performance than the original DBN-based RTCPM and the MLP based RTCPM. The most probable risk influencing path was identified as follows: speed on current segment (V) (time slice 2) → V (time slice 1) → speed on upstream segment (U_V) (time slice 1) → Traffic Performance Index (TPI) (time slice 1) → crash risk on current segment. The most sensitive contributor to crash risk in this path was V (time slice 2), followed by TPI (time slice 1), V (time slice 1), and U_V (time slice 1). These results indicate that the improved DBN-based RTCPM has the potential to predict crashes in real time for urban elevated expressway. Besides, it contributes to revealing the underlying mechanism of crash and formulating the real-time risk control measures.

1. Introduction

Predicting road crashes in real time is a hotspot in road safety under the context of active traffic management (ATM) over the past two decades. Real-time crash prediction refers to the assumption that the occurrence probability of a crash on a specific road segment can be predicted within a very short precrash time interval by adopting instantaneous traffic flow characteristics [1–3]. The development of Intelligent Transportation System (ITS) and advanced transportation information systems (ATIS) is helpful for easily

collecting traffic data in real time, promoting the effective and accurate assessment on crash risk on highways and expressways by use of RTCPMs [4–11].

In general, numerous RTCPMs studies establish a direct connection between traffic flow data (i.e., volume, speed, occupancy and their combinations) and crash data. In these models, the collinearity and correlation among dependent variables are avoided; thus, the independence of variables is guaranteed [12, 13]. However, road crash is a complex phenomenon involving coupling interdependency among multiple influencing factors. The concept of coupling

interdependency can be used to express the interaction between various risks. Although these complex system factors can exhibit many characteristics on their own, in reality these individual factors interact and couple with each other in even more complex ways in terms of coupling direction and coupling strength [14–16]. This interaction is called coupling interdependency, which can lead to an increased or a decreased risk of an accident [17]. Therefore, it is essential for RTCPMs to account for the interdependency among influencing factors. Additionally, the one-time interval of traffic data is frequently adopted for real-time crash prediction in a number of RTCPMs [6, 18]. However, for urban elevated expressway, the merging and lane-changing driving behaviours are frequent due to the dense-ramp setting. The traffic flow characteristic is prone to displaying dynamicity that varies over time, which is closely associated with crash risk [19]. Therefore, the dynamicity of traffic flow in the temporal dimension should be considered with the implementation of the RTCPM for predicting crashes on urban elevated expressway.

DBN, a particular form of Bayesian Network (BN), represents the dynamic evolution of some state space model through time [20]. It has been widely used to predict and assess the dynamically evolving process of risk in the field of maritime accidents, tunnel construction, ship-ice collision, etc. [21–23]. In order to express the dynamicity of traffic flow characteristics, some RTCPMs studies apply time-series traffic data consisting of several time intervals [24–27], which are proved to be feasible and robust. However, these researches ignore the investigation of interdependency among different traffic flow characteristics and simply connect each influencing factor to crash risk directly in the construction process of the graph structure. As the most critical step in the DBN construction, the interdependency of variables can be well assessed in the DBN model with the application of the structure learning algorithm. Besides, the neural network-based models (e.g., MLP) are also able to accommodate correlated dependent variables. However, the whole model should be rebuilt and recalibrated once the future new variables and knowledge from new data are input, whose tuning process can be highly resource-demanding [13].

Furthermore, considering the interdependency among influencing factors also helps to reveal the underlying mechanism of crash occurrences. The present study estimates the crash risk by quantifying the probability of crash occurrences. We hope this model can provide some real-time countermeasures to mediate risk when there is a high probability of crash. The formulation of countermeasures should be based on the identification of risk propagation path and significant risk contributors. However, there has been a dilemma between predictive and explanatory models: the models specialized in prediction are not the best in knowledge discovery, and vice versa [7, 28]. The DBN model has the advantage of implementing uncertainty analysis and probability reasoning and conducting bidirectional uncertainty investigation for prediction and diagnostic analyses. Combining with the sensitivity and strength of influences analysis methods can not only identify the most probable

risk propagation path, but also can recognise the most sensitive contributors in the propagation path [29]. Once the most sensitive risk contributors in the whole propagation path are revealed, the references for the sequence and emphasis of mediation can be provided, which helps to formulate appropriate real-time countermeasures to cut off the risk propagation path and decrease the probability of crash occurrence.

The existing DBN-based RTCPMs mainly emphasize the dynamicity of traffic flow characteristics, lacking investigation on the coupling interdependency among traffic flow characteristics. The main contributions of this study are (1) to apply the DBN structure learning algorithm in an example to predict road crashes; (2) to compare the performances of two DBN-based RTCPMs (considering the interdependency and not considering the interdependency) and the MLP-based RTCPM; and (3) to identify the most sensitive risk contributors in the propagation path by the use of the sensitivity and strength of influence analyses.

The manuscript is organized into five sections. The remainder is organized as follows. In Section 2, the materials and methods are presented. Section 3 presents the results and discussions. Section 4 provides some concluding remarks.

2. Materials and Methods

2.1. Study Area and Data Preparation. The 40 segments of the Yan'an elevated expressway in Shanghai, China, sequentially linking up to each other along the westbound and eastbound expressway, were selected as the study areas (see Figure 1). All segments are three-lane with detectors spaced at an approximate distance of 300–500 m. Each segment has similar road geometry and on/off-ramp arrangement; thus, the road geometries and ramp locations were not considered as influencing variables on the crash risk. There were 82 crashes that happened on the Yan'an expressway during August and September 2018. The dates, times, and segment IDs of the crashes were collected. Based on the matched case-control design, three corresponding noncrash cases for each crash case were randomly matched for the same segment and occurrence time (246 noncrash cases in total). Besides, traffic flow characteristics and weather variables were also obtained as inputs of the RTCPM, aiming at classifying the crash and noncrash states based on the investigation of relationship between crash risk, traffic flow characteristics, and weather conditions.

The existing dual-loop detectors in study areas are available for providing the average speed (km/h) and the average volume of a single lane (pcu/h) for each segment. Hourly weather variables, including visibility (km) and weather type (rainy or sunny), were collected from the Shanghai Xujiahui Observatory, which is 7.5 km far from the Yan'an expressway. In this study, the Traffic Performance Index (TPI) varying between 0 and 1 was applied as an indicator to measure the magnitude of congestion degree, where 1 is a traffic jam state and 0 is a free flow state (equation (1)). Consider

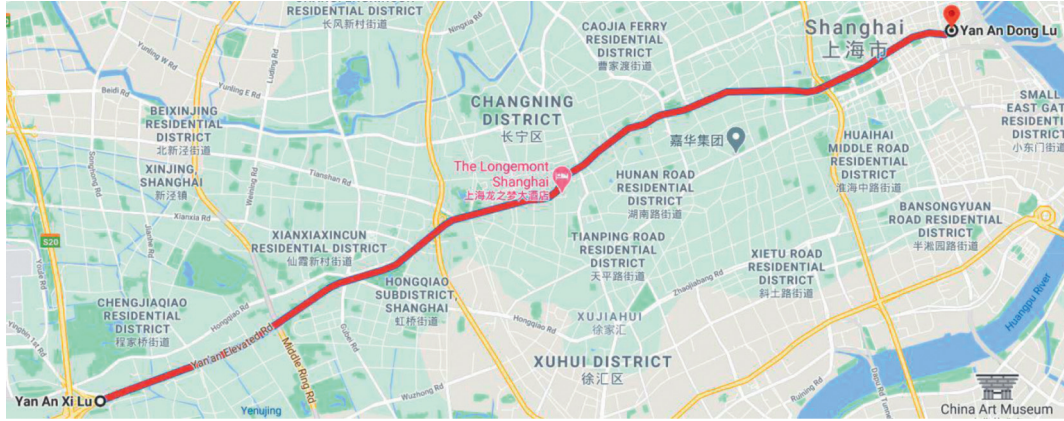


FIGURE 1: Yan'an elevated expressway, Shanghai, China.

$$TPI = \frac{(V_{\max} - V_i)}{V_{\max}}, \quad (1)$$

where V_{\max} is the maximum speed and V_i is the average speed at the i th time period.

The average speed data on the current, upstream, and downstream segments of the crash location and the TPI of the whole expressway were aggregated in 5-minute intervals. The evolution of traffic flow with time leading to a crash was a dynamic process; thus, the traffic flow characteristics of several time intervals before the crash should be combined to build the model. The intervals of 0–5 min (time slice 0), 5–10 min (time slice 1), and 10–15 min (time slice 2) prior to the crash were considered. The time slice 0 was excluded, because the crash warning system needs some time to recognise crash states, and the actual crash occurrence time and recorded time are not always completely consistent. Due to the raw weather data updated once an hour, the weather condition was regarded as a stable influencing variable across different time slices. Finally, the traffic flow and weather data corresponding to 82 crash cases and 246 noncrash cases were generated. In total, nine variables combining traffic flow characteristics on current, upstream, and downstream segments of the crash location with weather condition are shown in Table 1.

2.2. Random Forest (RF). The main purpose of constructing RTCPM is to evaluate crash risk in real time. High-dimensional variable space can increase the processing complexity of the RTCPM. Thus, Random Forest (RF), a widely used variable selection model, was implemented in this study to select influencing variables and reduce the redundancy of variables. Variable importance (VI) metric was used as the criterion to pick the mostly related variables [12, 30], which can be determined with the following steps.

- (1) Sample N amount of data from the learning set to build a tree classifier by bootstrap sample technique, and the remaining samples of the learning set were not used in the growth of the tree. The left-out samples, an effective internal test data set, were called out-of-bag (OOB) data, which were adopted to

obtain an unbiased error estimate. m number of variables were randomly selected from the original variable set M ($m < M$), and the best split variable in m at each tree node was adopted to split node. Each tree grew naturally without pruning. Repeat this step k times to construct RF consisting of k trees.

- (2) Each tree classifier produced a classification result by voting for the binary target (crash or noncrash) based on OOB samples, and the classification error rate R_i was calculated consequently.
- (3) Add random noise disturbance for the values of any variable in the OOB sample, and the new OOB sample was produced. Each tree that was implemented for crash/noncrash classification tests with the new OOB sample was used to calculate the classification error rate R_i' .
- (4) VI was calculated as the increase in the mean of the classification error rate of trees after adding random noise disturbance. The calculation formula was shown in the following equation:

$$VI = \frac{1}{k} \sum_{i=1}^k (R_i' - R_i). \quad (2)$$

2.3. Dynamic Bayesian Network (DBN). The Bayesian Network (BN) is a probabilistic graphical model that expresses the probability relationships among a set of variables that connect those variables in a directed acyclic graph (DAG). The BN has the advantages in learning causal relationships, predicting the consequences of intervention, and analyzing the most probable explanations of consequences. Some researchers have adopted BN to evaluate and analyze traffic accidents risk [31–33]. Most crashes did not happen based on a particular point in time, but they can be described through multiple traffic states among a series of time slices. The DBN is a kind of BN, which can couple time-series data to express the risk evolving process with time flowing forward [20]. With the application of the probabilistic inference, the critical step of BN generalization was to reveal the probabilistic dependencies of random variables, which are

TABLE 1: Information of the nine alternative variables.

Variable	Description
TPI	The average TPI of the whole expressway within 5 min interval
V	The average speed of current segment within 5 min interval (km/h)
U_V	The average speed of upstream segment within 5 min interval (km/h)
D_V	The average speed of downstream segment within 5 min interval (km/h)
Q	The volume of current segment within 5 min interval (pcu/h)
U_Q	The volume of upstream segment within 5 min interval (pcu/h)
D_Q	The volume of downstream segment within 5 min interval (pcu/h)
Visibility	The horizontal visibility within one hour (km)
Weather	The weather type in one hour, rainy or sunny

also expressed in time sequence in the DBN. Two types of dependencies existed in the DBN: dependencies within one time slice and dependencies among time slices. The DBN model consisted of observable evidence $X = \{x_1, x_2, \dots, x_t\}$ and hidden variables $Y = \{y_1, y_2, \dots, y_t\}$, which were traffic state variables and crash likelihood, respectively. When a Markov model and a BN were integrated to construct a DBN model, there were a transition model $P(x_t|x_{t-1})$, an observation model $P(y_t|x_t)$, and an initial state distribution $P(x_1)$. The joint probability distribution can be expressed as follows:

$$P(X, Y) = \prod_{t=2}^t P(x_t|x_{t-1}) \prod_{t=1}^t P(y_t|x_t)P(x_1). \quad (3)$$

There were three key steps to initialize a DBN model: (1) The ChiMerge algorithm was adopted to implement the discretization of continuous variables. (2) Structure learning was applied to present the graphic dependencies among variables. In this step, the DBN not only estimated the dependencies between variables within one time slice but also examined them among different time slices. The PC algorithm was used to build the structure of the BN within one slice among traffic state variables and crash likelihood. Then, the same variables among different slices were connected to build the structure of the DBN. (3) Parameter learning was conducted to learn the conditional probability distribution of variables within one time slice and across time slices. Parameter estimation was tested by the Expectation Maximization (EM) algorithm.

2.4. ChiMerge Algorithm. The continuous variables are usually problematic in DBNs because it fails to capture the relationships between the continuous variables [34]. The classical way to deal with continuous variables in DBNs is to discretize the variables [35]. Discretization is the operation of dividing continuous variables into a small number of intervals, where each interval is mapped to a discrete symbol. There are two widely used simple methods, the equal-width intervals, which divides the variables between the minimum and maximum values into a number of intervals in equal size, and the equal-frequency intervals, where the interval boundaries are chosen based on the fact that each interval contains the same number of samples. However, both of the

methods ignore the class of samples [36]. A good discretization has both the intrainterval uniformity and interinterval difference. ChiMerge algorithm performs merging operation by using the χ^2 statistic to test whether there are significant differences or similarities of relative class frequencies between adjacent intervals.

The ChiMerge algorithm is mainly consisted of several steps.

- (1) Sort the samples according to their value.
- (2) Calculate the χ^2 value for each pair of adjacent intervals with the following equation:

$$\chi^2 = \sum_{i=1}^m \sum_{j=1}^n \frac{(A_{ij} - E_{ij})^2}{E_{ij}}, \quad (4)$$

where $m = 2$ (the 2 intervals being compared), $n = 2$ (number of classes, i.e., crash and noncrash), A_{ij} = number of samples in the i th interval, j th class, and E_{ij} = expected frequency of A_{ij} .

- (3) Merge the pair of adjacent intervals with the lowest χ^2 value until all pairs of intervals with χ^2 values beyond χ^2 threshold. The χ^2 threshold is determined by a desired significance level (0.95 percentile level in this study) and the number of degrees of freedom (1 less than the number of classes). There are 2 classes (crash and noncrash); thus, the degree of freedom is 1. Finally, the χ^2 value is 3.841.

2.5. PC Algorithm. The PC algorithm is an efficient and classical algorithm used for structural learning in BN [37, 38]. The process of the PC algorithm mainly consists of three steps:

- (1) Determine the skeleton of the graph by conditional independence tests. Let $X = \{x_1, x_2, \dots, x_k\}$ be a set of random variables and $V = \{v_1, v_2, \dots, v_k\}$ be a set of nodes in a graph so that each node in V represents a random variable in X . Then, construct an undirected graph G where all nodes are connected to each other, and then the PC algorithm implements statistical tests to remove or maintain edges between adjacent nodes x_i and x_j given a conditioning x_γ in the graph by calculating the cross entropy $CE(x_i, x_j | x_\gamma)$:

$$\begin{aligned} \text{CE}(x_i, x_j | x_\gamma) &= \sum_{x_\gamma} P(x_\gamma) \sum_{x_i, x_j} P(x_i, x_j | x_\gamma) \\ &\cdot \log \frac{P(x_i, x_j | x_\gamma)}{P(x_i | x_\gamma) P(x_j | x_\gamma)}. \end{aligned} \quad (5)$$

The PC algorithm adopts G^2 test statistic, which equals $2n\text{CE}(x_i, x_j | x_\gamma)$ with n indicating the sample size, to verify the independence. The result of this first step is the skeleton of the graph.

- (2) Search the v -structures. If two variables x_i and x_j are not conditionally independent with given x_γ , then v_γ is determined as a collider node and a v -structure $v_i \rightarrow v_\gamma \leftarrow v_j$ is drawn, and the other edges remain undirected $v_i - v_\gamma - v_j$.
- (3) Confirm the directions of the rest of the edges. Combining with expert experience, some undirected edges between nodes are specified based on the principles where any cycle and any other v -configuration are not allowed.

2.6. Expectation Maximization (EM) Algorithm. The EM algorithm is a general algorithm to calculate maximal log likelihood and the performance has been proved to be effective in parameter learning of BN [39]. The basic theory of the EM algorithm is to learn the dependence among the nodes by iterating the process of parameters estimation [40]. The EM algorithm mainly consists of three steps:

- (1) Initialize θ : Given a set of unknown parameters θ , the value of a log likelihood is maximized. The object function is

$$\ell(\theta; X) = \log P(X|\theta) = \log \sum_Y P(Y, X|\theta). \quad (6)$$

Introduce a distribution $Q(Y)$: an initialization distribution of θ is defined based on Jensen's inequality:

$$\ell(\theta; X) = \log \sum_Y Q(Y) \frac{P(Y, X|\theta)}{Q(Y)} \geq \sum_Y Q(Y) \log \frac{P(Y, X|\theta)}{Q(Y)}. \quad (7)$$

- (2) E-Step: Calculate the distribution $Q(Y) = P(Y|X; \theta)$, which is viewed as the E-step.
- (3) M-Step: Optimize the parameters based on the estimation of the joint probability distribution, which is viewed as the M-step.

$$\theta' = \arg \max_{\theta} \sum_Y Q(Y) \log \frac{P(Y, X|\theta)}{Q(Y)}. \quad (8)$$

θ' replaces θ . The iterations process would be repeated until a local optimum of the estimated parameters is achieved.

2.7. Multilayer Perceptron (MLP). The neural network, an effective function approximator, is often used to solve

regression and prediction problems in various fields. A general multilayer perceptron model can be performed by the following 3 steps.

- (1) Initialize the MLP model. Assume that the original function can be approximated by a set of basic functions:

$$F(x) = \sum_{i=1}^m w_i \varphi_i(x) + e, \quad (9)$$

where F is the original function, x is the input vector, m is the number of network synapses, w is the weight of synapses, φ is the basis function allocated on synapses, commonly used functions with S-shaped curves (such as \tanh), and e is the error.

- (2) Load the sample point pair (x, y) and calculate the error between the predicted and true values:

$$e = \sum_i w_i \varphi_i(x) - y, \quad (10)$$

where y is the true value of the sample.

- (3) Adjust network synapse weights according to error feedback. The general calculation formula of the adjustment is

$$\Delta w = \varphi'(x) \sum_k w_k e_k, \quad (11)$$

where k is the layer after which the neuron to be adjusted is located. When the adjustment Δw is less than a preset threshold value η , this step would be terminated; otherwise, the weights would be updated and the process would go back to Step (2).

3. Results and Discussion

The DBN-based RTCPM was constructed based on the training dataset (involving 264 crash data and noncrash data) and validated based on the validation dataset (involving 64 crash data and noncrash data).

3.1. Variable Selection. Figure 2 shows the variable importance ranking which was determined by RF method. It is clear that the most important three variables were the TPI (0.151), V (0.144), and U_V (0.144) ($VI > 0.14$). The relative importance of other variables was less than 0.12. Therefore, the TPI, V, and U_V were selected as influencing variables to construct the DBN model. It is surprising that the visibility and weather played limited roles. It is probably explained by the collection time of the crash data (from August to September), when there were more daylight and less visibility differences (mean = 21.32 km, SD = 10.90 km). According to the Horizontal Visibility Grading of Chinese Standard (GB/T 33673-2017), when the visibility is greater than or equal to 10 km, the visual field is considered as a good level. Therefore, the overall good visibility did not contribute a lot to crash risk in this study. In addition, a classified weather variable, the weather type (rainy/sunny), was used as the

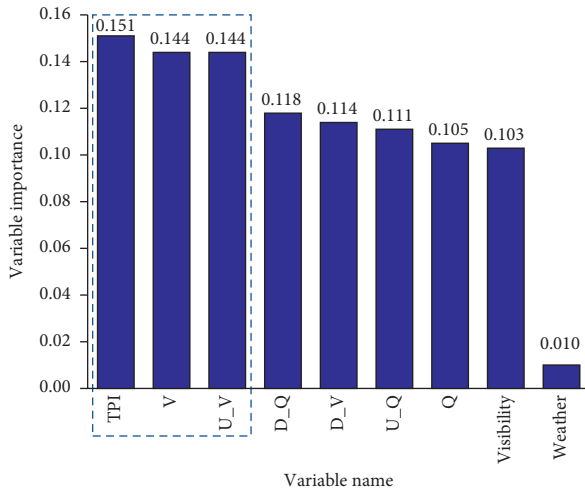


FIGURE 2: Variable importance ranking determined by Random Forest.

proxy to represent the weather condition in this study, rather than a quantized variable, rainfall. We assume that the relationship between the crash risk and rainfall might be more obvious than the weather type.

3.2. DBN Model Construction. The DBN models with and without considering the interdependence among traffic flow characteristics (TPI, V, and U_V) were both constructed based on the training dataset. The former model (the improved DBN-based RTCPM) was the main purpose, and the latter one (the original DBN-based RTCPM) was developed for comparison. Before constructing the graphical structure of the improved DBN-based RTCPM, the three traffic flow characteristics were discretized according to their corresponding crash cases using the ChiMerge algorithm. The number of discretization states of every variable was confined to 10 so that the calculation complexity in DBN models can be decreased. The discretization ranges of TPI, V, and U_V are presented in Figures 3–5, respectively. The results showed that the adjacent discretization intervals in every variable were characterized by distinguishable crash/non-crash ratio, indicating that the ChiMerge algorithm performs a good discretization.

After discretization, the PC algorithm and expert assessment were utilized to investigate the interdependency among traffic flow characteristics within one time slice. The dynamicity of traffic flow characteristics was reflected by connecting the same variables from time slice 2 to time slice 1. The dynamicity and interdependency determined the graphical structure of the improved DBN-based RTCPM (Figure 6). The original DBN-based RTCPM did not consider the interdependency among traffic flow characteristics, and its graphical structure was directly determined by connecting the traffic flow variables to crash risk within one time slice and connecting the same variables between two time slices (Figure 7).

Afterwards the parameter learning process was implemented using the EM algorithm. The initial states of the

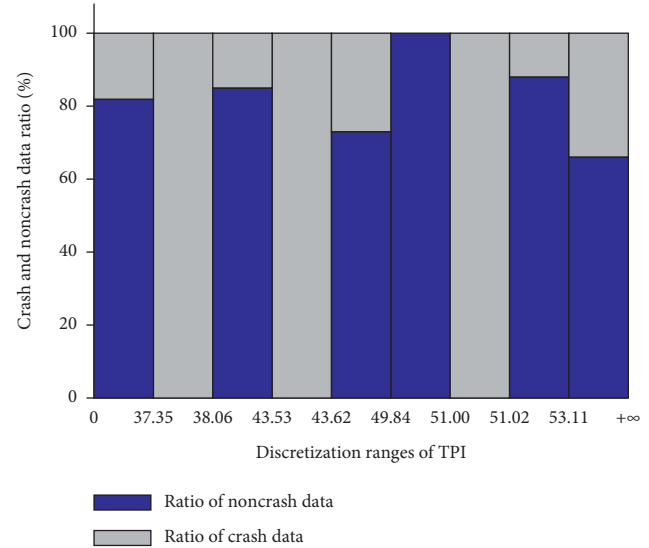


FIGURE 3: Discretization ranges of TPI.

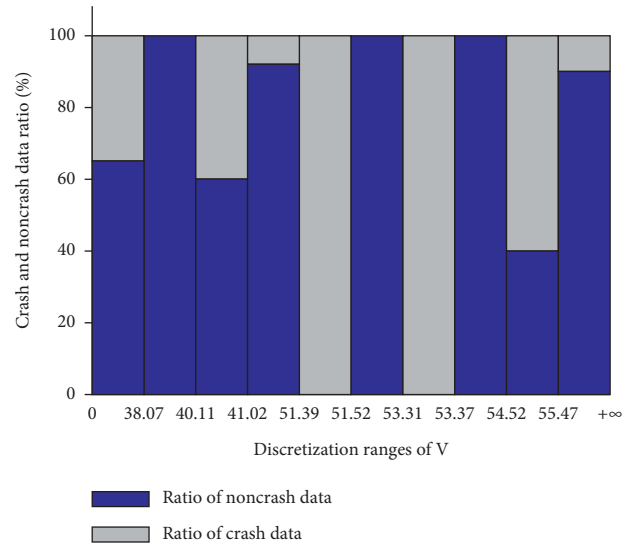


FIGURE 4: Discretization ranges of V.

improved DBN-based RTCPM and the original DBN-based RTCPM are presented in Figures 8 and 9, respectively. It was observed that their overall probabilities of a traffic flow state being associated with a crash were different (36% and 42%, respectively) when no new evidence was entered into the DBN. This difference suggested the importance of comparing the performance of the two types of DBN-based RTCPM.

3.3. Model Validation and Comparison. The validation dataset was used to validate the DBN models. When no new evidence was entered into the DBN, the marginal probability of crash risk node of initial state of DBN model was set as the classification threshold for evaluating the model performance. And then, each validation dataset was entered individually in the models. The crash risks, i.e., the posterior

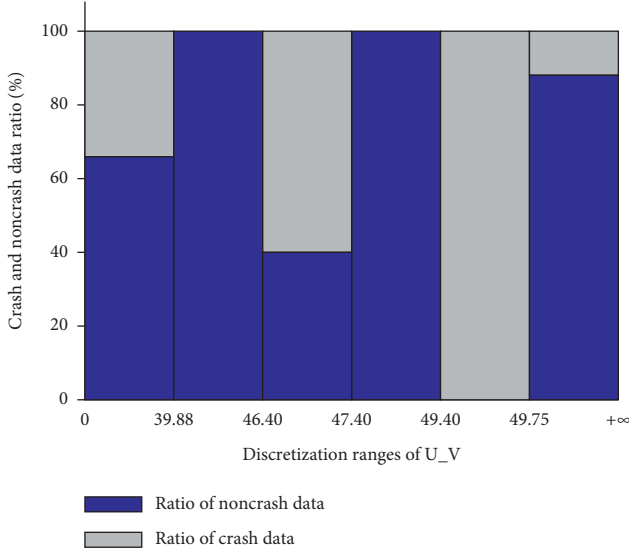


FIGURE 5: Discretization ranges of U_V.

probability of crash risk node, relating to the prone traffic condition, were calculated based on the prior probabilities. Several evaluation metrics based on the confusion matrix (Table 2) are presented in the following equations:

$$\text{overall_accuracy} = \frac{T_{\text{crash}} + T_{\text{noncrash}}}{T_{\text{crash}} + F_{\text{crash}} + F_{\text{noncrash}} + T_{\text{noncrash}}}, \quad (12)$$

$$\text{sensitivity} = \frac{T_{\text{crash}}}{(T_{\text{crash}} + F_{\text{noncrash}})}, \quad (13)$$

$$\text{specificity} = \frac{T_{\text{noncrash}}}{(T_{\text{noncrash}} + F_{\text{crash}})}, \quad (14)$$

$$\text{precision} = \frac{T_{\text{crash}}}{(T_{\text{crash}} + F_{\text{crash}})}, \quad (15)$$

$$\text{recall} = \frac{T_{\text{crash}}}{(T_{\text{crash}} + F_{\text{noncrash}})}, \quad (16)$$

$$F - \text{measure} = \frac{2 * \text{precision} * \text{recall}}{\text{precision} + \text{recall}}, \quad (17)$$

$$G - \text{means} = \sqrt{\text{sensitivity} * \text{specificity}}. \quad (18)$$

Besides the overall accuracy from equation (12), the sensitivity from equation (13), G -means from equation (17), and F -measure from equation (18) were used to compare the performance of two types of DBNs and MLP. For imbalanced classification, the overall accuracy metric is not sufficient due to its inability to examine the minor positive samples; thus, the sensitivity was chosen as the supplementary metric to examine the crash classification accuracy. The F -measure is the harmonic mean of precision and recall and represents the ability to detect crashes. Furthermore, the balanced classification ability can be reflected by G -means,

TABLE 2: Confusion matrix.

	Predicted crashes	Predicted noncrashes
Actual crashes	T_{crash}	F_{noncrash}
Actual noncrashes	F_{crash}	T_{noncrash}

which is the geometric mean of sensitivity and specificity. The comparison results are presented in Table 3.

As illustrated by Table 3, all the models can reach a good classification accuracy. Among them, the improved DBN-based RTCPM showed the best overall classification accuracy, followed by the original DBN-based RTCPM and MLP-based RTCPM. For the crash detection ability, the sensitivity metric indicated that the improved DBN-based RTCPM performed the best, and the relatively poor performance was seen in the original DBN-based RTCPM. Furthermore, the F -measure also suggested that the improved DBN-based RTCPM had better crash prediction ability than the original DBN-based RTCPM and MLP-based RTCPM. With respect to the balanced classification ability, the G -means revealed that the improved DBN-based RTCPM achieved better than the other models. For all the comparisons, the results demonstrated that the improved DBN-based RTCPM can achieve desirable overall prediction performance. It is also demonstrated that this model had an effective ability to monitor crashes in real time. Meanwhile, the model can keep the balance between crash and no-crash prediction. In summary, the prediction performance of DBN-based RTCPM can be improved by accounting for the interdependence of traffic flow characteristics.

3.4. Sensitivity and Strength of Influences Analysis. Investigation of the interdependency among the traffic flow also contributes to revealing the underlying mechanism of crash occurrence, which is helpful for formulating the real-time risk control measures. The sensitivity and strength of influences analysis were implemented in a professional DBN analysis software, Genie, to identify the most significant contributors to crash risk and the most probable risk propagation path.

3.5. Sensitivity Analysis. The sensitivity analysis of Genie can be utilized to identify which node had greater contribution to the target node in DBN. Setting the crash risk as the target node, conducting sensitivity analysis on it, and the contribution degrees of traffic flow characteristics on crash risks are presented in Figure 10 in a descending order. The results showed that the TPI in time slice 2 was the most sensitive factor that results in crash risk, followed by V in time slice 2, TPI in time slice 1, etc.

3.6. Strength of Influences Analysis. The strength of influences analysis was utilized to identify the most probable risk propagation path based on the improved interdependency structure. The strength of influence is always calculated from the distance between the probability distributions of the

TABLE 3: Performance comparison of two types of DBNs and MLP.

	Overall accuracy	Sensitivity	F-measure	G-means
Original DBN-based RTCPM	0.750	0.313	0.385	0.529
Improved DBN-based RTCPM	0.766	0.688	0.595	0.738
MLP-based RTCPM	0.725	0.556	0.476	0.656

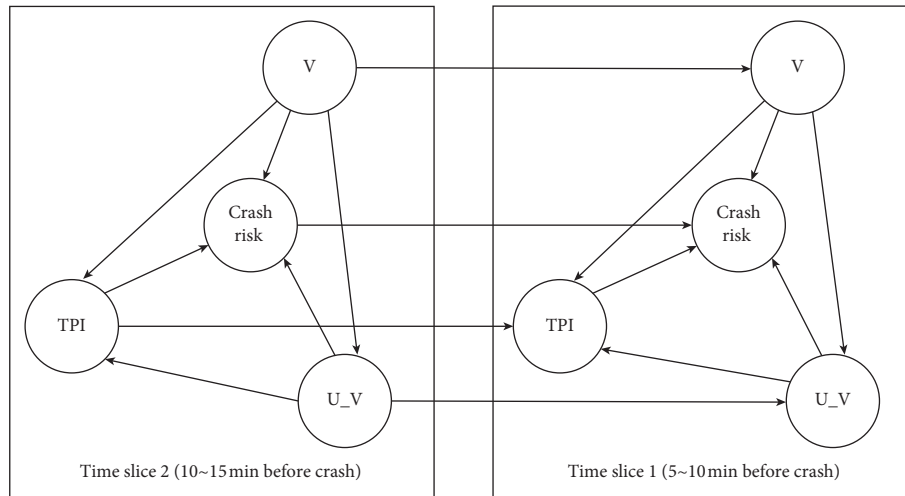


FIGURE 6: Graphical structural of the improved DBN-based RTCPM.

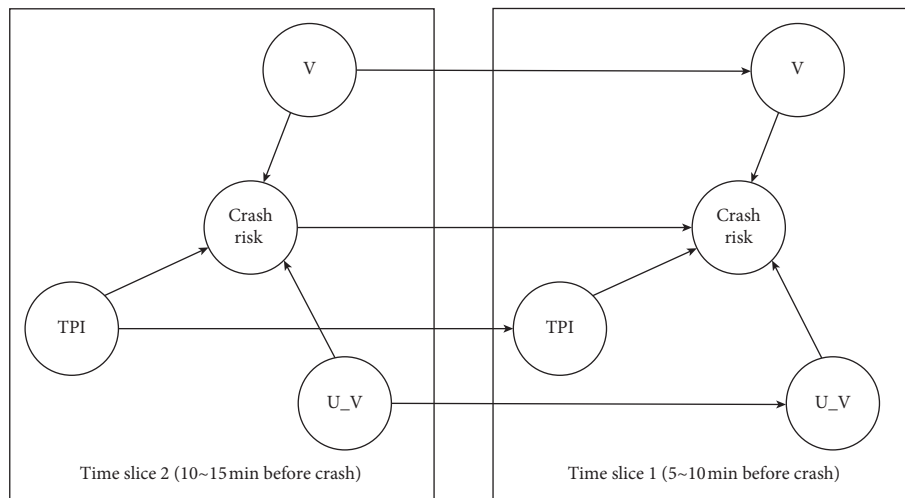


FIGURE 7: Graphical structural of the original DBN-based RTCPM.

child node conditional on the state of its parent node. As shown in Figure 11, the arcs have different values and thicknesses, presenting the strength of influence between connected nodes. The biggest accumulative value indicates that the most probable risk propagation path is V (time slice 2)→V (time slice 1)→U_V (time slice 1)→TPI (time slice 1)→crash risk on current segment.

Synthesizing the results of sensitivity and strength of influences analysis can be used to identify the most probable risk propagation path, as well as determine the most sensitive contributor in the propagation path. The results suggested that the sequence and emphasis of the real-time risk countermeasures should sequentially lay on V (time slice 2), TPI (time slice 1), V (time slice 1), and U_V (time slice 1).

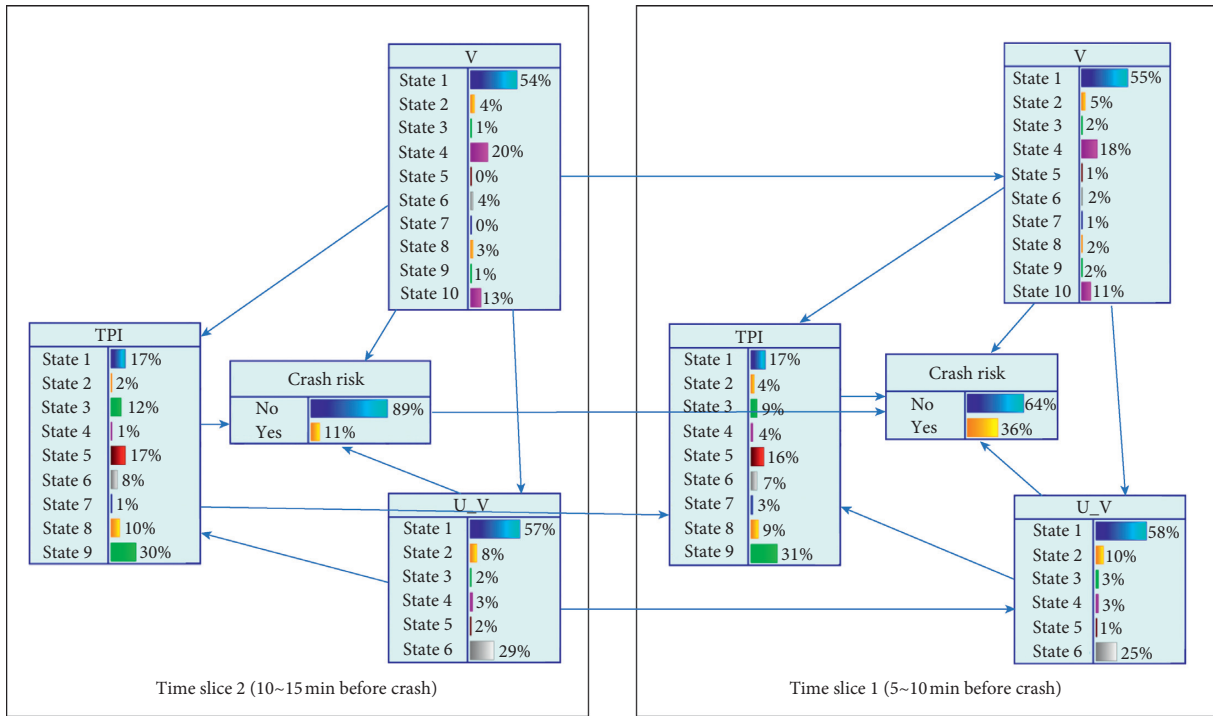


FIGURE 8: Initial state of the improved DBN-based RTCPM.

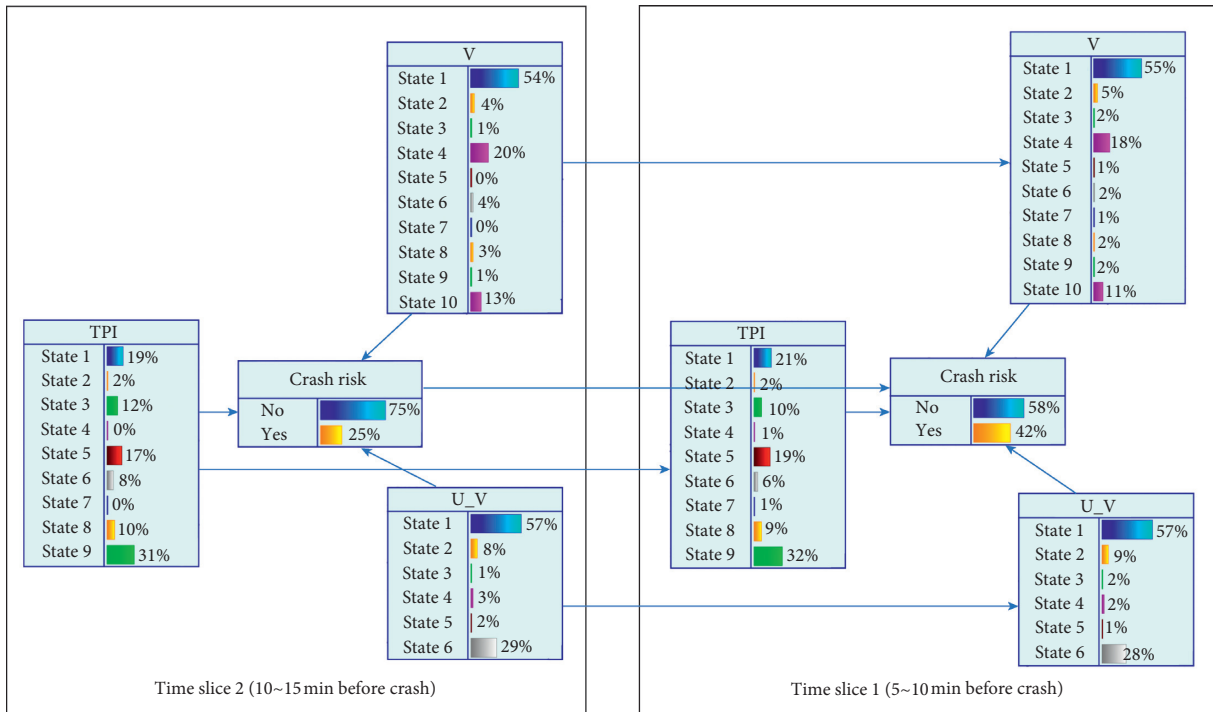


FIGURE 9: Initial state of the original DBN-based RTCPM.

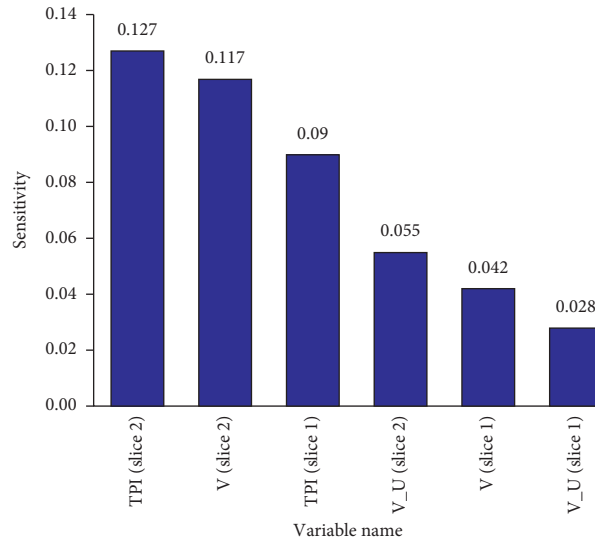


FIGURE 10: Results of sensitivity analysis.

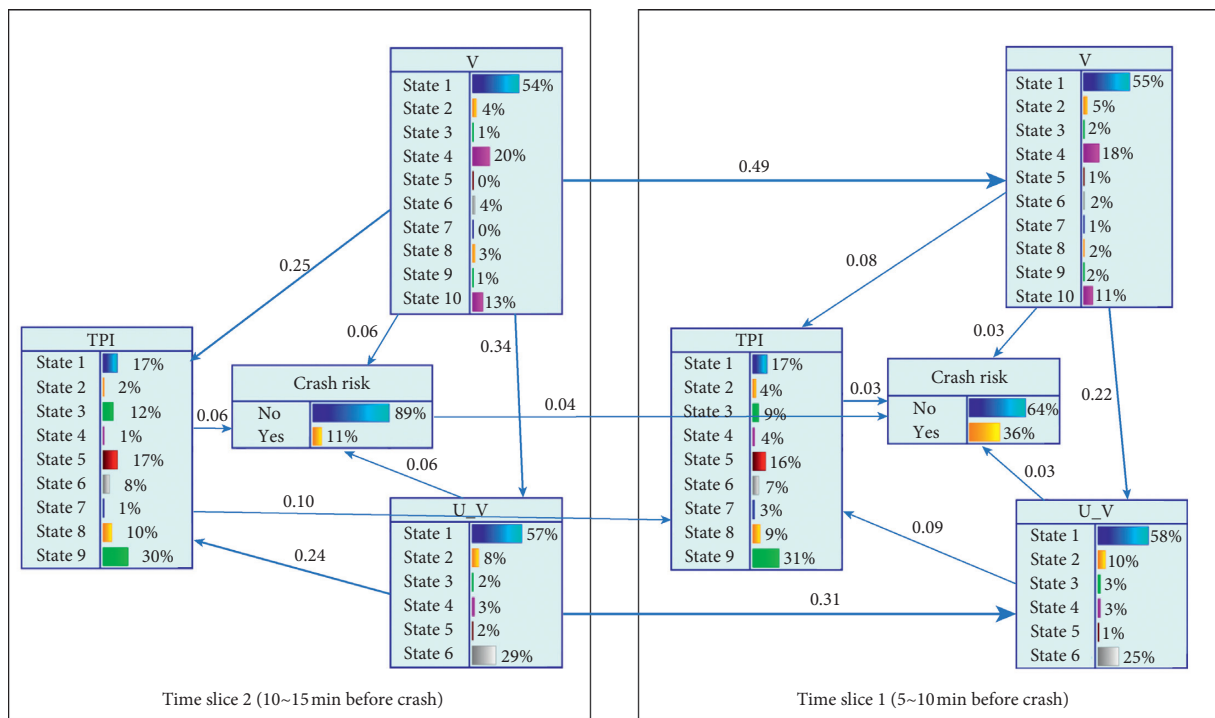


FIGURE 11: Results of strength of influences analysis.

4. Conclusions

This study aimed to build a RTCPM for urban elevated expressway by using the DBN model to capture the dynamicity and coupling interdependency among traffic flow characteristics before crash occurrence. The model was built and validated adopting traffic flow data collected on the Yan'an elevated expressway. Based on the DBN-based RTCPM, the sensitivity and strength of influences analysis were utilized to identify the most probable risk propagation path and the most sensitive contributors to crash risk. The main conclusions are as follows:

- (1) In model construction process, interdependency in the DBN model was determined by the PC algorithm and expert experience, and the dynamicity of traffic flow characteristics was expressed by adopting data in time slices. By validation, the improved DBN-based RTCPM got an overall accuracy of 76.6%, with a crash prediction accuracy of 68.8% and a crash/noncrash balanced classification accuracy of 73.8%. The results indicated that the model can achieve an effective crash prediction for urban elevated expressway.
- (2) Comparisons of the original DBN-based RTCPM and MLP-based RTCPM suggested that the improved DBN-based RTCPM can identify the interdependency among traffic flow characteristics before crash occurrences. The comparison results also indicated that the improved DBN-based RTCPM was more suitable for the prediction of real-time crashes for urban elevated expressway.
- (3) According to the results of sensitivity and strength of influences analysis, the most probable risk propagation path is V (time slice 2) $\rightarrow V$ (time slice 1) $\rightarrow U_V$ (time slice 1) $\rightarrow TPI$ (time slice 1) \rightarrow crash risk on current segment, and the most sensitive contributor to crash risk in this path is V (time slice 2), followed by TPI (time slice 1), V (time slice 1), and U_V (time slice 1). The results suggested that the formulation of the real-time risk countermeasures should sequentially focus on this sequence in the propagation path.

There would be two extensions in future research. On the one hand, the model was built and validated on the same urban elevated expressway; thus, the transferability of the model to another urban elevated expressway has not been discussed. On the other hand, the specific real-time risk countermeasures such as variable speed limit (VSL) can be investigated to improve crash risk.

Data Availability

The research data are available in the .CSV format file. They are available from the corresponding author upon request.

Conflicts of Interest

The authors declare that there are no conflicts of interest regarding the publication of this paper.

Acknowledgments

This study was supported by the National Natural Science Foundation of China (Grant no. 52072071).

References

- [1] C. Lee, B. Hellenga, F. Saccomanno et al., "Real-time crash prediction model for application to crash prevention in freeway traffic," *Transportation Research Record: Journal of the Transportation Research Board*, vol. 1840, no. 1, pp. 67–77, 2003.
- [2] M. Abdel-Aty, N. Uddin, A. Pande, M. F. Abdalla, and L. Hsia, "Predicting freeway crashes from loop detector data by matched case-control logistic regression," *Transportation Research Record: Journal of the Transportation Research Board*, vol. 1897, no. 1, pp. 88–95, 2004.
- [3] M. Abdel-Aty, N. Uddin, A. Pande et al., "Split models for predicting multivehicle crashes during high-speed and low-speed operating conditions on freeways," *Transportation Research Record: Journal of the Transportation Research Board*, vol. 1908, no. 1, pp. 51–58, 2005.
- [4] Q. Cai, M. Abdel-Aty, J. Yuan et al., "Real-time crash prediction on expressways using deep generative models," *Transportation Research Part C-Emerging Technologies*, vol. 117, 2020.
- [5] P. Li, M. Abdel-Aty, and J. Yuan, "Real-time crash risk prediction on arterials based on LSTM-CNN," *Accident Analysis and Prevention*, vol. 135, 2020.
- [6] C. Xu, W. Wang, P. Liu, R. Guo, and Z. Li, "Using the Bayesian updating approach to improve the spatial and temporal transferability of real-time crash risk prediction models," *Transportation Research Part C: Emerging Technologies*, vol. 38, pp. 167–176, 2014.
- [7] R. Yu, X. Wang, K. Yang, and M. Abdel-Aty, "Crash risk analysis for Shanghai urban expressways: a Bayesian semi-parametric modeling approach," *Accident Analysis & Prevention*, vol. 95, pp. 495–502, 2016.
- [8] Y. Guo, T. Sayed, L. Zheng, and M. Essa, "An extreme value theory based approach for calibration of microsimulation models for safety analysis," *Simulation Modelling Practice and Theory*, vol. 106, p. 102172, 2021.
- [9] Y. Guo, T. Sayed, and L. Zheng, "A hierarchical bayesian peak over threshold approach for conflict-based before-after safety evaluation of leading pedestrian intervals," *Accident Analysis & Prevention*, vol. 147, p. 105772, 2020.
- [10] Y. Guo, T. Sayed, and M. Essa, "Real-time conflict-based Bayesian Tobit models for safety evaluation of signalized intersections," *Accident Analysis & Prevention*, vol. 144, p. 105660, 2020.
- [11] Y. Guo, P. Liu, Y. Wu, and J. Chen, "Evaluating how right-turn treatments affect right-turn-on-red conflicts at signalized intersections," *Journal of Transportation Safety & Security*, vol. 12, no. 3, pp. 419–440, 2020.
- [12] M. Abdel-Aty, A. Pande, A. Das, and W. J. Knibbe, "Assessing safety on Dutch freeways with data from infrastructure-based intelligent transportation systems," *Transportation Research Record: Journal of the Transportation Research Board*, vol. 2083, no. 1, pp. 153–161, 2008.
- [13] M. Hossain and Y. Muromachi, "A Bayesian network based framework for real-time crash prediction on the basic freeway segments of urban expressways," *Accident Analysis & Prevention*, vol. 45, pp. 373–381, 2012.

- [14] D.-f. Chen, F. Luo, and Y. Feng, "Analysis of flight safety risk coupling based on fuzzy sets and complex network," in *Proceedings of 2013 International Conference on Management Science and Engineering*, pp. 329–334, Islamabad, Pakistan, November 2013.
- [15] T. Liu, F. Luo, and G. Yao, *Mathematical Analysis of Air Traffic Control Safety Risk Coupling*, 2012.
- [16] F. Zheng, M.-g. Zhang, J. Song, and F.-z. Chen, "Analysis on risk of multi-factor disaster and disaster control in oil and gas storage tank," *Procedia Engineering*, vol. 211, pp. 1058–1064, 2018.
- [17] J. Wang, J. Wu, X. Zheng, D. Ni, and K. Li, "Driving safety field theory modeling and its application in pre-collision warning system," *Transportation Research Part C: Emerging Technologies*, vol. 72, pp. 306–324, 2016.
- [18] C. Xu, W. Wang, and P. Liu, "A genetic programming model for real-time crash prediction on freeways," *IEEE Transactions on Intelligent Transportation Systems*, vol. 14, no. 2, pp. 574–586, 2013.
- [19] J. Sun, J. Sun, and P. Chen, "Use of support vector machine models for real-time prediction of crash risk on urban expressways," *Transportation Research Record*, vol. 2432, no. 1, pp. 91–98, 2018.
- [20] N. E. Fenton and M. Neil, *Risk Assessment and Decision Analysis with Bayesian Networks*, Taylor & Francis, Milton Park, ML, USA, 2013.
- [21] M. Jiang and J. Lu, "Maritime accident risk estimation for sea lanes based on a dynamic Bayesian network," *Maritime Policy & Management*, vol. 47, no. 5, pp. 649–664, 2020.
- [22] B. Khan, F. Khan, and B. Veitch, "A dynamic bayesian network model for ship-ice collision risk in the Arctic waters," *Safety Science*, vol. 130, 2020.
- [23] X. Wu, H. Liu, L. Zhang, M. J. Skibniewski, Q. Deng, and J. Teng, "A dynamic Bayesian network based approach to safety decision support in tunnel construction," *Reliability Engineering & System Safety*, vol. 134, pp. 157–168, 2015.
- [24] M. Hossain and Y. Muromachi, "A real-time crash prediction model for the ramp vicinities of urban expressways," *Iatss Research*, vol. 37, no. 1, pp. 68–79, 2013.
- [25] A. Roy, M. Hossain, and Y. Muromachi, "Enhancing the prediction performance of real-time crash prediction models: a cell transmission-dynamic bayesian network approach," *Transportation Research Record: Journal of the Transportation Research Board*, vol. 2672, no. 38, pp. 58–68, 2018.
- [26] A. Roy, R. Kobayashi, M. Hossain et al., "Real-time crash prediction model for urban expressway using dynamic bayesian network," *Journal of Japan Society of Civil Engineers Ser D3*, vol. 72, no. 5, pp. I_1331–I_1338, 2016.
- [27] J. Sun and J. Sun, "A dynamic Bayesian network model for real-time crash prediction using traffic speed conditions data," *Transportation Research Part C: Emerging Technologies*, vol. 54, pp. 176–186, 2015.
- [28] M. Hossain, M. Abdel-Aty, M. A. Quddus, Y. Muromachi, and S. N. Sadeek, "Real-time crash prediction models: state-of-the-art, design pathways and ubiquitous requirements," *Accident Analysis & Prevention*, vol. 124, pp. 66–84, 2019.
- [29] Y. F. Wang, T. Qin, B. Li, X. F. Sun, and Y. L. Li, "Fire probability prediction of offshore platform based on Dynamic Bayesian Network," *Ocean Engineering*, vol. 2017, 18 pages, Article ID 2525481, 2017.
- [30] L. Breiman, "Random forests," *Machine Learning*, vol. 45, no. 1, pp. 5–32, 2001.
- [31] A. Karimnezhad and F. Moradi, "Road accident data analysis using Bayesian networks," *Transportation Letters The International Journal of Transportation Research*, vol. 9, no. 1, pp. 12–19, 2015.
- [32] T. Tang, S. Zhu, Y. Guo et al., "Evaluating the safety risk of rural roadsides using a bayesian network method," *International Journal of Environmental Research and Public Health*, vol. 16, no. 7, 2019.
- [33] X. Zou and W. L. Yue, "A bayesian network approach to causation analysis of road accidents using netica," *Journal of Advanced Transportation*, 2017.
- [34] D. Geiger and D. Heckerman, "Learning Gaussian networks," *Uncertainty Proceedings 1994*, pp. 235–243, 1994.
- [35] S. Monti and G. F. Cooper, "A multivariate discretization method for learning bayesian networks from mixed data," arXiv preprint arXiv:1301.7403, 2013.
- [36] R. Kerber, "ChiMerge: discretization of numeric attributes," in *Proceedings of the 10th National Conference on Artificial Intelligence*, San Jose, CA, USA, July 1992.
- [37] M. Kalisch and P. Buehlmann, "Estimating high-dimensional directed acyclic graphs with the PC-algorithm," *Journal of Machine Learning Research*, vol. 8, pp. 613–636, 2007.
- [38] F. Musella, "A PC algorithm variation for ordinal variables," *Computational Statistics*, vol. 28, no. 6, pp. 2749–2759, 2013.
- [39] P. B. G. Lindsay, "Alternative EM methods for nonparametric finite mixture models," *Biometrika*, vol. 88, no. 2, pp. 535–550, 2001.
- [40] S. L. Lauritzen, "The EM algorithm for graphical association models with missing data," *Computational Statistics & Data Analysis*, vol. 19, no. 2, pp. 191–201, 1995.

Research Article

Modeling and Analysis on Minimum Safe Distance for Platooning Vehicles Based on Field Test of Communication Delay

Mengyan Hu , Xiangmo Zhao, Fei Hui , Bin Tian , Zhigang Xu , and Xinrui Zhang

College of Information Engineering, Chang'an University, No. 435, The Middle Section of South 2nd-Ring Road, Xi'an, Shaanxi 710064, China

Correspondence should be addressed to Bin Tian; tb@chd.edu.cn

Received 2 February 2021; Accepted 29 April 2021; Published 13 May 2021

Academic Editor: Yanyong Guo

Copyright © 2021 Mengyan Hu et al. This is an open access article distributed under the Creative Commons Attribution License, which permits unrestricted use, distribution, and reproduction in any medium, provided the original work is properly cited.

Vehicle platooning is a perspective technique for intelligent transportation systems (ITS). Connected and automated vehicles (CAVs) use dedicated short-range communication (DSRC) to form a convoy, in which the following vehicles can receive the information from their preceding vehicles to achieve safe automated driving and maintain a short headway. Consequently, a vehicle platoon can improve traffic safety and efficiency, further reducing fuel consumption. However, emergency braking inevitably occurs when the platoon meets an accident or a sudden mechanical failure. It is more critical when the wireless communication got delays. Therefore, “how to predefine a minimum safe distance (MSD) considering communication delay” is a challenging issue. To this end, a series of field tests were carried out to measure the communication delay of IEEE 802.11p that is the underlying protocol of DSRC. Subsequently, MSD is modeled and analyzed when the platoon travels at accelerating, cruising, and decelerating states. More importantly, the results of field tests are applied in the models to investigate the impact of communication delay on MSD in practice. The simulation results verify that the proposed model can effectively maintain the platooning vehicles' safety even if emergency braking happens with certain communication delays.

1. Introduction

Nowadays, roadway traffic continues to cause congestion, energy consumption, and pollution. To address these issues, researchers are studying connected and automated vehicle (CAV) technologies [1]. CAVs equipped with various on-board sensors and wireless communication systems can sense and exchange information between each other. Therefore, they can move quickly, safely, and smoothly and lead to a revolution in modern transportation systems. Among the CAV applications, vehicle platooning is an important application to achieve better traffic safety, efficiency, and lower fuel consumption by reducing the aerodynamic drag of the following vehicles. The safety of a vehicle platoon depends on two critical factors: the desired minimum safe distance (MSD) and the varying wireless communication delay caused by the complex traffic environments.

Many experienced drivers know that driving at a short gap from a vehicle ahead requires a lower throttle action to propel the vehicle forward owing to the reduced

aerodynamic drag [1]. Therefore, a vehicle platoon is a suitable solution to reduce emissions. Additionally, the total road capacity will also be increased when vehicles are arranged as a platoon with small spacing [2]. Hence, the determination of the MSD in vehicle platoon is very important for the following reasons: (1) it ensures that the vehicles in the platoon will not collide under any circumstances; (2) it is needed to determine the best balance point between the traffic safety and efficiency of the platoon; (3) it has an incremental relationship with the communication delay, although the impact of communication delay on MSD is very difficult to model; (4) it will be a critical parameter for the platoon controller if the MSD of platoon is modeled.

Vehicle platoon systems have attracted considerable attention in recent years. In a vehicle platoon system, several vehicles follow one leader vehicle and travel in a line maintaining a constant velocity. Each vehicle maintains a safe distance from its preceding vehicle. Owing to the shorter intervehicle distance in one lane, platoons can provide higher roadway throughput and better traffic flow control. It

can also help to reduce energy consumption by avoiding unnecessary fluctuations in speed [3]. Despite these advantages, a shorter intervehicle distance can lead to safety issue [4]. Therefore, it is important for a vehicle platoon to maintain a safe intervehicle distance.

Platooning is considered as one of the innovations in the automotive industry that aim to improve the safety, efficiency, mileage, and time of travel of vehicles while relieving traffic congestion, decreasing pollution, and reducing stress for passengers [5]. Also, platooning makes it possible for vehicles to travel together closely and safely. It can reduce the amount of space used by multiple vehicles on a highway, reducing traffic congestions [6].

To this end, this study first determines a practical upper bound of communication delay by testing IEEE 802.11p in the field (IEEE Std. 802.11p, 2010). Subsequently, MSD models are built considering communication delay so that a practical and solid MSD is provided for a vehicle platoon controller. Some explanations and assumptions are made as follows: we consider a platoon of six vehicles that exchange information with each other over a vehicular network. Each vehicle is assumed that it can process incoming information and update and broadcast its own state information over the vehicular network. All communication modules are assumed to be identical, and, as a result, messages all experience a uniform (identical) time delay even if the delay might be stochastic in the real world.

The main contributions of this study are summarized as follows:

- (1) Field tests were carried out to obtain the maximum communication time delay
- (2) By considering communication delay, MSD models were proposed to guarantee the safety of platooning vehicles when emergency braking happened during accelerating, cruising, and decelerating states
- (3) Simulation experiments were conducted to verify the correctness of the MSD models

The remainder of this paper is organized as follows: Section 2 presents related studies on the impact of a communication delay on CAV platoon control. Section 3 describes the necessary problem statement regarding MSD of platoon CACC string stability, in which the communication time delay, GPS errors, and mechanical responses of a vehicle are introduced. Section 4 introduces a field test that measures and calculates the communication delay of DSRC based on consecutive packets lost. The main idea of this study is elaborated on in Section 5. Three numerical models are developed to identify the MSD based on communication delay. Simulations carried out to verify the correctness and accurateness of the obtained MSD are then detailed in Section 6. Finally, the main points of the present study are summarized in Section 7.

2. Related Works

Platooning and related issues have been researched in several projects so far. PROMOTE CHAUFFEUR I + II European project [7, 8] explored truck platooning and driver assistant

functions. KONVOI German national project [9] explored truck-only platoons. For platooning vehicles, the PATH project [2] in the USA required exchange information between platooning vehicles and infrastructure and the platoon travels on dedicated lanes for autonomous driving.

String stability is an important performance for vehicle platoons [9]. It is related to the ability to suppress dynamics disturbance, for example, velocity or acceleration, which needs to be emphasized towards the upstream direction of a platoon, because that might lead to a collision in the platoon. To solve this problem, spacing errors between the vehicles in a platoon are often measured. Rajamani and Zhu [10] considered practical systems with adaptive cruise control, where both manually driven and automated cars can coexist. It was shown that the intermediate spacing can be reduced while maintaining string stability through wireless communication. Liang et al. [11] showed that the string stability can be obtained through an ordering strategy with respect to the vehicle mass. However, the string-stable performance cannot guarantee driving safety when emergency braking suddenly occurs by any vehicle in the platoon.

Collision avoidance has been studied in many areas of engineering, such as automotive engineering, maritime transportation, and unmanned aerial vehicles [12]. Nevertheless, few studies have considered safety strategies for CAVs in an emergency scenario. Recently, Ali [13] utilized reachability analysis tools for threat assessment and proposed a novel automotive safety function based on the vehicle state and road preview information.

Peters et al. [14] proposed a control strategy to achieve platooning stability with certain time delays by applying the leader state to the other members of the platoon. Kim et al. [15] presented an enhanced time-delay controller for the position control of autonomous vehicles and proposed an integral sliding-mode controller to improve the control precision. Zhang et al. [16] designed an adaptive sliding-mode controller considering the communication time delay and uncertainties to enhance vehicle mobility and safety. Song et al. [17] proposed a motion model based on a car-following model that describes the dependent motion of vehicles in the single-lane case to consider the motion dependence across vehicles. Zhao et al. [18] proposed a rear-end collision warning system (ReCWS) based on dedicated short-range communication (DSRC) information transmission delay and GPS error and verified the warning system by field tests. Ploeg et al. [19] proposed a control strategy for graceful degradation of one-vehicle look-ahead CACC to guarantee the platoon safety, which can degrade CACC to ACC when the communication network has latency and packet loss. Oncu et al. [20] approached the design of a CACC system from a Networked Control System (NCS) perspective and presented an NCS modeling framework. And they developed a technique to study the string stability of vehicle platoon. Abou et al. [21] proposed a novel CACC strategy to overcome the homogeneity assumption. This strategy can achieve string stability for uncertain heterogeneous platoons. These researchers also formulate an extended average dwell-time framework and an adaptive switched control strategy in order to handle the inevitable

communication losses. A summary table is shown in appendix. However, these studies did not investigate the safety issues during emergency braking while accompanied with communication delay.

Some studies have investigated the performance and time delay of the IEEE 802.11p protocol, as well as the platoon controller. Nevertheless, the influence of the communication time delay on the MSD of vehicles in platoon has not been investigated. Therefore, in this study, we attempt to fill this gap in the literature. The impact of communication time delay on MSD is investigated in an emergency braking scenario. Field test data are used to calculate the MSD of vehicle platoon in practice.

3. System Formulation

We assume that a platoon consists of a limited number of vehicles V_1, V_2, \dots, V_n . Vehicles are labeled in the order of platoon, where V_1 is the leader and V_2, \dots, V_n are the consecutive followers. The state of vehicles is represented by $[X_i, V_i]$, where X_i and V_i are the position and velocity of the i th vehicle, respectively. The state of the i th vehicle evolves in time according to the following stochastic differential equations:

$$dx_t^{(i)} = v_t^{(i)} dt, \quad (1)$$

$$dv_t^{(i)} = u_t^{(i)} dt + g d\delta_t^{(i)}, \quad (2)$$

where $u_t^{(i)}$ is the control input at time t and $g d\delta_t^{(i)}$ represents a noise generator affecting the dynamics of the vehicle that models the uncertainty diffused in the system. It is assumed that noise acts on every vehicle additively and independently of the noise from the other vehicles.

The noises may contain communication time delay, GPS error, mechanical response, surface friction, and so on. In this study, all the information of leader and predecessors is transmitted by wireless intervehicle communications. Therefore, communication time delay would be mainly investigated in theory and practice. The purpose of this study is to confirm the impact of the communication time delay on the MSD between platooning vehicles.

A predecessor-leader following topology is adopted to form a cooperative platoon [22], as shown in Figure 1. The topology is used to characterize the connectivity and information flow between vehicles under the vehicular network environment. Each vehicle in the platoon obtains the real-time dynamics states (i.e., position and speed) from the lead and preceding vehicles through the vehicle-to-vehicle (V2V) communications.

Figure 1 shows a schematic of the predecessor-leader following topology [22], which is used to characterize the connectivity between platoon vehicles under the connected environment. Each vehicle in the platoon obtains real-time information (i.e., position and speed) from the front and lead vehicles through the V2V communication system under this environment.

The objectives of platooning control are to ensure that two conditions are satisfied: (1) the pairwise difference

between the positions of two adjacent vehicles converges to zero; (2) the platoon reaches the same uniform speed under a steady state. These conditions can be synthesized a controller as follows:

$$u_t^{(i)} = \min(u_t^{(i,i-1)}, u_t^{(i,L)}), \quad (3)$$

$$u_t^{(i,i-1)} = k_i(v_{t-\tau}^{(i)} - v_{t-\tau}^{(i-1)}) + \beta k_i(x_{t-\tau}^{(i)} - x_{t-\tau}^{(i-1)} - (d_i - d_{i-1})), \quad (4)$$

$$u_t^{(i,L)} = k_i(v_{t-\tau}^{(i)} - v_{t-\tau}^{(L)}) + \beta k_i(x_{t-\tau}^{(i)} - x_{t-\tau}^{(L)} - (d_i - d_L)), \quad (5)$$

where τ is the communication time delay, k_i is the gain of speed error, βk_i is the gain of distance error, β is a tuning parameter, d_i is the distance traveled by vehicle i , and $u_t^{(i,i-1)}$ and $u_t^{(i,L)}$ are two optional desired controllers of i th vehicle calculated by using predecessor's state and leader's state, respectively.

Equation (3) indicates the final desired control should be the minimum of $u_t^{(i,i-1)}$ and $u_t^{(i,L)}$. The first and second terms in (4) and (5) represent the speed error and distance error. Equations (4) and (5) ensure that conditions (1) and (2) are satisfied and the pairwise difference converges to zero. The controller guarantees that the platoon reaches a uniform speed and a safe relative distance between two vehicles under a steady state.

4. Field Test of Communication Delay for DSRC

For modeling a practical MSD, field tests are carried out to determine the actual communication delay in a platoon. Nowadays, DSRC and C-V2X (cellular-vehicle-to-everything) are the two major techniques for the communication of CAVs. DSRC technique was developed by the IEEE (Institute of Electrical and Electronic Engineers) using IEEE 802.11p standard as its underlying protocol, while C-V2X technique was developed by 3GPP (3rd Generation Partnership Project) as LTE-V2X standard (an expansion of the LTE) and evolved to 5G.

For the vehicle platooning, direct vehicle-to-vehicle (V2V) communication in short range is needed. For this requirement, DSRC can well support that by its nature characteristic. LTE-V-Direct mode of C-V2X also can be used to satisfy the requirement. However, the LTE-V-Direct mode is proposed in Release 14 by 3GPP for a short period. There is no hardware module for its practical applications currently. By contrast, DSRC has been extensively tested and verified. The chips and modules of DSRC are relatively mature. In fact, the dedicated frequency for direct communications is similar between DSRC and C-V2X (LTE-V-Direct). Accordingly, DSRC devices are used to determine the actual communication delay for the vehicle platoon in this study.

4.1. Characteristic Analysis on DSRC. IEEE 802.11p is an amendment of WiFi that meets the relevant applications of intelligent transportation systems (ITS) and has already been used for DSRC [23]. Based on the standard of the IEEE

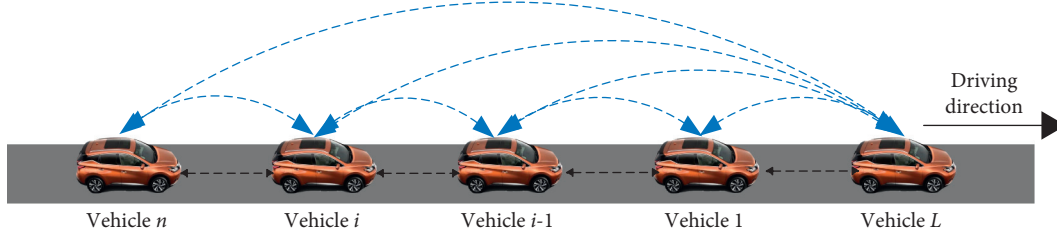


FIGURE 1: Flow topology of vehicle platoon.

802.11p protocol, a 75 MHz bandwidth from 5.850 to 5.925 GHz is allocated to DSRC by the Federal Communications Commission of the US [24]. This 75 MHz spectrum is divided into six service channels and one control channel of 10 MHz. Apart from the 802.11p, IEEE has also formulated a series of protocols for vehicular communication systems named Wireless Access for Vehicular Environment (WAVE). IEEE 802.11p is modified from 802.11a and defines the physical layer of the WAVE stack and part of the medium access control layer [24]. Based on the IEEE 802.11p standard, information such as position, speed, and direction is delivered from vehicle to other vehicles every 100 ms in a platoon. More detailed contents are elaborated in Appendix A.

4.2. Determination of DSRC Communication Delay by Field Test. In this study, two real vehicles BYD Yuan and Ford Focus as shown in Figure 2 equipped with DSRC on-board units are used.

On-Board Unit (OBU) is designed to transmit and process data between two connected vehicles, as shown in Figure 3. OBU includes two devices that are On-Board Diagnostics (OBD) and DSRC module. OBD is responsible for exchanging data between the vehicular system and the DSRC module (Figure 3(a)). DSRC module is in charge of transmitting packets between vehicles (Figure 3(b)). Figure 4 shows the bird's-eye view of the CAV test field of Chang'an University where the experiments were carried out.

The packet delivery rate (PDR) of the vehicles can be calculated as follows:

$$\text{PDR} = \frac{P_r}{P_s}, \quad (6)$$

where P_r and P_s are the number of data packets received by the destination node and sent by the source node, respectively.

Complete clock synchronization is difficult to achieve; thus, the round-trip time (RTT) is calculated to obtain the communication delay. The time taken for a data packet to be sent is denoted as T_1 ; the time elapsed after receiving the data packet is denoted as T_2 ; the time taken for the data packet to be transferred from the sender to the receiver is denoted as T_3 ; when the sender receives the data packet, record the time and record it as T_4 . Then, the RTT can be calculated as

$$\text{RTT} = (T_4 - T_1) - (T_3 - T_2), \quad (7)$$

and the communication delay can be calculated as

$$t_{iL} = \frac{\text{RTT}}{2}. \quad (8)$$

The following observations were made from the field test:

- (1) Neither the PDR nor the latency changes significantly when the distance between two vehicles is less than 400 m
- (2) The PDR and latency do not change as the speed of the vehicles increases up to 100 km/h
- (3) The average latency of 802.11p is approximately 5 ms with a PDR of 100%

There are pieces of literature to prove that the number of vehicles (nodes) would not have observable effects on the time delay unless it has a huge number of vehicles or the distances of vehicles are beyond the maximum communication distance of DSRC [25]. The communication time delay neither has observable differences that can affect safe distance under normal weather conditions (rain, fog, and cloudy day) [26]. Our experiments do not involve extreme weather, which can be considered as the next step of the research.

4.3. Time-Delay Calculation. Based on the standard 802.11p, the PDR is not lower than 90%. In the test above, the PDR was over 98%, which indicates that a maximum of 20 packets out of 1000 were lost. However, the MSD of vehicles in a platoon cannot be determined only based on the PDR. It cannot be known whether the packet loss has a uniform distribution or concentrated distribution. In this case, the number of consecutive packet losses will have a large impact on traffic safety. Yi et al. [27] proposed the Update Delay (UD) framework to represent the time elapsed between two consecutive successfully received CAMs from a specific transmitter at a specific receiver. Unlike the simulation result in [28], the test on the real vehicles showed that the maximum number of consecutive packet losses is two with a PDR of 98%. In the most extreme condition whereby the lead vehicle decelerates at the beginning of the delivery of one packet and two consecutive packets are lost, the maximum communication time delay is

$$t_d + 2t_p = 205\text{ms}, \quad (9)$$

where t_d is the average latency of 802.11p with a PDR of 100% and t_p is the time taken of the transmission with one

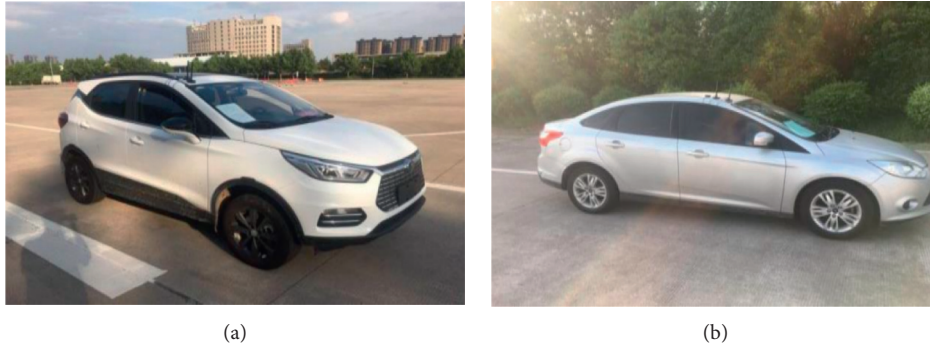


FIGURE 2: Vehicles used in the field test. (a) BYD Yuan. (b) Ford Focus.

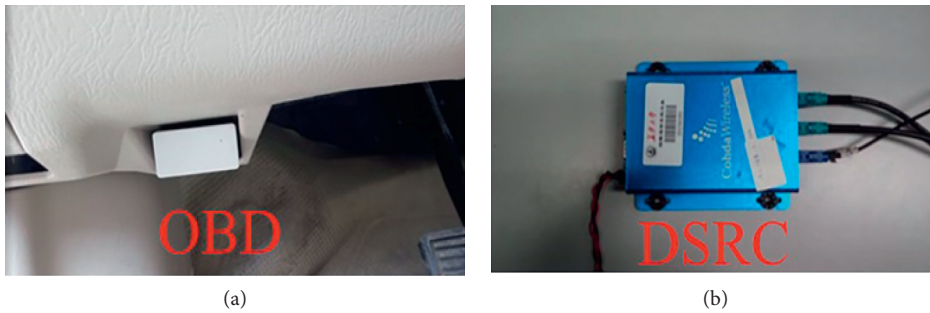


FIGURE 3: On-Board Unit (OBU) equipment. (a) On-Board Diagnostics (OBD) and (b) DSRC module.



FIGURE 4: Cav test field of Chang'an University.

packet. This is consistent with the observations. Considering a loss of three consecutive packets, the time delay is $t_d + 3t_p = 305\text{ms}$. Based on the standard of 802.11p, the packet loss rate should be no larger than 10%; otherwise, the communication network cannot be used on vehicle networking. We also tested the consecutive packet loss number with 100%–90% PDR; the consecutive packet loss number has no obvious change due to the CSMA/CA protocol.

Figures 5 and 6 show the influence of distance and PDR on communication time delay. A series of experiments have been performed to investigate the impact on the performance of platoon. The results indicate that the impact of PDR on time delay can be ignored compared with the influence of consecutive packet loss. On the other hand, the number of vehicles (nodes) would not have observable effects on the time delay, unless it has a huge number of vehicles or the distances of vehicles are beyond the maximum communication distance of DSRC [25]. In this study, the number of vehicles is 6; it is far less than the capacity of

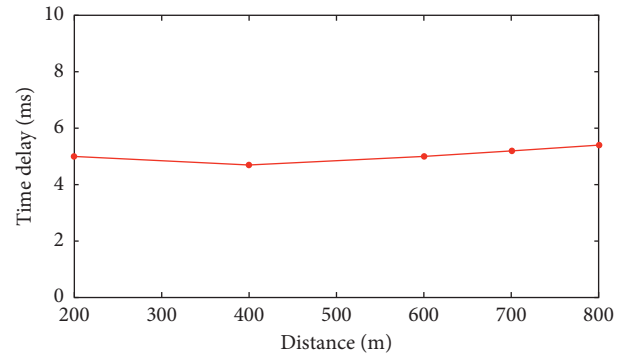


FIGURE 5: The influence of distance on time delay.

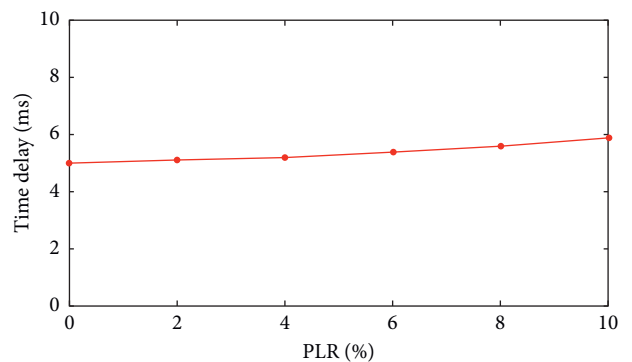


FIGURE 6: The influence of PLR (0–10%) on time delay.

DSRC. Therefore, the influence of traffic density is beyond our consideration.

5. Modeling and Analysis on MSD

Figure 7 shows the vehicle braking process of vehicles i and $i - 1$ in the platoon. The two vehicles in the right are the state of the vehicles i and $i - 1$ after braking; S is the gap between vehicles; S_i and S_{i-1} are the length of two adjacent vehicles; d_g is the gap after braking; and d_i and d_{i-1} are the distance between vehicles during the decelerating process, respectively.

In a platoon, an appropriate headway between two consecutive vehicles should be approached for driving safety. As above mentioned, the desired acceleration of each vehicle in the platoon would generally follow equation (3). However, the communication delay caused by the DSRC system also needs to be considered to guarantee the safety of vehicles. Figure 8 shows a flow diagram of the information transmission process in the vehicle platoon.

MSD models will be designed and proposed as in the following subsections. These models are formulated to define MSD for an emergency braking scenario during platooning vehicles cruising, accelerating, and decelerating.

5.1. MSD Model for Cruising State. In this paper, t_{ij} and t_{iL} denote the communication time delay between vehicles i and j and vehicle i and the lead vehicle L , respectively. The vehicle mechanical response delay τ is the same for each vehicle in the platoon. When a vehicle in a platoon of vehicles which drives at the same uniform speed under a steady state brakes, all vehicles finally reach a steady state. The time consumed during braking can be calculated as follows:

$$t_L = \frac{v_L - v_0}{a} + \tau, \quad (10)$$

$$t_i = \frac{v_i - v_0}{a} + t_{iL} + \tau, \quad (11)$$

where t_L and t_i are the time consumed by the leader and vehicle i , respectively, and v_0 is the final speed of the platoon. In this case, the difference in braking distance of vehicle i and the lead vehicle, denoted as d_i and d_L , respectively, can be calculated as follows:

$$d_L = \int_0^{(v_L - v_0)/a + \tau} v_L + a(t - \tau) dt, \quad (12)$$

$$d_i = \int_0^{(v_i - v_0)/a + t_{iL} + \tau} v_i + a(t - \tau - t_{iL}) dt. \quad (13)$$

Each vehicle in the platoon has the same velocity before braking, that is, $v_L = v_i$, and the acceleration a and the mechanical response delay τ are the same. From $d_L - d_i$, it can be seen that τ is irrelevant to the result of the difference in braking distance. This indicates that when the vehicles in the platoon have the same mechanical response delay, it would have no influence on the MSD.

From (10)–(13), the time taken for the deceleration process of the lead vehicle can be calculated as follows:

$$t_L = \frac{v_L - v_0}{a_{\max}}. \quad (14)$$

The time taken for vehicle i to slow down to the same speed as that of the leader is

$$t_i = \frac{v_i - v_0}{a_{\max}} + t_{iL}, \quad (15)$$

and the distance that vehicle travels during the decelerating process is

$$d_L = \int_0^{v_L - v_0/a_{\max}} v_L - a_{\max} t dt, \quad (16)$$

$$d_i = \int_0^{t_{iL}} v_i dt + \int_0^{v_i - v_0/a_{\max}} v_i - a_{\max} t dt. \quad (17)$$

Then, the difference in the distance traveled by the two vehicles is

$$d_i - d_L = \int_0^{t_{iL}} v_i dt + \int_0^{v_i - v_0/a_{\max}} (v_i - a_{\max} t) dt - \int_0^{v_L - v_0/a_{\max}} (v_L - a_{\max} t) dt. \quad (18)$$

Because the platoon is in a steady state at the start, v_i should be equal to v_L . Therefore, (10) can be rewritten as

$$d_i - d_L = v_i t_{iL} + v_i \frac{v_i - v_0}{a_{\max}} - \frac{1}{2} a_{\max} \left(\frac{v_i - v_0}{a_{\max}} \right)^2 - v_L \frac{v_L - v_0}{a_{\max}} + \frac{1}{2} a_{\max} \left(\frac{v_L - v_0}{a_{\max}} \right)^2. \quad (19)$$

From (18) it can be seen that the difference in the distance traveled by the two vehicles increases as v_0 decreases. Furthermore, the maximum value of $d_i - d_L$ should be used to calculate the MSD. In this case, the minimum value of v_0 , that is, 0, can be taken. Then, (18) can be written as

$$d_i - d_L = \int_0^{t_{iL}} v_L dt + \int_0^{v_L/a_{\max}} (v_L + a_{\max} t) dt - \int_0^{v_L/a_{\max}} (v_L + a_{\max} t) dt. \quad (20)$$

From (20), the difference in the distance traveled by the two vehicles can be obtained as follows:

$$d_i - d_L = v_L t_{iL}. \quad (21)$$

According to Yi et al. [27] and Suzuki et al. [29], the maximum deceleration of the vehicle with the emergency brake on is $a_{\max} \geq -4.5 \text{ m/s}^2$, and the maximum acceleration of vehicle that guarantees the comfort of the passengers is $a \leq 2.5 \text{ m/s}^2$.

The GNSS error of the CAV must be below 20 cm [30], and the tested vehicles met this requirement [31]. To ensure that the GNSS error of two vehicles does not influence traffic

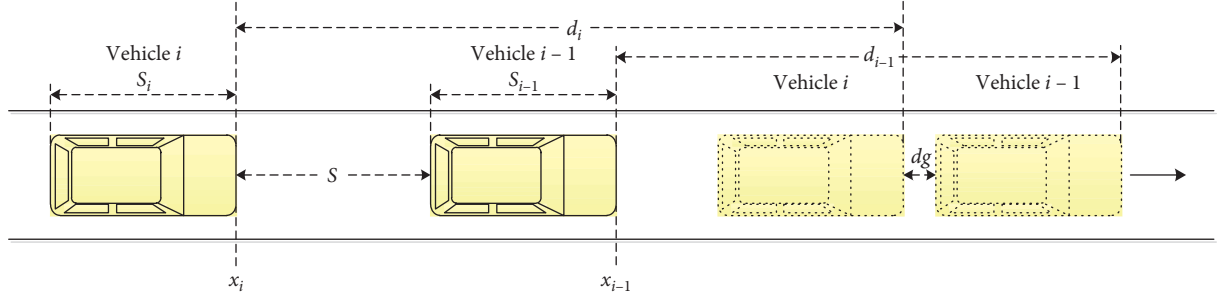


FIGURE 7: Schematic of vehicle braking process scenario.

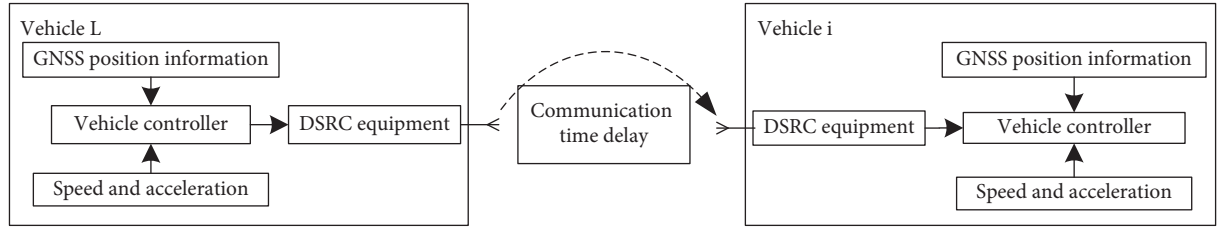


FIGURE 8: Information transmission process.

safety, it is necessary to add the error two times in the calculation of the MSD.

On the other hand, two vehicles need a gap of a certain volume when the velocity is 0. Based on the consideration of real traffic conditions, the gap was set to 1 m. Then, the MSD is

$$S = d_g + 2d_e + (d_i - d_L), \quad (22)$$

where d_g is the gap when the velocity is 0 and d_e is the maximum GNSS error.

5.2. MSD Model for Accelerating State. The calculation above shows the MSD with the platoon under a steady state (uniform motion). However, the emergency brake of the platoon could happen during the acceleration or deceleration motion. In this condition, the mechanical response τ cannot be ignored.

In the acceleration process, equations (16)–(18) can be written as

$$d_i = \int_0^{t_{iL} + \tau} (v_L + at) dt + \int_0^{v_L + a(t_{iL} + \tau) - v_0/a_{\max}} (v_L - a_{\max}t) dt, \quad (23)$$

$$d_L = \int_0^{\tau} (v_L + at) dt + \int_0^{v_L + a\tau - v_0/a_{\max}} (v_L - a_{\max}t) dt, \quad (24)$$

$$d_i - d_L = v_L t_{iL} + \frac{1}{2} a t_{iL}^2 + a t_{iL} \tau + \frac{a^2 t_{iL}^2 + 2a^2 t_{iL} \tau + 2v_L a t_{iL}}{2a_{\max}} \geq d_g. \quad (25)$$

In these equations, a represents the maximum acceleration of vehicle that guarantees the comfort of the passengers, which can be seen as the maximum acceleration in

the normal driving state. The mechanical response τ can be seen as 0.3 s based on the research of Davis [32].

5.3. MSD Model for Decelerating State. At the decelerating state, the mechanical response τ cannot be ignored as well due to the vehicles have different τ velocity when braking. The maximum deceleration also guarantees the comfort of the passengers. In the deceleration process, the equations can be written as

$$d_i = \int_0^{t_{iL} + \tau} (v_L - at) dt + \int_0^{v_L - a(t_{iL} + \tau) - v_0/a_{\max}} (v_L - a_{\max}t) dt, \quad (26)$$

$$d_L = \int_0^{\tau} (v_L - at) dt + \int_0^{v_L - a\tau - v_0/a_{\max}} (v_L - a_{\max}t) dt, \quad (27)$$

$$d_i - d_L = v_L t_{iL} - \frac{1}{2} a t_{iL}^2 - a t_{iL} \tau + \frac{a^2 (t_{iL}^2 + 2t_{iL} \tau) - 2v_L a t_{iL}}{2a_{\max}} \geq d_g. \quad (28)$$

5.4. Analysis of MSD Models. In Figure 9, it can be seen that the MSD in the three states grows with the increase of communication time delay. The result shows that communication delay indeed has a negative impact on the final MSD. Therefore, it is reasonable to consider communication delay in the MSD model. On the other hand, we also can observe that the MSD in the accelerating state is the largest, the one in the cruising state is in the middle, and the one in the deceleration state is the least. The reason for this phenomenon can be mainly understood as the energy change of vehicles. Speed can be an energy signal for platooning vehicles. The energy is continuously accumulated when the

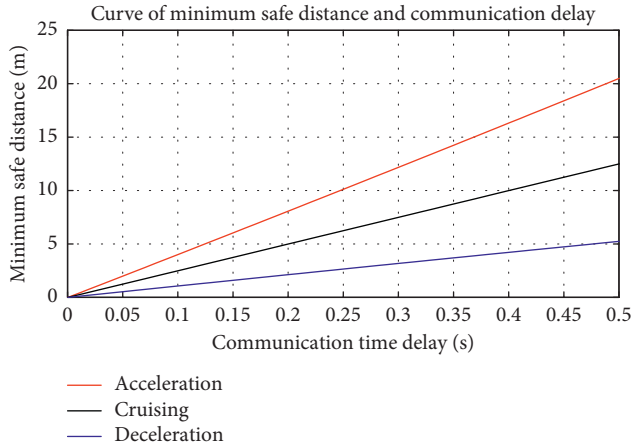


FIGURE 9: Relationship between time delay and MSD. X-axis is the communication time delay and Y-axis is the MSD. The red, black, and blue lines represent the acceleration, cruising, and deceleration condition.

vehicle is in the accelerating state. More energy is needed to be consumed by emergency braking. That means this process must experience a longer braking distance. Thus, the final MSD is longer than the other state. On the opposite, the energy has already been consumed during the decelerating state. The vehicle must take a short braking distance to stop if emergency braking happens at this time. For a similar reason, the MSD in the cruising state is in the middle level compared with the other two states.

Based on the three models, the MSD at different velocities can be calculated. Table 1 lists the results of the MSD at different velocities. The first column of minimum spacing is the safe distance when the platoon is accelerating; the second column is the safe distance when the platoon is traveling at a constant speed; the third column is the safe distance when the platoon is decelerating.

It can be seen from Table 1 that the MSD at three states has been calculated from velocity 5 km/h to 120 km/h. The values of MSD are relatively close at low velocity under the three states, while the difference of MSD is relatively large at high speed. It can also be observed that the MSD changes greatly at the accelerating state with the increase of velocity, that is, from 2.57 m to 17.49 m. On the opposite, the MSD changes less at decelerating state with the increase of velocity, that is, from 1.43 m to 5.69 m. These results accord with the rule of energy conversion that has been discussed in Figure 9.

6. Validation Based on Simulation Experiment

In the test, a one-lane one-way straight 2 km road section was selected. The platoon enters the starting point (the left side of the road in Figure 10) of the road section at a certain set speed, and the leader receives an emergency braking signal after 30 s. Table 2 lists the main platooning parameters.

TABLE 1: Minimum spacing in CAV platoon under different vehicle speeds.

Velocity (km/h)	Minimum spacing (m)
5	2.57/1.82/1.43
10	3.22/2.24/1.61
15	3.87/2.57/1.80
20	4.52/3.09/1.99
25	5.16/3.52/2.17
30	5.81/3.94/2.35
35	6.46/4.36/2.54
40	7.11/4.78/2.72
45	7.76/5.21/2.91
50	8.41/5.63/3.10
55	9.06/6.06/3.28
60	9.70/6.48/3.47
65	10.35/6.91/3.65
70	10.99/7.33/3.84
75	11.65/7.75/4.02
80	12.30/8.18/4.21
85	12.94/8.60/4.39
90	13.59/9.03/4.58
95	14.24/9.45/4.76
100	14.89/9.87/4.95
105	15.54/10.30/5.13
110	16.19/10.72/5.32
115	16.84/11.15/5.50
120	17.49/11.57/5.69

A vehicular network framework Veins 4.7 was used to test the MSD models in this study. Veins is an open-source framework composed of a network simulator OMNeT++ 4.7.1 and a road traffic simulator SUMO 0.25.0. OMNeT++ is used to simulate the V2V communication network based on the IEEE 802.11p standard, and SUMO is used to simulate the road traffic of vehicles in a platoon. These two simulators interact with each other through a standard traffic control interface (TraCI) by exchanging transmission control protocol messages.

The data rate is set to the data rate of 6 Mbit/s for IEEE 802.11p broadcasting; the transmission power is set to 300 mW. The Two-Ray Interference model propagation model is used. According to the setting of the propagation model, the radio communication range is about 366 m. The broadcast frequency could be changed to adapt to the requirements of an application. In this work, we use the same broadcast frequency for evaluating all the investigated protocols in the defined scenarios. Moreover, the size of beacon is set to 378 bytes, where the entry number of message list is set to 40. The beacon sending period is 1 s, and we focus mainly on the simulation of one-hop neighborhood worst-case refresh update. The simulation setting parameters are shown in Table 3.

A six-vehicle platoon is conducted to study the impact of the communication time delay on MSD models. The number of vehicles is chosen to ensure the efficiency of the simulation. It is worth noting that an excessive number of vehicles can cause data redundancy. In this paper, the platoon uses a predecessor-leader following network topology, in which the transmissions are unidirectional communications. Each

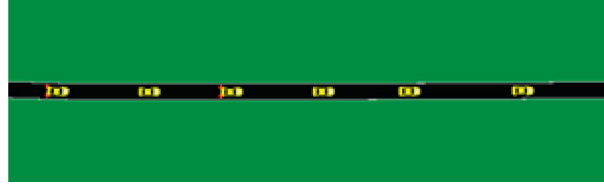


FIGURE 10: Closed platoon traffic simulation scene.

TABLE 2: Platooning parameters.

Parameter	Assumption value
Velocity	10–120 km/h
Vehicle length	5 m
Maximum acceleration	2.5 m/s ²
Maximum deceleration	4.5 m/s ²
Vehicles in platoon	6

TABLE 3: Simulation setting.

Physical layer	Frequency band	5.89 GHz
	Bandwidth	10 MHz
	Tx power	300 mW
	Receiver sensitivity	−100 dBm
	FSPL exponent α	3.0
	Thermal noise	−110 dBm
	Radio range (Friis)	~366 m
Link layer	Bit rate	6 Mbit/s
	CW	[15, 1023]
	Slot time	13 μ s
	SIFS	32 μ s
	DIFS	58 μ s
Data broadcasting	Broadcast frequency	10 Hz
	Data size	2312 bytes
Beaconing	Beacon frequency	1 Hz
	Beacon size	378 bytes
	Message list entries	40

vehicle only receives messages from the lead vehicle and the vehicle in the direct front. For the simplification of theory deduction and experimental simulation, we assume that the communication delay is constant, even if it has a random change in the reality.

The main purpose of this simulation is to ensure that the proposed MSD models would let vehicles have enough response time and distance to handle the emergency braking with a practical communication delay. The simulation was performed repetitively at a velocity from 5 to 120 km/h to guarantee the consistency of the results.

Figure 11 shows plots of the vehicle spacing after emergency braking as a function of the MSD of vehicles in the platoon with a communication delay of 305 ms; the area under the red line represents the condition in which a crash will occur. The points in Figure 11 represent the distribution of each simulation result. The five figures, respectively, represent five different gaps between the six vehicles in platoon. It can be seen from the figures that there is no point below the red line, which means that the MSD model was

suitable to avoid the crash. On the other hand, the distribution of points becomes more centralized from Figures 11(a)–11(e). This indicates that the time headway is tending to the minimum communication time delay from Figures 11(a)–11(e), which is 5 ms. This result is consistent with the characteristic of the information flow topology; that is, the lead vehicle will transmit the information to all the vehicles in the platoon.

Figures 12 and 13 show plots of the vehicle spacing after braking as a function of the MSD of vehicles in the platoon when traveling at a constant speed and decelerating. From Figures 11–13, it can be seen that, with all communication delays, the vehicles towards the front lead to more results close to the red line. Moreover, the tendency of the results is uniform with different communication time delay. On the other hand, the fact that there are always some points close to the red line indicates that the packet loss affects the MSD. In this study, the vehicle receives the information from the lead vehicle and the vehicle ahead. Once the vehicle i has packet loss from the

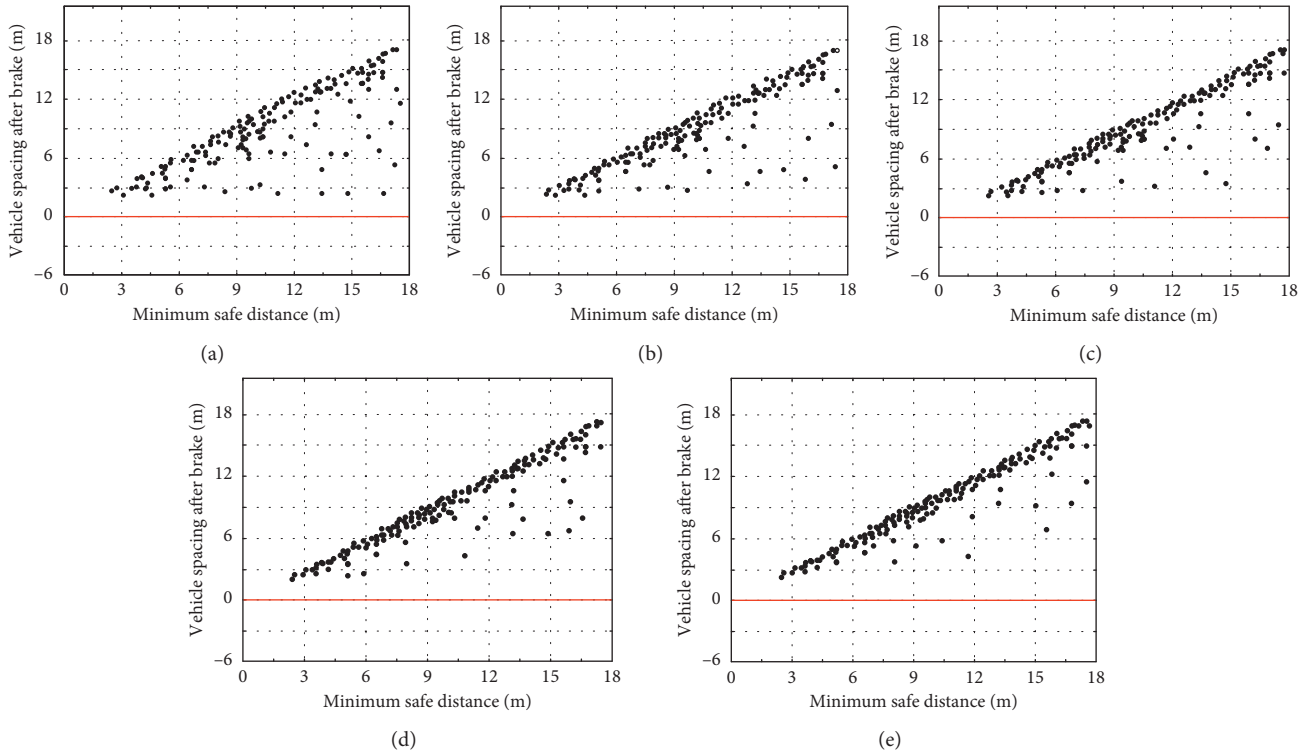


FIGURE 11: Vehicle spacing in platoon after emergency braking with 305 ms communication time delay during accelerating: spacing between (a) vehicle L and vehicle 1, (b) vehicle 1 and vehicle 2, (c) vehicle 2 and vehicle 3, (d) vehicle 3 and vehicle 4, and (e) vehicle 4 and vehicle 5.

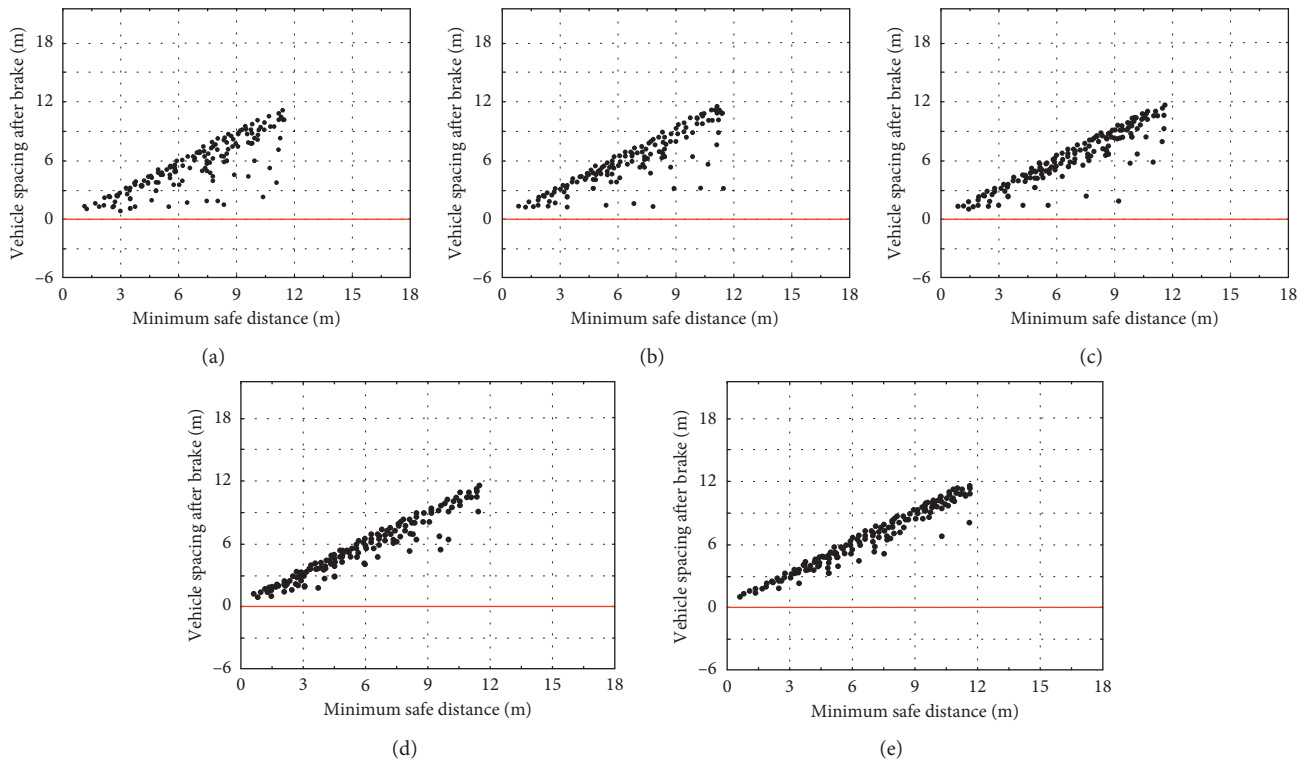


FIGURE 12: Vehicle spacing in platoon after braking with 305 ms communication time delay when traveling at a constant speed: spacing between (a) vehicle L and vehicle 1, (b) vehicle 1 and vehicle 2, (c) vehicle 2 and vehicle 3, (d) vehicle 3 and vehicle 4, and (e) vehicle 4 and vehicle 5.

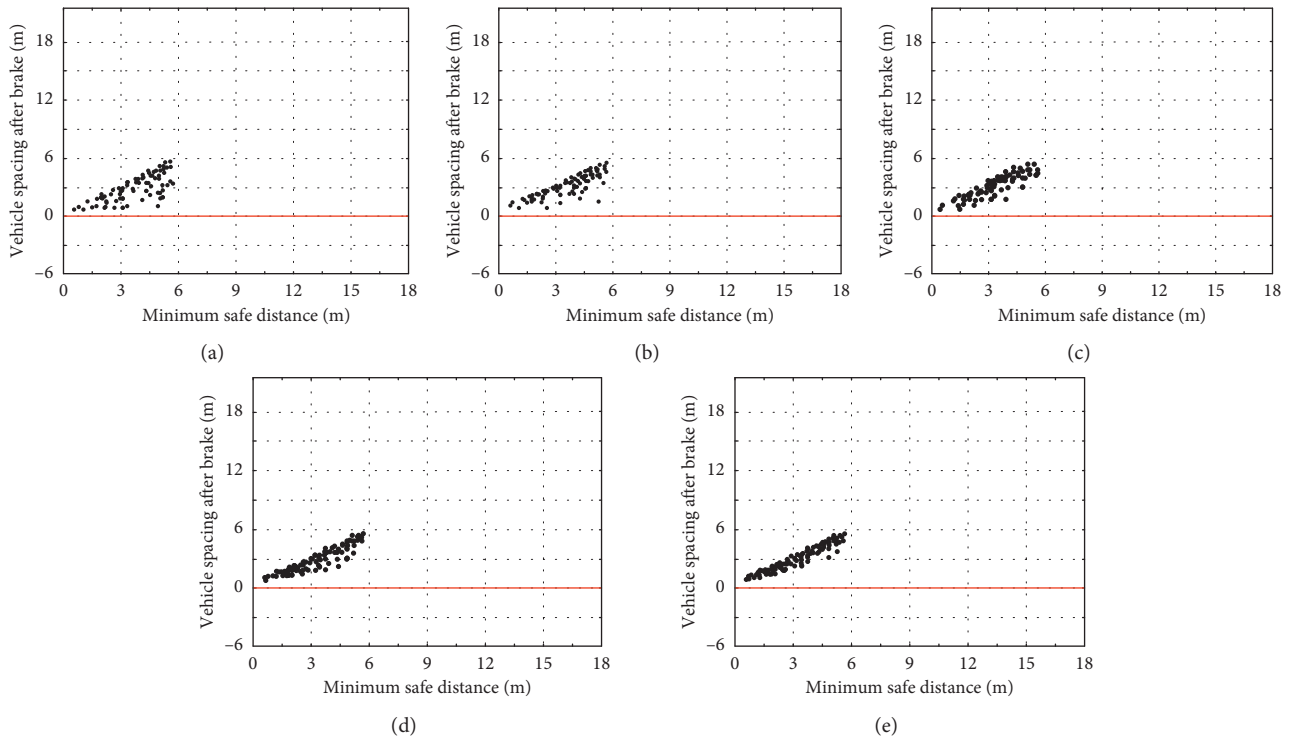


FIGURE 13: Vehicle spacing in platoon after braking with 305 ms communication time delay during decelerating: spacing between (a) vehicle L and vehicle 1, (b) vehicle 1 and vehicle 2, (c) vehicle 2 and vehicle 3, (d) vehicle 3 and vehicle 4, and (e) vehicle 4 and vehicle 5.

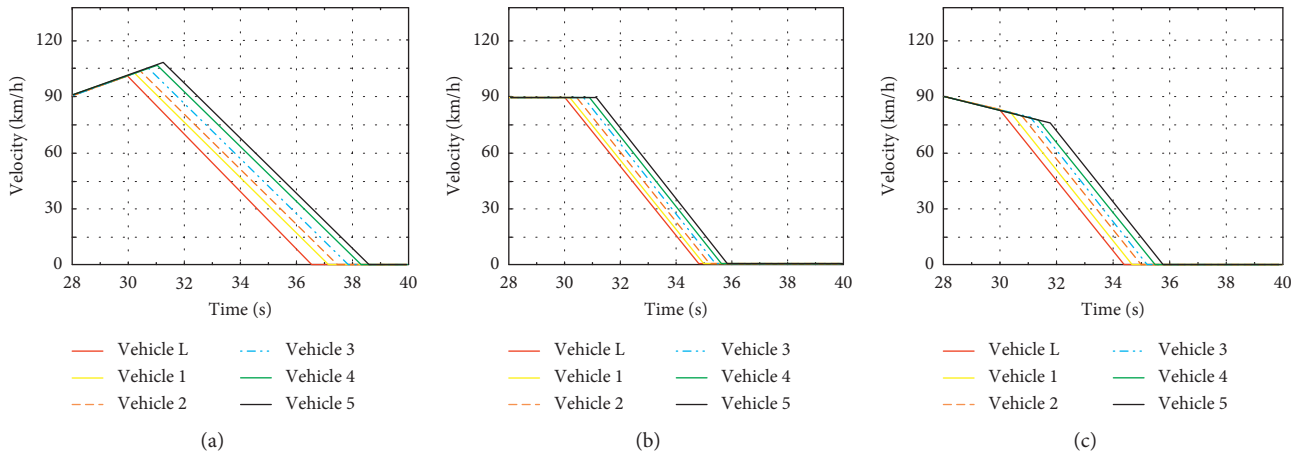


FIGURE 14: Vehicle velocity curve during the deceleration process at 90 km/h: (a) accelerating process; (b) traveling at a constant speed; (c) decelerating process.

lead vehicle, it can still receive the information from the vehicle ahead, which has the double insurance, and be able to combine the information of vehicles in front. In this case, the lower position of the vehicle in the platoon has a lower possibility of packet loss.

Figures 14 and 15 show plots of the vehicle velocity and travel distance during the braking process as a function of

the simulation time; the Y-axis in Figure 14 is the vehicle velocity and in Figure 15 is the distance that vehicles travel. Different colors of lines show each vehicle in platoon. The value shown in Figures 14 and 15 is the mean value of multiple experiments. It can be seen that the curve of the vehicle distance in the platoon is consistent with the calculation results.

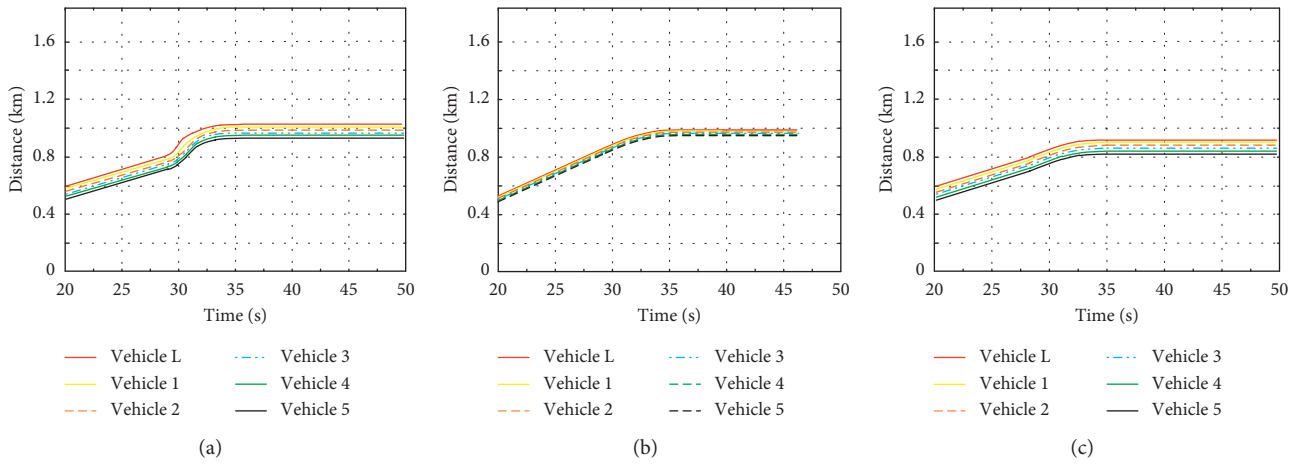


FIGURE 15: Vehicle travel distance in platoon at 90 km/h: (a) accelerating process; (b) traveling at a constant speed; (c) decelerating process.

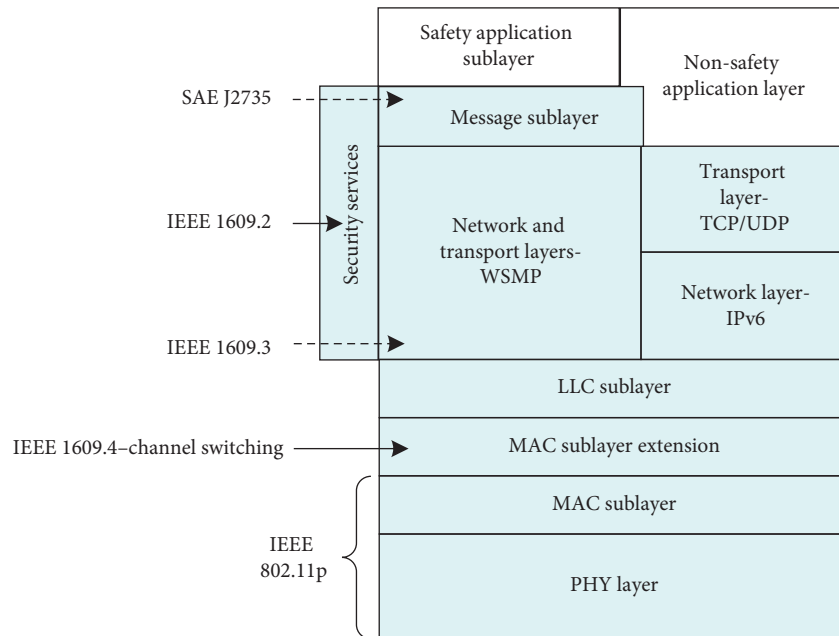


FIGURE 16: Layered architecture of DSRC technique.

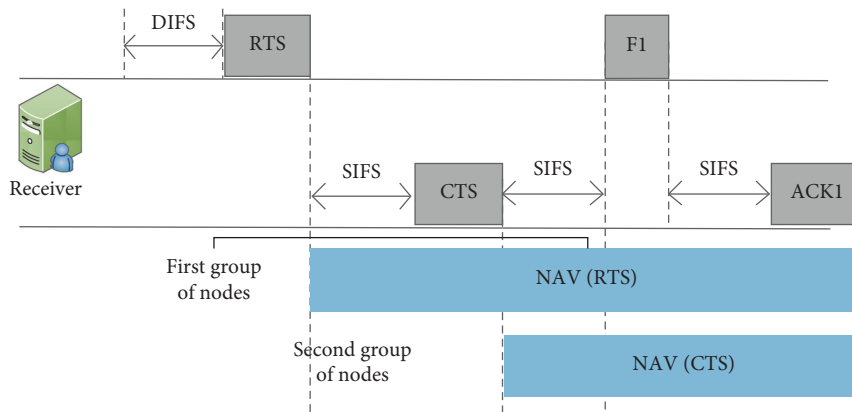


FIGURE 17: RTS/CTS mechanism sample graph.

TABLE 4: Access categories (ACs).

AC	Description
AC_BE	Best effort
AC_BK	Background
AC_VI	Video
AC_VO	Voice

TABLE 5: Default EDCA parameter set.

AC	AIFSN	CWmin	CWmax
AC_BE	9	aCWmin	aCWmax
AC_BK	6	aCWmin	aCWmax
AC_VI	3	$(aCWmin + 1)/2 - 1$	aCWmin
AC_VO	2	$(aCWmin + 1)/4 - 1$	$(aCWmin + 1)/2 - 1$

TABLE 6: Related works.

Sponsors/authors	Technologies	Functions	Simulations	Field tests
European (2001)	Promote	Truck platooning	×	✓
European (2007)	Chauffeur I + II	Driver assistant	×	✓
German (1996)	KONVOI	Truck platoon	×	✓
USA (2014)	PATH	V2X information exchange	×	✓
Swaroop et al. [9]	String stability	Suppress dynamics disturbance	✓	×
Rajamani et al. [10]	Practical systems with adaptive cruise control	Reduced intermediate spacing	✓	×
Liang et al. [11]	Ordering strategy with respect to the vehicle mass	String stability	✓	×
Ali et al. [13]	Collision avoidance	A novel automotive safety function	✓	×
Peters et al. [14]	Platooning stability	Applying the leader state to other members	✓	×
Kim et al. [15]	Enhanced time-delay controller and integral sliding-mode controller	Improve the control precision	✓	×
Zhang et al. [16]	Adaptive sliding-mode controller	Enhance vehicle mobility and safety	✓	×
Song et al. [17]	Motion model	Describe motion dependence across vehicles	✓	×
Zhao et al. [18]	Rear-end collision warning system	Ensure vehicle safety	×	✓
Ploeg et al. [19]	Graceful degradation of one vehicle	Platoon safety	✓	×
Oncu et al. [20]	NCS modeling framework	String stability	✓	×
Abou et al. [21]	CACC strategy	String stability	✓	×

7. Conclusion

We developed a numerical method to determine the MSD of CAVs in a platoon based on the communication time delay obtained by real vehicle field test, GNSS error, and mechanical response delay. In this method, the MSD is calculated by a modified Gipps' model adapted to the dynamic model of a CAV platoon. To test the effectiveness of the MSD calculation, a simulation based on SUMO and OMNeT++ was performed. The results show that the MSD determined by the proposed method can effectively avoid vehicle crashes in the platoon and is suitable for platoon control under the IEEE 802.11p protocol. The following conclusions can be drawn from this study. The communication time delay of DSRC caused by consecutive packets lost is obtained by field test, which is a maximum of 305 ms in the case of good communication. Afterwards, three models are built to represent the MSD of platoon under accelerating, cruising, and decelerating states. The communication delay obtained by field test is used for the calculation of MSD. Finally, the correctness of the

calculation results is verified through multiple sets of simulation experiments. The results of this study indicate that the vehicle spacing cannot be reduced indefinitely due to the communication delay of the 802.11p protocol. Although many influence factors have been considered, there are also some limitations in this study. The simulation only has 6 vehicles; the influence of traffic density has not been taken into account. On the other side, the vehicles' types are the same; the effect of vehicle type is not concerned. In future studies, other influencing factors of the MSD of the vehicles in platoon, for example, the accuracy of the speed sensor, road surface condition, and vehicle type, should be investigated [33].

Appendix

A. DSRC Technique and IEEE 802.11p Protocol

The layered architecture for the DSRC technique is shown in Figure 16. For IEEE 802.11p, the physical layer (PHY) employs the Orthogonal Frequency Division Multiplexing

(OFDM) which allows the digital data to be efficiently and reliably transmitted over a radio channel, even in multipath environments as the modulation scheme [34]. When there are multiple nodes in the channel, channel interference would become a problem under the 802.11p protocol. For this issue, the Media Access Control (MAC) layer employs the fully decentralized Carrier Sense Multiple Access with Collision Avoidance (CSMA/CA) protocol. This contention- and random-based MAC protocol cannot completely avoid packet collisions caused by simultaneous channel usage at high traffic densities, but the bandwidth and channel are enough for the six vehicles' platoon. Meanwhile, in order to provide a low-latency transmission guarantee for traffic safety applications, the multichannel mechanism of IEEE 802.11e (also known as IEEE 1609.4) is introduced in terms of the QoS of the IEEE 802.11p communication protocol.

In the field tests, it has been discovered that the channel interference problem exists and causes packet loss, which becomes the main factor of communication delay. Meanwhile, due to the existence of RTS/CTS mechanism in CSMA/CA protocol, there will be no long-term, large-scale packet loss during the communication. And the consecutive packet loss number with 100%–90% PDR has been tested, the results have no obvious change due to the CSMA/CA protocol. Therefore, very few consecutive packet loss becomes the main influence factor of the MSD.

The process of RTS/CTS mechanism is shown in Figure 17. The first group of nodes are around the sender. They start to mute after receiving the RTS until they receive the ACK. The second group of nodes are the ones around the receiver. They also start to mute after receiving the CTS until they receive the ACK.

IEEE 802.11p includes QoS channel access conforming to Enhanced Distributed Channel Access (EDCA) (i.e., 4 queues with different access categories) and accurately captures frame timing, modulation and coding, and channel models. IEEE 802.11p uses the EDCA mechanism to perform the channel access procedure. Frames are classified into four access categories (ACs), as shown in Table 4, providing different priorities for the data from higher layer. That is, the data with a higher priority will be transmitted first.

In EDCA of IEEE 802.11p, the Interframe Space (IFS) uses a new concept, namely, using Arbitration Interframe Space (AIFS) instead of DIFS in WiFi. The AIFS length and the maximum and minimum Content Window (CW) are based on the priority (category) of the data; as shown in Table 5, aCW_{min} and aCW_{max} are equal to 15 and 1023, respectively.

EDCA can improve the route queue capacity so that the route forwarding delay can be relaxed.

B. Summary Table of Related Works

Summary Table of Related Works is given in Table 6

Data Availability

No data were used to support this study.

Conflicts of Interest

The authors declare that there are no conflicts of interest regarding the publication of this paper.

Acknowledgments

This work was supported in part by the National Key Research and Development Program (Grant no. 2019YFB1600100); the National Natural Science Foundation of China (Grant no. 61973045); the Key Program of the National Natural Science Foundation of China (Grant no. U1864204); the Shaanxi Province Key Development Project (Grant no. S2018-YF-ZDGY-0300); the China Postdoctoral Science Foundation (Grant no. 2020M673323); and the Natural Science Foundation of Shaanxi Province (Grant no. 2018JQ6035).

References

- [1] A. A. Alam, A. Gattami, and K. H. Johansson, "An experimental study on the fuel reduction potential of heavy duty vehicle platooning," in *Proceedings of the 13th International IEEE Conference on Intelligent Transportation Systems*, October 2010.
- [2] A. Alam, A. Gattami, and K. H. Johansson, "Guaranteeing safety for heavy duty vehicle platooning: safe set computations and experimental evaluations," *Control Engineering Practice*, vol. 24, pp. 33–41, 2014.
- [3] V. Vukadinovic, K. Bakowski, P. Marsch et al., "3GPP C-V2X and IEEE 802.11 p for vehicle-to-vehicle communications in highway platooning scenarios," *Ad Hoc Networks*, vol. 74, pp. 17–29, 2018.
- [4] J. Wang and P. S. Wang, "Method and apparatus for measurement reporting and event-triggered periodic measurement reporting in an evolved universal terrestrial radio access network," 2009.
- [5] V. Arems, C. J. G. Bart, V. Driel, and R. Visser, "The impact of cooperative adaptive cruise control on traffic-flow characteristics," *IEEE Transactions on Intelligent Transportation Systems*, vol. 7, no. 4, pp. 429–436, 2006.
- [6] A. Davila, E. Del Pozo, E. Aramburu, and A. Freixas, "Environmental benefits of vehicle platooning," in *Proceedings of the Symposium on International Automotive Technology (SIAT 2013)*.
- [7] B. J. Harker, "Promote-chauffeur II & 5.8 GHz vehicle to vehicle communications system," in *Proceedings of the International Conference on Advanced Driver Assistance Systems*, September 2001.
- [8] S. E. Shladover, "Path at 20-history and major milestones," *IEEE Transactions on Intelligent Transportation Systems*, vol. 8, no. 4, pp. 584–592, 2007.
- [9] D. Swaroop and J. K. Hedrick, "String stability of interconnected systems," *IEEE Transactions on Automatic Control*, vol. 41, no. 3, pp. 349–357, 1996.
- [10] R. Rajamani and C. Zhu, "Semi-autonomous adaptive cruise control systems," *IEEE Transactions on Vehicular Technology*, vol. 51, no. 5, pp. 1186–1192, 2002.
- [11] K.Y. Liang, A. Alam, and A. Gattami, "The impact of heterogeneity and order in heavy duty vehicle platooning networks (poster)," in *Proceedings of the 2011 IEEE Vehicular Networking Conference (VNC)*, Amsterdam, Netherland, September 2011.

- [12] A. Ryan, M. Zennaro, A. Howell, R. Sengupta, and J. K. Hedrick, "An overview of emerging results in cooperative UAV control," in *Proceedings of the 2004 43rd IEEE Conference on Decision and Control (CDC)*, Nassau, Bahamas, May 2005.
- [13] M. Ali, "Decision making and control for automotive safety," Doctoral thesis, Chalmers University of Technology, Gothenburg, Sweden, 2012.
- [14] A. A. Peters, R. H. Middleton, and O. Mason, "Leader tracking in homogeneous vehicle platoons with broadcast delays," *Automatica*, vol. 50, no. 1, pp. 64–74, 2014.
- [15] J. Kim, H. Joe, Y. Son-Cheol, J. S. Lee, and M. Kim, "Time-delay controller design for position control of autonomous underwater vehicle under disturbances," *IEEE Transactions on Industrial Electronics*, vol. 63, no. 2, pp. 1052–1061, 2015.
- [16] L. Zhang, J. Sun, and G. Orosz, "Hierarchical design of connected cruise control in the presence of information delays and uncertain vehicle dynamics," *IEEE Transactions on Control Systems Technology*, vol. 26, no. 1, pp. 139–150, 2017.
- [17] D. Song, R. Tharmarasa, T. Kirubarajan, and X. N. Fernando, "Multi-vehicle tracking with road maps and car-following models," *IEEE Transactions on Intelligent Transportation Systems*, vol. 19, no. 5, pp. 1375–1386, 2017.
- [18] X. Zhao, Z. Wang, Z. Xu et al., "DSRC-based rear-end collision warning system—an error-component safety distance model and field test," *Transportation Research Part C: Emerging Technologies*, vol. 107, pp. 92–104, 2019.
- [19] J. Ploeg, E. Semsar-Kazerooni, G. Lijster et al., "Graceful degradation of cooperative adaptive cruise control," *IEEE Transactions on Intelligent Transportation Systems*, vol. 16, no. 1, pp. 488–497, 2015.
- [20] S. Oncu, J. Ploeg, N. Van De Wou, and H. Nijmeijer, "Cooperative adaptive cruise control: network-aware analysis of string stability," *IEEE Transactions on Intelligent Transportation Systems*, vol. 15, no. 4, pp. 1527–1537, 2014.
- [21] Y. Abou Harfouch, S. Yuan, and S. Baldi, "An adaptive switched control approach to heterogeneous platooning with intervehicle communication losses," *IEEE Transactions on Control of Network Systems*, vol. 5, no. 3, pp. 1434–1444, 2017.
- [22] Y. Li, C. Tang, P. Srinivas, and Y. Wang, "Nonlinear consensus-based connected vehicle platoon control incorporating car-following interactions and heterogeneous time delays," *IEEE Transactions on Intelligent Transportation Systems*, vol. 20, no. 6, pp. 2209–2219, 2018.
- [23] M. Shi, Y. Zhang, D. Yao, and C. Lu, "Application-oriented performance comparison of 802.11 p and LTE-V in a V2V communication system," *Tsinghua Science and Technology*, vol. 24, no. 2, pp. 123–133, 2018.
- [24] P. Sondi, L. Rivoirard, and M. Wahl, "Performance evaluation of vehicle-to-vehicle communications for a collective perception application in vehicular ad hoc networks," in *Proceedings of the 2018 IEEE 29th Annual International Symposium on Personal, Indoor and Mobile Radio Communications (PIMRC)*, pp. 602–603, IEEE, Bologna, Italy, September 2018.
- [25] S. Kim and M. Bennis, "Spatiotemporal analysis on broadcast performance of DSRC with external interference in 5.9 GHz band," 2019, <http://arxiv.org/abs/1912.02537>.
- [26] Y. Liu, Z. L. Wang, and B. G. Cai, "Investigation of a DSRC-based end of queue collision warning system by considering real freeway data," *Intelligent Transport Systems Iet*, vol. 13, no. 1, pp. 108–114, 2019.
- [27] K. Yi, I. Moon, and Y. D. Kwon, "A vehicle-to-vehicle distance control algorithm for stop-and-go cruise control," in *Proceedings of the 2001 IEEE Intelligent Transportation Systems*, pp. 478–482, Oakland, CA, USA, August 2001.
- [28] K. Yi and J. Chung, "Nonlinear brake control for vehicle CW/CA systems," *IEEE/ASME Transactions on Mechatronics*, vol. 6, no. 1, pp. 17–25, 2001.
- [29] Y. Suzuki, H. Ishizaka, A. Sakuma et al., "Development of braking systems for platoon-driving-development of energy-saving ITS technologies," in *Proceedings of the 2011 14th International IEEE Conference on Intelligent Transportation Systems (ITSC)*, pp. 1138–1143, IEEE, Washington DC, USA, October 2011.
- [30] X. Zhao, H. Min, Z. Xu, and W. Wang, "An ISVD and SFFSD-based vehicle ego-positioning method and its application on indoor parking guidance," *Transportation Research Part C: Emerging Technologies*, vol. 108, pp. 29–48, 2019.
- [31] H. Min, X. Wu, C. Cheng, and X. Zhao, "Kinematic and dynamic vehicle model-assisted global positioning method for autonomous vehicles with low-cost GPS/camera/in-vehicle sensors," *Sensors*, vol. 19, no. 24, p. 5430, 2019.
- [32] L. C. Davis, "Method of compensation for the mechanical response of connected adaptive cruise control vehicles," *Physica A: Statistical Mechanics and Its Applications*, vol. 562, 2021.
- [33] Proceedings of the IEEE Std 802.11p-2010: IEEE Standard for Information technology- telecommunications and information exchange between systems-local and metropolitan area networks-specific requirement, Part 11: wireless LAN Medium Access Control (MAC) and Physical Layer (PHY) specifications, 2010.
- [34] S. Arslan and M. Saritas, "The effects of OFDM design parameters on the V2X communication performance: a survey," *Vehicular Communications*, vol. 7, pp. 1–6, 2017.

Research Article

Quantification of Rear-End Crash Risk and Analysis of Its Influencing Factors Based on a New Surrogate Safety Measure

Qiangqiang Shangguan,^{1,2} Ting Fu ,^{1,2} Junhua Wang,^{1,2} Rui Jiang,³ and Shou'en Fang^{1,2}

¹The Key Laboratory of Road and Traffic Engineering, Ministry of Education, Tongji University, Shanghai 201804, China

²College of Transportation Engineering, Tongji University, 4800 Cao'an Highway, Shanghai 201804, China

³Investment and Development Department, China Shandong International Economic & Technical Cooperation Group Ltd., 1822A Shandong Hi-speed Group Mansion, Jinan 250098, Shandong, China

Correspondence should be addressed to Ting Fu; ting.fu@mail.mcgill.ca

Received 18 February 2021; Accepted 22 April 2021; Published 30 April 2021

Academic Editor: Yanyong Guo

Copyright © 2021 Qiangqiang Shangguan et al. This is an open access article distributed under the Creative Commons Attribution License, which permits unrestricted use, distribution, and reproduction in any medium, provided the original work is properly cited.

Traditional surrogate measures of safety (SMoS) cannot fully consider the crash mechanism or fail to reflect the crash probability and crash severity at the same time. In addition, driving risks are constantly changing with driver's personal driving characteristics and environmental factors. Considering the heterogeneity of drivers, to study the impact of behavioral characteristics and environmental characteristics on the rear-end crash risk is essential to ensure driving safety. In this study, 16,905 car-following events were identified and extracted from Shanghai Naturalistic Driving Study (SH-NDS). A new SMoS, named rear-end crash risk index (RCRI), was then proposed to quantify rear-end crash risk. Based on this measure, a risk comparative analysis was conducted to investigate the impact of factors from different facets in terms of weather, temporal variables, and traffic conditions. Then, a mixed-effects linear regression model was applied to clarify the relationship between rear-end crash risk and its influencing factors. Results show that RCRI can reflect the dynamic changes of rear-end crash risk and can be applied to any car-following scenarios. The comparative analysis indicates that high traffic density, workdays, and morning peaks lead to higher risks. Moreover, results from the mixed-effects linear regression model suggest that driving characteristics, traffic density, day-of-week (workday vs. holiday), and time-of-day (peak hours vs. off-peak hours) had significant effects on driving risks. This study provides a new surrogate safety measure that can better identify rear-end crash risks in a more reliable way and can be applied to real-time crash risk prediction in driver assistance systems. In addition, the results of this study can be used to provide a theoretical basis for the formulation of traffic management strategies to improve driving safety.

1. Introduction

Statistics from the World Health Organization (WHO) show that the number of deaths caused by road traffic crashes is about 1.35 million each year, ranking eighth among all causes of death [1]. The serious consequences of traffic crashes have driven researchers to investigate the causes of the crashes. Among the many causes, driving behavior has been found to be a crucial one. For example, a study conducted by National Highway Traffic Safety Administration (NHTSA) found that driver-related factors account for 94% of the critical reasons of these crashes, and most studies indicated that traffic crashes can largely result from risky

driving behaviors [2–4]. To reduce casualties and mitigate injuries from traffic crashes, understanding and identifying the crash risk is essential.

Among different types of traffic crashes, rear-end crashes are recognized as one of the most common types [5, 6]. Statistics from the NHTSA show that the rear-end crashes accounting for 32.4% of all accident types that cause personal injury [7]. Since most rear-end crashes occurred in car-following situations, it has become crucial to identify the rear-end crash risk during car-following process and explore its influencing factors [8–10].

Despite the efforts on rear-end crash risk identification and analysis, several research gaps still exist. Measures,

including time-to-collision (TTC), stop distance index (SDI), deceleration rate to avoid crash (DRAC), and others, have been proposed to study driving risks [11–13]. However, TTC based on constant velocity assumption ignores the response of the following vehicle (FV) and the changes in the states of the vehicle pairs. Therefore, measures which take the mechanism of driver response and the development of the crash into account should be developed for better representing risks during car-following events. Besides, the other traditional surrogate measures of safety (SMoS) cannot fully reflect the crash probability and crash severity at the same time. In addition, driving risks change with driver's personal characteristics and environmental factors [3, 14–16]. In-depth research on the risk of rear-end crash risk and its influencing factors is essential to formulate effective countermeasures to reduce the risk of rear-end crash.

Judging from the previous studies, the traditional SMoS cannot fully consider the crash mechanism or fail to reflect the crash probability and crash severity at the same time. In addition, just few previous studies have been conducted based on large-scaled naturalistic driving data and comprehensively consider driver heterogeneity, behavioral characteristics, and environmental characteristics to study the influencing factors of rear-end crash risk from the perspective of microscopic car-following behavior.

Therefore, this study aims to propose a reliable measure to quantify the driving risk in the process of car-following and investigate the impact of various influencing factors on the rear-end crash risk considering driver's heterogeneity. For that purpose, a new rear-end crash risk index (RCRI) was introduced, which fully considers the crash mechanism and integrates crash probability and crash severity. A total of 16,905 car-following events were extracted from Shanghai Naturalistic Driving Study (SH-NDS). Crash risks under different influencing factors were analyzed and compared based on the proposed RCRI. Then, the mixed-effects linear regression model was then employed to study the impact of the behavioral characteristics and environmental factors on rear-end crash risk.

2. Literature Review

2.1. Overview of Studies on Surrogate Measures of Safety (SMoS). High-risk car-following behaviors, such as close-driving to the leading vehicle (LV), may lead to a high probability of an accident [17]. Based on temporal and spatial proximity, various rear-end crash risk indexes have been proposed that can be used to evaluate driving risks. Among time-based surrogate measures, time-to-crash (TTC) was widely used in practice [11]. Meanwhile, the risk of rear-end crash also depends on driver's crash avoidance behavior. The crash can also be avoided if the FV brakes in time. Herein, deceleration rate to avoid crash (DRAC) was then introduced to evaluate the braking requirement during vehicle conflicts to quantify the risk of rear-end crash [13]. Besides, maintaining a safety distance between the LV and the FV is the key to avoiding rear-end crashes. Therefore, the stop distance index (SDI), which is based on the concept of safe stopping distance of the FV, was proposed by Oh et al.

[12]. To mitigate the risk of rear-end crash, the FV should maintain the safe headway distance from the LV.

Although the traditional SMoS was widely used in quantifying the risk of rear-end crash, they also have some limitations. Kuang et al. [18] summarized three main limitations of the SMoS presented above: (i) the driver's response characteristics when experiencing a conflict are not considered in these SMoS; (ii) due to the requirements of the boundary conditions, any situation where the speed of the FV is lower than the speed of the LV is considered a safe situation, which may be unreasonable for the situation where the vehicle is traveling at a similar speed and the headway distance is small; (iii) the arbitrary selection of the index threshold will also make the result inaccurate.

Researchers have also proposed some new surrogate measures to address the abovementioned problems. Xie et al. [19] proposed the time-to-crash with disturbance (TTCD) to quantify the risk of rear-end crash. This indicator solves the problem of inaccurate risk identification when the speed of the FV is less than the speed of the LV. Besides, Shi et al. [20] derived a new hybrid indicator named key risk indicator (KRI), which integrates time integrated time-to-crash (TIT), crash potential index (CPI), and stopping sight distance (PSD). However, these proposed surrogate measures cannot make up all the above three limitations. In view of this, Kuang et al. [18] proposed a surrogate measure based on tree structure to evaluate the rear-end crash risk, namely, aggregated crash index (ACI), which considers many major factors in rear-end crash, including disturbance of LV, driver's reaction characteristics, and available braking capacity of the FV. However, this method is not convenient due to its complicated leaf nodes, which makes it complicated to apply. In addition, this measure only discusses the occurrence probability of a rear-end crash event without considering the severity of the crash. Therefore, it is crucial to propose a new SMoS to address the above limitations and better quantify the risk of rear-end crash.

2.2. Overview of Studies on Driving Risk-Related Factors.

Driving risks are often considered to be related to multiple factors, including driver's individual characteristics and environmental factors [3, 14–16]. Several studies have explored the interaction between driving risks and various influencing factors. Table 1 summarizes these previous studies, which can be summarized into three main categories based on experimental methods: survey-based studies, driving simulation studies, and naturalistic driving studies.

Most of the initial research is based on reported survey data. However, the main problem is that the sample size of the data is limited and may be highly subjective. In addition, survey-based research pays more attention to the influence of driver characteristics on driving risks and ignores driving environmental factors. Alternatively, due to its high safety, controllability, and comprehensive data acquisition, driving simulators are used to study driver behavior characteristics to improve driving safety, especially in safety-critical conditions. However, studies based on driving simulation experiments are mostly limited to specific behavior in a limited

TABLE 1: Summary of studies on driving risk-related factors.

Author	Research purpose	Experimental methods	Sample size (number of participants)	Analytical methods	Main findings
Hayley et al. [23]	To investigate the influence of driver's personality characteristics on risky driving behavior.	Online survey	175 drivers (79 female) aged 18–64 years old.	Regression analyses	Risky driving has a greater correlation with emotion recognition and expression levels, and less correlation with age.
Harbeck et al. [24]	To examine risky driving in relation to psychological variables.	Online survey	601 participants (230 female) aged 17–25 years old.	Statistical analyses	The results of the proposed model show that young driver's risky driving is related to risk perception, response cost, and rewards.
Ulleberg and Rundmo [25]	To understand the underlying mechanism of risky driving behavior through the combination of personality traits and social cognitive methods.	Questionnaire	3942 participants (2208 female) aged 16–23 years old.	Structural equation model (SEM)	The personality of a driver indirectly affects risky driving behaviors mainly by influencing behavioral attitudes.
Tao et al. [2]	To investigate the relationship between gender, age, self-reported risky driving behaviors, and crash risk.	Questionnaire	511 participants (195 female) aged 36–45 years old.	Structural equation model (SEM)	The results show that both driving experience and dangerous driving behavior affect the risk of accidents. The driver's gender has little influence on dangerous driving behavior and accident risk.
Teye-Kwadjo [26]	To investigate the impact of driver's risk perception on risky driving behavior.	Questionnaire	519 participants (127 female) aged 20–59 years old.	Structural equation model (SEM)	The research results show that risk perception has an impact on drivers' risky driving behaviors. Male and female drivers and married and unmarried drivers have different preferences for risky driving behaviors.
Shangguan et al. [27]	To evaluate the rear-end crash risks under adverse environment.	Driving simulation	32 participants (12 female) aged 23–45 years old.	Survival analysis	The results show that the lower visibility leads to higher rear-end crash risk, and road alignment has a significant impact on crash risk.
Precht et al. [28]	To identify the main influencing factors contributing to driving risks.	Naturalistic driving data	108 trip segments.	Generalized linear mixed models (GLMMs)	Driving violations are related to anger, the presence of passengers, and personal differences. In addition, secondary tasks that cause distraction of the driver's visual attention and complex driving tasks are associated with high driving risks.
Pnina et al. [14]	To investigate the interactions between driving context and their associations with risky driving behaviors of young novice drivers.	Naturalistic driving data	81 teenager drivers (43 female), average age 16.48 years old (SD = 0.33).	Passion regression analyses	Driving own has a higher high-risk driving than shared vehicle, and driving during the day has a higher risky driving rate than driving at night.
Chen et al. [29]	To explore the contributing factors to crash risk during lane-changing process.	Naturalistic driving data	579 lane-changing vehicle groups	Mixed regression models	The distance between the lane-changing vehicle and the preceding vehicle in the lane before the lane-changing significantly affects lane-changing safety.

number of safety-critical scenarios and cannot truly reflect the external driving environment [21]. Research based on naturalistic driving data represents real-world driving situations. It is possible to extract significant driving behavior parameters from naturalistic driving data, such as speed, acceleration, relative position with surrounding vehicles, and environmental conditions to study the influencing factors of driving risk [22]. The collected data are more comprehensive and effective and may provide more valid results.

3. Data Preparation

3.1. Brief Introduction of the Shanghai Naturalistic Driving Study (SH-NDS). The real-world driving data used in this paper were collected by the SH-NDS, jointly conducted by Tongji University, General Motors (GM), and the Virginia Tech Transportation Institute (VTTI) from 2012 to 2016 [30, 31]. The 60 drivers participating in this naturalistic driving experiment are aged between 35 and 50 years old, and all of whom have a driving experience of more than five years. The total mileage that has been driven before participating in the experiment is more than 20,000 kilometers, and the average daily mileage is not less than 40 kilometers. Each driver drives the assigned experimental vehicle on the open road network, and the driving route is selected according to the driver's daily travel needs.

The video data of SH-NDS are mainly recorded by 4 cameras, which are installed in hidden locations that are not easy to observe. The video image is shown in Figure 1, which is composed of the front and rear vision of the vehicle, the driver's facial state, and the hand operation image.

3.2. Car-Following Event Extraction. In this study, the car-following events in the SH-NDS were extracted to analyze the influencing factors of rear-end crash risk. The SH-NDS data cover all daily trips of the drivers participated. Totally data of 18,242 trips were collected. In the SH-NDS, data were automatically collected using the data acquisition system, triggered by the ignition switch of the vehicle. Therefore, the database inevitably contains a large number of trip records that are not related to the research content (vehicle activities including fueling, car washing, maintenance, and other types of short-distance trip were all recorded). In addition, missing values and outliers also exist in the SH-NDS database. Data processing mainly includes the following four steps:

- (i) Step 1: eliminate invalid record files. Due to the large number of short-distance trip records in the SH-NDS database, considering the distance between adjacent entrances and exits on urban expressways, a trip includes at least entering the urban expressway, driving on the urban expressway, and exiting the urban expressway, so the trip files with the travel time less than 5 minutes should be removed.
- (ii) Step 2: remove driving data under discontinuous traffic flow. To extract the car-following event under

continuous traffic flow, a point-to-point map matching algorithm was used to match the driving trajectory measured by GPS with the electronic map road data to find the trip record on the urban expressway [32]. Then, each trip was verified through camera video recording to ensure the validity of the driving data selected for analysis. The weather and light conditions were also determined during the verification process.

- (iii) Step 3: handle missing values and outliers. In order to obtain data such as vehicle's speed, acceleration, relative space-time distribution of surrounding vehicles, and traffic environment conditions during the car-following process, data preprocessing is required. Linear interpolation was applied to deal with missing values. Then, outliers were eliminated based on pauta criterion, and the data were smoothed using the moving average filter.
- (iv) Step 4: extract data of car-following events. Car-following events were extracted by applying an automatic extraction algorithm proposed by Zhu et al. [33]; (1) radar target's identification number of $LV > 0$ and remained constant: guaranteeing the FV was preceded by the same LV; (2) $7\text{ m} < \text{longitudinal distance between the FV and the LV} < 120\text{ m}$: eliminating the congested-flow conditions; (3) $\text{lateral distance between the FV and the LV} < 2\text{ m}$: ensuring that the FV and the LV were in the same lane; (4) duration of the car-following event $> 15\text{ s}$: guaranteeing that each car-following event has enough data for analysis.

After the application of the above steps, 16,905 car-following events (about 135 h of total event duration) were extracted from 1,197 trips. Figure 2 shows the histogram of the duration of car-following events.

4. Methodology

The methodology of this research mainly includes three parts: (i) derivation of a new surrogate measure for rear-end crash risk, (ii) identification of influencing factors for rear-end crash risk, and (iii) mixed-effects linear regression for rear-end crash risk modeling and factor analysis.

4.1. Derivation of New Surrogate Measure for Rear-End Crash Risk

4.1.1. Rear-End Crash Mechanism. In the process of car-following maneuver, the driver will choose the appropriate speed and safe headway distance according to the movement status of the LV. The determination of the safe headway distance needs to consider the driver's reaction time and the vehicle's deceleration process. Otherwise, it may easily lead to a rear-end crash when the headway distance is too small. In this research, we imposed a hypothetical disturbance on the LV, assuming the LV decelerated at a certain deceleration rate. As can be seen in Figure 3, the FV will take appropriate evasive actions based on the initial driving

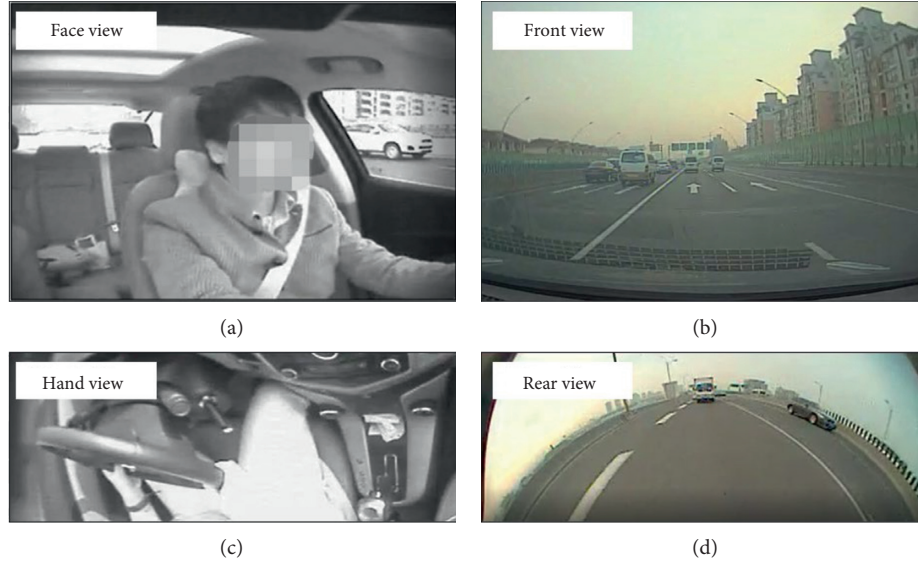


FIGURE 1: The video image of the SH-NDS.

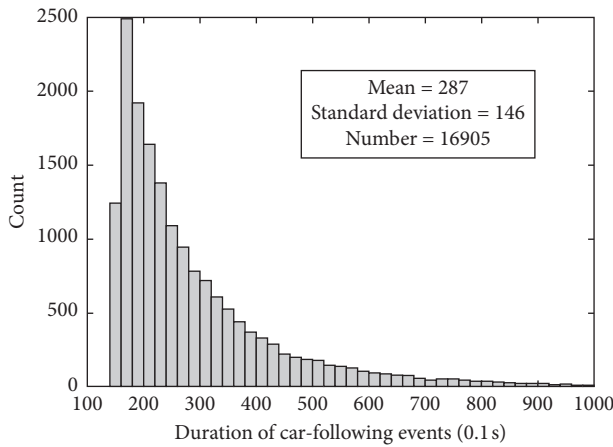


FIGURE 2: Histogram of the length of car-following events.

condition and the disturbance after reaction to avoid the crash. The crash outcome can be identified by evaluating the initial conditions, the disturbance, the driver's reaction characteristic, and the degree of evasive action [18, 34].

4.1.2. Rear-End Crash Risk Index (RCRI). Risk is the product of the possibility that a hazard event will occur and the consequence of the event. To address the limitations of SMOs mentioned above, we propose a new SMOs named RCRI, which considers the crash probability and crash severity at the same time, to quantify the risk of rear-end crash. According to the changes in the speed and distance of the LV and the FV before the crash, the process of rear-end crash can be divided into four categories, as shown in Figure 4 [35, 36].

Then, according to the characteristics of the rear-end crash, that is, the crash is plastic and the two vehicles tend to move together after the crash. In this study, the momentum

theorem was used to calculate the speed of the two vehicles after the rear-end crash, that is,

$$m_l v_{\text{pre-}l} + m_f v_{\text{pre-}f} = (m_l + m_f) v_c, \quad (1)$$

where m_l is the mass of the LV, m_f is the mass of the FV, $v_{\text{pre-}l}$ is the speed of the LV when the crash occurs, $v_{\text{pre-}f}$ is the speed of the FV when the crash occurs, and v_c is the speed of the LV and FV after the crash.

Calculate the energy loss ΔE of the two vehicles after rear-end crashes using the law of conservation of energy, as follows:

$$\begin{aligned} \Delta E &= \frac{1}{2} m_l v_{\text{pre-}l}^2 + \frac{1}{2} m_f v_{\text{pre-}f}^2 - \frac{1}{2} (m_l + m_f) v_c^2 \\ &= \frac{1}{2} \frac{m_l m_f}{(m_l + m_f)} (v_{\text{pre-}l} - v_{\text{pre-}f})^2. \end{aligned} \quad (2)$$

Therefore, this study uses the square of the absolute speed difference (SASD) at the time of the rear-end crash of two vehicles to express the severity of the rear-end crash.

To simplify the rear-end crash avoidance process, the model adopts two assumptions: (i) the braking process of the vehicle is regarded as a uniform deceleration process and (ii) the FV only adopts braking measures to avoid crash. Therefore, the braking stop distances of the two vehicles before the crash can be obtained, as shown in the following formula:

$$s_l = v_l t_c - \frac{1}{2} a_l t_c^2, \quad (3)$$

where s_l is the braking distance of the LV, v_l is the speed of the LV before braking, t_c is the time of crash, and a_l is the deceleration rate of the LV.

When $t_c \geq (v_l/a_l)$, the LV has been completely stopped, and the corresponding braking stop distance of LV is

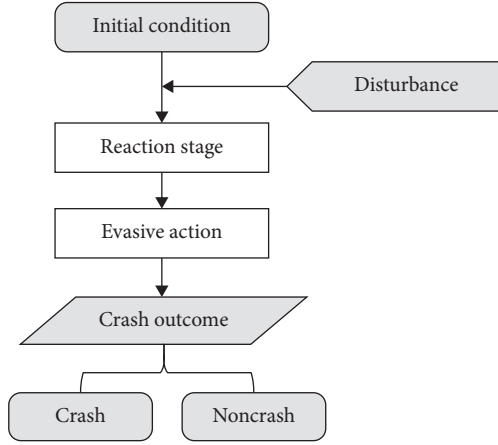


FIGURE 3: Schematic diagram of rear-end crash mechanism.

$$s_l = \frac{v_l^2}{2a_l}. \quad (4)$$

During the entire conflict process, during the reaction time t_R , the FV maintains a constant speed v_f and then decelerates at a constant deceleration rate a_f . When $0 \leq t_c \leq t_R$, the braking distance of the FV can be represented as

$$s_f = v_f t_c, \quad (5)$$

where s_f is the braking distance of the FV.

When $t_R \leq t_c \leq t_R + (v_f/a_f)$, the braking stop distance of the FV is

$$s_f = v_f t_R + v_f (t_c - t_R) - \frac{1}{2} a_f (t_c - t_R)^2. \quad (6)$$

Therefore, if the longitudinal distance between the FV and the LV is reduced to zero before the FV completely stopped, a crash will definitely occur, namely,

$$t_{c3} = \frac{(v_l - a_f t_R - v_f) \pm \sqrt{(a_f t_R + v_f - v_l)^2 + 2(a_l - a_f)((1/2)a_f t_R^2 + l)}}{a_l - a_f}. \quad (13)$$

If $a_l = a_f$, the solution is

$$t_{c3} = \frac{(1/2)a_f t_R^2 + l}{a_f t_R + v_f - v_l}, \quad (14)$$

$$\text{SASD}_3 = (v_l - a_l t_{c3}) - (v_f - (t_{c3} - t_R)a_f)^2.$$

$$t_{c4} = \frac{(v_f + a_f t_R) \pm \sqrt{(v_f + a_f t_R)^2 - 2a_f (v_l^2/2a_l) + l + (1/2)a_f t_R^2}}{a_f}, \quad (16)$$

$$\text{SASD}_4 = (v_f - (t_{c4} - t_R)a_f)^2.$$

$$s_l + l = s_f, \quad (7)$$

where l is the initial gap between LV and FV.

For scenario 1, where $0 \leq t_{c1} \leq t_R$ and $0 \leq t_{c1} \leq (v_l/a_l)$, when the crash occurs,

$$v_l t_{c1} - \frac{1}{2} a_l t_{c1}^2 + l = v_f t_{c1}. \quad (8)$$

The solution is

$$t_{c1} = \frac{(v_l - v_f) \pm \sqrt{(v_f - v_l)^2 + 2a_l l}}{a_l}, \quad (9)$$

$$\text{SASD}_1 = ((v_l - a_l t_{c1}) - v_f)^2.$$

For scenario 2, where $(v_l/a_l) \leq t_{c2} \leq t_R$, when the crash occurs,

$$\frac{v_l^2}{2a_l} + l = v_f t_{c2}. \quad (10)$$

The solution is

$$t_{c2} = \frac{(v_l^2/2a_l) + l}{v_f}, \quad (11)$$

$$\text{SASD}_2 = (v_f)^2.$$

For scenario 3, where $0 \leq t_{c3} \leq (v_l/a_l)$ and $t_R \leq t_{c3} \leq t_R + (v_f/a_f)$, when the crash occurs,

$$v_l t_{c3} - \frac{1}{2} a_l t_{c3}^2 + l = v_f t_R + v_f (t_{c3} - t_R) - \frac{1}{2} a_f (t_{c3} - t_R)^2. \quad (12)$$

If $a_l \neq a_f$, the solution is

For scenario 4, where $t_c \geq (v_l/a_l)$ and $t_R \leq t_c \leq t_R + (v_f/a_f)$, when the crash occurs,

$$\frac{v_l^2}{2a_l} + l = v_f t_R + v_f (t_c - t_R) - \frac{1}{2} a_f (t_c - t_R)^2. \quad (15)$$

The solution is

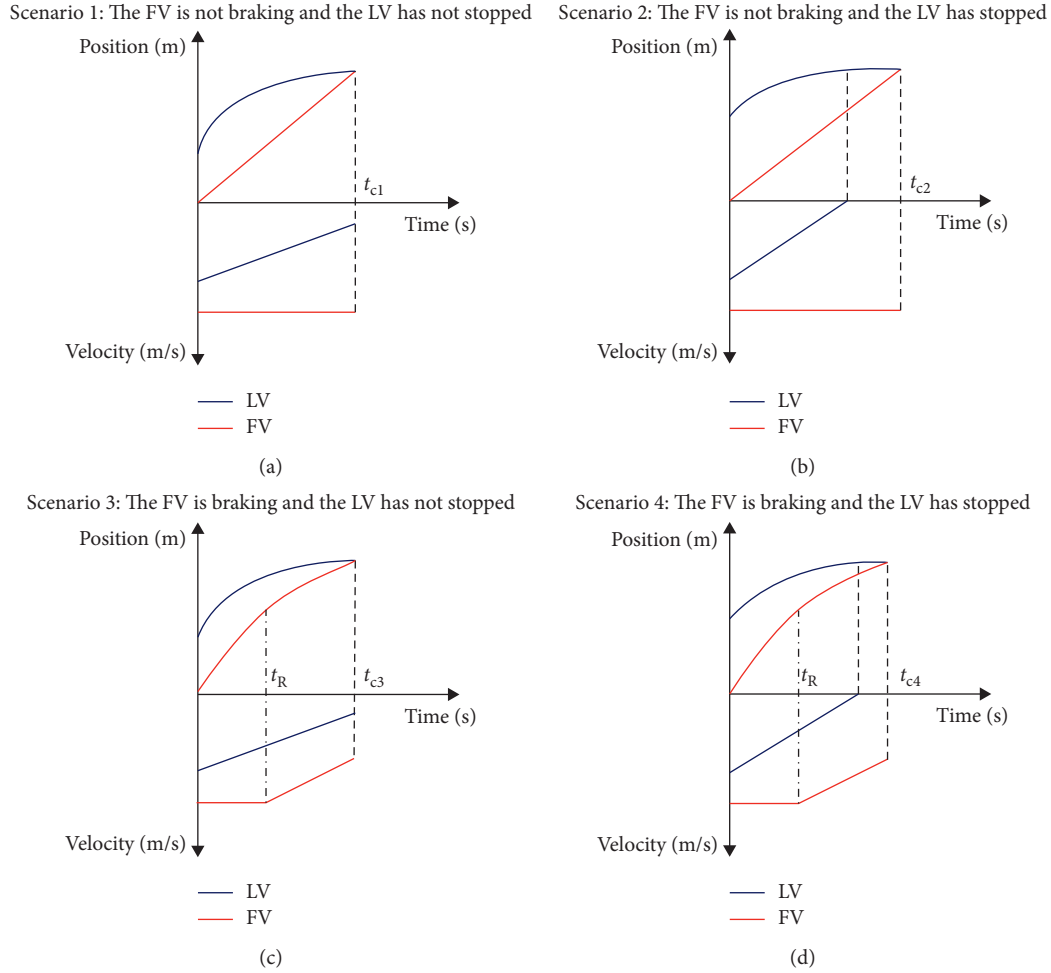


FIGURE 4: Descriptions of the four rear-end crash scenarios. *Note.* t_R – the reaction time of driver, t_c – the time of crash.

According to the previous studies, the deceleration rate taken by the LV follows a shifted gamma distribution (17.315, 0.128, 0.657), which was suggested and calibrated by Kuang et al. [18]. The reaction time of the FV follows a log-normal distribution (0.17, 0.44), and the braking coordination time is 0.175 s [37]. The maximum available deceleration rate (MADR) was assigned to be a truncated normal distribution with a mean of 8.45 m/s^2 and a variance of 1.4 m/s^2 between 4.23 m/s^2 and 12.68 m/s^2 [38].

The Monte Carlo simulation method was used to randomly select the deceleration rate taken by the LV, the reaction time of the driver, and the deceleration rate of the FV on the basis of the distribution function of each parameter mentioned above. According to the initial states of the LV and FV, the crash time (t) and the crash consequence (represented by SASD as discussed before) were calculated based on the above equations. Then, by integrating the possibility and consequences of the crash under the current car-following conditions, a new SMOs named RCRI can be calculated and expressed as below. It should be noted that the SASD needs to be normalized to a value between 0 and 1 before calculating RCRI. Therefore, the calculated RCRI range is also between 0 and 1:

$$\text{RCRI}_i = \frac{\sum_{j=1}^N \text{crash}_{ij} \times \text{SASD}_{ij}}{N}, \quad (17)$$

where RCRI_i represents the risk of rear-end crash at the i^{th} moment (0.1 s) in the car-following scenario; $N = 10,000$ is the number of random samples generated by the Monte Carlo simulation. When crash time t has a solution, that is, a crash occurs, $\text{crash}_{ij} = 1$; otherwise, $\text{crash}_{ij} = 0$.

It should be noted that SASD is dimensional, so it needs to be normalized before calculation.

4.2. Identification of the Influencing Factors for Rear-End Crash Risk

4.2.1. Definition of the Variables. As discussed in previous studies, the driving risk is mainly affected by driver's operational characteristics and the external driving environment [3, 14–16]. In order to quantify the various influencing factors for risks in the car-following process, this study extracted three categories of variables: behavioral variables, temporal variables, and environmental variables, as shown in Table 2.

TABLE 2: Summary of independent variables.

Categories	Variables	Conditions
Behavioral variables	Duration of car-following event	Continuous variable (0.1 s)
	Mean time headway	Continuous variable (s)
	Average speed difference	Continuous variable (km/h)
	Acceleration difference ratio	Continuous variable
Temporal variables	Day-of-week	Holiday, workday
	Time-of-day	Off peak, morning peak, evening peak
Environmental variables	Light condition	Daytime, nighttime
	Weather condition	Sunny, rainy
	Traffic density	High, median, low

The relevant variables of the driver's car-following behavior consider the duration of car-following event, time headway, and the driving speed and acceleration of the LV and FV. In order to eliminate the influence of the absolute value of the speed on the modeling, in terms of the speed indicator, this study adopted the average speed difference (ASD) between LV and FV, which is presented as

$$ASD = \frac{\sum_{t=1}^T |v_{l(t)} - v_{f(t)}|}{T}, \quad (18)$$

where $v_{l(t)}$ and $v_{f(t)}$ are the instantaneous speed of the LV and FV at its t -th record, and $t \in T$, T is the duration of car-following event.

Acceleration difference ratio (ADR) refers to the ratio of the standard deviation of the acceleration of the FV and LV. The ADR of one car-following event can be calculated as

$$ADR = \frac{\sigma_f}{\sigma_l}, \quad (19)$$

where σ_f and σ_l are the standard deviation of the acceleration of the FV and LV during one car-following period.

Peak hours increase the likelihood of congestion, resulting in a shortage of driving space, which in turn breeds risky driving behaviors. In order to consider the possible impact of the peak period, in this study, the car-following events within a day are divided into three categories: morning peak, evening peak, and off peak. Among them, the morning peak refers to 7:00 to 9:00, while the evening peak refers to 17:00 to 19:00. Besides, the traffic density was determined based on the speed of the FV and forward camera video recording, as described in Yang et al. [39].

To examine the effect of these independent variables on rear-end crash risk, the mean RCRI of a single car-following event was used as the dependent variable in this study.

4.2.2. Statistics Description of the Variables. As mentioned, we extracted 16,905 car-following events from 1,197 trips. Table 3 presents the descriptive statistics of the continuous variables and frequency information of the discrete independent variables in this study.

4.3. Mixed-Effects Linear Regression for Rear-End Crash Risk Modeling and Factor Analysis. In this research, all drivers participated in multiple car-following events, and car-following behavior characteristic variables were repeatedly collected from each participant. Therefore, the correlation problem between repeated observations will be exposed, that is, within-cluster correlation, and this problem can be solved by applying mixed-effects linear regression model [30, 40].

The mixed-effects linear regression model is an extension of the linear regression model, including fixed effects and random effects. Compared with the ordinary linear regression model, the mixed-effect linear regression model can well control the influence of the driver's personality factors. The results of the model can reflect the commonality of drivers and consider the internal correlation between samples, which is more suitable for solving the research problems.

In this paper, the fixed effects are the independent variables that the research focuses on. Besides, the drivers were treated as random effects to address the problem of within-cluster correlation.

Formally, the mixed-effects linear regression model can be written as

$$y = X\beta + Z\mu + \varepsilon, \quad (20)$$

where $y \in R^{N \times 1}$ is the dependent variable; $X \in R^{N \times p}$ is a matrix of the independent variables; $\beta \in R^{p \times 1}$ is the coefficients of the fixed effects; $Z \in R^{N \times q}$ is the matrix for random effects; $\mu \in R^{q \times 1}$ is the coefficients of the random effects; and $\varepsilon \in R^{N \times 1}$ is a column vector of the residuals. To recap,

$$\underbrace{y}_{N \times 1} = \underbrace{X}_{N \times p} \underbrace{\beta}_{p \times 1} + \underbrace{Z}_{N \times q} \underbrace{\mu}_{q \times 1} + \underbrace{\varepsilon}_{N \times 1}. \quad (21)$$

To better understand the structure of the model, here we provide an example where 16,905 (N) car-following events were collected from 58 (q) drivers. Our outcome y is the risk of car-following event. As mentioned above, we have 11 fixed effect predictors. The following equations represent the vectors and matrices provided in the previous equations:

TABLE 3: Summary of variables descriptive statistics.

<i>Independent variables (behavioral variables)</i>				
Variables	Mean	Std. Dev	Min	Max
Duration of car-following event (0.1 s)	286.66	146.44	151	1010
Mean time headway (s)	2.01	0.77	0.53	8.17
Average speed difference (m/s)	1.11	0.75	0.09	7.15
Acceleration difference ratio	0.91	0.38	0.00	4.08
<i>Independent variables (temporal variables)</i>				
Variables	Dummy variable	Count		
Day-of-week	Holiday	4200		
	Workday	12705		
	Off peak	9368		
Time-of-day	Morning peak	3873		
	Evening peak	3664		
<i>Independent variables (environmental variables)</i>				
Variables	Dummy variable	Count		
Light condition	Daytime	12456		
	Nighttime	4449		
Weather condition	Sunny	14587		
	Rainy	2318		
	High	1604		
Traffic density	Median	4495		
	Low	10806		
<i>Dependent variables (driving risk)</i>				
Variables	Mean	Std. Dev	Min	Max
RCRI	0.0031	0.0061	0.0000	0.7736

$$\begin{aligned}
 y &= \begin{bmatrix} \text{risk} \\ 0.013 \\ 0.002 \\ \dots \\ 0.006 \end{bmatrix}_{16,905 \times 1}, \\
 X &= \begin{bmatrix} \text{Intercept} & \dots & \text{Density} \\ 1 & \dots & 1 \\ 1 & \dots & 1 \\ \dots & \dots & \dots \\ 1 & \dots & 2 \end{bmatrix}_{16,905 \times 11}, \\
 \beta &= \begin{bmatrix} 0.004 \\ 0.001 \\ 0.005 \\ \dots \\ -0.001 \end{bmatrix}_{11 \times 1}, \\
 Z &= \begin{bmatrix} \text{Driver}_1 & \dots & \text{Driver}_{58} \\ 1 & \dots & 0 \\ 0 & \dots & 0 \\ \dots & \dots & \dots \\ 0 & \dots & 1 \end{bmatrix}_{16,905 \times 58}.
 \end{aligned} \quad (22)$$

The random effects μ in the regression model are a column vector containing random intercepts. However, it is not necessary to estimate μ in actual regression modeling.

Instead, the model assumes that μ follows a normal distribution, with a mean of zero and a variance of σ^2 :

$$\mu \sim N(0, \sigma^2). \quad (23)$$

Parameters of all components were estimated using the mixed procedure in Stata/MP 16.0. The statistical significance level was set at 0.05.

5. Results and Discussion

5.1. Rear-End Crash Risk Identification Using SH-NDS Data and RCRI. To better illustrate the rear-end crash risk identification measure proposed in this study, TTC, DRAC, SDI, and RCRI were all employed to quantify the risk for one car-following event. According to the previous studies, the thresholds of each SMoS are chosen as follows. The threshold of TTC is normally chosen as 3 s [41], and the threshold of DRAC is 3.4 m/s² [42]. In the SDI calculation, it is assumed that the deceleration speed is 3.3 m/s² and the reaction time is 1.0 s [20]. A portion of the vehicle movement data during one car-following event is presented in Table 4. The risks identified at intervals of 0.1 s are shown in Figure 5.

As mentioned in the methodology, the RCRI is calculated based on the assumed disturbance. This measure can be used to quantify the risk in any scenario, even when the LV's speed is greater than that of the FV. Besides, the RCRI takes into account the most critical variables in crash mechanisms such as driver reaction characteristics and vehicle braking performance and comprehensively considers the crash probability and consequences. Moreover, the RCRI is a continuous variable, so it has better flexibility to quantify the

TABLE 4: The vehicle movement data and risk identification results for one car-following event.

Time interval (0.1 s)	FV speed (m/s)	FV speed - LV speed (m/s)	Headway distance (m)	Risk (TTC)	Risk (DRAC)	Risk (SDI)	Risk (RCRI)
...
158	16.9	9.4	38.7	0	0	1	0.08
159	16.7	9.7	37.9	0	0	1	0.10
160	16.4	10.2	36.5	0	0	1	0.16
161	16.1	10.4	35.7	0	0	1	0.18
162	15.9	10.5	34.9	0	0	1	0.21
163	15.6	10.7	33.3	0	1	1	0.27
164	15.2	10.7	32.5	0	1	1	0.30
165	14.9	10.8	31.7	1	1	1	0.31
166	14.6	11.2	30.0	1	1	1	0.43
...

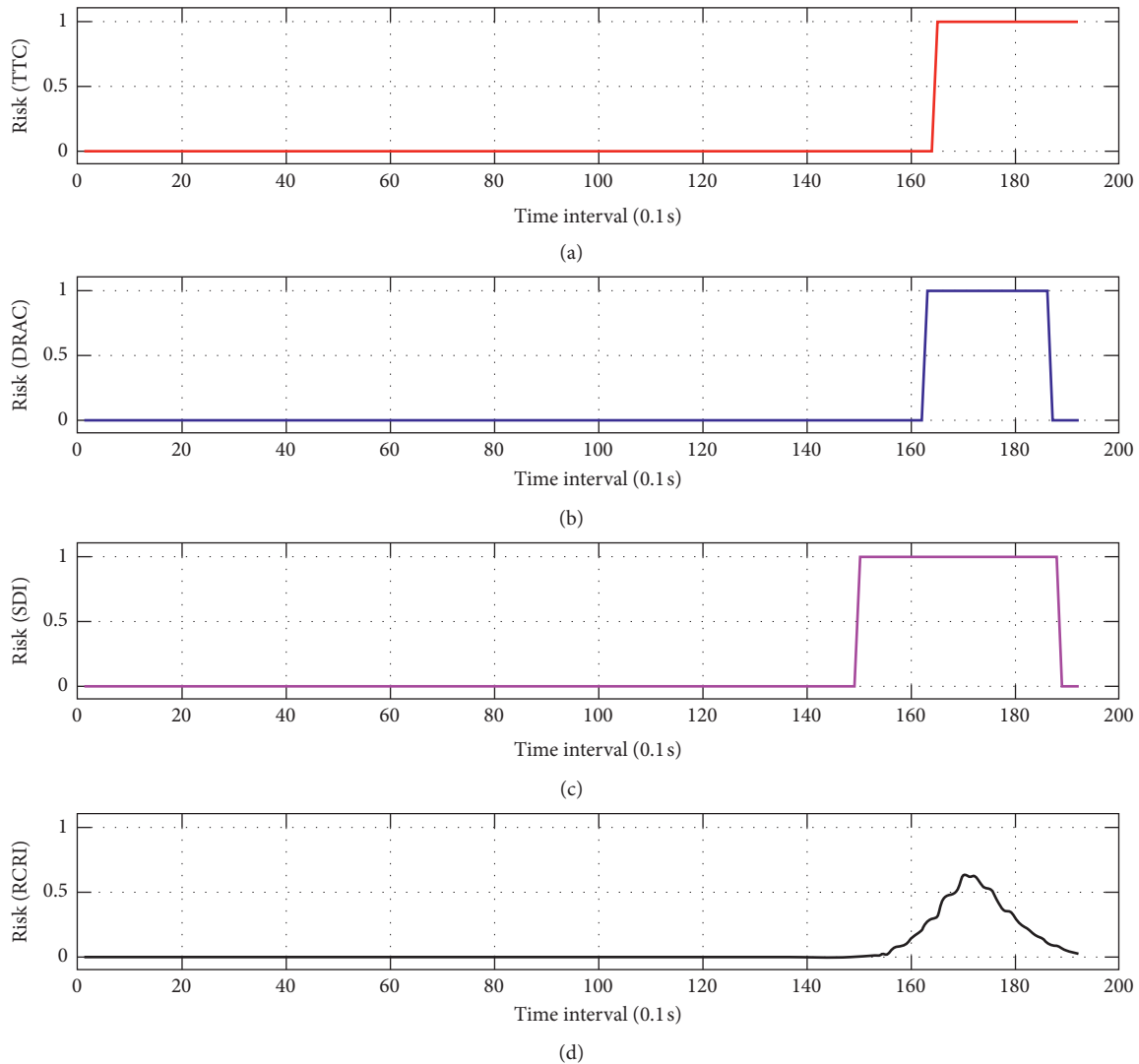


FIGURE 5: Rear-end crash risk identified by TTC, DRAC, SDI, and RCRI for one car-following event.

real-time change process of rear-end crash risk. On the contrary, the risk quantification results based on TTC, DRAC, and SDI are dummy variables. Therefore, the RCRI can more accurately represent the risk and has wider applicability.

5.2. Comparative Analysis of Rear-End Crash Risk under Different Influencing Factors. Before the significance test, the Kolmogorov-Smirnov (K-S) test was employed to verify the distribution of rear-end crash risks under different influencing factors. The results of the K-S test show that rear-end

TABLE 5: Significant main effects for rear-end crash risk.

Variables	Statistical results	Dummy variables	Rear-end crash risk	
			Mean	Std. Dev.
Day-of-week	$F = 58.1, p < 0.001$	Holiday	0.0028	0.0031
		Workday	0.0032	0.0033
Time-of-day	$F = 18.5, p < 0.001$	Off peak	0.0030	0.0033
		Morning peak	0.0034	0.0033
		Evening peak	0.0032	0.0032
Light condition	$F = 8.8, p = 0.003$	Daytime	0.0032	0.0032
		Nighttime	0.0030	0.0034
Weather condition	$F = 0.7, p = 0.408$	—	—	—
Traffic density	$F = 1655.0, p < 0.001$	High	0.0049	0.0027
		Median	0.0049	0.0033
		Low	0.0021	0.0029

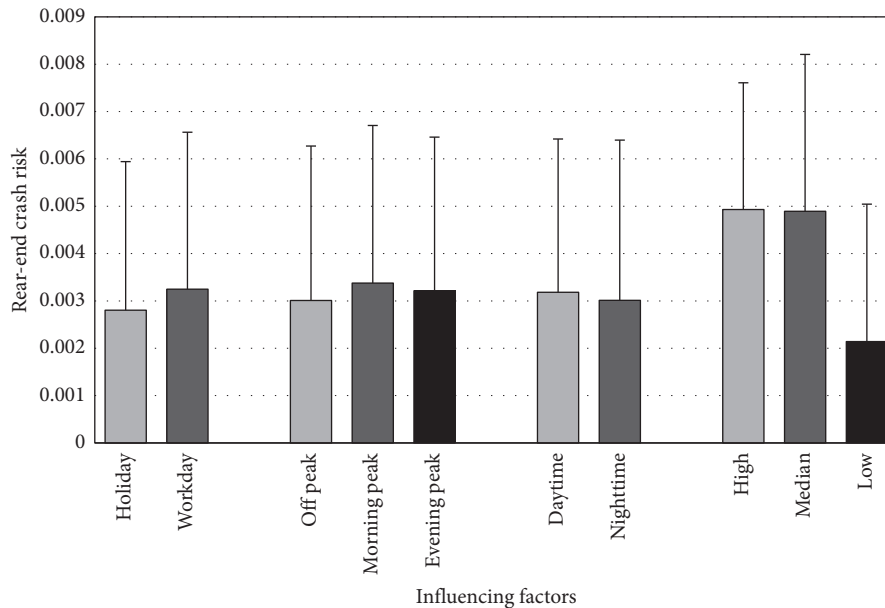


FIGURE 6: Rear-end crash risk under different influencing factors.

crash risk under different influencing factors meets the requirements of homogeneity of variance and normal distribution. Therefore, the analysis of variance (ANOVA) was then applied to test the significance of difference in rear-end crash risk under different influencing factors. Table 5 provides the summary statistics of the driving risk under these significant influencing factors. It can be seen from Table 5 that the rear-end crash risk under most influencing factors, such as day-of-week, time-of-day, light condition, and traffic density, is significantly different.

Figure 6 shows the comparison results of rear-end crash risk under different influencing factors. Specifically, for day-of-week, driving risk increased with the workday (by 14.3% from 0.0028 to 0.0032). In addition, the driving risks are 0.0030, 0.0034, and 0.0032 respectively in the three cases of off peak, morning peak, and evening peak. The significant differences in the risks of these temporal variables indicate that the driving risks are different for different travel

purposes. The decrease in driving risk was slight but significant by 0.0002 (6.3%) from daytime to nighttime. The driving risk decreased from 0.0049 in high traffic density to 0.0021 (by 57.1%) in low traffic density, indicating that traffic congestion leads to a decrease in driving safety.

5.3. Results of Mixed-Effects Linear Regression Model. Based on the car-following behavior variables and environmental factors variables obtained from SH-NDS, the influencing factors of rear-end crash risk are investigated. Table 6 presents the results of mixed-effects linear regression model. As shown in Table 6, the results of chi-squared goodness of fit indicate that the mixed-effects regression model fits well ($\chi^2(11) = 11198.24$, $\text{Prob} > \chi^2(11) = 0.00$). Except for the morning peak in temporal variables and weather conditions, all the variables listed in Table 6 are significant at 95% confidence level.

TABLE 6: Estimated parameters of the the mixed-effects linear regression model.

Explanatory variables		β	Std. Err.	Z	$P> Z $	95% CI	
						Lower	Upper
<i>Fixed effects (behavioral variables)</i>							
Duration of car-following event		$-9.52e-07$	$1.29e-07$	-7.36	<0.001	$-1.20e-06$	$-6.98e-07$
Mean time headway		-0.00200	0.00003	-65.32	<0.001	-0.00206	-0.00194
Average speed difference		0.00029	$8.18e-06$	35.07	<0.001	0.00027	0.00030
Acceleration difference ratio		0.00099	0.00005	18.80	<0.001	0.00088	0.00109
<i>Fixed effects (temporal variables)</i>							
Day-of-week	Holiday (baseline)	—	—	—	—	—	—
	Workday	0.00022	0.00005	4.88	<0.001	0.00013	0.00031
Time-of-day	Off peak (baseline)	—	—	—	—	—	—
	Morning peak	0.00010	0.00005	1.91	0.056	$2.57e-06$	0.00020
	Evening peak	-0.00012	0.00005	-2.42	0.016	-0.00023	-0.00002
<i>Fixed effects (environmental variables)</i>							
Light condition	Daytime (baseline)	—	—	—	—	—	—
	Nighttime	—	—	—	—	—	—
Weather condition	Sunny (baseline)	—	—	—	—	—	—
	Rainy	0.00013	0.00006	2.30	0.021	0.00002	0.00023
Traffic density	High (baseline)	—	—	—	—	—	—
	Median	-0.00203	0.00007	-27.10	<0.001	-0.00217	-0.00188
	Low	-0.00542	0.00007	-73.05	<0.001	-0.00557	-0.00527
Fixed effects (intercept)		0.00915	0.00016	58.55	<0.001	0.00884	0.00946
<i>Random effects (group name: driver)</i>							
		Estimate	Std. Err.			95% conf. interval	
Variance of intercept		$5.53e-07$	$1.05e-07$		$3.81e-07$	$8.01e-07$	
Variance of residual		$5.69e-06$	$6.21e-08$		$5.57e-06$	$5.82e-06$	
		$\chi^2(11) = 11198.24, \text{Prob} > \chi^2(11) = 0.0000$					
Log likelihood					77997.65		
LR test vs. linear model					$\chi^2 = 1216.65, \text{Prob} > \chi^2 = 0.00$		
Number of observations					16,905		
Number of groups					58		

As shown in Table 6, all selected behavioral variables affect the driving risk. The longer the duration of car-following event, the lower the driving risk. This can be understood as the risk of driving increases when the LV is changed frequently. Clearly, the larger the time headway, the lower the driving risk. This result is consistent with Duan et al. [9], who evaluated risk perception in car-following process. In addition, based on the SH-NDS data, Zhu et al. [43] concluded that the aggressive drivers have a shorter time gap than conservative drivers. Existing studies found evidence that speed dispersion is also an important factor in determining crash risk [44–46]. The larger speed difference between LV and FV is associated with a higher crash rate, which is generally consistent with our findings. In addition to the speed difference, this paper investigates the impact of acceleration difference on driving risk. The results show that the higher the acceleration difference ratio, the higher the risk, which indicates that the driving risk will increase when the FV uses more frequent acceleration and deceleration operations than the LV during car-following processes.

Qin et al. [47] suggested that due to the different travel purposes (to/from work) of drivers, the probability of a crash during working day and nonworking day is different, and the probability of crashes on working days is higher. This finding is consistent with the results of the regression model in this paper; that is, working days lead to higher driving risks. Furthermore, from the regression coefficients of this study, it

can be concluded that the crash risk is higher for the morning peak compared with other times of the day, and the evening peak is the lowest risk period of the day. The results are further confirmed that there is a significant correlation between driving risk and driving purpose. The driving risk of drivers on the way to work is higher than the risk of leaving work.

As for the diverse environment, compared with sunny days, the risk of rear-end crash is higher for drivers on rainy days, which is consistent with Das et al. [48] and Jung et al. [49]. From the obtained results, we can draw the conclusion that traffic density has a greater impact on rear-end crash risk [50]. The variable of median-density and low-density show a negative coefficient ($\beta = -0.002$ for median-density and $\beta = -0.005$ for low-density), indicating that driving risk decreased in lower density traffic. The high-density traffic flow leads to an increase in the uncertainty of traffic flow and increases the driving risk. This result is consistent with Huang et al. [22], who investigated the driving risks under different conditions using naturalistic driving study and driver attitude questionnaire.

6. Conclusions

This study proposes a new SMOs to quantify driving risks in car-following situations and investigates the impact of different influencing factors (behavioral factors, temporal

factors, and environmental factors) on rear-end crash risk considering driver's heterogeneity. A total number of 16,905 car-following events were extracted from SH-NDS database. Risks of rear-end crash under different influencing factors were compared. In addition, a mixed-effects linear regression model was then applied to investigate the relationship between rear-end crash risk and various influencing factors. Several key conclusions can be drawn:

- (i) Different from TTC, DRAC, SDI, and other indicators, the surrogate measure RCRI was proposed based on crash mechanism and comprehensively considers the crash probability and consequences. This measure can be applied in any car-following situation, even when the speed of the LV is greater than the speed of the FV. The RCRI proposed in this study is a continuous variable, so it can be more flexible to quantify the risk of rear-end crash.
- (ii) Among different temporal variables, workday and morning peak hour had the highest mean value of driving risk. For different light conditions, the crash risk increased for daytime compared to nighttime. As for different traffic density, the driving risks corresponding to low-density traffic flows are significantly lower than those corresponding to high-density and medium-density traffic flows.
- (iii) The mixed-effects linear regression model performed well in quantitatively evaluating the impact of various influencing factors on rear-end crash risk. The developed models demonstrated that duration of car-following event, mean time headway, average speed difference, acceleration difference ratio, day-of-week, time-of-day, weather condition, and traffic density had significant effects on rear-end crash risk. Workday and morning peak negatively affected driver safety. As for environmental variables, rainy and high-density traffic decreased driver safety.

As the main contribution, this paper utilizes a new SMOs and naturalistic driving data to quantify rear-end crash risk and identify the impacts of different influencing factors on the crash risks. Research was conducted based on naturalistic driving data, which objectively reflects the real operation of drivers. The new SMOs can not only be used to investigate the driving safety of drivers under different driving environments but also be used for driving risk evaluation and real-time risk prediction. Results from the mixed-effects linear regression model can be used to improve driving safety by adopting appropriate countermeasures. For example, traffic safety management can be strengthened during working days and morning peak hours to ensure safe driving.

Still, limitations exist in this study. The proposed indicators mainly focus on the risk of rear-end crash and cannot comprehensively consider other types of crash risks. In addition, no crash data were obtained from SH-NDS database that can be used to verify the effectiveness of RCRI. For future work, further validation will be applied to evaluate the effectiveness of RCRI based on crash data.

Moreover, the RCRI will be used to predict the real-time change process of driving risk and explore the impact of risky driving.

Data Availability

The data used in this paper are available from the corresponding author upon request.

Conflicts of Interest

The authors declare that there are no conflicts of interest regarding the publication of this paper.

Acknowledgments

This paper was jointly supported by the Chinese National Natural Science Foundation (71871161) and the Science and Technology Commission of Shanxi Province (19-JKCF-02).

References

- [1] WHO, *Global Status Report on Road Safety 2018*, World Health Organization, Geneva, Switzerland, 2018.
- [2] D. Tao, R. Zhang, and X. Qu, "The role of personality traits and driving experience in self-reported risky driving behaviors and accident risk among Chinese drivers," *Accident Analysis & Prevention*, vol. 99, pp. 228–235, 2017.
- [3] X. Zhang, X. Qu, D. Tao, and H. Xue, "The association between sensation seeking and driving outcomes: a systematic review and meta-analysis," *Accident Analysis & Prevention*, vol. 123, pp. 222–234, 2019.
- [4] S. Singh, *Critical Reasons for Crashes Investigated in the National Motor Vehicle Crash Causation Survey*, National Highway Traffic Safety Administration, Washington, DC, USA, 2015.
- [5] L. Dimitriou, K. Stylianou, and M. A. Abdel-Aty, "Assessing rear-end crash potential in urban locations based on vehicle-by-vehicle interactions, geometric characteristics and operational conditions," *Accident Analysis & Prevention*, vol. 118, pp. 221–235, 2018.
- [6] Y. Wu, M. Abdel-Aty, Q. Cai, J. Lee, and J. Park, "Developing an algorithm to assess the rear-end collision risk under fog conditions using real-time data," *Transportation Research Part C: Emerging Technologies*, vol. 87, pp. 11–25, 2018a.
- [7] National Highway Traffic Safety Administration, *Traffic Safety Facts 2015. Report No. DOT HS 812 384*, National Highway Traffic Safety Administration, Washington, DC, USA, 2017.
- [8] K. L. M. Broughton, F. Switzer, and D. Scott, "Car following decisions under three visibility conditions and two speeds tested with a driving simulator," *Accident Analysis & Prevention*, vol. 39, no. 1, pp. 106–116, 2007.
- [9] J. Duan, Z. Li, and G. Salvendy, "Risk illusions in car following: is a smaller headway always perceived as more dangerous?" *Safety Science*, vol. 53, pp. 25–33, 2013.
- [10] X. Li, X. Yan, J. Wu, E. Radwan, and Y. Zhang, "A rear-end collision risk assessment model based on drivers' collision avoidance process under influences of cell phone use and gender-A driving simulator based study," *Accident Analysis & Prevention*, vol. 97, pp. 1–18, 2016.
- [11] J. C. Hayward, "Near miss determination through use of a scale of danger," *Transportation Research Record*, vol. 384, pp. 24–34, 1972.

- [12] C. Oh, S. Park, and S. G. Ritchie, "A method for identifying rear-end collision risks using inductive loop detectors," *Accident Analysis & Prevention*, vol. 38, no. 2, pp. 295–301, 2006.
- [13] D. F. Cooper and N. Ferguson, "Traffic studies at t-junctions. 2. A conflict simulation record," *Traffic Engineering Control*, vol. 17, 1976.
- [14] G. Pnina, E. Johnathon, Z. Chunming et al., "Vehicle ownership and other predictors of teenagers risky driving behavior: evidence from a naturalistic driving study," *Accident Analysis & Prevention*, vol. 118, pp. 96–101, 2018.
- [15] B. Simons-Morton, N. Lerner, and J. Singer, "The observed effects of teenage passengers on the risky driving behavior of teenage drivers," *Accident Analysis & Prevention*, vol. 37, no. 6, pp. 973–982, 2005.
- [16] B. Yu, Y. Chen, S. Bao, and D. Xu, "Quantifying drivers' visual perception to analyze accident-prone locations on two-lane mountain highways," *Accident Analysis & Prevention*, vol. 119, pp. 122–130, 2018.
- [17] Y. Wu, M. Abdel-Aty, J. Park, and R. M. Selby, "Effects of real-time warning systems on driving under fog conditions using an empirically supported speed choice modeling framework," *Transportation Research Part C: Emerging Technologies*, vol. 86, pp. 97–110, 2018.
- [18] Y. Kuang, X. Qu, and S. Wang, "A tree-structured crash surrogate measure for freeways," *Accident Analysis & Prevention*, vol. 77, pp. 137–148, 2015.
- [19] K. Xie, D. Yang, K. Ozbay, and H. Yang, "Use of real-world connected vehicle data in identifying high-risk locations based on a new surrogate safety measure," *Accident Analysis & Prevention*, vol. 125, pp. 311–319, 2019.
- [20] X. Shi, Y. D. Wong, M. Z. F. Li, and C. Chai, "Key risk indicators for accident assessment conditioned on pre-crash vehicle trajectory," *Accident Analysis & Prevention*, vol. 117, pp. 346–356, 2018.
- [21] T. Fu, L. Miranda-Moreno, and N. Saunier, "A novel framework to evaluate pedestrian safety at non-signalized locations," *Accident Analysis & Prevention*, vol. 111, pp. 23–33, 2018.
- [22] H. Huang, Y. Li, X. Zheng, J. Wang, Q. Xu, and S. Zheng, "Objective and subjective analysis to quantify influence factors of driving risk," in *Proceedings of the 2019 IEEE Intelligent Transportation Systems Conference (ITSC)*, pp. 4310–4316, IEEE, Auckland, New Zealand, October 2019.
- [23] A. C. Hayley, B. d. Ridder, C. Stough, T. C. Ford, and L. A. Downey, "Emotional intelligence and risky driving behaviour in adults," *Transportation Research Part F: Traffic Psychology and Behaviour*, vol. 49, pp. 124–131, 2017.
- [24] E. L. Harbeck, A. I. Glendon, and T. J. Hine, "Young driver perceived risk and risky driving: a theoretical approach to the "fatal five"" *Transportation Research Part F: Traffic Psychology and Behaviour*, vol. 58, pp. 392–404, 2018.
- [25] P. Ulleberg and T. Rundmo, "Personality, attitudes and risk perception as predictors of risky driving behaviour among young drivers," *Safety Science*, vol. 41, no. 5, pp. 427–443, 2003.
- [26] E. Teye-Kwadjo, "Risky driving behaviour in urban Ghana: the contributions of fatalistic beliefs, risk perception, and risk-taking attitude," *International Journal of Health Promotion and Education*, vol. 57, no. 5, pp. 256–273, 2019.
- [27] Q. Shangquan, T. Fu, and S. Liu, "Investigating rear-end collision avoidance behavior under varied foggy weather conditions: a study using advanced driving simulator and survival analysis," *Accident Analysis & Prevention*, vol. 139, Article ID 105499, 2020.
- [28] L. Precht, A. Keinath, and J. F. Krems, "Identifying the main factors contributing to driving errors and traffic violations—results from naturalistic driving data," *Transportation Research Part F: Traffic Psychology and Behaviour*, vol. 49, pp. 49–92, 2017.
- [29] Q. Chen, R. Gu, H. Huang, J. Lee, X. Zhai, and Y. Li, "Using vehicular trajectory data to explore risky factors and unobserved heterogeneity during lane-changing," *Accident Analysis & Prevention*, vol. 151, Article ID 105871, 2021.
- [30] X. Wang, M. Yang, and D. Hurwitz, "Analysis of cut-in behavior based on naturalistic driving data," *Accident Analysis & Prevention*, vol. 124, pp. 127–137, 2019.
- [31] M. Zhu, X. Wang, and J. Hu, "Impact on car following behavior of a forward collision warning system with headway monitoring," *Transportation Research Part C: Emerging Technologies*, vol. 111, pp. 226–244, 2020.
- [32] J. Wang, T. Luo, and T. Fu, "Crash prediction based on traffic platoon characteristics using floating car trajectory data and the machine learning approach," *Accident Analysis & Prevention*, vol. 133, Article ID 105320, 2019.
- [33] M. Zhu, X. Wang, A. Tarko, and S. E. Fang, "Modeling car-following behavior on urban expressways in shanghai: a naturalistic driving study," *Transportation Research Part C: Emerging Technologies*, vol. 93, pp. 425–445, 2018.
- [34] C. Johnsson, A. Laureshyn, and T. De Ceunynck, "In search of surrogate safety indicators for vulnerable road users: a review of surrogate safety indicators," *Transport Reviews*, vol. 38, no. 6, pp. 765–785, 2018.
- [35] J. Carbaugh, D. N. Godbole, and R. Sengupta, "Safety and capacity analysis of automated and manual highway systems," *Transportation Research Part C: Emerging Technologies*, vol. 6, no. 1-2, pp. 69–99, 1998.
- [36] J. Wang, Y. Kong, T. Fu, and J. Stipanovic, "The impact of vehicle moving violations and freeway traffic flow on crash risk: an application of plugin development for micro-simulation," *PLoS One*, vol. 12, 2017.
- [37] D. Wang, *Traffic Flow Theory*, China Communications Press, Beijing, China, 2002.
- [38] F. Cunto and F. F. Saccomanno, "Calibration and validation of simulated vehicle safety performance at signalized intersections," *Accident Analysis & Prevention*, vol. 40, no. 3, pp. 1171–1179, 2008.
- [39] M. Yang, X. Wang, and M. Quddus, "Examining lane change gap acceptance, duration and impact using naturalistic driving data," *Transportation Research Part C: Emerging Technologies*, vol. 104, pp. 317–331, 2019.
- [40] H. Gan and Y. Bai, "The effect of travel time variability on route choice decision: a generalized linear mixed model based analysis," *Transportation*, vol. 41, no. 2, pp. 339–350, 2014.
- [41] C. Chai, X. Zeng, X. Wu, and X. Wang, "Safety evaluation of responsibility-sensitive safety (RSS) on autonomous car-following maneuvers based on surrogate safety measurements," in *Proceedings of the 2019 IEEE Intelligent Transportation Systems Conference (ITSC)*, pp. 175–180, IEEE, Auckland, New Zealand, October 2019.
- [42] G. Guido, F. Saccomanno, A. Vitale, V. Astarita, and D. Festa, "Comparing safety performance measures obtained from video capture data," *Journal of Transportation Engineering*, vol. 137, no. 7, pp. 481–491, 2011.
- [43] M. Zhu, X. Wang, and Y. Wang, "Human-like autonomous car-following model with deep reinforcement learning," *Transportation Research Part C: Emerging Technologies*, vol. 97, pp. 348–368, 2018.

- [44] L. Aarts and I. Van Schagen, "Driving speed and the risk of road crashes: a review," *Accident Analysis & Prevention*, vol. 38, no. 2, pp. 215–224, 2006.
- [45] O. M. J. Carsten and F. N. Tate, "Intelligent speed adaptation: accident savings and cost-benefit analysis," *Accident Analysis & Prevention*, vol. 37, no. 3, pp. 407–416, 2005.
- [46] T. Stübig, M. Petri, C. Zeckey et al., "Alcohol intoxication in road traffic accidents leads to higher impact speed difference, higher ISS and MAIS, and higher preclinical mortality," *Alcohol*, vol. 46, no. 7, pp. 681–686, 2012.
- [47] X. Qin, J. N. Ivan, N. Ravishanker, J. Liu, and D. Tepas, "Bayesian estimation of hourly exposure functions by crash type and time of day," *Accident Analysis & Prevention*, vol. 38, no. 6, pp. 1071–1080, 2006.
- [48] S. Das, A. Dutta, and S. R. Geedipally, "Applying Bayesian data mining to measure the effect of vehicular defects on crash severity," *Journal of Transportation Safety & Security*, pp. 1–17, 2019.
- [49] S. Jung, X. Qin, and D. A. Noyce, "Modeling highway safety and simulation in rainy weather," *Transportation Research Record: Journal of the Transportation Research Board*, vol. 2237, no. 1, pp. 134–143, 2011.
- [50] Y. Guo, T. Sayed, and M. Essa, "Real-time conflict-based Bayesian Tobit models for safety evaluation of signalized intersections," *Accident Analysis & Prevention*, vol. 144, Article ID 105660, 2020.

Research Article

Pedestrian Crash Exposure Analysis Using Alternative Geographically Weighted Regression Models

Seyed Ahmad Almasi ¹, Hamid Reza Behnood ¹, and Ramin Arvin ²

¹Department of Transportation Planning, Faculty of Engineering, Imam Khomeini International University, Qazvin, Iran

²Department of Civil & Environmental Engineering, University of Tennessee, Knoxville, USA

Correspondence should be addressed to Hamid Reza Behnood; hr.behnood@gmail.com

Received 30 November 2020; Revised 25 January 2021; Accepted 8 February 2021; Published 18 February 2021

Academic Editor: Mohamed Hussein

Copyright © 2021 Seyed Ahmad Almasi et al. This is an open access article distributed under the Creative Commons Attribution License, which permits unrestricted use, distribution, and reproduction in any medium, provided the original work is properly cited.

In order to develop a sustainable, safe, and dynamic transportation system, proper attention must be paid to the safety of pedestrians. The purpose of this study is to analyze the surrogate measures related to pedestrian crash exposure in urban roads, including the use of sociodemographic characteristics, land use, and geometric characteristics of the network. This study develops pedestrian exposure models using geographical spatial models including geographically weighted regression (GWR), geographically weighted Poisson regression (GWPR), and geographically weighted Gaussian regression (GWGR). In general, the results of the GWPR model show that the presence of a bus station, population density, type of residential use, average number of lanes, number of traffic control cameras, and sidewalk width are negatively associated with increasing the number of crashes. In this study, in order to identify traffic analysis zones (TAZ) based on the observed and predicted crash data, spatial distance-based methods using GWPR outputs have been used. This study shows the dispersion and density of pedestrian crashes without possessing the volume of pedestrians. Comparison of the performance of GWPR and Poisson models shows a significant spatial heterogeneity in the analysis.

1. Introduction

Pedestrians are known as vulnerable road users, and the severity of pedestrian injuries in motor vehicle crashes is relatively high. Today, ensuring the safe movement of pedestrians is one of the most challenging concerns for transportation engineers. In general, in urban accidents, drivers and passengers have the largest share of the comprehensive cost of traffic accidents (94%) [1]. In order to develop a sustainable, safe, and dynamic transportation system, proper attention must be paid to the safety of pedestrians. The proportion of pedestrian casualties in the world has increased by an average of 11 percent to 14 percent over the past decade, so addressing pedestrian safety and raising awareness about safe pedestrianization is an important issue. This study was conducted with the aim of addressing the safety of pedestrians and identifying the extent of exposure to pedestrian crashes in urban areas and

identifying accident-prone areas. Obviously, the number of people walking on the streets (i.e., pedestrian trips) and the factors that cause the presence of more pedestrians on the streets is one of the best measures for pedestrian exposure [2–5].

However, continuous measurement of pedestrian travels is difficult considering all the effective variables because it requires the use of significant resources and many factors that play a role in creating pedestrian travels. The purpose of this study is to investigate the available criteria and select the most effective measures in order to predict the variable of pedestrian exposure (pedestrian trips) and identify areas prone to pedestrian crashes. In other words, the purpose of this study is to analyze the surrogate measures related to pedestrian exposure in urban roads, including the use of sociodemographic characteristics, land use, and geometric characteristics of the network. The three-step process in the study involves the development of exposure models using

geographical spatial models including geographically weighted regression (GWR), geographically weighted Poisson regression (GWPR), and geographically weighted Gaussian regression (GWGR). Exposure models in this study are compared with the study model developed by Lee et al. [5] which were performed using Tobit method and generalized linear models (GLMs) and predicted pedestrian travel. In their study, it was suggested that the effect of the geographical location of exposure variables for pedestrian crashes be investigated in future studies. In the current study, the effect of spatial exposure variables based on their geographical location has also been investigated. Then, in order to identify the best exposure model between GWR, GWPR, and GWGR models, the Akaike Information Criterion (AIC) index and P value were used after validating the models to predict pedestrian crashes. This method can be described as a pedestrian safety analysis on urban roads (microlevel) with macrolevel data. Also in this study, in order to identify traffic analysis zones (TAZs) based on the observed and predicted crash data, spatial distance-based methods using GWPR outputs have been used.

The city of Tehran in Iran and its urban areas have been considered in this study. Although the two-step process (i.e., first identifying pedestrian collision variables and second crash prediction and identifying high-risk areas) has a relatively larger modeling error than the one-step model (pedestrian crash prediction only), but still by analyzing the volume of pedestrians and crashes, their output can lead to a better understanding of safety [5]. This study addresses pedestrian safety in the study area by identifying the best model for dealing with pedestrian crashes on major urban roads (first- and second-degree arteries and collector streets) as well as creating a safety analysis process for regions where pedestrian crash data are not available. This process can help transportation authorities create safer paths for pedestrians by implementing appropriate safety interventions.

2. Literature Review

Pedestrian safety is a growing concern, and so extensive studies have been conducted to ensure pedestrian safety. Researchers have tried to identify the factors contributing to pedestrian fatalities as well as identifying the urban areas with the highest risk of crashes for pedestrians by developing spatial relationships. For this purpose, in this section, past studies on the development of exposure models and spatial analysis of crashes have been reviewed.

Lee and Abdel-Aty [6] conducted a comprehensive study of pedestrian crashes at intersections in Florida. This study followed the Keall [7] method to use pedestrian personal travel data to create a rational model of a pedestrian exposure with crashes. In the proposed exposure measure, different walking patterns were reflected by different age groups of pedestrians. Miranda-Moreno et al. [8] analyzed two important relationships between land development and pedestrianization: (a) between land use and pedestrian activities and (b) between risk exposure (pedestrian and vehicle activities) and pedestrian crash frequency. The authors concluded that the land use pattern affects the level of

pedestrian activities with a direct impact on pedestrian safety. Ukkusuri et al. [9] developed a pedestrian count crash frequency model for New York City using a negative binomial model and a stochastic parameter. This model found that the ratio of illiterate population, business areas, school areas, functional characteristics of the intersection, type of access control on the roads, and the number of lanes had a positive effect on pedestrian crashes.

In order to select the variables used in the proposed exposure model, several previous studies have been reviewed. Previous researchers have shown that pedestrian volume is a significant measure of exposure that has a positive effect on the occurrence of vehicle-pedestrian collisions [2–5, 10]. Another significant measure of exposure is the effects of land use patterns that have long been studied by researchers [5, 11–13]. Wier et al. [13] found that the number of pedestrian crashes is relatively higher in commercial and residential areas. There are many studies that describe the impact of demographic and socioeconomic characteristics on pedestrian safety (e.g., [12]).

Although previous researchers have attempted to explain pedestrian exposure, there are very few studies that specifically identify the exact causes of this criterion. Another issue is the reliability of pedestrian volume data. There have been many cases where pedestrian volume data were not available or were not sufficiently accurate to perform a safety analysis. A reliable process for identifying surrogate measures is needed to express the pedestrian exposure criteria in such cases. Apart from these issues, the use of the negative binomial (NB) or even zero-inflated negative binomial (ZINB) model in microlevel safety analysis has been questioned by many authors [5, 14–16]. However, some authors have confirmed it in macrolevel analysis [17].

In general, spatial prediction of crashes using localized parameters gives us more accurate predictions compared to methods in Highway Safety Manual [18] that use global parameters. In addition, traffic exposure criteria (such as AADT and length of segment) are considered as predictors of crash frequency and have been widely used by transportation professionals to predict the occurrence of crashes at a particular site. Therefore, in the field of safety performance functions (SPFs), understanding the different spatial relationships between the main factors of exposure and the frequency of crashes has significant potential for the development of localized SPFs that can potentially provide more accurate crash predictions at separate sites [19].

In the current study, in order to identify high-risk TAZs based on observed and predicted crash data, two methods have been adopted: (1) frequency-based methods and (2) distance-based models. The first group measures the severity of point events based on the density of an area. These methods include kernel density estimation (KDE). The second group measures the spatial dependence of point events based on the distance of points from each other. This group includes methods such as nearest neighbor distances, K -functions, and Moran I [20, 21]. Hadayeghi et al. [22] presented traditional crash prediction models for 463 TAZs in Toronto using traditional NB (global) and GWPR general regression models. The results showed that GWPR models

were able to partially deal with spatial dependence as well as spatial heterogeneity resulting from these factors and TAZs. Xu and Huang [23] modeled the total crash frequency as a function of road length density, population density, average household income, and percentage of road sections with different speed limits and showed that the GWPR model due to the instability of the crash location has acceptable accuracy compared to the NB model with random parameter. A parametric GWPR model was also developed to estimate some parameters globally and some locally [24]. Similarly, a study by Rhee et al. [25] investigated traffic accidents with spatial correlation and spatial relevance using advanced spatial modeling methods. The results showed that the statistical performance of GWR was superior in the correlation coefficient of localization.

3. Methods

In this study, in the first step, which is the identification of exposure variables, several statistical methods have been used to identify these variables and the crash frequency is examined based on different modeling methods. In the second step, crash prediction models are presented at the TAZ level using surrogate variables. The following is a brief description of the modeling techniques used in these two steps.

3.1. Models Used to Identify Exposure Variables

3.1.1. Generalized Linear Models. Generalized linear models (GLMs) are a general class of statistical models that include many common models with specific features. A typical GLM is as follows:

$$Y = \sum_{i=1}^m \beta_i \chi_i + \varepsilon_i. \quad (1)$$

In this equation, Y is the linear prediction and ε_i is the error parameter. In the generalized linear model, the assumptions of independent and normal distribution in Y are given. This distribution includes such cases as normal, Poisson, gamma, and binomial distributions [26]. The GLM is a flexible generalization of ordinary linear regression that allows the use of response variables that have error distribution models other than the normal distribution.

3.1.2. Tobit Model. In this study, in order to eliminate any negative prediction of pedestrian crash, Tobit model was used to identify the measure of exposure. The Tobit model is a statistical model used to describe the relationship between a censored dependent variable y_i and an independent variable (or vector) x_i . The Tobit model is as follows:

$$y_i^* = \beta \chi_i + \varepsilon_i \quad i = 1, 2, \dots, N, \\ y_i = \begin{cases} y_i^*, & \text{if } y_i^* > 0, \\ 0, & \text{if } y_i^* \leq 0. \end{cases} \quad (2)$$

In this relation, y_i^* is a hidden variable that can only be seen if it is positive. Also, N is the number of observations, y_i is a dependent variable, x_i is a vector of explanatory variables, β is a vector of estimable parameters, and ε_i is a normal and independent distribution. The error parameter also has a mean of zero and a variance of σ^2 [27].

3.1.3. Variable Importance for Exposure Model Using Random Forest. Important explanatory variables can be determined using a random forest exposure model. The first step in this process is to place a random forest of data. During the fitting of this process, an out-of-bag error (a method for measuring random forest prediction error) is recorded for each data point and averaged in the forest. In order to measure the importance of the j^{th} attribute after training, the values of the j^{th} attribute can be changed among the training data and the out-of-bag error is re-estimated in this turbulent dataset [28].

3.2. TAZ Level Crash Predictive Models

3.2.1. Network KDE. As mentioned earlier, many recent studies have used the KDE network method developed by Okabe et al. [29] to examine the spatial correlation of point events in a road network. In this study, the KDE network method has been used to estimate the density of road sections in the Tehran road network. This method is based on the study method of Okabe and Sugihara [30].

In this study, the KDE network was performed on 1000-meter sections, similar to those proposed by Xie and Yan [20] and Nie et al. [31]. Also, according to studies [32, 33] in order to achieve more accurate KDE results, three values of 100, 200, and 500 meters have been considered for bandwidth measure. See Okabe and Sugihara [30] for more details on the computational process.

3.2.2. Geographically Weighted Regression Models. Geographically weight regression (GWR) is an exploratory method that has been adopted in the relevant literature mainly to deal with spatial variables. Past studies on the relationship between urban form and pedestrian behavior have mainly used global regression models. However, since the present study includes urban areas with the main arterial functional class and collectors, the behavioral characteristics of pedestrians may be different in each one. Therefore, it is likely that the relationship between urban form and walking varies across the study area.

In this study, a Gaussian GWR model is used to evaluate the relationship between exposure variables (land use and street characteristics around houses as independent variables). To determine which model is appropriate, a comparison was made between Gaussian GWR and geographically weighted regression and geographically weighted Poisson regression. A model with lower AIC values is a more appropriate model [34–36].

A GWPR model is also used in this study. In a GWPR model, the frequency of crashes is predicted by a set of

explanatory variables in which the parameters are allowed to change in space. This model can be written as follows [37]:

$$\ln(\lambda_i) = \beta_0(u_i, v_i) + \beta_1(u_i, v_i)\ln(E_{vi}) + \sum_{k=1}^k \beta_k(u_i, v_i)x_{ij}. \quad (3)$$

In this relation, (u_i, v_i) specifies the coordinates of region i . It should be noted that, in GWPR, $\beta_k(u_i, v_i)$ is a function of the coordinates of the center for region i .

In this study, GWR4.0 software was used to identify high-risk points in which the chances of determining the walking exposure variable increase because changes in independent variables are given in the first step of modeling. The results of GWR, GWPR, and GWGR in ArcGIS, version 10.2, were mapped to visualize spatial relationships. Also, even if there is a discontinuity in the study area, the optimal bandwidth has been selected based on several experiments to ensure that the blank spaces are outside the crash points of the study area.

3.3. Measures of Goodness of Fit. To evaluate and compare the performance of the models, three statistics were used to measure the accuracy of the estimates. First, we used AIC, which indicates that the lower the AIC, the better the model [38]. The AIC is measured as follows:

$$\begin{aligned} \text{AIC} &= D + 2K, \\ \text{AICc} &= \text{AIC} + \frac{2k(k+1)}{n-k-1}, \end{aligned} \quad (4)$$

where D represents the model deviation and k is the number of parameters. In GWPR, due to the nonparametric framework of the model, the number of parameters is meaningless. Therefore, an effective number of parameters must be considered, which can be written as follows [39]:

$$\begin{aligned} K &= \text{trace}(S), \\ \text{MAD} &= \frac{\sum_{i=1}^n |y_{\text{pred}} - y_{\text{obs}}|}{n}, \\ \text{RMSE} &= \sqrt{\frac{\sum_{i=1}^n (y_{\text{pred}} - y_{\text{obs}})^2}{n}}, \end{aligned} \quad (5)$$

where S is the hat matrix. In addition to AIC, we also used mean absolute error (MAE) and root mean square error (RMSE) to compare model performance. Lower MAE and RMSE values indicate better model performance. Finally, Moran's I statistics model was used to validate the models. Statistically, Moran's I statistics is a measure of spatial correlation. In this study, the Moran test was used to examine whether the residuals of city-wide crash predictions were spatially related to neighboring TAZs. Negative (positive) value of Moran's I statistics indicates a negative (positive) spatial correlation at the overall level.

3.4. Data Preparation. The main source of data for this study is Tehran Municipality. The data used in this study are shown in Table 1. In this study, the analyzed zones have been considered for model development based on the variables of exposure in TAZs, which are 560 zones for Tehran. Of course, it should be considered that, in order to match the analyzed zones, the whole city can be divided into equal units, but due to the lack of homogeneous distribution of pedestrian crashes, many of the identical zones will have zero observed crashes.

The TAZ characteristics selected for the crash analysis include all the variables in Table 1. All items selected as exposure variables are items that affect the frequency of crashes. Crash data variable (CR) shows the total number of pedestrian crashes in Tehran. The density of speed cameras (TCC) indicates a risk factor at their installation site, as these devices are typically installed in locations where drivers need more focus and are at greater risk of road crashes [32]. Bus station (BS) can be a risk factor as a large number of pedestrians get on and off in one place and some of them tend to cross the street [5]. The presence of schools (SC) is one of the most important places to attract pedestrians, so the presence of schools in TAZs during the hours of the day is a risk factor for pedestrian crashes [5]. The presence of a pedestrian bridge (PB) based on studies has improved pedestrian safety in conflicting with vehicles [5]. Also, the presence of intersections in any zone increases the risk of pedestrian collisions. It is obvious that population density (TP0) in each zone and the density of vulnerable users (TP1 and TP2) increase the risk of pedestrian collisions [5, 32, 33]. This study was conducted in two steps including [1] identifying the variables of pedestrian exposure and [2] investigating the spatial-geographical relationship between the variables and the spatial crash prediction at the TAZ level. GIS and SPSS software were used to extract and process data for the first step and GWR4 for the second step. The integration of the database with all the information collected in TAZs is done with the help of standard tools in GIS that allow spatial search, layer addition, and spatial operations based on topological relationship.

Table 1 shows the pedestrian crash dataset of Tehran, which includes 1231 observed cases. Descriptive variables were also classified into three categories: "demographic and socioeconomic," "land use," and "traffic and geometric". Out of 25 variables collected, 15 variables are listed in Table 1 based on the results of the first step in the study. Road network in Tehran, including arterial roads and collectors, has been used for analysis. Data were collected from various sources. Figure 1 shows the study area and the status of existing crashes. Figure 2 shows the KDE crash density function based on crash point and crash density per kilometer in three bandwidths of 100, 200, and 500 meters.

The correlation between the descriptive variables used in the Tobit model (selected model based on the results of the first step of the study) was investigated before the modeling process. Pairs of variables with correlation coefficients higher than 0.6 are not included in the models simultaneously [5]. In the modeling process, first the explanatory variables with the lowest correlation values were included in

TABLE 1: Description of variables used in the study.

Variable	Description
Crash data (CR)	Pedestrian crash data for the years 2017 to 2019 in Tehran
Bus stops (BS)	Location of bus stops in the existing situation and detailed plan of Tehran
Schools (SC)	Location of all schools in Tehran urban zones including both existing and planned schools
Pedestrian bridges (PB)	Location of pedestrian overpasses
Intersections (TS)	Location of all controlled and noncontrolled intersections
Total population (TP0)	Based on the last census in 2016
Children population (TP1)	Based on the last census in 2016
Elder people population (TP2)	Based on the last census in 2016
Motorcycles (TM)	Based on the data recorded in the 2016 census and registered in police databases
Vehicles (TC)	Based on the data recorded in the 2016 census and registered in police databases
Residential land use (RE)	Data gathered by Tehran Municipality's staff in 2017
Business land use (BU)	Data gathered by Tehran Municipality's staff in 2017
Recreational land use (RCE)	Data gathered by Tehran Municipality's staff in 2017
Average road width (AW)	Based on GIS layers of the Tehran Municipality
Average number of lanes (AL)	Based on GIS layers of the Tehran Municipality
Average length of median refuges (TR)	Based on GIS layers of the Tehran municipality
Average sidewalk width (PP)	Average sidewalk width in each traffic zone based on aerial photos
Average speed (SA)	Based on the data adopted from the Traffic Control Center of Tehran Municipality
Average road slope (AS)	Based on GIS layers of the Tehran Municipality
Speed cameras (TCC)	Based on the data adopted from the Traffic Control Center of Tehran Municipality

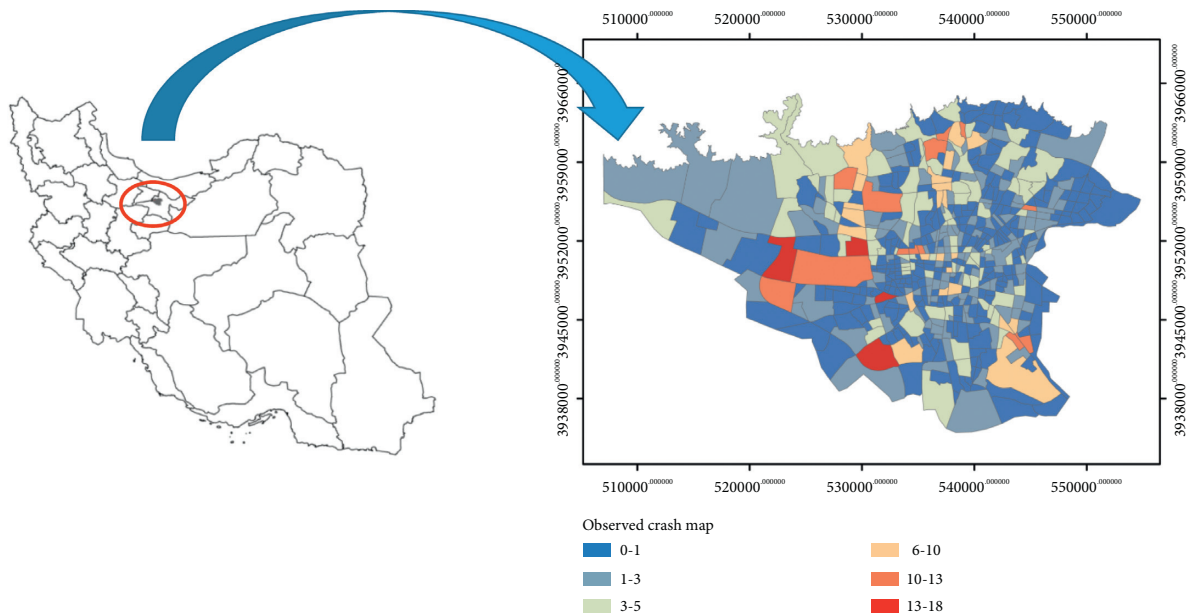


FIGURE 1: The study area and the status of existing crashes.

the model and the variables with relatively lower correlation values were preferred in the model (Tables 2 and 3).

4. Results and Discussion

A total of six exposure models have been developed in this study (Table 4). Because two different modeling methods are used (GLM vs. Tobit) to compare the best model, it is not appropriate to compare the Akaike Information Criterion (AIC) or the Bayesian Information Criterion (BIC). Therefore, to compare the models, the mean absolute deviation (MAD) and the root mean square error (RMSE) for each model have been used [5]. Table 4 shows that the Tobit

model using all variables performs best with the lowest MAD and RMSE values. The Tobit model also shows any predicted negative pedestrian crashes using the exposure variables equal to zero because the lower limit is set at zero.

Between 2017 and 2019, 1228 pedestrian crashes were reported in Tehran, in which 44 people died and 1184 were injured. A total of 4979 schools, 4831 bus stops, 927 pedestrian bridges, 801 lighted intersections, and 5386 traffic control cameras located in 560 different TAZs were included in this analysis (Table 1), with an average number of variables ranging from 0 to 80 in all TAZs. This initial benchmark shows that the difference between the scatterings of exposure variables at the level of TAZs is significant. The

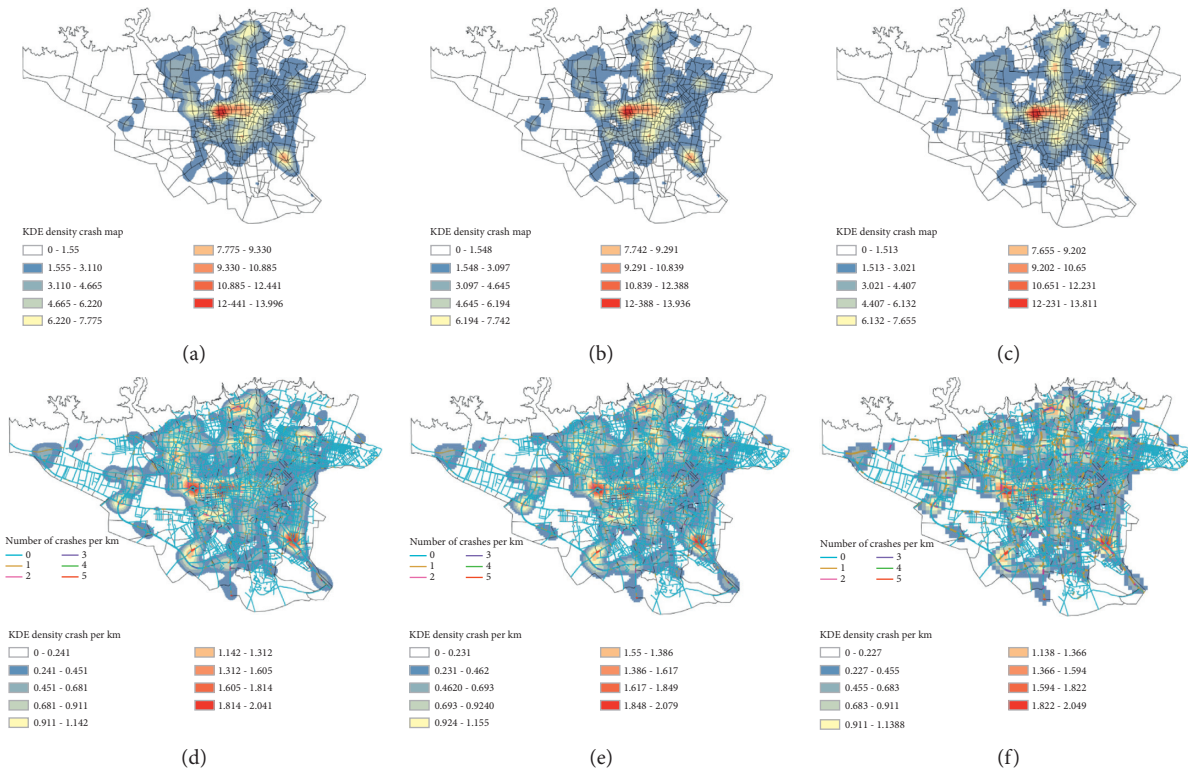


FIGURE 2: KDE crash density functions in different bandwidths. (a) KDE crash density function for bandwidth = 100 m. (b) KDE crash density function for bandwidth = 200 m. (c) KDE crash density function for bandwidth = 500 m. (d) KDE crash density function per km for bandwidth = 100 m. (e) KDE crash density function per km for bandwidth = 200 m. (f) KDE crash density function per km for bandwidth = 500 m.

TABLE 2: Pearson correlation coefficients.

Correlation		SC	BS	PB	TS	TP0
SC	Pearson Sig.	1				
BS	Pearson Sig.	0.54** 0.00	1			
PB	Pearson Sig.	0.39** 0.00	0.60** 0.00	1		
TS	Pearson Sig.	0.36** 0.00	0.41** 0.00	0.21** 0.00	1	
TP0	Pearson Sig.	0.63** 0.00	0.60** 0.00	0.47** 0.00	0.37** 0.00	1

*Correlation is significant at the 0.05 level (2-tailed). **Correlation is significant at the 0.01 level (2-tailed).

results of GWR, GWGR, and GWPR models are shown in Tables 5–7, respectively. Table 8 compares the GWR, GWGR, and GWPR models. According to the results shown in these tables, the GWPR model has a higher accuracy in predicting crashes based on exposure variables. In Figure 3, based on crash predictive models and using ArcGis software, a pedestrian crash map of Tehran has been produced. Table 9 shows the ANOVA values for the GWPR model.

Tables 5–9 show the results of the GWR, GWGR, and GWPR models with adaptive bisquare kernel for predicting crashes. In the kernel density function model, the lowest AICC value was obtained based on the adaptive bisquare

kernel. Notably, we found that the results were largely consistent with the adaptive bisquare kernel. Also, the Lagrange coefficient values for the GWPR model and the global model were 0.12 and 0.15, respectively, which is less than the critical Lagrange value (3.48). The study by Hezaveh et al. [1] also confirms the adaptive bisquare kernel in relation to the Gaussian adaptive for urban TAZs.

The comparison of AIC, AICc, deviation, MAE, and RMSE presented in Table 8 shows that the GWPR model is more appropriate than the global model. The value of Moran I (0.031) indicates that, in the GWPR model, the residues are not related to each other. In addition, VIF values

TABLE 4: Comparison of the exposure models developed in the study.

Model type (exposure)	MAD	RMSE
Exposure model (GLM) using all variables	26.91	40.12
Exposure model (GLM) using PCA variables	37.21	49.26
Exposure model (Tobit) using all variables	22.69	37.99
Exposure model (GLM) using random forest variables	31.06	42.40
Exposure model (Tobit) using RF variables	33.76	42.43
Exposure model (Tobit) using PCA variables	30.61	43.24

TABLE 5: Summary results of the GWR model for predicting crashes.

Variables	Intercept 2.053	C-export	Residual -0.044	R ² (local) 0.39	Std. error	Std. resid -0.024
SC		0.248			0.183	
BS		0.228			0.196	
PB		0.118			0.120	
TS		0.178			0.085	
TP0		0.725			0.210	
TM		-0.423			0.248	
TC		0.354			0.155	
RE		-0.423			0.122	
BU		0.572			0.135	
RCE		-0.028			0.123	
AW		0.39			0.190	
TR		0.121			0.088	
TCC		-0.055			0.012	
TP1		0.514			0.145	
TP2		0.325			0.162	
AL		0.254			0.065	
PP		-0.416			0.321	
SA		0.213			0.174	
AS		0.085			0.162	

TABLE 6: Summary results of the GWGR model for predicting crash.

Variables	Estimate	Stand. error	Z (Est/SE)	Mean	Std.	Min	Max	Median	Lower quartile	Upper quartile	Local
Intercept	2.173	0.101	21.462	1.046	1.810	3.093	-2.52	2.009	1.922	2.284	Yes
SC	0.209	0.150	1.394	0.214	0.228	0.531	-0.36	0.285	0.150	0.381	Yes
BB	-0.084	0.170	-0.494	0.553	0.513	1.809	-0.41	0.332	0.128	0.862	Yes
PB	0.012	0.164	0.071	0.227	0.337	0.898	-0.22	0.324	0.181	0.501	Yes
TS	0.202	0.121	1.676	0.173	0.179	0.555	-0.42	0.164	0.107	0.275	Yes
TP0	-0.548	0.519	-1.057	1.081	0.344	3.677	-1.79	-0.007	-0.342	0.817	Yes
TP1	-0.137	0.411	-0.333	1.311	-0.13	4.750	-2.03	-0.518	-0.907	0.385	Yes
TP2	0.154	0.322	0.477	0.742	0.301	1.933	-1.31	0.188	-0.219	0.796	Yes
TM	0.273	0.187	1.465	0.519	0.246	1.123	-2.04	0.330	0.098	0.536	Yes
TC	0.091	0.419	0.218	1.292	-1.32	0.605	-4.83	-1.137	-1.925	-0.244	Yes
RE	-0.429	0.143	-2.999	0.343	-0.56	-0.03	-1.45	-0.545	-0.835	-0.235	Yes
BU	0.229	0.116	1.970	0.520	-0.08	0.923	-1.23	-0.038	-0.509	0.350	Yes
REC	0.556	0.133	4.172	0.253	0.769	1.429	0.139	0.718	0.636	0.886	Yes
AW	0.086	0.121	0.716	0.158	0.005	0.497	-0.39	0.008	-0.125	0.064	Yes
AL	-0.348	0.117	-2.970	2.477	-1.16	-0.00	-11.6	-0.234	-0.576	-0.140	Yes
TR	0.641	0.191	3.347	0.373	0.386	1.473	-0.33	0.324	0.124	0.621	Yes
AS	0.232	0.112	2.068	0.208	0.170	0.715	-0.46	0.201	0.050	0.266	Yes
TCC	0.795	0.175	4.548	0.456	0.813	2.017	0.114	0.665	0.470	1.085	Yes
PP	-0.423	0.125	-3.25	-0.25	0.145	1.025	-0.21	0.361	0.251	0.189	Yes

(mean = 1.8; maximum = 3.9) indicate that the local multicollinearity issue is not critical in this study.

In the study by Lee et al. [5], it is proposed to investigate the local effect of pedestrian crash exposure variables. The

statistical results of the second step models in the current study show that, in the GWPR model, all variables had a local effect. Figure 3 shows the spatial effect of the estimated parameter on crashes. This figure shows only those

TABLE 7: Summary results of the GWPR model for predicting crash.

Variables	Estimate	Stand. error	Z (Est/SE)	Mean	Std.	Min	Max	Median	Lower quartile	Upper quartile	Local
Intercept	-13.165	0.033	-399.863	-14.48	3.208	-31.32	-12.16	-13.15	-14.101	-12.813	Yes
SC	0.104	0.036	2.883	0.111	0.126	-0.160	0.436	0.110	0.008	0.213	Yes
BS	-0.355	0.040	-8.943	-0.028	0.294	-0.824	0.732	-0.073	-0.226	0.139	Yes
PB	0.042	0.038	1.100	0.062	0.168	-0.358	0.433	0.058	-0.068	0.183	Yes
TS	0.218	0.032	6.771	0.077	0.157	-0.401	0.284	0.117	-0.006	0.198	Yes
TP0	-0.312	0.122	-2.559	0.681	1.509	-2.625	5.228	0.402	-0.415	1.370	Yes
TP1	-0.401	0.109	-3.672	-0.467	1.147	-3.593	2.591	-0.618	-1.044	0.201	Yes
TP2	-0.055	0.074	-0.744	0.286	0.416	-0.822	1.068	0.312	-0.012	0.631	Yes
TM	0.254	0.044	5.724	-0.004	0.473	-2.010	1.211	0.026	-0.241	0.290	Yes
TC	0.343	0.105	3.257	-1.014	0.917	-3.034	1.017	-0.992	-1.831	-0.254	Yes
RE	-0.230	0.041	-5.627	-0.224	0.189	-0.709	0.200	-0.261	-0.365	-0.043	Yes
BU	-0.012	0.026	-0.464	-0.220	0.359	-1.242	0.727	-0.101	-0.508	0.049	Yes
REC	0.201	0.026	7.724	0.212	0.189	-0.117	0.764	0.148	0.055	0.328	Yes
AW	0.139	0.034	4.017	-0.019	0.172	-0.631	0.412	0.005	-0.103	0.097	Yes
AL	-0.153	0.039	-3.920	-3.683	7.218	-40.32	0.502	-0.146	-2.609	-0.056	Yes
TR	0.327	0.044	7.352	0.181	0.314	-0.555	1.083	0.157	-0.064	0.367	Yes
AS	0.211	0.028	7.588	0.124	0.323	-0.527	1.141	0.084	-0.078	0.245	Yes
TCC	-0.251	0.037	-6.715	-0.005	0.252	-0.709	0.621	-0.029	-0.149	0.136	Yes
PP	-13.165	0.033	-399.863	-14.48	3.208	-31.32	-12.16	-13.15	-14.101	-12.813	Yes

TABLE 8: Comparison and fitted goodness model.

Models	Global model result		Regression model
	GWGR	GWPR	GWR
Unbiased sigma estimate	2.3961	2.4921	2.1748
-2 log-likelihood	2569.6562	2989.7522	2347.2654
AIC	2587.4516	2767.4426	2507.5604
AICc	2589.0339	2799.0559	2534.7239
Adjusted R square	0.3214	0.44	0.41
MAD	0.851	0.482	0.952
RMSE	1.052	0.591	1.34
Moran's index	0.042	0.031	0.061
P value	<0.001	<0.001	<0.001

coefficients that have a significant effect and the small coefficients are shown in white. It is noteworthy that the estimated coefficients in common fixed models are in the range of similar values in spatial models [1] and this shows that the estimated parameters in global models (i.e., fixed models) are characteristics of the average of the factors affecting the dependent variable.

VIF values do not change between 1.12 and 3.9 (the critical value of VIF between 5 and 10 means a complete spatial correlation between the independent variables). This could be due to excessive scatter in the exposure variables. According to studies [1, 23, 40], the location of VIF in this limit can also justify the geographical distribution of Poisson in crash prediction, but this issue can be explored in the future. Traffic parameters such as intersections and speed cameras have a significant impact on pedestrian crashes and in TAZs where the speed camera density is higher, and fewer crashes will occur due to the variable estimation coefficient (negative).

The model predicts that crashes decrease as population density increases. The sign of population density is negatively associated with crash frequency which is consistent with previous studies [41]. This could be due to the fact that,

in residential areas without commercial and recreational land uses, due to the low speed of vehicles and the presence of speed bumps, as well as distracting effects, the crash density has decreased. In general, the results of the GWPR model show that the presence of a bus station, population density, type of residential land use, average number of lanes, number of traffic control cameras, and sidewalk width have a negative effect on increasing the number of crashes. In the GWR model, the number of motorcycles, residential land use, recreational land use, the average number of lanes, and the number of speed cameras in TAZs had a negative relation with increasing pedestrian crashes. Finally, in the GWGR model, the number of bus stops, population density, residential land use density, average number of lanes, and the number of speed cameras were negatively associated with increasing crashes. It should be noted that, in the three mentioned models, a significant relationship between dependent variable and independent variables has been obtained, which has been confirmed by previous studies (e.g., [13, 40, 42]).

One of the explanations for the negative sign of the bus station in urban areas can be the reduction of the volume of motor vehicles around the residential area, which reduces

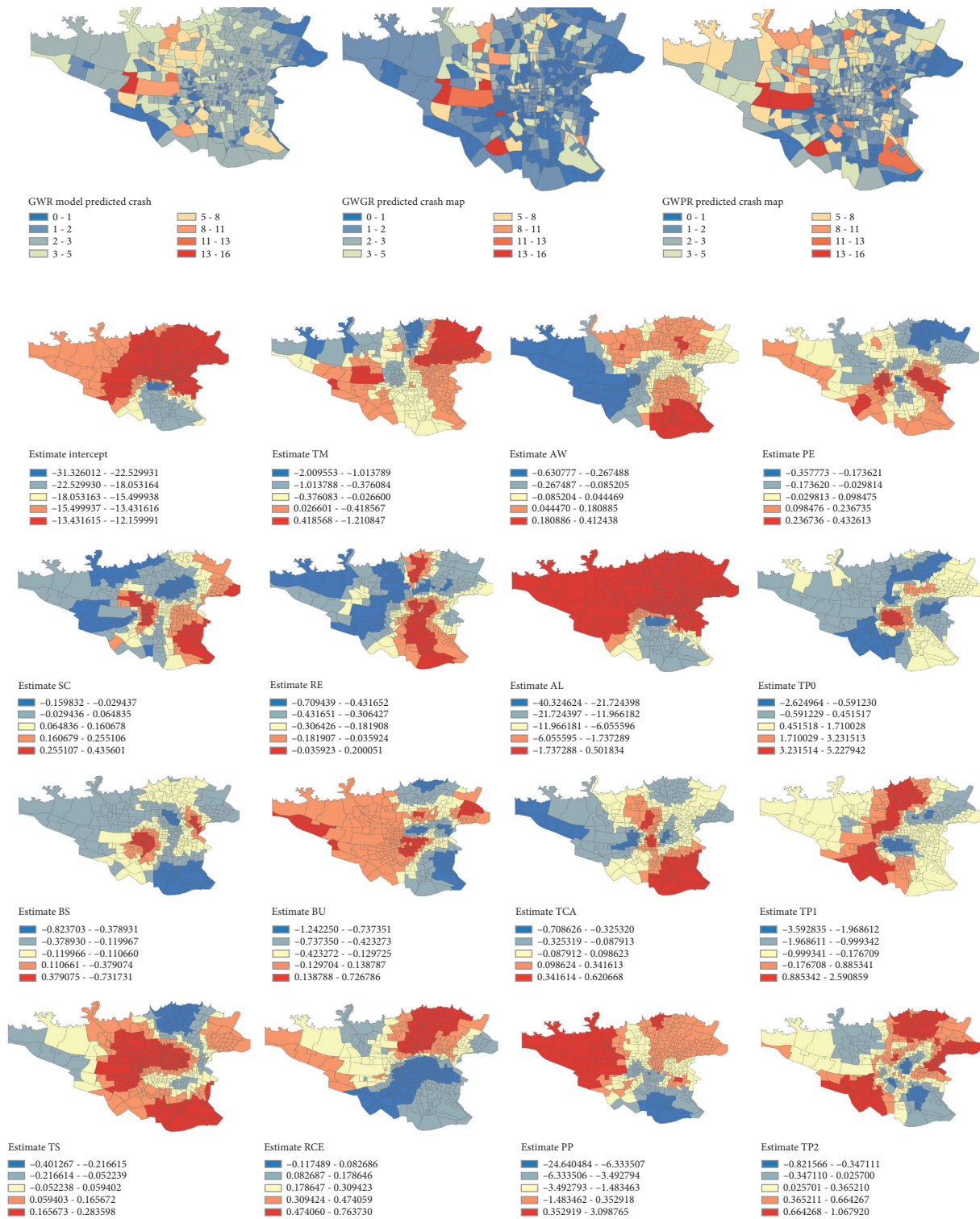


FIGURE 3: Crash predictive maps for GWR, GWGR, and GWPR models.

traffic congestion and ultimately exposes the motor traffic of other residents [1, 5]. On the other hand, poor design of a multimode network can negatively affect the safety of nonmotorized users and public transportation. The difference between the signs of the estimated coefficients in several different models requires more details in future studies. We

may expect older people to suffer more severe injuries due to vulnerability [1]. Conversely, older people travel less than other groups [43–45]. As a result, in this study, the percentage of elderly people compared to other age groups was negatively associated with the increase in crash density in the GWPR model. The negative sign of motorcycle users on the

TABLE 9: ANOVA table for GWPR model.

Source	SS	DF	MS	F	P value
Global residuals	3111.824	542			0.001
GWPR improvement	943.826	83.0214	11.286		0.001
GWPR residuals	2168.097	458.2651	4.730	2.3861	0.001

increase of pedestrian crashes can be due to the increase in motorcycle travel; hence, the number of pedestrian trips has decreased. In this study, the variables of number of schools, number of intersections, and pedestrian bridges have been shown with a positive sign, in which the impact of intersections on pedestrian crashes is not significant but has a positive effect on causing crash, which is confirmed by the study by Lee et al. [5]. Due to the presence of parents and children on the school routes, there is more walking activity in TAZs with more schools. Households with less than two vehicles (0 or 1 vehicle) are another important source of pedestrian activity. Car ownership is directly related to household income levels, which reflects the socioeconomic impact on pedestrian activity [5]. It is obvious that family members without transportation meet their transportation needs through public transportation or walking. On the other hand, the amount of car ownership in TAZs also has a significant impact on increasing pedestrian crash exposure. Of course, the crash may occur with vehicles that are outside the TAZ and collide with a pedestrian while traveling in different TAZs. In this study, the TC variable is the vehicle ownership variable in the study area, considering the two factors, and the model results show a positive effect on pedestrian exposure. As mentioned earlier, in this study, the average width of the sidewalk was negatively associated with pedestrian exposure and did not cause crashes, which is consistent with previous studies (e.g., [5, 45, 46]). These findings are also consistent with studies of human factors that show that some groups (e.g., low income, low education, and young urban road users) are more prone to abnormal behaviors [1, 47, 48].

According to the modeling results, the effect of slope and average width of the route on crashes is positive and the reason could be that pedestrians in wider passages have to travel longer to cross the street so they are more exposed in the passage of vehicles. Also, the medium slope has a positive effect on pedestrian crashes compared to zero-slope roads due to more difficult control of vehicles in adverse weather conditions.

5. Conclusion

In this study, a systematic approach has been developed that uses pedestrian surrogate measures based on exposure information. In this study, in the first step, which is the identification of exposure variables, several statistical methods have been used to identify these variables and the frequency of crashes is investigated based on different modeling methods. In the second step, crash prediction models were presented at the zone level using surrogate variables. In this study, three models GWR, GWGR, and GWPR have been used to spatially predict the crash frequency based on exposure variables, and the results of the study showed that the GWPR model makes more accurate predictions. In addition, identifying effective criteria such as

the presence of school, car and motorcycle ownership, bus station, sidewalk width, pedestrian bridges, type of intersection control and the presence of midroad refuge, population density, type of land use, width of roads, average number of routes, average road slopes, and number of speed cameras in dealing with pedestrians is important in this study. In this study, it is emphasized that while providing safety measures for pedestrians, cases such as improving traffic calming should be done in areas with high density of schools as well as schools in the area of intersections and increase the width of sidewalks in areas with more bus stations, because in areas where the bus is the main mode of transportation, there is a tendency to walk and consequently pedestrians are exposed to crashes.

The proposed two-step method in this study involves two consecutive modeling processes. The first model identifies the exposure variables in pedestrian crashes and the second model estimates the number of pedestrian crashes using three spatial models GWR, GWGR, and GWPR. However, this trend is limited because the result can be affected by the errors accumulated in the first stage due to the existence of an uncontrollable confounding variable as well as information biases. It is possible to solve the problem by adopting a simultaneous modeling approach. This study has shown the dispersion and density of pedestrian crashes without possessing the volume of pedestrians and thus by taking safety measures in places prone to pedestrian crashes, social costs, and casualties can be decreased. In this study, Poisson regression was used to evaluate the relationship between sociological variables and crashes at the zone level. Comparison of the performance of GWPR and Poisson models shows a significant spatial heterogeneity in the analysis. The increase in residential density in urban areas has been associated with a decrease in speed and therefore has led to a reduction in crash frequency. On the other hand, increasing travel time and consequently increasing traffic exposure affect the social costs of crashes. Identifying traffic-prone zones can be a useful element in developing policies to support mitigation measures related to pedestrian exposure to traffic. We expect that, in future studies, negative geographic binomial distribution models and the experimental Bayesian geographic model will be used to identify pedestrian exposure variables.

Data Availability

The data used to support the findings of this study are available from the corresponding author upon request.

Conflicts of Interest

The authors declare that they have no conflicts of interest.

Acknowledgments

The authors of this article would like to thank the Deputy of Transportation and Traffic of Tehran Municipality, Legal Medicine Organization, Statistics Center of Iran, and Deputy of Architecture and Urban Planning of Tehran Municipality in order to collect the required data and cooperate in field visits and geometric information of the road network.

References

- [1] A. M. Hezaveh, R. Arvin, and C. R. Cherry, "A geographically weighted regression to estimate the comprehensive cost of traffic crashes at a zonal level," *Accident Analysis & Prevention*, vol. 131, pp. 15–24, 2019.
- [2] D. G. Davis and J. P. Braaksma, "Adjusting for luggage-laden pedestrians in airport terminals," *Transportation Research Part A: General*, vol. 22, no. 5, pp. 375–388, 1988.
- [3] X. Qin and J. N. Ivan, "Estimating pedestrian exposure prediction model in rural areas," *Transportation Research Record: Journal of the Transportation Research Board*, vol. 1773, no. 1, pp. 89–96, 2001.
- [4] W. W. Y. Lam, S. Yao, and B. P. Y. Loo, "Pedestrian exposure measures: a time-space framework," *Travel Behaviour and Society*, vol. 1, no. 1, pp. 22–30, 2014.
- [5] J. Lee, M. Abdel-Aty, and I. Shah, "Evaluation of surrogate measures for pedestrian trips at intersections and crash modeling," *Accident Analysis & Prevention*, vol. 130, pp. 91–98, 2019.
- [6] C. Lee and M. Abdel-Aty, "Comprehensive analysis of vehicle-pedestrian crashes at intersections in Florida," *Accident Analysis & Prevention*, vol. 37, no. 4, pp. 775–786, 2005.
- [7] M. D. Keall, "Pedestrian exposure to risk of road accident in New Zealand," *Accident Analysis & Prevention*, vol. 27, no. 5, pp. 729–740, 1995.
- [8] L. F. Miranda-Moreno, P. Morency, and A. M. El-Geneidy, "The link between built environment, pedestrian activity and pedestrian-vehicle collision occurrence at signalized intersections," *Accident Analysis & Prevention*, vol. 43, no. 5, pp. 1624–1634, 2011.
- [9] S. V. Ukkusuri, S. Hasan, and H. M. A. Aziz, "Random parameter model used to explain effects of built-environment characteristics on pedestrian crash frequency," *Transportation Research Record: Journal of the Transportation Research Board*, vol. 2237, no. 1, pp. 98–106, 2011.
- [10] W. W. Y. Lam, B. P. Y. Loo, and S. Yao, "Towards exposure-based time-space pedestrian crash analysis in facing the challenges of ageing societies in Asia," *Asian Geographer*, vol. 30, no. 2, pp. 105–125, 2013.
- [11] R. Cervero, "Mixed land-uses and commuting: evidence from the American housing survey," *Transportation Research Part A: Policy and Practice*, vol. 30, no. 5, pp. 361–377, 1996.
- [12] D. J. Graham and D. A. Stephens, "Decomposing the impact of deprivation on child pedestrian casualties in England," *Accident Analysis & Prevention*, vol. 40, no. 4, pp. 1351–1364, 2008.
- [13] M. Wier, J. Weintraub, E. H. Humphreys, E. Seto, and R. Bhatia, "An area-level model of vehicle-pedestrian injury collisions with implications for land use and transportation planning," *Accident Analysis & Prevention*, vol. 41, no. 1, pp. 137–145, 2009.
- [14] D. Lord, S. P. Washington, and J. N. Ivan, "Poisson, Poisson-gamma and zero-inflated regression models of motor vehicle crashes: balancing statistical fit and theory," *Accident Analysis & Prevention*, vol. 37, no. 1, pp. 35–46, 2005.
- [15] D. Lord, S. Washington, and J. N. Ivan, "Further notes on the application of zero-inflated models in highway safety," *Accident Analysis & Prevention*, vol. 39, no. 1, pp. 53–57, 2007.
- [16] Y. J. Kweon, "Development of crash prediction models with individual vehicular data," *Transportation Research Part C: Emerging Technologies*, vol. 19, no. 6, pp. 1353–1363, 2011.
- [17] Q. Cai, J. Lee, N. Eluru, and M. Abdel-Aty, "Macro-level pedestrian and bicycle crash analysis: incorporating spatial spillover effects in dual state count models," *Accident Analysis & Prevention*, vol. 93, pp. 14–22, 2016.
- [18] American Association of State Highway Transportation Officials (AASHTO), *Highway Safety Manual*, AASHTO, Washington, DC, USA, 2010.
- [19] J. Liu, A. J. Khattak, and B. Wali, "Do safety performance functions used for predicting crash frequency vary across space? Applying geographically weighted regressions to account for spatial heterogeneity," *Accident Analysis & Prevention*, vol. 109, pp. 132–142, 2017.
- [20] Z. Xie and J. Yan, "Kernel density estimation of traffic accidents in a network space," *Computers, Environment and Urban Systems*, vol. 32, no. 5, pp. 396–406, 2008.
- [21] T. Steenberghen, K. Aerts, and I. Thomas, "Spatial clustering of events on a network," *Journal of Transport Geography*, vol. 18, no. 3, pp. 411–418, 2010.
- [22] A. Hadayeghi, A. S. Shalaby, and B. N. Persaud, "Development of planning level transportation safety tools using geographically weighted poisson regression," *Accident Analysis & Prevention*, vol. 42, no. 2, pp. 676–688, 2010.
- [23] P. Xu and H. Huang, "Modeling crash spatial heterogeneity: random parameter versus geographically weighting," *Accident Analysis & Prevention*, vol. 75, pp. 16–25, 2015.
- [24] R. Amoh-Gyimah, M. Saberi, and M. Sarvi, "The effect of variations in spatial units on unobserved heterogeneity in macroscopic crash models," *Analytic Methods in Accident Research*, vol. 13, pp. 28–51, 2017.
- [25] K.-A. Rhee, J.-K. Kim, Y.-I. Lee, and G. F. Ulfarsson, "Spatial regression analysis of traffic crashes in Seoul," *Accident Analysis & Prevention*, vol. 91, pp. 190–199, 2016.
- [26] U. Olsson, *Generalized Linear Models: An Applied Approach*, Lightning Source, La Vergne, TN, USA, 2002.
- [27] S. P. Washington, M. G. Karlaftis, and F. Mannering, *Statistical and Econometric Methods for Transportation Data Analysis*, CRC Press, Boca Raton, FL, USA, 2010.
- [28] L. Breiman, "Random forests," *Machine Learning*, vol. 45, no. 1, pp. 5–32, 2001.
- [29] A. Okabe, T. Satoh, and K. Sugihara, "A kernel density estimation method for networks, its computational method and a GIS-based tool," *International Journal of Geographical Information Science*, vol. 23, no. 1, pp. 7–32, 2009.
- [30] A. Okabe and K. Sugihara, *Spatial Analysis along Networks: Statistical and Computational Methods*, John Wiley & Sons, Hoboken, NJ, USA, 2012.
- [31] K. Nie, Z. Wang, Q. Du, F. Ren, and Q. Tian, "A network-constrained integrated method for detecting spatial cluster and risk location of traffic crash: a case study from Wuhan, China," *Sustainability*, vol. 7, no. 3, pp. 2662–2677, 2015.
- [32] M. J. T. L. Gomes, F. Cunto, and A. R. Da Silva, "Geographically weighted negative binomial regression applied to zonal level safety performance models," *Accident Analysis & Prevention*, vol. 106, pp. 254–261, 2017.
- [33] D. Chimba, A. Musinguzi, and E. Kidando, "Associating pedestrian crashes with demographic and socioeconomic

- factors,” *Case Studies on Transport Policy*, vol. 6, no. 1, pp. 11–16, 2018.
- [34] A. S. Fotheringham, C. Brunsdon, and M. Charlton, *Geographically Weighted Regression: The Analysis of Spatially Varying Relationships*, John Wiley & Sons, Hoboken, NJ, USA, 2003.
- [35] J. Tu and Z. Xia, “Examining spatially varying relationships between land use and water quality using geographically weighted regression I: model design and evaluation,” *Science of the Total Environment*, vol. 407, no. 1, pp. 358–378, 2008.
- [36] Q. Wang, J. Ni, and J. Tenhunen, “Application of a geographically-weighted regression analysis to estimate net primary production of Chinese forest ecosystems,” *Global Ecology and Biogeography*, vol. 14, no. 4, pp. 379–393, 2005.
- [37] A. Ramin, M. Kamrani, A. Khattak, and J. Rios-Torres, *Safety Impacts of Automated Vehicles in Mixed Traffic*, Oak Ridge National Lab.(ORNL), Oak Ridge, TN (United States), 2018.
- [38] H. Bozdogan, “Model selection and Akaike’s information criterion (AIC): the general theory and its analytical extensions,” *Psychometrika*, vol. 52, no. 3, pp. 345–370, 1987.
- [39] T. Nakaya, A. S. Fotheringham, C. Brunsdon, and M. Charlton, “Geographically weighted Poisson regression for disease association mapping,” *Statistics in Medicine*, vol. 24, no. 17, pp. 2695–2717, 2005.
- [40] D. Lord and F. Mannering, “The statistical analysis of crash-frequency data: a review and assessment of methodological alternatives,” *Transportation Research Part A: Policy and Practice*, vol. 44, no. 5, pp. 291–305, 2010.
- [41] W. E. Marshall and N. N. Ferenchak, “Assessing equity and urban/rural road safety disparities in the US,” *Journal of Urbanism: International Research on Placemaking and Urban Sustainability*, vol. 10, no. 4, pp. 422–441, 2017.
- [42] N. Dong, H. Huang, J. Lee, M. Gao, and M. Abdel-Aty, “Macroscopic hotspots identification: a Bayesian spatio-temporal interaction approach,” *Accident Analysis & Prevention*, vol. 92, pp. 256–264, 2016.
- [43] A. F. Williams and O. Carsten, “Driver age and crash involvement,” *American Journal of Public Health*, vol. 79, no. 3, pp. 326–327, 1989.
- [44] D. L. Massie, K. L. Campbell, and A. F. Williams, “Traffic accident involvement rates by driver age and gender,” *Accident Analysis & Prevention*, vol. 27, no. 1, pp. 73–87, 1995.
- [45] KRTPO, *2008 East Tennessee Household Travel Survey Final Report*, Knoxville Regional Transportation Planning Organization, Austin, TX, USA, 2008.
- [46] A. J. Khattak and D. Rodriguez, “Travel behavior in neo-traditional neighborhood developments: a case study in USA,” *Transportation Research Part A: Policy and Practice*, vol. 39, no. 6, pp. 481–500, 2005.
- [47] J. Davey, D. Wishart, J. Freeman, and B. Watson, “An application of the driver behaviour questionnaire in an Australian organisational fleet setting,” *Transportation Research Part F: Traffic Psychology and Behaviour*, vol. 10, no. 1, pp. 11–21, 2007.
- [48] T. Nordfjærn, A. M. Hezaveh, and A. R. Mamdoohi, “An analysis of reported driver behaviour in samples of domestic and expatriate Iranians,” *Journal of Risk Research*, vol. 18, no. 5, pp. 566–580, 2015.

Research Article

Can I Trust You? Estimation Models for e-Bikers Stop-Go Decision before Amber Light at Urban Intersection

Jing Cai ¹, Jianyou Zhao ², Yusheng Xiang ³, Jing Liu ^{2,4}, Gang Chen ¹, Yueqi Hu ², and Jianhua Chen ⁵

¹School of Transportation Engineering, Chang'an University, Xi'an 710064, China

²School of Automobile, Chang'an University, Xi'an 710064, China

³Institute of Vehicle System Technology, Karlsruhe Institute of Technology, Karlsruhe 76131, Germany

⁴School of Mechanical and Electrical Engineering, Anhui Jianzhu University, Hefei 230601, China

⁵Transportation Information Center, China Academy of Transportation Sciences, Beijing 100029, China

Correspondence should be addressed to Jianyou Zhao; jyzhao@chd.edu.cn

Received 26 October 2020; Revised 16 November 2020; Accepted 13 December 2020; Published 24 December 2020

Academic Editor: Feng Chen

Copyright © 2020 Jing Cai et al. This is an open access article distributed under the Creative Commons Attribution License, which permits unrestricted use, distribution, and reproduction in any medium, provided the original work is properly cited.

Electric bike (e-bike) riders' inappropriate go-decision, yellow-light running (YLR), could lead to accidents at intersection during the signal change interval. Given the high YLR rate and casualties in accidents, this paper aims to investigate the factors influencing the e-bikers' go-decision of running against the amber signal. Based on 297 cases who made stop-go decisions in the signal change interval, two analytical models, namely, a base logit model and a random parameter logit model, were established to estimate the effects of contributing factors associated with e-bikers' YLR behaviours. Besides the well-known factors, we recommend adding approaching speed, critical crossing distance, and the number of acceleration rate changes as predictor factors for e-bikers' YLR behaviours. The results illustrate that the e-bikers' operational characteristics (i.e., approaching speed, critical crossing distance, and the number of acceleration rate change) and individuals' characteristics (i.e., gender and age) are significant predictors for their YLR behaviours. Moreover, taking effects of unobserved heterogeneities associated with e-bikers into consideration, the proposed random parameter logit model outperforms the base logit model to predict e-bikers' YLR behaviours. Providing remarkable perspectives on understanding e-bikers' YLR behaviours, the predicting probability of e-bikers' YLR violation could improve traffic safety under mixed traffic and fully autonomous driving condition in the future.

1. Introduction

In recent years, the transportation system has been undergoing huge change. Not only is the nonmotor vehicle characterized as one of the popular transportation modes in some Asian countries (i.e., China, Malaysia, and Thailand) [1], but also it is the widely used mode of transportation in developed countries (i.e., Australia, Sweden, and Germany) [1–3]. Cycling possesses plenty of advantages compared to other transportation modes, which is in terms of its flexibility, easy manoeuvrability, easy parking, lower cost, and convenience in congestion traffic [1]. In China, the transportation system has been undergoing huge change in recent years. Electric bicycle (e-bike) has increased dramatically

and constituted about 34% of all transportation modes in China, and the number of e-bikes has been in excess of 250 million in 2018 [4]. Without a doubt, with the growing popularity of e-bike, many countries have experienced a tremendous growth in traffic crashes involving e-bike. Because e-bike is defined as nonmotor vehicle by most countries in the world, e-bikers are not required to have driving license which may cause them to overestimate their cycling technique. Due to the unskilled cycling performance and being not protected by any metal structures, the casualties of e-bikers were about 32579 in traffic accident from 2016 to 2017 [4, 5]. Moreover, e-bike crashes were composed of 70% Chinese nonmotor traffic accidents in 2015 [4]. Intersection is one of the most dangerous parts in road

network. Particularly, intersection is one of the most dangerous parts in road network since statistics show that the vast majority of accidents occurred at intersection [6]. Signal violation including red-light running (RLR) and YLR could be the main reasons behind more than 60% of fatal crashes involving nonmotor vehicles in intersection [7]. Based on motor vehicle-oriented perspectives in road networks design, the signal indications are not supposed to fit nonmotor vehicles. Because of the different performance between motors and nonmotors, the complicated decision-making process for e-bikers at the beginning of amber light at intersection may incur a rear-end collision for the inappropriate stop-decision (emergency braking) or a right-angle collision for the inappropriate go-decision (yellow-light running). It is clear that those frequent inappropriate decisions could have negative effects not just on e-bikers' safety but also on other road users, especially on self-driving vehicles. However, although a series of studies have shown the prediction models for the behaviours of e-bikers during the red light, the research about the YLR behaviours of e-bikers is still a research gap. Therefore, it is indispensable to devote efforts to find out the contributing factors associated with e-bikers' YLR violation at the beginning of amber light to improve traffic safety under mixed traffic and fully autonomous driving condition in the future.

Amber light plays a crucial role in the efficiency and safety of a signalized intersection. Stop-go decision is required to make by drivers when they face the beginning of amber light. Gaizis et al. proposed the drivers' stop-pass model defined as Gazis-Herman-Maradudin model (GHM) [8]. Following Gaizis's research, many researchers studied drivers' stop-go decision in the signal change interval. Several lines of studies suggested that the likelihood of YLR increases when the vehicle has a high speed at the beginning of amber light [9–15]. It is now well established from a variety of studies that critical crossing distance (CCD) significantly impacts on drivers' stop-go decision [9, 10, 12–14, 16]. These studies reported that a vehicle has shorter CCD, and drivers are more likely to run against the amber light signal. Amer et al. and Lu et al. showed that the changes of vehicle's acceleration rate also have significant impacts on drivers' YLR violation when drivers approach to the intersection during yellow phase [10, 11]. In addition, drivers' stop-go decision at the beginning of amber light is not a simple function of vehicles' operation characteristics, but also it depends on various driver demographics. Research studies developed by Rakha et al., Campisi et al., and Savolainen found that the propensity of YLR for female drivers is vastly lower than male individuals [17–19]. Compared to young- and middle-age groups, the old-age drivers are with propensity to stop at the beginning of amber light [17]; however, the effect of age on drivers' YLR behavior is not consistent. Savolainen found that young- and middle-age male drivers are the most likely to stop at the signal change interval among all participants in their experiment [19].

The existing researches explored two typical types of e-bikers' signal violation behavior, i.e., e-bike riders' RLR and YLR. First, many researchers focused on the effects of

contributing factors which may have influence on e-bikers' RLR violation. Many studies examined the demographic factors associated with e-bikers' RLR behavior. There is a consensus that male riders have higher risk propensity to cross against the red indications than female e-bikers [20, 21]. The age of e-bikers has been extrapolated to be a significant variable for estimating their RLR behaviors. Young-age riders are more inclined to running the red-light, and the old e-bikers have lower likelihood of RLR than the young- and middle-age ones. In terms of psychological factors, Yang et al. and Tang et al. revealed that attitude and perceived behavioral control are significant predictors for the intention of RLR behavior [22, 23]. A number of research studies have identified a link between e-bikers' RLR behaviors and environment factors. Previous studies on the number of riders waiting behind the stop mark have identified that the more riders wait behind the stop mark for next green light, the less riders cross against the red light [24, 25]. Mei et al. and Yan et al. have shown that the RLR rate for e-bike is higher in off-peak hours in which the volume of motor vehicles is lower than that in peak hours [25, 26]. Many studies have explored the relationship between the infrastructure of intersection and the e-bike riders' RLR behaviours. There is evidence that nonmotorized lanes separated from vehicle lanes [3, 20], the PCSD infrastructure [27], and sunshields [28] are effective in preventing e-bike riders' RLR behaviours.

In addition, with respect to e-bikers' YLR behaviours, Tang et al. reported that the potential time (PT) is the dominant factor to explain the stop-go decision for e-bikers. PT is the time to stop mark when e-bikers make a go-decision without changing their initial approaching speed [29]. Various researchers analyzed the environment factors contributing to e-bikers' decision of YLR. Dong et al. focused on the effects of flash green signal on the YLR violation and they found that flashing green signals not just almost eliminate the DZ but also enlarge the OZ for e-bikers [30]. Tang et al. concluded that the green-light time and intersection's form are the most significant factors to e-bikers' GR near-violation which is also called YLR violation [31].

In terms of e-bikers' signal violation in modeling identification, many analytical methods have been established to solve this problem. Logistics regression is widely utilized to analyze the RLR behavior for e-bikers [20, 28, 32, 33]. Yang et al. and Mei et al. developed survival analysis model to investigate e-bikers' risky crossing behaviours [21, 25]. The theory of planned behavior (TPB) model was used to predict for e-bikers' intention of RLR in these studies conducted by Yang et al. and Tang et al. [22, 23]. A Hidden Markov Driving model proposed by Dong et al. and Li et al. [30, 34, 35] was used to explain the YLR behaviour of motor drivers and e-bikers. An integrated regression analysis developed by Tang et al. was used to explain the probability of e-bikers' YLR behaviours [31]. Numerous researchers have tried to use many methods identifying the factors influencing e-biker's signal violation. However, the violation behaviour might occur under distinct conditions and influencing by other unobserved influential factors of individuals, which may lead to omitting the

unobserved heterogeneity and making the wrong analysis for the results [24, 36]. To provide some insights into this problem, some researchers established random parameter logit model (RPLM) which is also called mixed logit model [19, 24, 37] to eliminate the effects of unobserved heterogeneity. Wang et al. identified variables contributing to RLR behavior of pedestrians and e-bikers using the RPLM [24]. Zheng et al. established a random coefficient logistics model to identify factors associated with the violation of pedestrian and cyclists on the Brooklyn Bridge promenade [36]. And the RPLM was used to investigate the effect of factors in other traffic safety researches [38, 39]; for instance, the studies analyzed the injury severity for drivers [40–42].

The aim of our paper is to analyze the factors contributing to e-bikers' YLR violation. Based on the natural observation data, two analytical logit models (i.e., a base logit model and a random parameter logit model) were established to explain the effects of contributing factors. There are three advantages of this study. First, we analyzed the impact factors, where the e-bikers' personal characteristics and their operating characteristics are included, on e-bikers' YLR violation using massive amount of crossing trajectories in the case of signal change interval, by extracting the real-time data from high-resolution event-based recorded data. Secondly, we first classified e-bikers' YLR behaviours in terms of how many times e-bikers changed his/her stop-go decision in 6 s before the end of green light into normal yellow-light running (NYLR) and aggressive yellow-light running (AYLR) and also classified e-bikers' YLS behaviours into normal yellow-light stopping (NYLS), aggressive yellow-light stopping (AYLS), and conservative yellow-light stopping (CYLS), which has clearly shown the decision-making process for e-bikers in the signal change interval. Thirdly, the use of random parameter logit model (RPLM) in this study has advantages in that it can account for the unobserved heterogeneity which is likely to present the e-bikers' individuals' differences.

The structure of rest paper is as follows. The data collection process is presented in Section 2, in which a method is also developed to categorize YLR and yellow-light stopping (YLS) e-bikers into different types according to the changes of acceleration rate during 6-second green light before the beginning of amber light. Section 3 briefly introduces the two logit models. In Section 4, the statistics analysis of observation, the analysis of different types for YLR and YLS behaviours, and the results of the two models are presented. Section 5 gives a discussion of the model estimating results. Finally, concluding remarks and the perspectives for further research are given.

2. Data Collection and Process

2.1. Site Selection and Description. It has been proved that direct observation can provide quite useful information to study road users' behavior by previous researches [11, 29, 30, 36]. In this study, a natural observation was conducted in Xi'an, China, which has 10 million residents, and the ownership of e-bike has been over 3 million [4]. A typical four-leg intersection located in Huancheng South

Road, which is the major corridor connecting east and west of Beilin district, and Wenyi North Road (H-W intersection) was selected for natural observation. H-W intersection is with the following characteristics. (a) An exclusive non-motorized lane exists in upstream of the intersection, which could separate the nonmotors including e-bikes and regular bikes from motors in order to reduce the interactive impact. (b) The landscape trees do not exist on the side of non-motorized lane, which may help clearly observe e-bikers' crossing behaviour in signal change interval. (c) A countdown signal device (CSD) is installed in H-W intersection, all motor drivers and cyclists who are approaching the intersection in the same direction should obey the CSD timer. A traffic signal phase in which a 6 s countdown green signal is displayed at the end of green-light and a 3 s amber light signal following this countdown signal is used in this intersection (the traffic light phase at H-W intersection is shown in Figure 1). (d) H-W intersection has a moderate e-bike traffic volume that does not cause the traffic jam and the e-bikers could smoothly clear the intersection without queueing.

2.2. Data Collecting. The main equipment used in this natural observation were an unmanned aerial vehicle (DJI Inspire 1) and a video camera (Sony FDR-AX45) to obtain high-resolution videos of e-bikers' stop-go decision-making process in signal change interval. In this natural observation, a 2-hour video was collected during weekday's morning and evening peak hours under good weather conditions for 2 weeks in October 2019; i.e., totally we recorded 20-hour tapes. To avoid buses and vehicles' crossing behaviours hindering e-bikes' crossing trajectory in the videotape, the UAV hovered for an altitude of 50 m over the nonmotorized lane located in upstream intersection and adjusted the lens angle of the camera to clearly record the riders' entire crossing process and the traffic signal indications (the first step shown in Figure 2). And the other synchronized camera was mounted on the telegraph poles that were located in the roadside of the intersection, to avoid being spotted by e-bikes and consequently causing their crossing behaviours changes. The lens angle of this camera was pointed towards the riders to obtain their detailed personals (the first step shown in Figure 2). These two cameras' time parameter was set identically and a synchronous remote control was used, which made them synchronize temporally and spatially to record e-bikers' crossing behaviours.

2.3. Data Processing. A data processing framework of this study is briefly presented in Figure 2. All the e-bike riders who entered the scope of the cameras and crossed the intersection were recorded; however, only the e-bikers who crossed straight through the intersection in the signal change interval were coded. Right-turn and left-turn e-bikers were excluded since their crossing trajectories may be hindered by turning motor vehicles.

Using two synchronized cameras with different perspectives, we obtained two temporally and spatially synchronous tapes. After that, we manually matched,

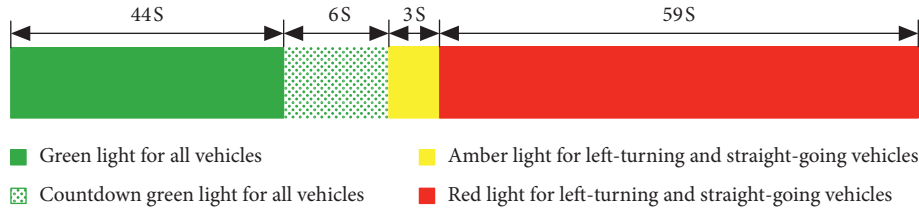


FIGURE 1: Traffic light phase at H-W intersection.

numbered, and then recorded the target e-bikers according to the identical schedule and the e-bikes' appearance in two videos (the third step shown in Figure 2). Utilizing a trajectory analysis software Tracker, we extracted the target e-bike position and trajectories in the period of 9 seconds before the light turns red, including 3 seconds of amber light and the last 6 seconds of green light. As the input for the trajectory software, we measured the road traffic marking in the middle of the intersection as a reference to evaluate the objects' sizes in the videos, so that the software can automatically extract the X and Y data of e-bikes position in real time. Obviously, the calculations for meaningful information of e-bikes were described in equations (1)–(3). Equation (1) calculates the displacement of the e-bike. The following equation calculates the displacement of e-bike in frame i denoted as S_i (m):

$$S_i = \sqrt{(x_i - x_{i-1})^2 + (y_i - y_{i-1})^2}, \quad (1)$$

where x_i is the displacement of e-bike on the X -axis in frame i , y_i is the displacement of e-bike on the Y -axis in frame i , and i is the number of the frame.

The following equation is used to calculate the instantaneous speed denoted as v_i (m/s):

$$v_i = \frac{S_i}{t}, \quad (2)$$

where t is the time length of frame i .

The following equation calculates the instantaneous accelerated speed denoted as a_i (m/s²):

$$a_i = \frac{v_i}{t} - \frac{v_{i-1}}{t} = \frac{S_i - S_{i-1}}{t^2}. \quad (3)$$

Meanwhile, the data related to e-biker's personalities, including gender, estimated age group, and e-bike type, were labelled according to the appearance of e-bikes and riders from the videotape by two students, who were trained to be familiar with common e-bike models and learned the standards for classifying the e-bikers' age group. In order to avoid data recording mistake, recoding reliability was calculated by Cohen's kappa for categorical variables and intraclass correlation for continuous variables. All the coefficients ranged from 0.81 to 0.98, which ensured the reliability of extracting process.

The possible contributing factors (independent variables) were including gender (GEN), established age group (AGE), vehicle type (VT), the number of acceleration rate changes (NA), approaching speed (AS), and critical crossing distance (CCD). The details of independent variables are

presented in Table 1. Three-category variables, namely, AGE and NA, were changed to two dummy variables for calculating BLM and RPLM, respectively. The old-age group and the e-bikers with acceleration rate change once time group were considered as the base variables; other age groups and times of acceleration rate change groups have been incorporated in the models as dummy variables. The variable AGE was converted into two dummy variables. The first dummy variable was young vs. old with 0 denoting the young and 1 denoting the old ones. The second dummy variable was middle-age vs. old with 0 denoting the middle-age riders and 1 denoting the old individuals. And the variable acceleration rate change once time was denoted 1, while without acceleration rate change and the acceleration rate change more than 2 times were denoted 0 in the two dummy variables, respectively.

2.4. Classification of Stop-Go Decision-Making Process. Based on the Chinese Road Traffic Safety Law [43], we define the yellow-light running behaviour as that instead of stopping behind the stop mark at the beginning of amber light; the e-bikers continue going through the stop mark. After collecting the e-bikers' crossing trajectory data, YLR riders can be easily identified. The identifying reliability was calculated by Cohen's kappa coefficient and the value of coefficient is 0.94, ensuring the reliability of identifying process.

2.4.1. Yellow-Light Running Behaviour Categorization. As a consequence of the e-bikes' manual operation power system, the acceleration rate is positive when e-bikers continue going forward. On the contrary, the acceleration rate is negative when e-bikers decide to stop. It was proved by previous study that the operating characteristics may reflect the physiological characteristics of drivers during the actual driving process [44]. The e-bikers' stop-go decision-making process could be precisely presented by the real-time acceleration rate. In this study, YLR behaviour is classified into normal yellow-light running (NYLR) and aggressive yellow-light running (AYLR), based on how many times e-bikers changed their stop-go decision in the last 6 seconds of green light. NYLR behaviour is defined if the riders make a decision to speed up through the stop mark after observing that the countdown green light began to flash but fail to pass it before the beginning of amber light. This category is shown in Figure 3(a), the speed increased due to the acceleration rate increase and maintained positive as the e-bikers made a go-decision to pass through the stop mark before the

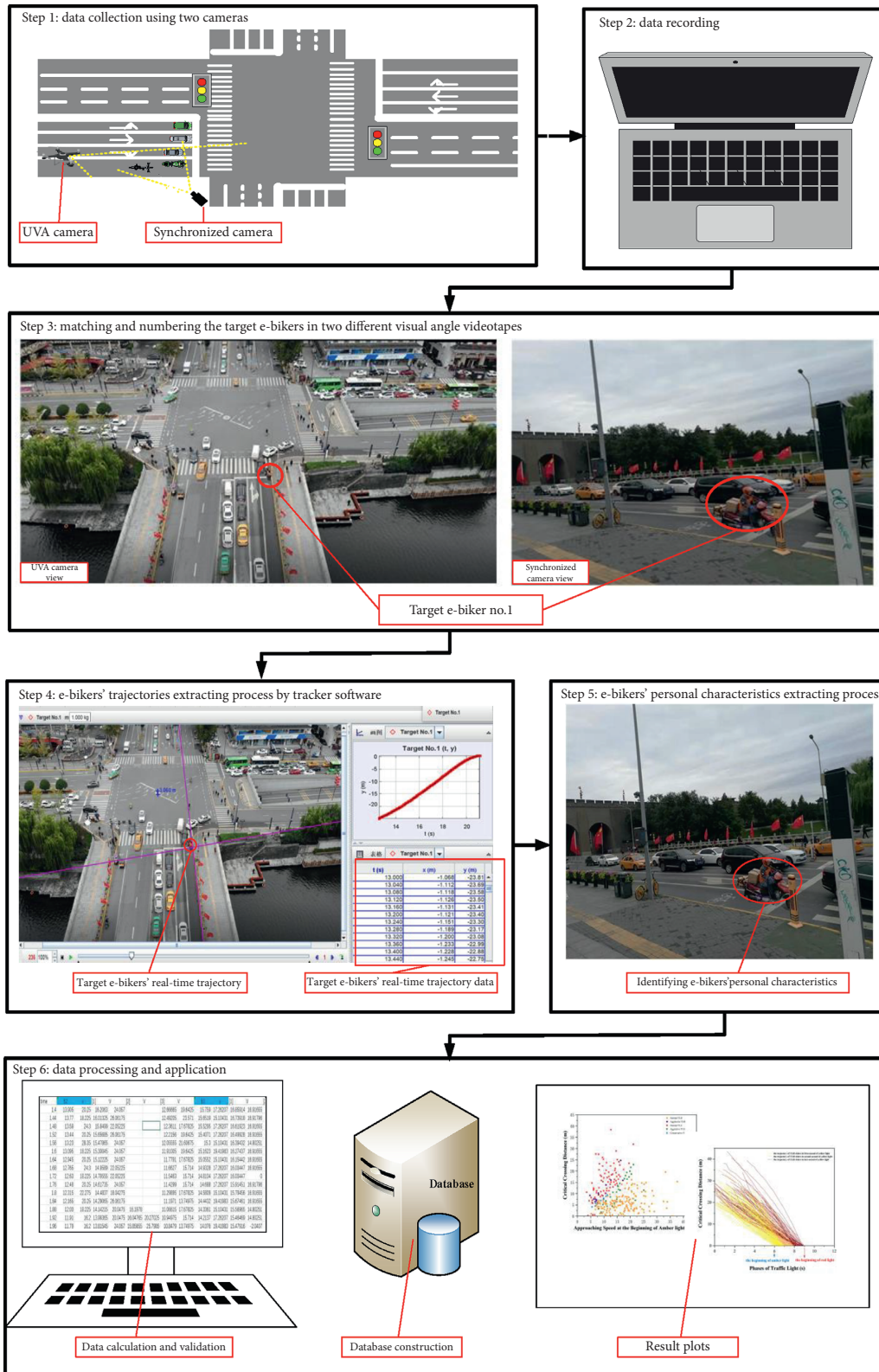


FIGURE 2: Data processing framework.

beginning of amber light. AYLRL referred to the riders who firstly decided to decelerate but made a second decision to accelerate to cross through the stop mark; however, they

failed to pass it before the beginning of amber light. Figure 3(b) presented the speed and acceleration/deceleration rate of typical types for AYLRL violation. It can be seen

TABLE 1: Definition of variables coded.

Variable	Description	Coding value
GEN	Male	0
	Female	1
AGE	Young-age group (<30)	0
	Middle-age group (30–50)	1
	Old-age group (>50)	2
VT	Bicycle electric bike	0
	Scooter electric bike	1
NA	0 changes	0
	More than 2 changes	1
	1 change	2
AS	The speed of e-bike when it approached intersection at the beginning of amber light.	The real-time value
CCD	The distance of e-bike away from stop mark at the beginning of amber light.	The real-time value

AGE: estimated age group. Using estimated age group could be effective to extract e-bikers' individual information. The groups were divided into young-age riders (<30), middle-age riders (30–50), and old-age riders (>50) reported by Wu et al. [7]. VT: vehicle type. Bicycle e-bike can ride the pedal to provide power for going forward, while the scooter e-bike's power is only provided by electromotor. NA: number of acceleration rate changes. The number of times that acceleration rate changes from positive to negative, or from negative to positive.

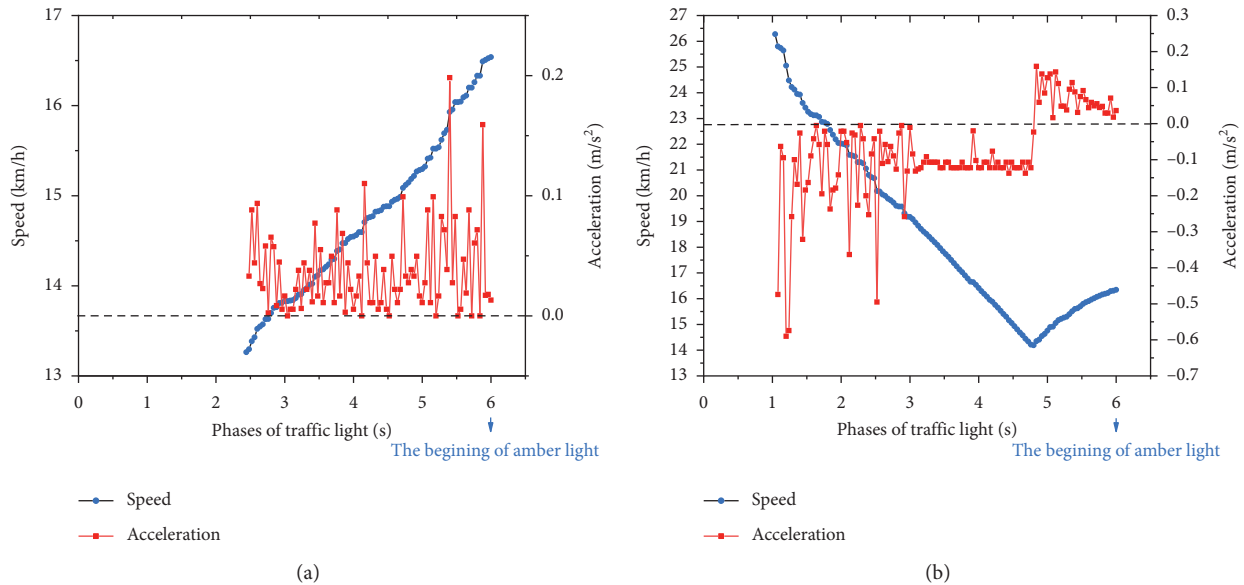


FIGURE 3: Typical approaching speed and acceleration rate profile of NYLR and AYLR e-bikers.

that the speed dropped off due to the acceleration rate decrease below zero when e-bikers made a stop-decision at the beginning of countdown green light, and then the speed distinctly increased with the increase of acceleration before the beginning of amber light. We conjecture that they may change their initial idea and decide to pass through the intersection based on their newly gathered circumstance information, such as critical crossing distance and the volume of nonmotors and motors.

2.4.2. Yellow-Light Stopping Behaviour Categorization.

Yellow-light stopping (YLS) behaviour is defined as that riders stopped in appropriate position, i.e., behind the stop mark, before the end of amber light signal. The decision-making process distinguished three different types of YLS

behavior, i.e., normal yellow-light stopping (NYLS), aggressive yellow-light stopping (AYLS), and conservative yellow-light stopping (CYLS). NYLS is the behaviour that e-bikers initially decided to stop slowly and could stop behind the stop mark before the onset of red light. Figure 4(a) shows the speed and deceleration rate of typical types for NYLS behaviour. It is clear that with the acceleration rate decreasing below zero, the speed of e-bike gone down almost to zero before the beginning of red light. Defined as AYLS, the behaviour is considered as that riders who decided to pass through stop mark at the onset of the countdown green light but later they changed their initial decisions from passing to stopping caused by the changing environment or other reasons. Figure 4(b) shows the opposite trend to Figure 3(b). The speed increased with the increase of acceleration rate at the beginning of countdown

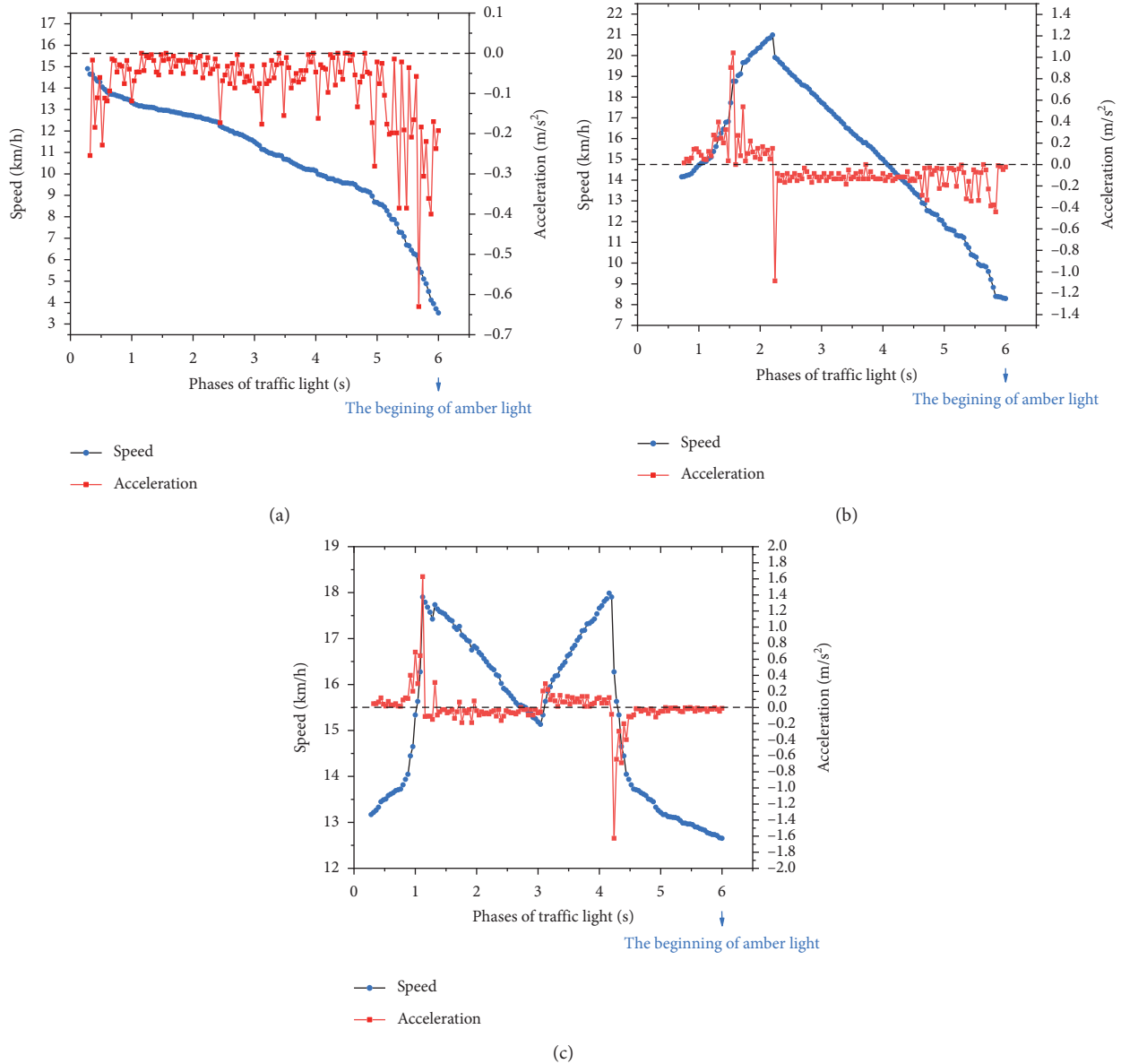


FIGURE 4: Typical approaching speed and acceleration rate profile of NYLS, AYLR, and CYLS e-bikers.

green light, and then it decreased for the acceleration rate decreasing below zero before the beginning of amber light. CYLS can be described as the behaviour that the e-bikers made multiple go-stop decisions from the onset of countdown green light to the end of it, but they finally stopped behind the stop mark. Figure 4(c) displays the speed and acceleration rate for typical types for CYLS behaviour. It can be seen that the speed of e-bike fluctuated over the change of acceleration rate, which happened because the e-bikers made multiple stop-go decisions during the countdown green-light time.

3. Methodology

Logistics regression has been widely applied to analyze the risk behaviour of road users in previous researches, especially to examine the factors contributing to RLR and YLR illegal behaviour [4, 20, 28, 32, 33, 45]. In this study, we

developed two logit models, namely, a base logit model and a random parameter logit model, to analyze the e-bikers' behaviour with respect to the stop-go decision when they were facing the signal change from green to yellow. In our two logit models, $Y = 1$ denoted YLR e-bikers and $Y = 0$ denoted YLS e-bikers. The outcome of rider i 's decision to go through the stop mark at the beginning of amber light represented as Y_i is shown in the following equation:

$$Y_i = \beta X_i + \varepsilon_i, \tag{4}$$

where β is a vector of estimable regression parameters; X_i is a vector of the observed variables which may affect the YLR behaviour; and ε_i is an error term.

The probability of the e-biker i 's infringement of the amber light was obtained from the base logit model in the following equation:

$$p_i = (y_i = 1 | x_0, x_1, \dots, x_n) = \frac{\text{EXP}(\beta \mathbf{X}_i)}{1 + \text{EXP}(\beta \mathbf{X}_i)} \quad (5)$$

In this base logit model, p_i is the probability that YLR events occurred, and β_i is the corresponding coefficient of x_i estimated by the method of maximum likelihood. However, the base logit model has drawbacks which cannot analyze the potential effects of unobserved heterogeneity in riders' individual characteristics and cannot allow unobserved environment factors of utility to be correlated. All these random effects may result in erroneous parameter estimation and prejudices in estimation of the model, and the heterogeneity (i.e., some riders are prone to stop at the amber light interval and have lower risk propensity) may damage the Independence from Irrelevant Alternatives (IIA) assumption [15, 19, 24, 37, 40, 46]. To obtain an accurate estimation of variables, we proposed a random parameter logit model to analyze e-bikers' YLR behavior. The rider YLR propensity function was proposed in the following equation:

$$T_i = \beta_i \mathbf{X}_i + \varepsilon_i, \quad (6)$$

where β_i is the special parameter vector for the final decision of rider i which may vary across observed individual riders.

As mentioned above, substituting equation (6) into equation (5), the random parameter logit model was established as follows:

$$p_i = (y_i = 1 | x_0, x_1, Lx_n) = \int \frac{\text{EXP}(\beta_i \mathbf{X}_i)}{1 + \text{EXP}(\beta_i \mathbf{X}_i)} f(\beta_i | \phi) d\beta_i, \quad (7)$$

where $f(\beta_i | \phi)$ is the probability density function of β_i , and ϕ refers to a vector of parameters for the function (mean and variance).

The probability of the rider i 's infringement of the amber light estimated by equation (7) cannot be calculated exactly because of involving a multidimensional integral which is not close to solution. Quasirandom numbers generated by Halton, also called Halton's draws, were proved to be an efficient alternative to pseudorandom numbers by Bhat and Train [37]. In this study, we used Halton's draws to draw the values of β_i from $f(\beta_i | \phi)$. 200 Halton draws, the number of Halton draws, were used to calculate the accurate parameter estimation which has been proved to be a sufficient number in prior studies [19, 24, 46]. In addition, all parameters were assumed to follow normal distribution as presented in Wang and Savolainen's studies [19, 27].

Furthermore, the goodness-of-fit statistics measure Akaike Information Criterion (AIC) was used for model comparison. The value of AIC was calculated in the following equation:

$$\text{AIC} = -2LL + 2p, \quad (8)$$

where LL is the log-likelihood at convergence for the estimated model and p is the number of parameters in the model.

4. Results

4.1. Description Statistics of e-Bikers' Yellow-Light Running and Yellow-Light Stopping Behaviour. A total of 297 first-to-stop and first-to-go e-bikers (186 e-bikers with YLR behavior and 111 e-bikers with YLS behaviors) approaching the intersection during the signal change interval were observed in 20 h high-resolution videos. The following e-bikers were excluded to eliminate the influence of the leading e-bikes in the queue on their crossing behaviours.

The trajectories of YLR e-bikers are shown in Figure 5. The majority of YLR behavior (accounting for more than 70% of all YLR e-bikers) occurred during the early stages (i.e., the first and second) of an amber light. All the 297 observed e-bikers, divided into different types of YLR and YLS according to their decision-making process, were summarized as follows.

As shown in Tables 2 and 3, the descriptive statistics for the number of e-bikers' infringement behaviour in different groups were tested by chi-square test. Firstly, male e-bikers were prone to have YLR violation than female e-bikers (128 vs. 58, $p < 0.01$). In addition, the riders who rode bicycle e-bikes were less likely to have YLR behaviour than the riders who rode scooter e-bikes (136 vs. 50, $p < 0.05$). However, there was no statistical difference in the number of YLR in different age groups ($p = 0.235$).

As shown in Table 2, the overall proportion of YLR e-bikers who made one decision to run against the amber light, also called normal yellow-light running riders, was 93%. The majority of YLR e-bikers did a go-decision and did not change their initial decisions when they were facing the appearance of countdown green-light indications; only 7% of e-bikers modified their initial stop-decisions to go-decisions. A chi-square test was used to analyze the number of different YLR types' behaviours in different groups of e-bikers' personal characteristics. The occurrence rate of female NYLR riders was slightly greater than that of male NYLR riders (94.8% vs. 92.2%, $p < 0.001$), while the rate of male AYLR riders was larger than that of female AYLR riders (7.8% vs. 5.2%, $p < 0.001$). These results suggested that a large percentage of female YLR e-bikers decided to cross through the stop mark and did not change their initial go-decision after observing the onset of countdown green-light indications and that male YLR riders were more likely to change their initial stop-decision to continue crossing through the stop mark to run against the amber light. Based on the statistically significant difference, scooter e-bikers were more likely to have AYLR behaviours (7.4% vs. 6%, $p < 0.05$). A higher proportion of NYLR e-bikers and a lower proportion of AYLR e-bikers were observed in the old-age group than the young- and middle-age riders (100% vs. 93.9% and 87.7%, 0% vs. 6.1% and 12.3%); however, the difference cannot be observed in the number of different YLR types for different age groups from the results of chi-square test ($p = 0.179$).

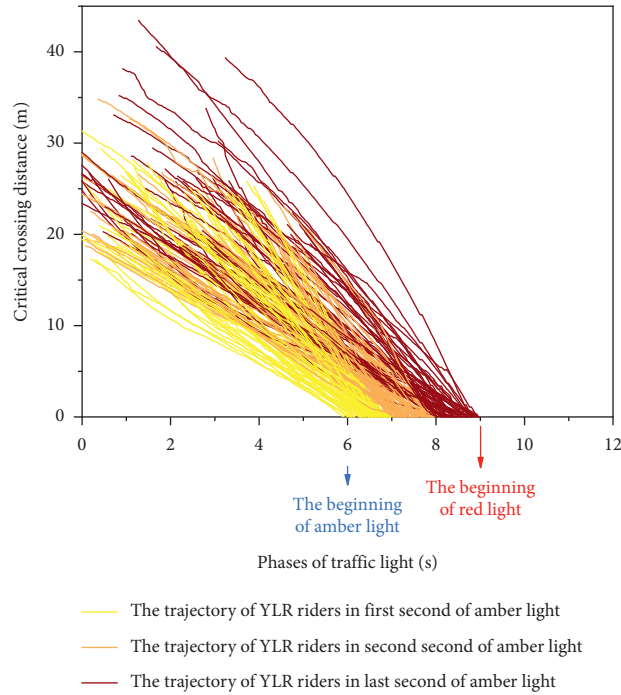


FIGURE 5: YLR e-biker's trajectories at the intersection.

TABLE 2: Statistics of yellow-light running behaviour by each subcategory.

Running behavior type	Number of YLR riders	
	Normal running	Aggressive running
<i>Gender</i>		
Male	92.2% (118/128)	7.8% (10/128)
Female	94.8% (55/58)	5.2% (3/58)
<i>Age group</i>		
Young	93.9% (92/98)	6.1% (6/98)
Middle-age	87.7% (50/57)	12.3% (7/57)
Old	100% (31/31)	0% (0/31)
<i>Vehicle type</i>		
Bicycle-style electric-bike	94.0% (47/50)	6.0% (3/50)
Scooter-style electric-bike	92.6% (126/136)	7.4% (10/136)
Overall	93.0% (173/186)	7.0% (13/186)

TABLE 3: Statistics of yellow-light stopping behaviour by each subcategory.

Stopping behavior type	Number of YLS riders		
	Normal stopping	Aggressive stopping	Conservative stopping
<i>Gender</i>			
Male	54.5% (24/44)	43.2% (19/44)	2.3% (1/44)
Female	76.2% (51/67)	11.9% (8/67)	11.9% (8/67)
<i>Age group</i>			
Young	28.6% (6/21)	57.1% (12/21)	14.3% (3/21)
Middle-age	78.3% (54/69)	14.5% (10/69)	7.2% (5/69)
Old	71.4% (15/21)	23.8% (5/21)	4.8% (1/21)
<i>Vehicle type</i>			
Bicycle-style electric-bike	79.5% (54/68)	17.6% (12/68)	2.9% (2/68)
Scooter-style electric-bike	48.8% (21/43)	34.9% (15/43)	16.3% (7/43)
Overall	67.6% (75/111)	24.3% (27/111)	8.1% (9/111)

Table 3 presents the observation of NYLS riders, AYLS riders, and CYLS riders being 75, 27, and 9, respectively. A majority of observed YLS riders had NYLS behaviours (67.6%), which indicated that upon facing the countdown green-light indications, most of e-bikers decided to smoothly decelerate until stopped behind the stop mark. When they observed the onset of countdown green light, 33 riders changed their stop-go decisions at least once time. The Pearson chi-square test was applied to identify whether there were significant differences in the number of YLS types among different groups. There was statistically significant difference in the number of different YLS types in the gender group ($p < 0.01$), as well as in age group ($p < 0.05$). Most of female e-bikers were more likely to decide decelerating until stopped without changing their stop-decision (76.2%), while over 40% of male e-bikers did a two-step or a multiple-step stop-go decision after the onset of countdown green light. Further, YLS riders within middle-age and old groups were more likely to do NYLS behaviour than that of young group (78.3% and 71.4% vs. 28.6%). A large percentage of young riders (i.e., $57.1\% + 14.3\% = 71.4\%$) decided to stop after the onset of countdown green light but modified their decision more than once. However, the number of YLS types had no significant difference in different vehicle types group ($p > 0.1$).

4.2. Descriptive Statistics of e-Bikers' Approaching Speed and Critical Crossing Distance. Approaching speed is a crucial factor related to YLR behavior as mentioned above. The YLR and YLS e-bikers' AS at the beginning of amber light is presented in the cumulative frequency curve as shown in Figure 6. The average AS of YLR e-bikers was 16.5 km/h, which was less than 25 km/h that is the limit speed of e-bike based on the China Road Safety Law [4]. And the average AS of YLS e-bike riders was 11.83 km/h at the beginning of amber light. The result of independent sample Student's t -test indicated that the AS of YLR and YLS e-bikers had significant difference ($F = 3.387, p < 0.01; t = 5.848, p < 0.01$) and that the AS of YLR riders was significantly higher than that of YLS ones.

Further, the AS of different YLR types was analyzed by Levene's test prior to the Student t -test. The result showed that the AS of different types for YLR and YLS e-bikers was significantly different at the level of 0.01. As indicated in Figure 7(a), the NYLR riders had an average AS of 17.03 km/h with a standard deviation of 6.43 km/h which was higher than that of AYLR e-bikers ($M = 9.40$ km/h, $SD = 3.90$ km/h). The one-way ANOVA results showed that the AS of different types for YLS riders had significant difference ($F = 21.307, p < 0.001$). A post hoc test, using Least Significant Difference (LSD) method, revealed that the AS for AYLS was significantly higher than that of NYLS and CYLS riders ($p < 0.001$), but there was no significant difference of the AS between NYLS and CYLS riders ($p = 0.106$) (see Figure 7(b)).

e-bike riders' critical crossing distance at the beginning of amber light also has significant impact on riders' decision of YLR behaviour. Based on the data we extracted from the

videos, sample e-bikes of AS and CCD for different types of YLR and YLS at the beginning of amber light were indicated by the solid plots in Figure 8. It was found that the e-bikers could make different stop-go decisions, even a contrary decision with similar AS and CCD from this figure which showed the complexities of the riders' stop-go decision.

For the purpose of comparison, the independent sample Student t -test was used to analyze the CCD for YLR and YLS groups' e-bikers. The CCD were significantly different between YLR group and YLS group ($F = 46.658, p < 0.001; t = 12.2, p < 0.001$). The YLR e-bikers were closer to stop mark than YLS ones at the beginning of amber light (6.29 m vs. 14.24 m). By applying Student's t -test, we compared the values of CCD for different YLR types. The results of tests indicated that the CCD of different YLR types were significantly different at the level of 0.01. NYLS riders were closer to stop mark than AYLS riders (5.93 m vs. 11.06 m), as shown in Figure 9(a). A one-way ANOVA test was carried out and the significant difference can be observed from the result for the CCD in different YLS types ($p < 0.001$). Using LSD method, the result of post hoc test revealed that NYLS riders was the farthest from the stop mark than AYLS and CYLS riders ($p < 0.001$). And the CCD for the CYLS riders was significantly closer to stop mark than that of AYLS riders at the beginning of amber light ($p < 0.001$) (see Figure 9(b)).

4.3. Modeling Result. Both base logit model (BLM) and random parameter logit model (RPLM) were established to identify and evaluate the contributing factors on the e-bikers' YLR infringement. WinBUGS software developed by the University of Cambridge was used to estimate these models. Table 4 presents the final results from two developed models (i.e., BLM and RPLM). In RPLM, the standard deviations were included for those parameter estimates which were observed to vary across individual riders.

Also, AIC was used to compare the goodness of fit of these two models. It is noteworthy that the RPLM provided a statistically superior fit relative to the BLM as indicated by the AIC value of RPLM smaller than that of BLM (1071.4 vs. 1336.3), shown in Table 5.

5. Discussion

The objective of our study was to analyze the contributing factors to e-bikers' YLR behaviour at signalized intersection. Owing to the lack of risk perception and safety riding awareness, traffic signal violation, especially YLR behaviour, is common in e-bikers' crossing behaviour in China. In our study, the natural observation results showed that 63% of e-bikers had a YLR violation when they arrived at intersection facing signal change interval, which is slightly lower than the result proposed by Bharat [13] (the proportion of YLR violation was 68.6% in motorized two wheel). However, the proportion of YLR e-bikers is relatively higher than the result reported by Tang et al. [31] (the proportion of the GR near-violation, also called YLR violation, was 32%). The difference between these two studies may be caused by the

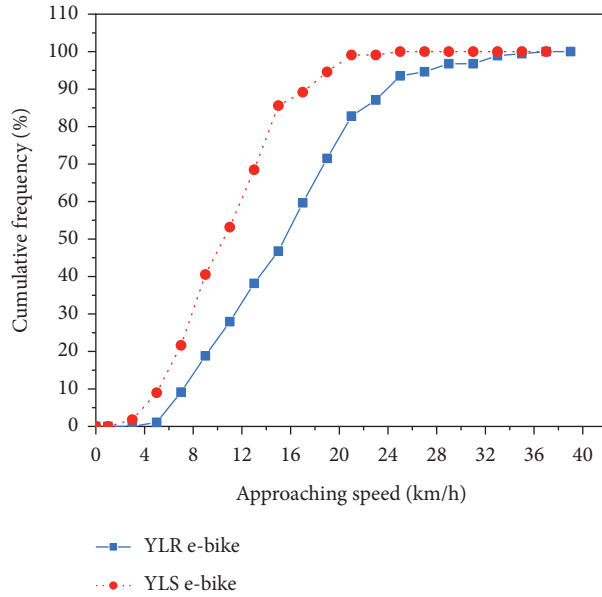


FIGURE 6: Cumulative frequency curve of approaching speed for YLR and YLS e-bike.

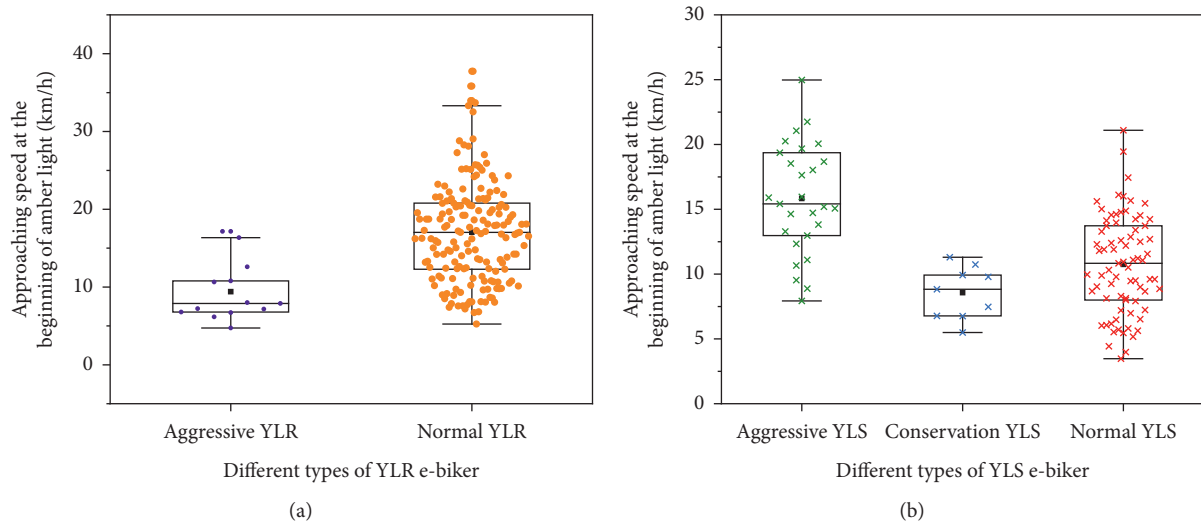


FIGURE 7: Box plots of approaching speed for different types of YLR and YLS e-bikers.

different data collection process, which is that we only collected the e-bike riders’ crossing behaviour who faced the signal change interval, while in Tang’s study the authors recorded all e-bike riders’ crossing behaviours during peak hours.

Two logistics regression models (i.e., BLM and RPLM) were applied to test the factors which affected e-bikers’ YLR behaviour. Given that the RPLM outperforms the BLM (the value of AIC in RPLM model is smaller than that of BLM), we selected RPLM for evaluating the contributing factors on e-bikers YLR behaviour. e-bikers’ gender, age group, and the operation attributes including AS, CCD, and NA were found to have significant effects on YLR behaviour. To analyze the effects of these contributing factors on the likelihood of infringement behaviour, the odds ratio (OR) was used. The

OR could be defined as the effect of a one-unit increase in a contributing factor to the odds of YLR violation with other factors being controlled for.

5.1. Analysis of Approaching Speed. As mentioned above, results from Student’s *t*-test and the one-way ANOVA model implied that riders’ AS was significantly different in different types of YLR and YLS behavior. The AS of NYLR was higher than that of AYLR, indicating that the NYLR e-bikers decided to pass through the stop mark without any decelerating. On the other hand, the lowest value of AS was observed in CYLS e-bikers who changed their stop-go decision more than 2 times. As shown from the result of RPLM in Table 4, AS was found to be significant associated with

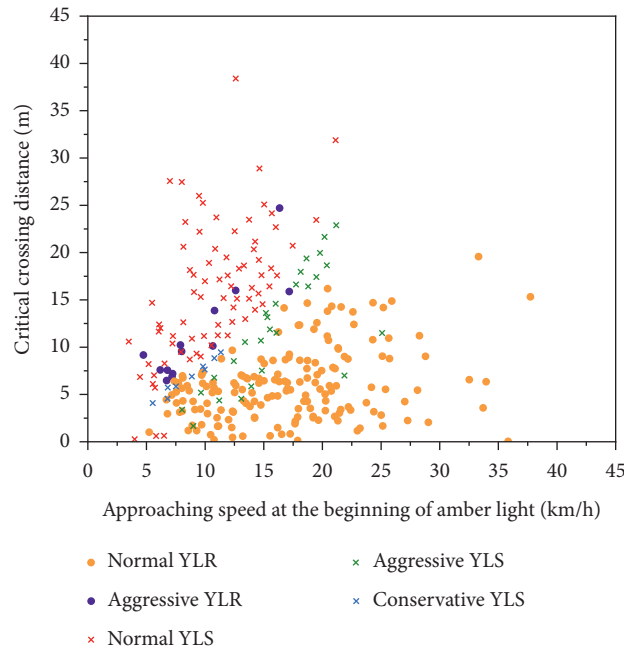


FIGURE 8: Stop-go decision types in the AS-CCD diagram.

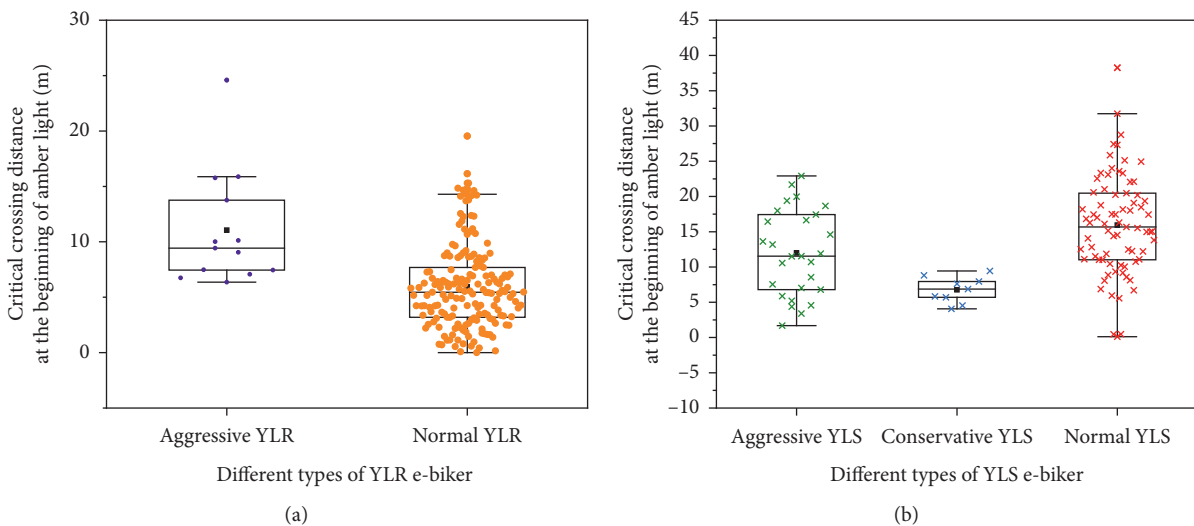


FIGURE 9: Box plots of critical crossing distance for different types of YLR and YLS e-bikers.

e-bikers' YLR behavior. The RPLM illustrated that the value of OR was 1.53 ($e^{0.427}$). This value was indicated that when the e-biker was riding 1 km/h (one unit) faster than others, he/she would have 1.53 times to do a YLR behaviour. This finding was consistent with previous studies that the larger the e-bike and motorcycles approaching speed had, the higher the probability of YLR was in the drivers' crossing behaviour [13, 30]. The result in e-bike vehicles was also in accord with previous researches on motor vehicle YLR violation [11–13]. The parameter for AS was a normal distribution with a mean of 0.427 and a standard deviation of 0.688. According to the cumulative probability function of the AS distribution, the figures suggested that 72.9% samples were greater than 0 and 27.1% samples were less than 0. This

demonstrated that the effect of AS on 72.9% of samples was positive which indicated that the probability of YLR behavior increased. On the other hand, the effect of AS on 27.1% of samples was negative which indicated that the probability of YLR behavior decreased. The approaching speed of e-bike was a significant predictor to predict the YLR violation, which may be caused by the fact that motorcyclists who regarded themselves as "speeder" were more likely to run against signal [47, 48].

5.2. Analysis of Critical Crossing Distance. YLR could be caused by that amber light time is not long enough for e-bike to cross through stop mark before the signal indication turns to

TABLE 4: Estimates of parameters in BLM and RPLM for e-bikers' YLR behaviour.

Variables	BLM		RPLM	
	Mean	SE	Mean	SE
Intercept	-1.337***	0.681	-1.041**	0.699
Gender				
Male vs. female	-0.672**	0.028	-0.661***	0.024
Std. dev. of parameter distribution			0.451***	0.033
Age				
Young vs. old	-1.174***	0.876	-0.874**	0.076
Std. dev. of parameter distribution			0.815***	0.030
Middle-age vs. old	0.342*	0.057	0.212**	0.038
Std. dev. of parameter distribution			0.638**	0.231
Vehicle type (VT)				
Bicycle-style e-bike vs. scooter-style e-bike	0.332	0.041	0.446	0.124
Std. dev. of parameter distribution			0.265	0.066
Number of acceleration rate changes (NA)				
Zero changes vs. one change	-1.267**	0.650	-1.312***	0.049
Std. dev. of parameter distribution			1.592	0.234
More than 2 changes vs. one change	-0.72	0.102	-0.634	0.048
Std. dev. of parameter distribution			0.961	0.085
Approaching speed (AS)	0.391***	0.098	0.427***	0.086
Std. dev. of parameter distribution			0.688***	0.026
Distance to the stop-line (DTS)	-0.256***	0.058	-0.312***	0.064
Std. dev. of parameter distribution			0.201***	0.049

*Statistically significant at $\alpha = 0.10$. **Statistically significant at $\alpha = 0.05$. ***Statistically significant at $\alpha = 0.01$.

TABLE 5: Goodness-of-fit measures for BLM and RPLM.

	BLM	RPLM
Number of observations	297	297
Log-likelihood at zero, LL(0)	-511.13	-501.59
Log-likelihood at convergence, LL (β)	-661.02	-486.71
Akaike Information Criterion (AIC)	1336.3	1071.4

red; therefore, critical crossing distance at the beginning of amber light is an important indicator for intersection safety. Based on the results we analyzed above, the average value of CCD for NYLR riders was the smallest than other observed e-bikers at the beginning of amber light, which means that NYLR riders were close to stop mark at the beginning of amber light. Thus, they would be confident with the enough time in which they can cross the stop mark safely without waiting next green light. But it is also true that the AYLR riders who had a longer CCD had YLR behaviour. This may explain the random effects of CCD on e-bikers' YLS behaviour as suggested by the estimated parameters with a mean of -0.312 and a standard deviation of 0.201. The results indicated that the effect of CCD on the YLR was negative and was in line with some previous studies in which the researchers concluded that drivers who drove close to the stop mark had higher likelihood to run against traffic signal in signal change interval [8, 13, 30].

5.3. Analysis of the Number of Acceleration Rate Changes.

Due to the low power output, the acceleration rate or deceleration rate, which also can be seen as the e-bike riders' stop-go decision, was the most critical factor affecting the speed of e-bike. With regard to the number of acceleration rate changes for e-bikers, consistent with the study proposed

by Tang [31], the e-bikers who could know the remaining time of amber light from the countdown timer are more likely to accelerate to clear the intersection. e-bikers who decided not to change their initial acceleration rate (keep accelerating to pass the stop line) were found to have YLR violation with the probability of 271% higher than the riders who change their initial decision once time. Similar findings that vehicles would change speed to cross the intersection were reported in many researches [24, 49, 50]. In natural observation, e-bike riders could assess the viability of passing through the stop mark based on the environment constraints and the acceleration rate of their e-bike. The number of YLR riders who decided not to change their initial accelerating behaviour was much more than that number of YLR riders who had changed their acceleration once time. However, the second dummy variable's effect on YLR behaviour was not statistically significant. The result could be caused by the fact that there were no riders who repetitively changed their stop-go decision, which also can be seen as acceleration rate changed more than 2 times, and had YLR behaviour in our natural observation.

5.4. Analysis of e-Bikers' Characteristics. The crucial explanatory variable gender has negative effect on e-bikers' YLR violation. Compared to male, female e-bikers were

found less likely to have YLR behaviour with a mean of -0.661 and a standard deviation of 0.451 . The figures of cumulative probability function implied that 7% of female e-bikers tended to run against the amber light indications despite the decreased probability of YLR behaviour for the majority of female. The result was consistent with the findings proposed by previous researches. For example, female drivers including e-bikers and motor drivers are found to be less likely to be involved in YLR behaviour [4, 9, 10, 17]. In addition, other studies have found that male e-bikers have more propensity to disobey traffic rules [20, 25, 31]. The female drivers are more prone to obey the traffic regulation [51] and have higher level of risk perception [52], which mean that female drivers were more cautious than the male drivers in risky driving situations. The higher violation of male driver may be caused by human or physiological factors. The research developed by Parker et al. suggested that facing the traffic light changes, males would react more angrily and aggressively in driving than female drivers. The male riders would not tolerate to wait the next green-light; therefore, they are prone to infringe the traffic regulation. And males are more likely to engage in risky behaviours (i.e., traffic light violation) [53].

e-bikers' age was found to be significantly related to riders' YLR behaviours. The estimated age group was a three-category variable; two dummy variables were set for BLM and RPLM as mentioned above. The effect of the first dummy variable was with a mean of -0.874 and a standard deviation of 0.815 , which meant that the old-age riders were 0.42 times less likely to run against the amber light than the young-age individuals. Given the distribution, 86% of the distribution was below 0, while 14% of distribution was above 0. This implied that most old e-bikers (86%) were less prone to have YLR behaviour, and a minority of old-aged (14%) had a higher probability to do YLR. This tied with the previous studies proposed by Bernhoft and Carstensen [54] and Chung and Zamani [55, 56] in which the authors found that young-age drivers have more propensity to engage in risky driving behaviours and involve in severe accidents. In contrast, old riders appeared to have an opposite tendency compared to middle-age riders. The old riders were more likely to be involved in YLR behaviour. The indicator variable for the second dummy variable leads to a random parameter with a mean of 0.212 and a standard deviation of 0.638 , suggesting that 62.9% of old e-bikers had an increased probability to have YLR behaviour while the remaining old individuals (37.1%) were less likely to run against the amber light indication. This result reflected the heterogeneity of old e-bikers. However, this finding was inconsistent with Wu [57] and Feng [58], which concluded that middle-age riders have higher probability to have aberrant driving behaviors than other drivers.

In terms of vehicle type, the rate of YLR for bicycle e-bike was 16.8% (50/297) and the rate for scooter e-bike was 45.8% (136/297). Despite the different rate of YLR for two different vehicle types of e-bike, the vehicle type's effect on e-bike YLR was not significant according to the result of RPLM. This may be caused by that although e-bikers ride different types of e-bike, they tend to have similar behaviours in same

cycling environment. This finding was similar with the conclusion that the bicycle riders and e-bike riders do not have significant impact on the immediate RLR behaviours [24].

6. Conclusions

To improve the intersection safety under mixed traffic condition, especially under fully autonomous driving condition in the near future, we have found out factors contributing to e-bikers' stop-go decision to cross through stop mark during the signal change interval. Using a UAV and a synchronized camera, high-resolution videos of e-bikers' stop-go decision-making process in the signal change interval were obtained. We identified 297 cases for e-bikers' crossing behaviour during amber light period. Two analytical models including a base logit model and a random parameter logit model were established based on the e-bike individuals' characteristic data, i.e., gender, age group, vehicle type, and the operations characteristic data, i.e., the approaching speed, the critical crossing distance, and the number of acceleration rate changes to investigate the relationship between explanatory variables and the e-bike YLR violation. Accordingly, several key conclusions can be made as follows:

- (1) In order to increase the accuracy of predicting e-bikers' YLR violation and to better understand the e-bikers' decision-making process, we believe the further classification of the e-bikers is essential. YLR riders should be categorized into NYLR and AYLR, whereas YLS individuals ought to be divided into NYLS, AYLS, and CYLS. Based on the statistical analysis, the conclusions indicate that the AS and CCD are significantly different for different types of YLR and YLS cases. Concretely, the AS for NYLR riders is higher than that of AYLR; nevertheless, the CCD of AYLR is larger than that of NYLR. AYLS e-bikers' AS is significantly faster than the other two types of YLS individuals, yet they are closer to the stop mark than NYLS e-bikers.
- (2) We recommend to adopt RPLM as the prediction model for e-bikers' YLR violation since the value of AIC showed the statistical superiority of the RPLM compared to the BLM. Also, taking unobserved heterogeneities effects into consideration could improve the prediction probability of e-bikers' YLR behaviours.
- (3) By taking additional factors, such as approaching speed, critical crossing distance, and especially the number of acceleration rate change into account, our proposed estimation model can more accurately predict probability of the traffic rules violation based on e-bike drivers' behaviours before the beginning of the amber light. For instance, e-bikers who have the higher AS, shorter CCD and do not change their initial acceleration rate would increase their probabilities to run against the amber light. In addition, female and middle-age e-bikers are less likely to have YLR behaviours.

Although this study provided insights into e-bike riders' YLR behaviour, there are some limitations should be done in further works. Firstly, the data was only collected in a four-leg intersection which may not reflect general environment of intersections. Secondly, the observation was conducted on individual e-biker. The objective e-bikers are not linked with other riders which may ignore the impact of platoons. Last but not least, the dataset we used is only including limited samples; thus, we encourage other researchers to test our approach on their larger dataset. Future works should take more observations and the effects of platoons into consideration to validate the findings of our study.

Data Availability

The data used to support the findings of this study have not been made available due to data privacy.

Conflicts of Interest

The authors declare that there are no conflicts of interest with respect to the research, authorship, and/or publication of this article.

Acknowledgments

This work was supported in part by the National Key Research and Development Program of China under Grants 2017YFC0803900 and 2018YFC0807500, in part by the National Natural Science Foundation of China under Grants U1664264 and 51878066, in part by the Central Universities and Colleges of Chang'an University under Grant 300102229201, and in part by Henan Provincial Science and Technology Foundation under Grant no. 2019G-2-11.

References

- [1] S. Das and A. K. Maurya, "Modelling of motorised two-wheelers: a review of the literature," *Transport Reviews*, vol. 38, pp. 1–23, 2018.
- [2] A. N. Stephens, J. Brown, L. De Rome, M. R. J. Baldock, R. Fernandes, and M. Fitzharris, "The relationship between motorcycle rider behaviour questionnaire scores and crashes for riders in Australia," *Accident Analysis & Prevention*, vol. 102, pp. 202–212, 2017.
- [3] K. Schleinitz, T. Petzoldt, S. Kröling, T. Gehlert, and S. Mach, "(E-) cyclists running the red light—the influence of bicycle type and infrastructure characteristics on red light violations," *Accident Analysis & Prevention*, vol. 122, pp. 99–107, 2018.
- [4] J. Cai, J. Zhao, J. Liu, K. Shen, X. Li, and Y. Ye, "Exploring factors affecting the yellow-light running behavior of electric bike riders at urban intersections in China," *Journal of Advanced Transportation*, vol. 2020, Article ID 8573232, 12 pages, 2020.
- [5] Z. Wang, R. Neitzel, X. Xue, W. Zheng, and G. Jiang, "Awareness, riding behaviors, and legislative attitudes toward electric bikes among two types of road users: an investigation in Tianjin, a municipality in China," *Traffic Injury Prevention*, vol. 20, pp. 72–78, 2019.
- [6] A. Jahangiri, H. Rakha, and T. A. Dingus, "Red-light running violation prediction using observational and simulator data," *Accident Analysis & Prevention*, vol. 96, pp. 316–328, 2016.
- [7] C. Wu, L. Yao, and K. Zhang, "The red-light running behavior of electric bike riders and cyclists at urban intersections in China: an observational study," *Accident Analysis & Prevention*, vol. 49, pp. 186–192, 2012.
- [8] D. Gazis, R. Herman, and A. Maradudin, "The problem of the amber signal light in traffic flow," *Operations Research*, vol. 8, no. 1, pp. 112–132, 1960.
- [9] P. Papaioannou, "Driver behaviour, dilemma zone and safety effects at urban signalised intersections in Greece," *Accident Analysis & Prevention*, vol. 39, no. 1, pp. 147–158, 2007.
- [10] A. Amer, H. Rakha, and I. El-Shawarby, "Agent-based behavioral modeling framework of driver behavior at the onset of yellow indication at signalized intersections," in *Proceedings of the 2011 14th International IEEE Conference on Intelligent Transportation Systems (ITSC)*, Washington, WA, USA, October 2011.
- [11] G. Lu, Y. Wang, X. Wu, and H. X. Liu, "Analysis of yellow-light running at signalized intersections using high-resolution traffic data," *Transportation Research Part A: Policy and Practice*, vol. 73, pp. 39–52, 2015.
- [12] H. Köll, M. Bader, and K. W. Axhausen, "Driver behaviour during flashing green before amber: a comparative study," *Accident Analysis & Prevention*, vol. 36, no. 2, pp. 273–280, 2004.
- [13] B. K. Pathivada and V. Perumal, "Analyzing dilemma driver behavior at signalized intersection under mixed traffic conditions," *Transportation Research Part F: Traffic Psychology and Behaviour*, vol. 60, pp. 111–120, 2019.
- [14] S. Biswas and I. Ghosh, "Modeling of the drivers' decision-making behavior during yellow phase," *KSCE Journal of Civil Engineering*, vol. 22, no. 11, pp. 4602–4614, 2018.
- [15] M. M. Haque, A. D. Ohlhauser, S. Washington, and L. N. Boyle, "Decisions and actions of distracted drivers at the onset of yellow lights," *Accident Analysis & Prevention*, vol. 96, pp. 290–299, 2016.
- [16] J. Li, X. Jia, and C. Shao, "Predicting driver behavior during the yellow interval using video surveillance," *International Journal of Environmental Research and Public Health*, vol. 13, no. 12, p. 1213, 2016.
- [17] H. Rakha, I. El-Shawarby, and J. R. Setti, "Characterizing driver behavior on signalized intersection approaches at the onset of a yellow-phase trigger," *IEEE Transactions on Intelligent Transportation Systems*, vol. 8, no. 4, pp. 630–640, 2007.
- [18] T. Campisi, G. Tesoriere, A. Canale et al., "Comparison of red-light running (RLR) and yellow-light running (YLR) traffic violations in the cities of Enna and thessaloniki," *Transportation Research Procedia*, vol. 45, pp. 947–954, 2020.
- [19] P. T. Savolainen, "Examining driver behavior at the onset of yellow in a traffic simulator environment: comparisons between random parameters and latent class logit models," *Accident Analysis & Prevention*, vol. 96, pp. 300–307, 2016.
- [20] L. Bai, P. Liu, Y. Guo, and H. Yu, "Comparative analysis of risky behaviors of electric bicycles at signalized intersections," *Journal of Crash Prevention & Injury Control*, vol. 16, pp. 424–428, 2014.
- [21] X. Yang, M. Huan, M. Abdel-Aty, Y. Peng, and Z. Gao, "A hazard-based duration model for analyzing crossing behavior of cyclists and electric bike riders at signalized intersections," *Accident Analysis & Prevention*, vol. 74, pp. 33–41, 2015.
- [22] H. Yang, X. Liu, F. Su, C. Cherry, Y. Liu, and Y. Li, "Predicting e-bike users' intention to run the red light: an application and extension of the theory of planned behavior," *Transportation*

- Research Part F: Traffic Psychology and Behaviour*, vol. 58, pp. 282–291, 2018.
- [23] T. Tang, H. Wang, X. Zhou, and H. Gong, “Understanding electric bikers’ red-light running behavior: predictive utility of theory of planned behavior vs prototype willingness model,” *Journal of Advanced Transportation*, vol. 2020, Article ID 7097302, 2020.
- [24] W. Wang, Z. Yuan, Y. Liu, X. Yang, and Y. Yang, “A random parameter logit model of immediate red-light running behavior of pedestrians and cyclists at major-major intersections,” *Journal of Advanced Transportation*, vol. 2019, Article ID 2345903, 2019.
- [25] H. Mei, X. Yang, and B. Jia, “Crossing reliability of electric bike riders at urban intersections,” *Mathematical Problems in Engineering*, vol. 2013, Article ID 108636, 2013.
- [26] F. Yan, B. Li, W. Zhang, and G. Hu, “Red-light running rates at five intersections by road user in Changsha, China: an observational study,” *Accident Analysis & Prevention*, vol. 95, pp. 381–386, 2016.
- [27] R. Yu, H. Zhao, C. Zhang, and Z. Wang, “Analysis of risk-taking behaviors of electric bicycle riders in response to pedestrian countdown signal devices,” *Traffic Injury Prevention*, vol. 20, no. 2, pp. 1–7, 2019.
- [28] Y. Zhang and C. Wu, “The effects of sunshields on red light running behavior of cyclists and electric bike riders,” *Accident Analysis & Prevention*, vol. 52, pp. 210–218, 2013.
- [29] K. Tang, S. Dong, F. Wang, Y. Ni, and J. Sun, “Behavior of riders of electric bicycles at onset of green and yellow at signalized intersections in China,” *Transportation Research Record: Journal of the Transportation Research Board*, vol. 2317, no. 1, pp. 85–96, 2012.
- [30] S. Dong, J. Zhou, and S. Zhang, “Determining E-bike drivers’ decision-making mechanisms during signal change interval using the hidden Markov driving model,” *Journal of Advanced Transportation*, vol. 2019, Article ID 7341097, 2019.
- [31] T. Tang, H. Wang, J. Ma, and X. Zhou, “Analysis of crossing behavior and violations of electric bikers at signalized intersections,” *Journal of Advanced Transportation*, vol. 2020, Article ID 3594963, 2020.
- [32] W. Du, J. Yang, B. Powis et al., “Understanding on-road practices of electric bike riders: an observational study in a developed city of China,” *Accident Analysis & Prevention*, vol. 59, pp. 319–326, 2013.
- [33] X. Yang, M. Abdel-Aty, M. Huan, B. Jia, and Y. Peng, “The effects of traffic wardens on the red-light infringement behavior of vulnerable road users,” *Transportation Research Part F: Traffic Psychology and Behaviour*, vol. 37, pp. 52–63, 2016.
- [34] J. Li, Q. He, H. Zhou, Y. Guan, and W. Dai, “Modeling driver behavior near intersections in hidden Markov model,” *International Journal of Environmental Research and Public Health*, vol. 13, p. 1265, 2016.
- [35] J. Li, B. Jiang, C. Dong, J. Wang, and X. Zhang, “Analysis of driver decisions at the onset of yellow at signalized intersections,” *Journal of Advanced Transportation*, vol. 2020, pp. 1–12, 2020.
- [36] L. Zheng, T. Sayed, and Y. Guo, “Investigating factors that influence pedestrian and cyclist violations on shared use path: an observational study on the Brooklyn bridge promenade,” *International Journal of Sustainable Transportation*, vol. 14, no. 7, pp. 503–512, 2020.
- [37] T. Zeng, *Essays on the Random Parameters Logit Model*, Louisiana State University, Baton Rouge, LA, USA, 2011.
- [38] F. Chen, S. Chen, and X. Ma, “Analysis of hourly crash likelihood using unbalanced panel data mixed logit model and real-time driving environmental big data,” *Journal of Safety Research*, vol. 65, pp. 153–159, 2018.
- [39] B. Dong, X. Ma, F. Chen, and S. Chen, “Investigating the differences of single-vehicle and multivehicle accident probability using mixed logit model,” *Journal of Advanced Transportation*, vol. 2018, pp. 11.11–11.19, 2018.
- [40] Y. Guo, Y. Wu, J. Lu, and J. Zhou, “Modeling the unobserved heterogeneity in E-bike collision severity using full bayesian random parameters multinomial logit regression,” *Sustainability*, vol. 11, no. 7, p. 2071, 2019.
- [41] F. Chang, P. Xu, H. Zhou, A. H. S. Chan, and H. Huang, “Investigating injury severities of motorcycle riders: a two-step method integrating latent class cluster analysis and random parameters logit model,” *Accident Analysis & Prevention*, vol. 131, pp. 316–326, 2019.
- [42] F. Chen and S. Ma, “Investigation on the injury severity of drivers in rear-end collisions between cars using a random parameters bivariate ordered probit model,” *International Journal of Environmental Research and Public Health*, vol. 16, no. 14, p. 2632, 2019.
- [43] Government, C.C. Road Traffic Safety Law of the People’s Republic of China. 2011.
- [44] Z. Feng, M. Yang, W. Zhang, Y. Du, and H. Bai, “Effect of longitudinal slope of urban underpass tunnels on drivers’ heart rate and speed: a study based on a real vehicle experiment,” *Tunnelling and Underground Space Technology*, vol. 81, pp. 525–533, 2018.
- [45] W. Zhang, K. Wang, L. Wang, Z. Feng, and Y. Du, “Exploring factors affecting pedestrians’ red-light running behaviors at intersections in China,” *Accident Analysis & Prevention*, vol. 96, pp. 71–78, 2016.
- [46] P. C. Anastasopoulos and F. L. Mannering, “An empirical assessment of fixed and random parameter logit models using crash- and non-crash-specific injury data,” *Accident Analysis & Prevention*, vol. 43, no. 3, pp. 1140–1147, 2011.
- [47] K. Chorlton, M. Conner, and S. Jamson, “Identifying the psychological determinants of risky riding: an application of an extended theory of planned behaviour,” *Accident Analysis & Prevention*, vol. 49, pp. 142–153, 2012.
- [48] M. A. Elliott, “Predicting motorcyclists’ intentions to speed: effects of selected cognitions from the theory of planned behaviour, self-identity and social identity,” *Accident Analysis & Prevention*, vol. 42, no. 2, pp. 718–725, 2010.
- [49] K. Shaaban, D. Muley, and A. Mohammed, “Analysis of illegal pedestrian crossing behavior on a major divided arterial road,” *Transportation Research Part F: Traffic Psychology and Behaviour*, vol. 54, pp. 124–137, 2018.
- [50] C. Havard and A. Willis, “Effects of installing a marked crosswalk on road crossing behaviour and perceptions of the environment,” *Transportation Research Part F: Traffic Psychology and Behaviour*, vol. 15, no. 3, pp. 249–260, 2012.
- [51] F. Fraboni, V. Marín Puchades, M. De Angelis, L. Pietrantonio, and G. Prati, “Red-light running behavior of cyclists in Italy: an observational study,” *Accident Analysis & Prevention*, vol. 120, pp. 219–232, 2018.
- [52] K. Wang, W. Zhang, J. Liu et al., “Exploring the factors affecting myopic drivers’ driving skills and risk perception in nighttime driving,” *Cognition, Technology & Work*, vol. 21, no. 2, pp. 275–285, 2019.
- [53] C. Wang, W. Zhang, Z. Feng, K. Wang, and Y. Gao, “Exploring factors influencing the risky cycling behaviors of young cyclists aged 15–24 Years: a questionnaire-based study in China,” *Risk Analysis*, vol. 40, no. 8, p. 1554, 2020.

- [54] I. M. Bernhoft and G. Carstensen, "Preferences and behaviour of pedestrians and cyclists by age and gender," *Transportation Research Part F: Traffic Psychology and Behaviour*, vol. 11, no. 2, pp. 83–95, 2008.
- [55] Y.-S. Chung and J.-T. Wong, "Beyond general behavioral theories: structural discrepancy in young motorcyclist's risky driving behavior and its policy implications," *Accident Analysis & Prevention*, vol. 49, pp. 165–176, 2012.
- [56] F. Zamani-Alavijeh, S. Niknami, M. Bazargan et al., "Risk-taking behaviors among motorcyclists in Middle East countries: a case of Islamic Republic of Iran," *Traffic Injury Prevention*, vol. 11, no. 1, pp. 25–34, 2010.
- [57] W. U. Ou and Q. M. Liu, "Electric bicycle related injury and risk factors in hangzhou," *Journal of Environmental & Occupational Medicine*, vol. 29, no. 9, 2012.
- [58] Z. Feng, J. Zhan, C. Wang, C. Ma, and Z. Huang, "The association between musculoskeletal disorders and driver behaviors among professional drivers in China," *International Journal of Occupational Safety and Ergonomics*, vol. 26, no. 3, pp. 551–561, 2020.

Research Article

Analysis of Freeway Secondary Crashes in Different Traffic Flow States by Three-Phase Traffic Theory

Bo Yang ¹, Yao Wu ^{1,2} and Weihua Zhang ³

¹Jiangsu Key Laboratory of Urban ITS, Southeast University,
Jiangsu Province Collaborative Innovation Center of Modern Urban Traffic Technologies, Si Pai Lou #2, Nanjing 210096, China

²Department of Civil Engineering, The University of British Columbia, 6250 Applied Science Lane, Vancouver,
BC V6T 1Z4, Canada

³School of Automobile and Traffic Engineering, Hefei University of Technology, Hefei 230009, China

Correspondence should be addressed to Yao Wu; wuyaomaster@126.com

Received 27 July 2020; Revised 19 August 2020; Accepted 1 September 2020; Published 27 September 2020

Academic Editor: Neng-Chao Lyu

Copyright © 2020 Bo Yang et al. This is an open access article distributed under the Creative Commons Attribution License, which permits unrestricted use, distribution, and reproduction in any medium, provided the original work is properly cited.

The objective of this study is to analyse the relationship between secondary crash risk and traffic flow states and explore the contributing factors of secondary crashes in different traffic flow states. Crash data and traffic data were collected on the I-880 freeway in California from 2006 to 2011. The traffic flow states are categorised by three-phase traffic theory. The Bayesian conditional logit model has been established to analyse the statistical relationship between the secondary crash probability and various traffic flow states. The results showed that free flow (F) state has the best safety performance of secondary crash and synchronized flow (S) state has the worst safety performance of secondary crashes. The traditional logistic regression model has been used to analyse the contributing factors of secondary crashes in different traffic flow states. The results indicated that the contributing factors in different traffic flow states are significantly different.

1. Introduction

Exploring the crash mechanism and contributing factors plays an important role in preventing crash and reducing crash severity to freeway traffic surveillance systems. The occurrence of a crash can generate the turbulence of traffic flow which may lead to further crashes. Secondary crash (SC) occurs within the spatial and temporal impact ranges of the turbulent traffic conditions caused by the primary crash (PC). Previous studies suggested that 2.2% to 3.9% of freeway crashes can result in SC [1–3].

With the widespread use of freeway real-time traffic surveillance systems, researchers have started using high-resolution dynamic traffic flow data to identify the traffic condition before SC occurrences. In general, SC can be affected by various contributing factors, including traffic flow characteristics, geometric design factors, weather conditions, PC characteristics, etc. [4–7]. In addition, many researchers have paid close attention to the identification

method of SC. The common methods include static threshold method (STM) [8–10] and dynamic methods (DM) [11–14].

Although many studies have studied the identification method and crash mechanism of SC, few studies focused on the difference of SC in various traffic conditions. In different traffic conditions, there is a significant difference of traffic flow characteristics that affect the spatial-temporal evolution [15–18] and safety performance [19,20]. The typical divided methods of traffic flow include three-phase traffic theory [15,16], four-phase traffic theory [17], six levels of services [18], etc. It has been proved that the safety performance of SC associated with various traffic conditions has a significant difference [3,21].

In this study, the traffic flow is divided by three-phase traffic theory. The main purpose is to analyse the difference of safety performance for SC in different traffic flow states and explore how contributing factors affect the probability of SC in different traffic flow states. The SC related data were

collected from the I-880 freeway in the United States from 2006 to 2011. The Bayesian conditional logit models have been established to analyse the statistical relationship between the SC probability and traffic flow states. The traditional logistic regression models were established to quantify the effects of various variables on the SC probability in different traffic flow states. This research can help traffic management personnel better understand which traffic flow state is more dangerous for the occurrence of SC and realize the contributing factors of SC in different traffic flow states. The results can be applied to develop effective countermeasures and reduce the SC probability in different traffic flow states.

2. Literature Review

In early studies, STM was usually applied to identify SC. The STM is defined by the fixed spatial and temporal influence areas of traffic flow caused by a prior crash. Numerous studies have utilized the STM to analyse SC, such as Raub [22], Karlaftis et al. [23], Moore et al. [8], Zhan et al. [9], Hirunyanitwattana and Mattingly [10], etc. However, there is an obvious limitation for STM. The determination of the scope in STM is too subjective to have objective and reasonable identification method [24]. In subsequent studies, to overcome the limitation of STM, many researchers adopt DM to identify SC [25–28]. DM has a dynamic boundary of influence area based on speed contour plot [14], shock wave [27], etc.

In recent studies, many researchers have analysed and predicted SC with statistical method or intelligent learning approaches. For example, Wang and Jiang proposed an identification method of SC by the speed contour plot and the spatiotemporal evolution of shockwaves [4]. The results indicated that the identification method based on an integer programming model can reduce the misidentification probability of SC. Kitali et al. used random forest to extract the important variables [5]. The results of Bayesian random effect complementary log-log model showed that some traffic flow variables, the PC types, and severities can significantly affect the probability of SC. In subsequent studies, Kitali et al. utilized the penalized logistic regression model to improve the predictive accuracy of the SC risk model [6]. The results of model indicated that the traffic flow variables and the PC characteristics can significantly affect the probability of SC. Specifically, the traffic flow variables include the occupancy, speed, variation of hourly flow, etc. The PC characteristics include the impact duration, types, occurrence time, etc. Yang et al. confirmed the PC boundary with the clustering method and metaheuristic optimization algorithm [7]. Then, a novel identification method is introduced to identify SC. The results showed that the accuracy of identifying SC can rise to 95% with the market penetration rate increasing from 5% to 25%. Subsequently, Yang et al. summarized and discussed the previous studies from three perspectives, including the identification method of SC, the predictive models of SC risk, and the prevention measures of SC [11]. Goodall predicted the probability of SC by empirical queuing and estimated volumes [12]. It was

found that SC occurred on average once every 10 crashes and 54 disabled vehicles. In the author's previous study, a two-step identification method of SC combined with the speed contour map and the shock wave was applied, and the random effect logit regression was utilized to analyse the contributing factors of SC [13]. The results indicated that the number of significant contributing factors increases with increasing of the threshold value. In addition, the collision type, road surface, speed, and traffic flow can significantly affect the probability of SC.

However, few researchers have analysed SC combined with the traffic flow states. Park et al. applied stochastic gradient boosting and rule extraction techniques to improve the accurate and comprehensible predictions of SC [21]. The results indicated that the unexpected traffic congestion caused by a crash has a significant effect on the occurrence of SC. Xu et al. used the zero-inflated ordered probit regression model to explore the relationship between the SC risk and traffic related variables, including traffic flow variables, geometric design factors, weather conditional factors, and PC characteristics [3]. The results showed that there is a significant difference of contributing factors between the SC-prone state and the SC-free state.

Although some researchers have considered the traffic flow states into the studies of SC, no researchers have studied the difference of SC mechanism in different traffic flow states divided by classical macroscopic traffic flow theory. The common methods of classical macroscopic traffic flow theory have been widely used in numerous areas of transportation engineering, including six levels of service [18], four-phase traffic theory [17], and three-phase traffic theory [15,16]. In these common theories, the three-phase traffic theory is one of the accepted approaches for modelling freeway traffic flow [15,16]. According to the three-phase traffic theory, freeway traffic flow can be classified into three phases, including free-flow phase (F), synchronized flow phase, and wide moving jams [15,16].

To make up for the shortcomings of previous studies without considering the classical macroscopic traffic flow theory in the analysis of SC, the three-phase traffic theory is applied in this study to explore the difference of SC mechanism in various traffic flow states.

3. Materials and Methods

3.1. Data Sources. Data were obtained from a 34-mile section on the I-880 freeway in the California, United States, between 2006 and 2011. There are 119 loop detector stations along the selected freeway section with an average spacing of 0.5 miles. A total of 3 weather stations are located along the selected freeway section. The weather data were obtained from the National Climate Data Center (NCDC) website which provides hourly weather information. The geometric and traffic data were collected from the nearest loop detector stations to each collision location and obtained from the Highway Performance Measurement System (PeMS) maintained by the California Department of Transportation (Caltrans). Crash data were obtained from the Statewide Integrated Traffic Records System (SWITRS) of the Caltrans.

Specifically, vehicle count, speed, and occupancy were collected in 30 s for each lane. The related crash data included traffic flow variables, environmental factors, geometric design factors, and others. A total of 9,919 crashes were used in this study. There were three types of crashes, including SC, PC, and NC. PC are defined as the crashes that led to SC, while NC are defined as the crashes that did not lead to SC. The method of identification of SC and the number of SC, PC, and NC are given in Section 2. For each crash, to compensate for the possible inaccuracies in the reported collision occurrence time and identify hazardous traffic conditions ahead of the crash occurrence time, traffic data were collected for the 5–10 min prior to crash occurrence [13,19]. Non-crash cases were extracted based on crash locations and times, and the ratio between crash and non-crash is 1:4 [19].

In Table 1, the 30 s raw data of 5-minute intervals for each crash were further converted into the 19 traffic flow variables, in addition to 4 environment variables, 4 geometric characteristics variables, and 5 crash characteristics variables. A total of 32 candidate variables were considered.

3.2. The Identification of Traffic Flow States. Previous studies have suggested that the traffic states defined by the three-phase traffic theory can be identified by the traffic flow characteristics measured from loop detector stations. According to the three-phase traffic theory, the traffic flow is separated into three steady states, including free flow (F), synchronized flow (S), and wide moving jams (J). In addition to the three steady states, there are four traditional states in this study, including the transitional state from free flow to synchronized flow (F→S), the transitional state from synchronized flow to free flow (S→F), the transitional state from synchronized flow to wide moving jams (S→J), and the transitional state from wide moving jams to synchronized flow (J→S). However, previous studies have demonstrated that the wide moving jams generally do not emerge with the free flow phase [25]. Thus, the transitional state from free flow to wide moving jams was not considered in the present study. The identification method of these traffic flow states has been introduced as follows [29–32]:

- (1) The free flow (F) is characterized by high vehicle speeds and low traffic density. The free flow phase can be easily distinguished from congested flow using the time series plot of speed and occupancy.
- (2) The synchronized flow (S) is characterized by weak correlation between flow rate and density, with a correlation parameter lower than 0.2.
- (3) The wide moving jams (J) are identified by strong correlation between density and flow rate, with a correlation parameter greater than 0.5.
- (4) The transitional states between free flow (F) and synchronized flow (S) are identified by a sudden change in the time series plot of speed and occupancy. The reduction in speed overtime is considered an indicator for the transitional state from free flow to synchronized flow (F→S), and vice versa.

- (5) The transitional states between synchronized flow (S) and wide moving jams (J) are identified by the correlation between density and flow rate, with a correlation parameter between 0.2 and 0.5. The reduction in speed overtime is considered an indicator for the transitional state from synchronized flow to wide moving jams (S→J), and vice versa.

3.3. The Identification of Secondary Crash. The method based on speed contour figure was applied to identify SC in this study. This method uses real-time traffic flow data to determine the spatial and temporal influencing range of a prior crash and simultaneously takes the effects of recurrent congestions into account. The identification method is introduced in detail as follows [13]:

- (1) The 5 min speed data were extracted to produce a speed contour figure for a prior crash. Specifically, the speed data were extracted from the loop detectors within 10 miles upstream and 10 miles downstream the prior crash during the time interval between 6 hours before and 6 hours after the prior. Figure 1(a) shows an example of a speed contour figure. It can be clearly seen from the figure that congestions and queue formations occur after the prior crash. However, less information has been offered by the figure about whether the queue formations resulted from recurrent congestions or the prior crash. To eliminate the effects of recurrent congestions, the spatial and temporal influencing range of the prior crash should be determined, which is given by the following two steps.
- (2) The 5 min speed data for the same time and same location in step one, however, from crash-free days, were extracted for the whole year in this step. For instance, the prior crash in Figure 1(a) happened at 11:45 am on September 20, 2010, at milepost 3.95. Following this step, the speed data for the same time and location in Figure 1(a) were collected from all crash-free days in 2010. Subsequently, the speed data for each time and location were averaged over all the crash-free days.
- (3) To eliminate the potential effects of recurrent congestions, the average speed in step two was subtracted from the speed data for each time and location in step one. A new speed contour figure was developed using the differences between speeds in step two and step one for various times and locations. The new speed contour figure as shown in Figure 1(b) was then used to determine the spatial and temporal influencing range of the prior crash.
- (4) The crashes that happened within the spatial and temporal influencing ranges of a prior crash were identified as SC. The crashes that did not lead to SC were identified as NC.

Following the above four steps of identification method, the summary of SC, PC, and NC in different traffic flow states is given in Table 2, respectively. Compared to the previous study by authors, only speed contour figure was

TABLE 1: Candidate variables.

Variable category	Symbol	Variables
Traffic flow characteristics	C	Correlation coefficient between occupancy and flow during 5–10 minutes
	Cnt/Spd/Occ	Average 30 s vehicle count/speed/detector occupancy during 5–10 minutes (veh/30 s)/(mile/h)/(%)
	StdC/StdS/StdO	Std. dev. of 30 s vehicle count/speed/detector occupancy during 5–10 minutes (veh/30 s)/(mile/h)/(%)
	Cc/Cs/Co	Coefficient of variation of 30 s vehicle count/speed/detector occupancy during 5–10 minutes (veh/30 s)/(mile/h)/(%)
	Dc/Ds/Do	The difference in average 30 s vehicle count/speed/detector occupancy between 15–20 min and 5–20 min (veh/30 s)/(mile/h)/(%)
	Lcnt/Lspd/Locc	Average difference in 30 s vehicle count/speed/detector occupancy between adjacent lanes during 5–10 minutes (veh/30 s)/(mile/h)/(%)
	Lstdc/Lstds/Lstdo	Std. dev. of difference in 30 s vehicle count/speed/detector occupancy between adjacent lanes during 5–10 minutes (veh/30 s)/(mile/h)/(%)
Environmental characteristics	Vi	Visibility (mile)
	We	1 = bad weather condition; 0 = otherwise
	Rs	1 = otherwise; 0 = dry road surface
	Li	1 = bad light; 0 = otherwise
Geometric characteristics	Lw	Lane width (ft)
	Is	Inner shoulder width (ft)
	Os	Outer shoulder width (ft)
	Ra	1 = ramp segment; 0 = otherwise
Crash characteristics	Tr	1 = the crash including a truck; 0 = otherwise
	Se	1 = the injury crash; 0 = otherwise
	Ho	1 = the hit object crash; 0 = otherwise
	Ss	1 = the sideswipe crash; 0 = otherwise
	Re	1 = the rear end crash; 0 = otherwise

used to identify SC without considering the shockwave in the present study [13], because this study focused on the difference in safety performance of SC associated with various traffic flow states.

3.4. Bayesian Conditional Logit Model. As discussed in the literature review section, although some researchers have considered the traffic flow states into the studies of SC, no researchers have studied the difference in safety performance of SC associated with various traffic flow states divided by classical macroscopic traffic flow theory. The conditional logit model was applied to quantitatively analyse the relative safety performance of SC in different traffic flow states while controlling for the effects of other traffic related variables, such as weather condition, geometric metric design, road pavement, etc. The model can be written as [33–37]

$$y_{ijk} \sim \text{Bernoulli}(p_{ijk}),$$

$$P(y_{itk}) = \frac{1}{\{1 + \exp[-\alpha_i + \sum_{k=1}^K \beta_k x_{ijk}]\}}, \quad (1)$$

where x_{ijk} is the k th unmatched variable for the case ($j=0$) or the j th control in the i th matched set. Therefore, $X = \{x_{ijk}\}$ consists of all the cases, and all matched sets are controlled, where $i = 1, 2, \dots, I$; $j = 0, 1, \dots, J$; $k = 1, 2, \dots, K$. I represents the total number of matched sets; J represents the number of controls in each matched set; and K represents the number of contributing variables.

TABLE 2: The summary of different crash types in different traffic flow states.

Traffic flow states	Normal crash	Primary crash	Secondary crash	Total
F	7584	50	27	7661
S	825	14	16	855
J	273	4	15	292
F→S	367	8	10	385
S→F	336	8	10	354
S→J	195	10	11	216
J→S	145	3	8	156
Total	9725	97	97	9919

α_i is the effect of matching variables on the probability of SC occurrence for each matched set; β_k represents the estimated coefficients for explanatory variables; and x_k is the unmatched contributing variables applied in this study.

A conditional probability is used to account for the selection bias of the matched case-control design. The conditional probability that the first vector of the contributing variables x_{i0} in the i th matched set corresponds to the case, conditional on $x_{i0}, x_{i1}, \dots, x_{iJ}$ being the vectors of contributing variables in the i th matched set, is shown as

$$P_i^c = \frac{\exp(\sum_{k=1}^K \beta_k x_{i0k})}{\exp(\sum_{k=1}^K \beta_k x_{i0k}) + \sum_{j=1}^J \exp(\sum_{k=1}^K \beta_k x_{ijk})}. \quad (2)$$

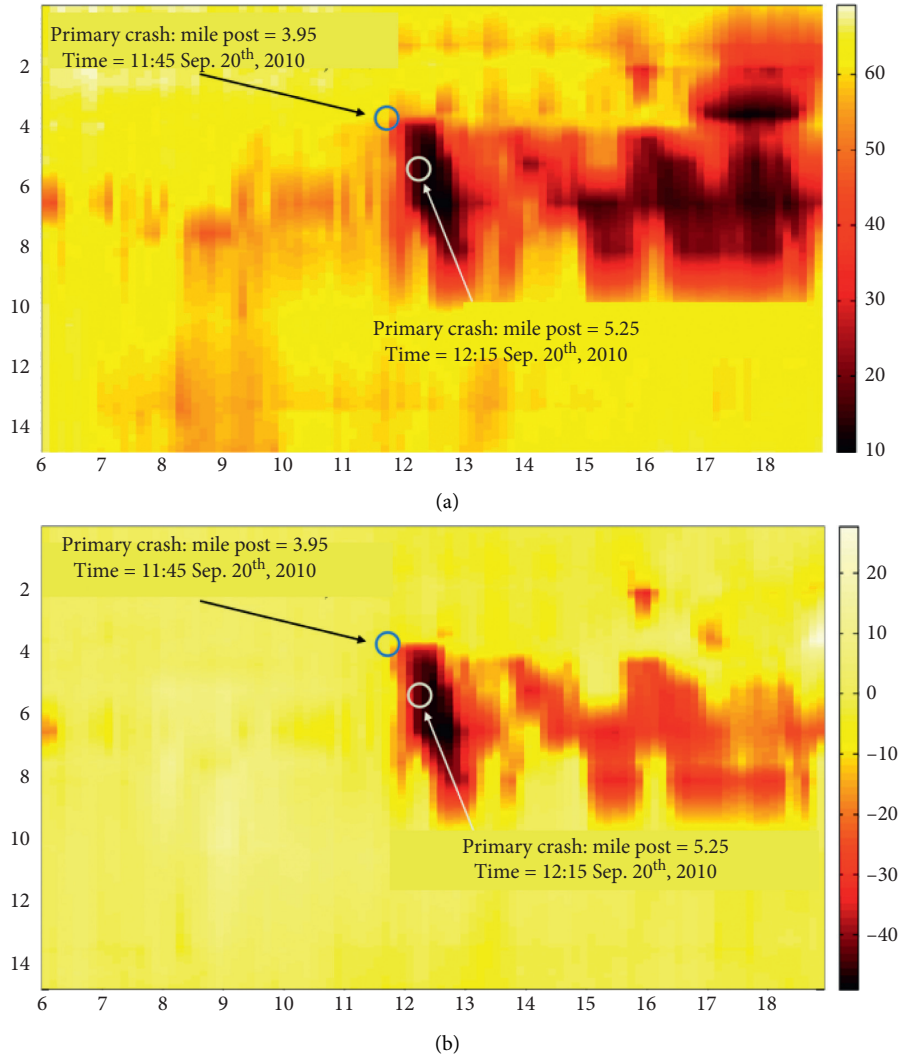


FIGURE 1: Initial identification of SC. (a) Speed contour plot without accounting for the recurrent congestions. (b) Speed contour plot accounting for the recurrent congestions.

Therefore, the probability function of the conditional logit model is expressed as

$$\begin{aligned}
 f(Y|\beta) &= \prod_{i=1}^I f(y_{i0} = 1|\beta) = \prod_{i=1}^I P_i^c \\
 &= \exp \left\{ \sum_{i=1}^I \sum_{k=1}^K (\beta_k x_{i0k}) - \sum_{i=1}^I \log \left[\sum_{j=0}^J \exp \left(\sum_{k=1}^K \beta_k x_{ijk} \right) \right] \right\}. \quad (3)
 \end{aligned}$$

This study applied the Bayesian inference method based on Markov Chain Monte Carlo (MCMC) for the specification of the conditional logit model. Compared to the point estimations of the traditional maximum likelihood estimation (MLE) method, the Bayesian modelling technique regards all unknown parameters as random variables with a prior distribution. The estimates of the mean, standard deviation, and quartiles of the coefficients can be affected by the posterior distribution. Based on the Bayes'

theory, the posterior distribution of parameters can be expressed as

$$f(\beta|Y) = \frac{f(Y, \beta)}{f(Y)} = \frac{f(Y|\beta)\pi(\beta)}{\int f(Y, \beta)d\beta} \propto f(Y|\beta)\pi(\beta), \quad (4)$$

where $f(\beta|Y)$ is the posterior joint distribution of parameters β conditional upon dataset Y , $f(Y, \beta)$ is the joint probability distribution of dataset Y and model parameters β , $f(Y|\beta)$ denotes the likelihood conditional on model parameters β , and The function $\pi(\beta)$ is the prior distribution of model parameters β . The non-informative prior distributions were applied for the model parameters, which can be written as

$$\beta \sim \text{Normal}(0_K, 10^6 I_K), \quad (5)$$

where 0_K represents a $K \times 1$ vector of zeros and I_K represents a $K \times K$ identity matrices. Based on the specification of the

prior distributions for the model parameters β , the posterior joint distribution $f(\beta|Y)$ is expressed as

$$f(\beta|Y) \propto f(Y|\beta)\pi(\beta) = \prod_{i=1}^I f(y_{i0} = 1|\beta) \times \prod_{k=1}^K N\left(\beta_k \left| \mu_k, \sum_k \right.\right) \quad (6)$$

$$\propto \exp\left\{\sum_{i=1}^I \sum_{k=1}^K (\beta_k x_{i0k}) - \sum_{i=1}^I \log\left[\sum_{j=0}^J \exp\left(\sum_{k=1}^K \beta_k x_{ijk}\right)\right] - \frac{1}{2} \sum_{k=1}^K \frac{(\beta_k)^2}{10^6}\right\}.$$

The Markov Chain Monte Carlo (MCMC) method was used to generate realizations from the posterior joint distribution of the model parameters and draw parameters sequentially from equation (6). Compared to the nonstandard conditional distributions in equation (6), the Metropolis-Hasting sampling approach was applied to generate random draws. The inference was used based on the remaining draws after discarding the draws during the burn-in period.

In the present study, only Bayesian conditional logit model was used to analyse the difference in safety performance of SC associated with various traffic flow states. To compare the models, in terms of which one is better in future studies, DIC and AUC values can be adopted. DIC is recognized as Bayesian generalization of AIC (Akaike information criterion) and it was adopted for model comparisons. DIC is a combination of model fit measurement and the effective number of parameters; the smaller DIC indicates a better model fit. AUC value, which is area under the receiver operating characteristic (ROC) curve, was chosen to evaluate and compare these models; larger AUC values indicate a better goodness-of-fit and classification power [38].

4. Results and Discussion

4.1. Safety Performance of Secondary Crash in Different Traffic Flow States. In this study, compared to other studies based on the Bayesian conditional logit model, the Bayesian conditional logit model was used to quantify the difference in the safety performance of SC associated with various traffic flow states divided by three-phase traffic theory. The group variables are separated based on case and control samples. In models, the events (the value of dependent variable is 1) are PC that induced SC and the non-events (the value of dependent variable is 0) are NC that did not induce SC. Because the traffic flow in this study is divided into seven states, including free flow (F), synchronized flow (S), wide moving jams (J), the transitional state from free flow to synchronized flow (F→S), the transitional state from synchronized flow to free flow (S→F), the transitional state from synchronized flow to wide moving jams (S→J), and the transitional state from wide moving jams to synchronized flow (J→S), thus, in this method, the free flow (F) state is considered as the reference level, and the other six

traffic flow states are considered as six independent variables. Finally, the odds ratio can be used to quantify the difference in the safety performance of SC between free flow (F) and the other six traffic flow states. This model did not include other traffic flow variables such as speed and density, because the traffic flow states were highly correlated with traffic flow variables [39].

Three parallel MCMC chains were constructed for Bayesian inference. Each MCMC chain consisted of 10 000 iterations, including an initial “burn-in” period of 4000 iterations [39]. The estimations of each parameter from the MLE method were considered initial values. The initial values for multiple MCMC chains were dispersed throughout the 90% confidence intervals of the estimated parameters from the MLE. The convergence of the posterior distribution samples was checked by the visual inspection of the trace plots, posterior density plots, and autocorrelation function plots. In addition, the Gelman Rubin potential scale reduction (PSR) was also checked. If the PSR was lower than 1.1, the multiple chains were considered converged [39]. The estimation results of the Bayesian conditional logit models are given in Table 3. The 95% credible interval for each parameter in Table 3 indicates that the traffic flow states significantly affect the probability of SC occurrences. The odds ratio for each variable was used to quantify the safety performance of SC in different traffic flow states.

In the Bayesian conditional logit models, as shown in Table 3, the results suggest that the odds ratios of synchronized flow (S), the transitional state from free flow to synchronized flow (F→S), the transitional state from synchronized flow to free flow (S→F), the transitional state from synchronized flow to wide moving jams (S→J), and the transitional state from wide moving jams to synchronized flow (J→S) are significantly greater than free flow (F), and the odds ratio of wide moving jams (J) is not significantly greater than free flow (F). Accordingly, free flow (F) has the best safety performance in terms of the lowest SC likelihood. However, synchronized flow (S) has the highest SC likelihood, followed by the transitional state from synchronized flow to wide moving jams (S→J). The probabilities of SC occurrence associated with F→S, S→F, and J→S are very similar to each other. In detail, the SC probability of synchronized flow (S) is 8.561 times higher than free flow (F). The SC probability of the transitional state from free flow to synchronized flow (F→S) is 2.488 times

TABLE 3: The estimation results of Bayesian conditional logit models.

Traffic flow states	Mean	MC error	2.50%	97.50%	Odds ratio
S	2.258	0.016	1.368	3.190	9.561
J	1.258	0.025	-0.115	2.634	3.519
F→S	1.249	0.018	0.445	2.066	3.488
S→F	1.512	0.019	0.627	2.434	4.535
S→J	2.191	0.018	1.082	3.327	8.943
J→S	1.585	0.025	0.430	2.769	4.881

^aFree flow (F) is the reference level.

higher than free flow (F). The SC probability of the transitional state from synchronized flow to free flow (S→F) is 3.535 times higher than free flow (F). The SC probability of the transitional state from synchronized flow to wide moving jams (S→J) is 7.943 times higher than free flow (F). The SC probability of the transitional state from wide moving jams to synchronized flow (J→S) is 3.881 times higher than free flow (F).

4.2. The Contributing Factors of Secondary Crash in Different Traffic Flow States. To identify how different contributing factors affect the SC probability in different traffic flow states, the traditional logistic regression models were applied [40]. The events are PC that induced SC and the non-events are NC that did not induce SC. In models, 1 is PC and 0 is NC. *P* value of 0.1 was employed for parameter estimate significance in these models. The models were estimated using the software package STATA. To avoid the biased results caused by multicollinearity, the Pearson correlation parameters between different candidate variables were calculated. The highly correlated explanatory variables were avoided to be included into the model simultaneously. The significant variables of the traditional logistic regression models in different traffic flow states are presented in Table 3. The meaning of symbols in Table 4 has been explained in Table 1.

In free flow (F), as shown in Table 4, *Stdc* and *Lstdo* were found to be positively related to the SC probability, but *Spd* and *Ss* were found to be negatively related to the SC probability. The difference of occupancy between adjacent lanes was found to be related to lane-change frequency [41]. The results indicated that the free flow with low speed and more lane changing behaviours can result in the increasing of SC risk. Moreover, the non-sideswipe prior crash can significantly increase the SC risk in free flow. In summary, the preventive measures for SC in free flow (F) are rapid evacuation of congestion and decreasing the interaction between vehicles.

In synchronized flow (S), *Lw*, *Os*, *Occ*, *Lspd*, and *Ho* were found to be positively related to the SC probability, and *Stdo* was found to be negatively related to the SC probability. In synchronized flow, there is a tendency to the synchronization of speeds on each lane and across different lanes [19]. The results showed that the congested flow and synchronization of traffic flow can lead to the increasing of SC likelihood. In addition, larger lane width and outer shoulder width may encourage drivers to take advantage of large space

TABLE 4: The estimation results of the traditional logistic regression models.

Variables	Coefficient	S.D.	$P> z $	2.50%	97.50%
Free flow (F)					
<i>Spd</i>	-0.144	0.022	0.0001	-0.187	-0.100
<i>Stdc</i>	0.472	0.146	0.001	0.185	0.759
<i>Lstdo</i>	13.093	4.187	0.002	4.886	21.300
<i>Ss</i>	-1.306	0.533	0.014	-2.351	-0.261
Cons	2.511	1.487	0.091	-0.403	5.425
Synchronized flow (S)					
<i>Lw</i>	3.295	1.005	0.001	1.325	5.264
<i>Os</i>	0.274	0.126	0.029	0.027	0.520
<i>Occ</i>	12.822	4.849	0.008	3.318	22.325
<i>Stdo</i>	-9.711	4.097	0.018	-17.742	-1.681
<i>Lspd</i>	0.087	0.043	0.043	0.003	0.171
<i>Ho</i>	1.403	0.829	0.091	-0.222	3.027
Cons	-48.560	13.309	0.0001	-74.645	-22.476
Wide moving jams (J)					
<i>Stdo</i>	20.025	8.668	0.021	3.037	37.014
<i>Lcnt</i>	-1.685	0.576	0.003	-2.813	-0.556
Cons	-6.809	1.697	0.0001	-10.135	-3.483
The transitional state from free flow to synchronized flow (F→S)					
<i>Is</i>	-0.275	0.126	0.029	-0.521	-0.029
<i>Dc</i>	-0.764	0.280	0.006	-1.313	-0.215
<i>Occ</i>	26.222	9.524	0.006	7.556	44.888
<i>Co</i>	8.109	2.639	0.002	2.936	13.281
<i>Lstdo</i>	-23.091	10.220	0.024	-43.122	-3.060
Cons	-8.399	2.144	0.0001	-12.602	-4.197
The transitional state from synchronized flow to free flow (S→F)					
<i>C</i>	-4.475	1.635	0.006	-7.681	-1.270
<i>Ds</i>	0.077	0.047	0.100	-0.015	0.170
<i>Ss</i>	1.459	0.789	0.065	-0.088	3.005
Cons	-1.254	0.912	0.169	-3.041	0.534
The transitional state from synchronized flow to wide moving jams (S→J)					
<i>Is</i>	-0.241	0.118	0.041	-0.473	-0.010
<i>Dc</i>	-0.695	0.288	0.016	-1.258	-0.131
<i>Stdo</i>	9.106	4.366	0.037	0.548	17.663
Cons	-1.586	1.119	0.156	-3.780	0.607
The transitional state from wide moving jams to synchronized flow (J→S)					
<i>Tr</i>	7.849	3.412	0.021	1.161	14.536
<i>Cs</i>	-27.593	14.976	0.065	-56.945	1.759
Cons	0.442	2.240	0.844	-3.948	4.831

to pass the congested flow which is caused by a prior crash. Thus, the SC probability will increase in larger lane width and outer shoulder width situation. If the prior crash is a hit object crash, the SC probability will also increase. In summary of the preventive measures for SC in synchronized flow (S), relieving the traffic congestion as soon as possible, reducing the number of lanes, and reducing outer shoulder width can decrease the SC risk while a prior crash occurs, especially a hit object prior crash.

In wide moving jams (J), *Stdo* was found to be positively related to the SC probability, and *Lcnt* was found to be negatively related to the SC probability. The results indicated that the synchronization of vehicles between different adjacent lanes can significantly increase the SC likelihood. The large variation of occupancy in wide moving jams can

significantly increase the SC likelihood. Therefore, making full use of available lanes and relieving the traffic congestion quickly, while a prior crash occurs, can help to reduce the SC risk in wide moving jams (J).

In the transitional state from free flow to synchronized flow ($F \rightarrow S$), Occ and Co were found to be positively related to the SC probability, but Is, Dc, and Lstdo were found to be negatively related to the SC probability. The results implied that the significant tendency from free flow to synchronized flow can result in more congestion, less space, and more lane-change behaviours; the SC likelihood will increase with the traffic flow more and more congested in $F \rightarrow S$. In addition, the evacuation of congested flow can benefit from the larger inner shoulder width, and the larger inner shoulder width can provide more space for drivers to apply crash avoidance measures. Thus, the larger inner shoulder width can decrease the SC likelihood.

In the transitional state from synchronized flow to free flow ($S \rightarrow F$), Ds and Ss were found to be positively related to the SC probability, and Cc was found to be negatively related to the SC probability. Similar to the results of $F \rightarrow S$, the more congested the transitional state tends to be, the larger the SC probability will get. In addition to the traffic flow characteristics, if the prior crash is a sideswipe crash, the SC probability will also increase. In summary of the preventive measures for SC in $S \rightarrow F$ state, relieving the traffic congestion quickly can help to reduce the SC risk while a prior crash occurs, especially a sideswipe prior crash.

In the transitional state from synchronized flow to wide moving jams ($S \rightarrow J$), Stdo was found to be positively related to the SC probability, but Is and Dc were found to be negatively related to the SC probability. Synchronized flow and wide moving jams are both congested flow. In this transitional state, more congested flow will decrease the SC probability. This result is opposite to the results in $F \rightarrow S$ and $S \rightarrow F$. It is because the less available space for drivers will lead to less dangerous driving behaviours. In this transitional state, similar to the results of $F \rightarrow S$, the larger inner shoulder width can provide more space for drivers to apply crash avoidance measures.

In the transitional state from wide moving jams to synchronized flow ($J \rightarrow S$), Tr was found to be positively related to the SC probability, and Cs was found to be negatively related to the SC probability. In previous studies, it has been proved that the prior crash including a truck is found to be a significant factor of SC [11]. In this transitional state, the results showed that the prior crash including a truck also significantly affects SC risk.

5. Conclusion

In this study, the traffic flow is divided by three-phase traffic theory. The main purpose is to analyse the difference of safety performance for SC in different traffic flow states and explore how contributing factors affect the probability of SC in different traffic flow states. The SC related data were collected from the I-880 freeway in the United States from 2006 to 2011. The Bayesian conditional logit models have

been established to analyse the statistical relationship between the SC probability and traffic flow states. The traditional logistic regression models were established to quantify the effects of various variables on the SC probability in different traffic flow states.

More specifically, the results of the Bayesian conditional logit model have been summarized as follows:

- (1) F has the best safety performance in terms of the lowest SC likelihood
- (2) S has the highest SC likelihood, followed by $S \rightarrow J$
- (3) The probabilities of SC occurrence associated with $F \rightarrow S$, $S \rightarrow F$, and $J \rightarrow S$ are very similar to each other
- (4) J is not significantly greater than F

In addition, the results of the traditional logistic regression model have been summarized as follows:

- (1) In free flow (F), rapid evacuation of congestion and decreasing the interaction between vehicles can reduce the SC risk while a prior crash occurs, especially a non-sideswipe prior crash
- (2) In synchronized flow (S), relieving the traffic congestion as soon as possible, reducing the number of lanes, and reducing outer shoulder width can decrease the SC risk while a prior crash occurs, especially a hit object prior crash
- (3) In wide moving jams (J), making full use of available lanes and relieving the traffic congestion quickly, while a prior crash occurs, can help to reduce the SC risk
- (4) In the transitional state from free flow to synchronized flow ($F \rightarrow S$) and the transitional state from synchronized flow to wide moving jams ($S \rightarrow J$), larger inner shoulder width can decrease the SC likelihood
- (5) In the transitional state from synchronized flow to free flow ($S \rightarrow F$), relieving the traffic congestion quickly can help to reduce the SC risk while a prior crash occurs, especially a sideswipe prior crash
- (6) In the transitional state from wide moving jams to synchronized flow ($J \rightarrow S$), the prior crash including a truck also significantly affects SC risk

This research can help traffic management personnel better understand which traffic flow state is more dangerous for the occurrence of SC and realize the contributing factors of SC in different traffic flow states. The results can be applied to develop effective countermeasures and reduce the SC probability in different traffic flow states. However, there are still several issues and potential future studies as follows:

- (1) More PC characteristics need to be considered in the analysis of SC risk. In this study, only four crash types were taken into account in models
- (2) In this study, the traffic flow is only divided by three-phase traffic theory. More macroscopic traffic flow theories should be studied in the future

- (3) Additional research is needed to test for the transferability of the research findings to other freeways
- (4) In future studies, more models should be used to compare with the Bayesian conditional logit model and the traditional logistic regression model in this study

Data Availability

The weather data were obtained from the National Climate Data Center (NCDC) website which provides hourly weather information. The geometric and traffic data were collected from the nearest loop detector stations to each collision location and obtained from the Highway Performance Measurement System (PeMS) maintained by the California Department of Transportation (Caltrans). Crash data were obtained from the Statewide Integrated Traffic Records System (SWITRS) of the Caltrans.

Conflicts of Interest

The authors declare that there are no conflicts of interest regarding the publication of this paper.

Acknowledgments

This research was sponsored by the Projects of the National Natural Science Foundation of China (71701046 and 51878236).

References

- [1] C. Zhan, A. Gan, and M. Hadi, "Identifying secondary crashes and their contributing factors," *Transportation Research Record: Journal of the Transportation Research Board*, vol. 2102, no. 1, pp. 68–75, 2009.
- [2] H. Zhang and A. Khattak, "What is the role of multiple secondary incidents in traffic operations?" *Journal of Transportation Engineering*, vol. 136, no. 11, pp. 986–997, 2010.
- [3] C. Xu, S. Xu, C. Wang, and J. Li, "Investigating the factors affecting secondary crash frequency caused by one primary crash using zero-inflated ordered probit regression," *Physica A: Statistical Mechanics and Its Applications*, vol. 524, pp. 121–129, 2019.
- [4] Z. Wang and H. Jiang, "Identifying secondary crashes on freeways by leveraging the spatio-temporal evolution of shockwaves in the speed contour plot," *Journal of Transportation Engineering Part A-Systems*, vol. 146, no. 2, Article ID 04019072, 2020.
- [5] A. E. Kitali, P. Alluri, T. Sando, H. Haule, E. Kidando, and R. Lentz, "Likelihood estimation of secondary crashes using Bayesian complementary log-log model," *Accident Analysis & Prevention*, vol. 119, pp. 58–67, 2018.
- [6] A. E. Kitali, P. Alluri, T. Sando, and W. Wu, "Identification of secondary crash risk factors using penalized logistic regression model," *Transportation Research Record: Journal of the Transportation Research Board*, vol. 2673, no. 11, pp. 901–914, 2019.
- [7] H. Yang, Z. Wang, K. Xie, and D. Dai, "Use of ubiquitous probe vehicle data for identifying secondary crashes," *Transportation Research Part C: Emerging Technologies*, vol. 82, pp. 138–160, 2017.
- [8] J. E. Moore, G. Giuliano, and S. Cho, "Secondary accident rates on los angeles freeways," *Journal of Transportation Engineering*, vol. 130, no. 1, pp. 280–285, 2004.
- [9] C. Zhan, L. Shen, and M. Hadi, "Understanding the characteristics of secondary crashes on freeways," in *Proceedings of the Presented at 87th Annual Meeting of the Transportation Research Board*, Washington, DC, USA, January 2008.
- [10] W. Hirunyanitawattana and S. P. Mattingly, "Identifying secondary crash characteristics for the california highway system," in *Presented at 85th Annual Meeting of the Transportation Research Board*, Washington, DC, USA, January 2006.
- [11] H. Yang, Z. Wang, K. Xie, K. Ozbay, and M. Imprialou, "Methodological evolution and frontiers of identifying, modeling and preventing secondary crashes on highways," *Accident Analysis & Prevention*, vol. 117, pp. 40–54, 2018.
- [12] N. J. Goodall, "Probability of secondary crash occurrence on freeways with the use of private-sector speed data," *Transportation Research Record: Journal of the Transportation Research Board*, vol. 2635, no. 1, pp. 11–18, 2017.
- [13] B. Yang, Y. Guo, and C. Xu, "Analysis of freeway secondary crashes with a two-step method by loop detector data," *IEEE Access*, vol. 7, pp. 22884–22890, 2019.
- [14] M.-I. M. Imprialou, F. P. Orfanou, E. I. Vlahogianni, and M. G. Karlaftis, "Methods for defining spatiotemporal influence areas and secondary incident detection in freeways," *Journal of Transportation Engineering*, vol. 140, no. 1, pp. 70–80, 2014.
- [15] B. S. Kerner and H. Rehborn, "Experimental properties of complexity in traffic flow," *Physical Review E*, vol. 53, no. 5, pp. 4275–4278, 1996.
- [16] B. S. Kerner, "Experimental features of self-organization in traffic flow," *Physical Review Letters*, vol. 81, no. 17, pp. 3797–3800, 1998.
- [17] N. Wu, "A new approach for modeling of Fundamental Diagrams," *Transportation Research Part A: Policy and Practice*, vol. 36, no. 10, pp. 867–884, 2002.
- [18] Transportation Research Board, *Highway Capacity Manual*, Transportation Research Board of the National Academies, Washington, DC, USA, 2010.
- [19] C. Xu, P. Liu, W. Wang, and Z. Li, "Safety performance of traffic phases and phase transitions in three phase traffic theory," *Accident Analysis & Prevention*, vol. 85, pp. 45–57, 2015.
- [20] C. Xu, P. Liu, and F. W. Zhang, "Development of a real-time crash risk prediction model incorporating the various crash mechanisms across different traffic states," *Traffic Injury Prevention*, vol. 16, no. 1, pp. pp28–35, 2015.
- [21] H. Park, A. Haghani, S. Samuel, and M. A. Knodler, "Real-time prediction and avoidance of secondary crashes under unexpected traffic congestion," *Accident Analysis & Prevention*, vol. 112, pp. 39–49, 2018.
- [22] R. A. Raub, "Occurrence of secondary crashes on urban arterial roadways," *Transportation Research Record: Journal of the Transportation Research Board*, vol. 1581, no. 1, pp. 53–58, 1997.
- [23] M. G. Karlaftis, S. P. Latoski, N. J. Richards et al., "Empirical analysis of secondary crash causes," in *Presented at 77th Annual Meeting of the Transportation Research Board*, Washington, DC, USA, January 1998.
- [24] C.-S. Chou and E. Miller-Hooks, "Simulation-based secondary incident filtering method," *Journal of Transportation Engineering*, vol. 136, no. 8, pp. 746–754, 2010.

- [25] H. Zhang, M. Cetin, and A. J. Khattak, "Joint analysis of queuing delays associated with secondary incidents," *Journal of Intelligent Transportation Systems*, vol. 19, no. 2, pp. 192–204, 2015.
- [26] H. Park and A. Haghani, "Real-time prediction of secondary incident occurrences using vehicle probe data," *Transportation Research Part C: Emerging Technologies*, vol. 70, pp. 69–85, 2016.
- [27] J. Wang, L. Boya, Z. Lanfang, and D. R. Ragland, "Modeling secondary accidents identified by traffic shock waves," *Accident Analysis and Prevention*, vol. 87, pp. 141–147, 2016.
- [28] C. Xu, P. Liu, B. Yang, and W. Wang, "Real-time estimation of secondary crash likelihood on freeways using high-resolution loop detector data," *Transportation Research Part C: Emerging Technologies*, vol. 71, pp. 406–418, 2016.
- [29] Y. Toshiyuki and V. Shankar, "Bivariate ordered-response probit model of driver's and passenger's injury severities in collisions with fixed objects," *Accident Analysis and Prevention*, vol. 36, pp. 869–879, 2004.
- [30] W. Knospe, L. Santen, A. Schadschneider et al., "Single-vehicle data of highway traffic: microscopic description of traffic phases," *Physical Review E*, vol. 65, pp. 1–16, 2002.
- [31] J. Carroll, "Generalization of canonical correlation analysis to three or more sets of variables," in *Presented at 76th Annual Meeting of the Transportation Research Board*, Washington, DC, USA, January 1968.
- [32] V. Burg, *Nonlinear Canonical Correlation and Some Related Techniques*, DSWO Press, Leiden, Netherlands, 1988.
- [33] N. Bruce, D. Pope, and D. Stanistreet, *Quantitative Methods for Health Research: A Practical Interactive Guide to Epidemiology and Statistics*, John Wiley & Sons, Hoboken, NJ, USA, 2008.
- [34] Y. Guo, P. Liu, Y. Wu, and J. Chen, "Evaluating how right-turn treatments affect right-turn-on-red conflicts at signalized intersections," *Journal of Transportation Safety & Security*, vol. 12, no. 3, pp. 419–440, 2020.
- [35] Y. Guo, Z. Li, P. Liu, and Y. Wu, "Modeling correlation and heterogeneity in crash rates by collision types using full bayesian random parameters multivariate Tobit model," *Accident Analysis & Prevention*, vol. 128, pp. 164–174, 2019.
- [36] Y. Guo, Z. Li, and T. Sayed, "Analysis of crash rates at freeway diverge areas using bayesian tobit modeling framework," *Transportation Research Record: Journal of the Transportation Research Board*, vol. 2673, no. 4, pp. 652–662, 2019.
- [37] Y. Guo, Z. Li, P. Liu, and Y. Wu, "Exploring risk factors with crashes by collision type at freeway diverge areas: accounting for unobserved heterogeneity," *IEEE Access*, vol. 7, pp. 11809–11819, 2019.
- [38] R. Yu, X. Wang, K. Yang, and M. Abdel-Aty, "Crash risk analysis for Shanghai urban expressways: a Bayesian semi-parametric modeling approach," *Accident Analysis & Prevention*, vol. 95, pp. 495–502, 2016.
- [39] C. Xu, Y. Wang, P. Liu, W. Wang, and J. Bao, "Quantitative risk assessment of freeway crash casualty using high-resolution traffic data," *Reliability Engineering and System Safety*, vol. 169, pp. 299–311, 2018.
- [40] Z. Li, W. Wang, R. Chen, P. Liu, and C. Xu, "Evaluation of the impacts of speed variation on freeway traffic collisions in various traffic states," *Traffic Injury Prevention*, vol. 14, no. 8, pp. 861–866, 2013.
- [41] D. C. Gazis, R. Herman, and G. H. Weiss, "Density oscillations between lanes of a multilane highway," *Operations Research*, vol. 10, no. 5, pp. 658–667, 1962.

Research Article

A Framework for Intersection Traffic Safety Screening with the Implementation of Complex Network Theory

Xueyu Mi,^{1,2} Chunfu Shao,¹ Chunjiao Dong ,¹ Chengxiang Zhuge,³ and Yan Zheng¹

¹Key Laboratory of Transport Industry of Big Data Application Technologies for Comprehensive Transport, Ministry of Transport, Beijing Jiaotong University, Beijing 100044, China

²College of Civil and Architectural Engineering, North China University of Science and Technology, He Bei, Tang Shan 063210, China

³Department of Land Surveying and Geo-Informatics, The Hong Kong Polytechnic University, Hong Kong, China

Correspondence should be addressed to Chunjiao Dong; cjdong@bjtu.edu.cn

Received 12 August 2020; Revised 7 September 2020; Accepted 13 September 2020; Published 27 September 2020

Academic Editor: Feng Chen

Copyright © 2020 Xueyu Mi et al. This is an open access article distributed under the Creative Commons Attribution License, which permits unrestricted use, distribution, and reproduction in any medium, provided the original work is properly cited.

The traffic safety screening could provide guidance for determining the use of resources for traffic safety improvements and is critical for the traffic management. To account for the impacts of traffic safety and the effects of intersection as a node in the roadway network, a framework with six indicators and four strategies is proposed for intersection traffic safety screening. The traffic flow has been incorporated into the process of developing three indicators from the perspective of the complex network theory to measure the node importance. For the assessment of traffic safety, other than the observed and estimated crash frequency and modified time-to-collision, a distance that describes the nonlane-based movements has been proposed from the perspective of traffic safety. A multilayer entropy-weighted VIKOR (MEW-VIKOR) approach is proposed to compute the ranking results, and four strategies have been developed to better account for the effects of the six indicators simultaneously. A roadway network with 28 intersections in Shenzhen has been adopted to verify the effectiveness of the proposed framework for intersection traffic safety screening. The results indicate that the proposed framework with two layers could represent the features of traffic safety and the characteristics of node importance and satisfy the expectation from the public, government, and research institutes. With an appropriate threshold setting, the ranking results are consistent with the intersection safety investigation and contribute significantly to the reduction of false-positive and false-negative cases in identifying the black spot intersections.

1. Introduction

Intersections indicate a complicated and hazardous roadway environment involving human factors, vehicle characteristics, roadway design features, and traffic flow movements. The presence of conflicted traffic flow movements, mixed roadway users, diversified driver actions and behaviors, and complicated roadway design features creates a challenging and confusing condition to the roadway users that leads to greater crash frequencies with serious severity. Traffic crashes at intersections place a huge burden on society and public in terms of death, injury, and property damage [1, 2]. Once a traffic crash occurred at an intersection, as the critical component and important node of the roadway network, the condition of

the intersection will impact the operation efficiency and safety of neighboring zones, and even the overall roadway network. The influencing degree and extent depend on the importance of the intersection as a node in the roadway network. Hence, the measurement of importance of intersection as a node in the roadway networks can provide insights into understanding the spread rate and extent of traffic congestions and the loss of network efficiency that caused by the occurrences of traffic crashes. To reduce the impacts of intersection-related traffic crashes on the roadway network, there is a need to identify the most important intersections with traffic safety issues in the roadway network and ensure that the necessary countermeasures are designed and applied to prevent the occurrences of traffic crashes and reduce the crash severity.

2. Literature Review

As part of the roadway management process, the traffic safety screening of hazardous intersections and identification of high-risk traffic crash intersections are of great interest from safety specialists and roadway agencies. In the process of traffic safety analyses, the term of black spot (BS) is adopted to describe the locations that have a greater crash rates than an average. The identification, ranking, and treatment of black spots have been referred to a standard methodology of safety management for over 30 years, which effectively reduce and prevent the occurrences of traffic crashes [3]. Since conducting a detailed engineering study for all roadway locations is expensive, the traffic safety screening is critical, which helps the engineers to identify the locations with potential for safety improvements. For the roadway network screening, the most crash-prone sites can be identified. The identified locations can be the school zones, corridors, intersections, and others. In practice, screening at intersection level for the entire roadway network is required for various reasons that include the need to meet drivers' expectations of homogeneous infrastructure conditions across the roadway network.

Although the methods, such as the Empirical Bayes (EB) method, are recommended for network screening by the Highway Safety Manual (HSM), the simplistic approaches that rely only on observed crash frequency or crash severity are commonly used by researchers [4, 5]. Rahman et al. [6] identified the most crash-prone school zones based on crash rates in Orange and Seminole Counties in Florida. Three countermeasures were proposed for the identified school zones, and the simulation experiments were designed to evaluate the implemented effects using microsimulation. Meuleners et al. [7] assessed the effectiveness of the black spot programs in Western Australia. The crash rate reduction and the economic benefits of the treatments at the treated locations were computed. The results showed that the programs have reduced the reported crash rate by 15%. The estimated cost savings and net savings were 50.8 and 40.4 million Australian dollars, respectively. The benefit cost ratio across all treated locations was 4.9.

The commonly used black spot identification (BSID) methods include crash frequency method (crashes per year or crashes per km per year), crash rate method (crashes per vehicle per kilometers or per vehicles), and a combination of the two methods [8, 9]. Since the methods are not based on the statistical models, the results can vary in the analyzed period. To overcome the limitations of the commonly used BSID methods, the empirical Bayesian (EB) techniques have been proposed, which combines the features and benefits of the observed and predicted crash frequencies [10, 11]. The crash frequencies can be predicted by using a safety performance function (SPF) that is developed from historical crash data. Based on the reliability level of the predicted crash frequencies, a statistical model could be used to weight the observed and predicted crash frequencies in the EB methods. The safety effects of a black spot program that was implemented in Flanders-Belgium have been evaluated by Pauw et al. [12] using an empirical Bayes method before and

after study. The effects of general trends and the stochastic nature of crashes, including regression to the mean, have been considered. The results show that the implementation of the program has resulted in a 24–27% and 46–57% reduction in injury and fatal crashes, respectively.

Using observed crash frequencies and rates might result in a volume bias, a segment length bias, and a regression-to-the-mean bias [13]. Errors in BSID can result in false-positive and false-negative cases [14]. In other words, crashes can occur in both safe and unsafe locations, and the essential is to identify the most dangerous locations with greater impacts. Other than the crash frequency/rate methods and the EB methods, the research explored a variety of methods in traffic safety screening. Fan et al. [15] proposed a feature-based depth neural network identifying the black spots, and the accuracy is 89%. Cafiso and Di Silvestro [16] investigated the performance of safety indicators in black spot identification for two-lane rural roads. A Monte Carlo simulation was proposed to produce theoretical crash data that were used to define a priori hazardous sites. The results showed that the indicators that are based on the EB estimation should be used for safety improvement from the perspective of practice. Geurts et al. [17] conducted a sensitivity analysis regarding the identification and ranking of the black spots. The results indicated that the injury weighting values that are relating to the attitude of the traffic safety problem and the usage of estimated crash counts have important impacts on the selection and ranking of black spots in terms of ranking order and traffic safety decisions.

Though there are a large number of studies focusing on the development of BSID methods, few research studies have been conducted to analyze and compare the model performances. A site and method consistency test and total rank differences test were proposed by Cheng and Washington [11] to compare the performances of four commonly used BSID methods. The EB methods showed the best consistency among the other BSID methods and were recommended to be used as the standard in the identification of BS. The same conclusion was obtained by Montella [18], whose study also proved the effectiveness of the EB method compared with the other seven BSID methods. To understand the impacts of roadway network segmentation on the performances of BSID methods, four commonly used BSID methods (empirical Bayesian (EB), excess EB, crash frequency, and crash ratio) and four segmentation methods (spatial clustering, constant traffic volume, constant length, and the standard Highway Safety Manual segmentation method) have been analyzed by Ghadi and Török [19]. The results showed that there is a significant relationship between the performances of BSID methods and segmentation methods. In general, the EB methods have superior performance compared with other methods, regardless of the segmentation approaches. The results are consistent with that of Montella's study [18], which showed that the EB method is the most reliable method for identifying the black spots.

To identify the intersection with potential for safety improvements and understand the impacts of intersection-related crashes on roadway networks, in the research, a framework of intersection traffic safety screening is

developed by considering the indicators of traffic safety and node importance. To account for the traffic safety assessment and node importance simultaneously, with the developed six indicators, four strategies are proposed in the framework of intersection traffic safety screening. One is incorporating the ranking results of node importance in the procedure of traffic safety assessment. Second is incorporating the traffic safety assessment results as a factor to calculate the node importance. The third is to compute ranking results with the developed six indicators. The fourth is combining the ranking results of traffic safety assessment and node importance. To overcome the limitation of the conventional evaluation methods that are using the subjective weigh factors, a multilayer entropy-weighted VIKOR (MEW-VIKOR) method is proposed to compute the ranking results. The developed framework of intersection traffic safety screening can be used for assessing the entire intersections in the roadway network and identifying the intersections with potential for safety improvements from a combined perspective by accounting for traffic safety and node importance simultaneously. The identified intersections with a ranking order are recommended for further investigation with detailed traffic safety countermeasures.

3. Modeling Framework and Formulation

The intersection traffic safety screening can be defined as the process of searching and ranking the intersections in roadway networks with a greater safety risk and potential of significant impacts on the traffic flow states of the roadway network. In the research, a framework that incorporates the traffic safety assessment and node importance has been proposed for intersection traffic safety screening and a multilayer entropy-weighted VIKOR (MEW-VIKOR) method is developed for the ranking. The motivation of the research is to measure the traffic safety and node importance simultaneously in the process of traffic safety screening. It would be great that all the impact factors have been considered and more indicators have been developed. However, more indicators means more complicated interaction between the variables. In the research, the six indicators are recommended to capture the characteristics of traffic safety and node importance simultaneously. In practice, based on the data and other actual situations, the indicators can be modified under the framework of traffic safety screening.

3.1. Indicators of Intersection Node Importance. The commonly used methods of node importance can be classified into the social network-based models and system science-based models [20]. Based on the assumption that a node importance is relevant to the connection between the nodes, the social network models were proposed to determine the network attributes, such as shortest path, degree, and closeness to highlight the difference among nodes. With the assumption that the nodes can be removed from the network, the system science methods were proposed to determine the node importance by changing the network topology and assessing the destructiveness. In the research,

the node importance of intersection is computed based on the principle of the social network-based models since the assumption of the social network-based models is acceptable and satisfied in the roadway network with the intersection as the nodes.

Given that the roadway network can be considered as an undirected network, let $\mathbf{G} = (\mathbf{I}, \mathbf{S}, \mathbf{A})$ represents the roadway network that takes the intersections as the nodes, where $\mathbf{I} = \{i_1, i_2, \dots, i_n\}$ denotes the set of all intersections, $|\mathbf{I}| = n$; $\mathbf{S} = \{s_1, s_2, \dots, s_l\} \subseteq \mathbf{I} \times \mathbf{I}$ denotes the set of connection segments, and $|\mathbf{S}| = l$; $\mathbf{A} = \{a_{ij}\}$ denotes the adjacency matrix. Accordingly, three indicators can be defined to measure the node importance of the intersections. One is the closeness centrality [20, 21], one is the betweenness centrality [22], and the third is the degree centrality. Different from the conventional closeness centrality that are measured by the path length to other nodes, the closeness centrality of intersection i is computed by the sum of traffic flow and the reciprocal of the sum of path length to other intersections, which is defined as

$$CC(i) = \frac{\sum_{j=1}^n q_{ij}}{(1/(n-1))\sum_{j=1}^n d_{ij}q_{ij}}, \quad (1)$$

where $CC(i)$ is the closeness centrality of intersection i ; q_{ij} is the traffic flow on the shortest path between intersections i and j ; and d_{ij} denotes the length of shortest path between intersections i and j . When there is no available path between intersections i and j , then $d_{ij} = \infty$ ($1/d_{ij} = 0$). The greater $CC(i)$ indicates that the i intersection is more important.

The indicator of betweenness centrality indicates the importance of an intersection controlling the traffic flow along the shortest path in the roadway network, which can be defined as

$$BC(i) = \frac{2(\sum_{r,s \neq i} (t_{rs}(i)q_{rs}(i))/t_{rs}q_{rs})}{n(n-1)}, \quad (2)$$

where $BC(i)$ is the betweenness centrality of intersection i ; t_{rs} is the number of the shortest paths between intersections r and s , and $t_{rs}(i)$ is the number of the shortest paths between intersections r and s that go through the intersection i ; q_{rs} is the traffic flow of the shortest paths between intersections r and s , and $q_{rs}(i)$ is the traffic flow of the shortest paths between intersections r and s that go through the intersection i ; and n is the number of the intersections, and the formulation of $n(n-1)/2$ is employed to normalize the betweenness centrality. The greater $BC(i)$ indicates that the intersection i is more important.

The degree centrality indicates the property that an intersection connects with other intersections directly, which can be defined as

$$DC(i) = \frac{\sum_{j=1}^n a_{ij}q_{ij}}{(n-1)Q}, \quad (3)$$

where a_{ij} is the adjacency factor and Q is the total traffic flow on the roadway network. When there is a roadway segment between intersections i and j , $a_{ij} = 1$; otherwise, $a_{ij} = 0$.

Compared with the conventional CC (i), BC (i), and DC (i) that used for node importance computing, the proposed CC (i), BC (i), and DC (i) account for the impacts of traffic flow, which could better represent the spatial topological relationship of roadway networks.

3.2. Indicators of Intersection Traffic Safety. Regarding the assessment of intersection traffic safety, the commonly employed methods could be classified into two categories [23]. One is a reactive approach, and the crash data that include historical crash records and predicted crashes could be used. Another is a proactive approach, and the Surrogate Measures of Safety (SMoS) were used to identify the crash-prone locations where an observable noncrash event could lead to a crash [24, 25]. Although the reactive approaches have many limitations such as missing crash records, small sample size, and unobserved causal factors of the crashes, the methods are essential for the greatest benefit of BSID because the observed and predicted crash counts indicate the effects of risk factors that are involving geometric design features, traffic conditions, and environmental characteristics. The SMoS approach, on the other hand, without relying on a huge number of crash data, developed the trajectory-based measures to identify the noncrash event that could be further converted into the corresponding crash frequency. In the research, the reactive and proactive approaches have been developed simultaneously since the traffic safety of intersection includes the interactions among human factors, vehicle characteristics, roadway design features, and traffic flow movement.

For the reactive approaches, the empirical Bayesian (EB) techniques that combine the benefit of observed and estimated crash frequencies have been employed [19]. The observed and estimated crash frequencies are weighted in a statistical model:

$$Y_i = (1 - \omega_i)y_{io} + \omega_i y_{ip}, \quad (4)$$

where Y_i is the expected crash frequency for intersection i ; y_{io} and y_{ip} are the observed and estimated crash frequencies for intersection i in the research period; and the weight factor ω_i represents the reliability level of the estimated crashes y_{ip} .

The estimated crash frequencies y_{ip} could be computed by a negative binomial regression model:

$$y_{ip} = \exp\left(\alpha + \sum_j \beta_j x_{ij}\right), \quad (5)$$

where α is the intercept and β_j is the regression coefficients of the corresponding explanatory variables x_{ij} .

Since not all the impact factors that could potentially cause the occurrences of traffic crashes could be observed and measured, there is a need to develop some effective and efficiency SMoS for intersection traffic safety screening. Commonly used SMoS, such as time-to-collision (TTC) [26] and postencroachment time (PET) [23], are inappropriate for intersection traffic safety screening since the characteristics of vehicle movements at intersections, such as frequently acceleration and nonlane-based vehicle

movements, have not been taken into account. Based on Newton's equations of motion, a traffic crash could be occurred when the distances traveled by the following vehicle is equal to or greater than the sum of the initial relative distance between the leading and following vehicles and the distance traveled by the leading vehicle [27]:

$$v_f t + \frac{1}{2} a_f t^2 \geq v_l t + \frac{1}{2} a_l t^2 + s, \quad (6)$$

where v_f and v_l represent the speed of the following and leading vehicles, respectively, t is the time gap; a_f and a_l represent the acceleration of the following and leading vehicles, respectively, and s denotes the initial relative distance.

Let Δv and Δa be the relative speed and acceleration of the interacting vehicles, respectively, the Modified TTC (MTTC) can be obtained from equation (5):

$$\text{MMTC} = \begin{cases} \min(t_1, t_2), & \text{if } \Delta a, t_1, t_2 > 0, \\ t_1, & \text{if } \Delta a, t_1 > 0, t_2 \leq 0, \\ t_2, & \text{if } \Delta a, t_2 > 0, t_1 \leq 0, \\ t_3, & \text{if } (\Delta a \leq 0 \text{ or } t_1, t_2 \geq 0) \text{ and } t_3 > 0, \end{cases} \quad (7)$$

where t_1 and t_2 are the two values that are derived from equation (5); and t_3 is the original TTC:

$$\begin{aligned} t_1 &= \frac{-\Delta v + \sqrt{\Delta v^2 + 2\Delta a s}}{\Delta a}, \\ t_2 &= \frac{-\Delta v - \sqrt{\Delta v^2 + 2\Delta a s}}{\Delta a}, \\ t_3 &= \frac{s}{\Delta v}. \end{aligned} \quad (8)$$

The MTTC could be computed based on the vehicle trajectories that are obtained from a video record. Other than the MTTC, to account for the effects of nonlane-based vehicle movements, a distance that is based on the longitudinal gap and lateral overlap is proposed to identify the vehicle interaction characteristics:

$$d = \sqrt{(x_l - x_f - L_l)^2 + \left(|y_l - y_f| - \frac{w_l}{2} - \frac{w_f}{2}\right)^2}, \quad (9)$$

where (x_l, y_l) is the center coordinate of the leading vehicle, (x_f, y_f) is the center coordinate of the following vehicle, L_l is the length of the leading vehicle, w_l is the width of the leading vehicle, and w_f is the width of the following vehicle.

An interaction between the leading and following vehicles is identified as critical if the path of the two vehicles is overlapped. In other words, the interactions are critical if the d is less than $\sqrt{L_l^2 + 1/2(w_l + w_f)^2}$. Such critical interactions could be identified for individual vehicle in the intersection area at every instant.

3.3. A Framework for Combining the Traffic Safety Assessment and Node Importance. To obtain more comprehensive and effective results, the multi-attribute decision-making

(MADM) methods could be used to account for the effects of the proposed six indicators [28]. As the commonly used MADM methods, the Technique for Order Preference by Similarity to an Ideal Object (TOPSIS) methods and Visekriterijumsko KOMpromisno Rangiranje (VIKOR) methods have been proposed based on an aggregating function representing the concept of closeness to the ideal [29, 30]. The TOPSIS methods compare the distance of individual alternative to the ideal and anti-ideal solution, and the VIKOR methods have been developed to provide compromise solutions to discrete multiple indicators that include noncommensurable and conflicting indicators. In the research, the VIKOR methods have been employed to screen and rank the intersection with multiple indicators since the indicators of traffic safety and node importance are not commensurable. In addition, a multilayer entropy-weighted VIKOR (MEW-VIKOR) method is proposed to better account for the effects of traffic safety indicators and node importance indicators, simultaneously.

Suppose the set of indicators is $C = \{c_1, c_2, \dots, c_m\}$, then the normalized decision matrix can be expressed as

$$\mathbf{D} = \begin{bmatrix} x_{11} & x_{12} & \cdots & x_{1m} \\ x_{21} & x_{22} & \cdots & x_{2m} \\ \vdots & \vdots & \ddots & \vdots \\ x_{n1} & x_{n2} & \cdots & x_{nm} \end{bmatrix}, \quad (10)$$

$$x_{ij} = \frac{c_{ij}}{\sqrt{\sum_{i=1}^n (c_{ij})^2}},$$

where x_{ij} is the normalized value of c_{ij} and c_{ij} is the value of j th indicator for the i th intersection, and $i = 1, 2, \dots, n$; $j = 1, 2, \dots, m$.

To overcome the limitation of the conventional VIKOR methods that are using the subjective weigh factors, the entropy-weighted (EW) method is adopted to compute the weight of individual indicator. By accounting for the information entropy, the weight of the j th indicator of the proposed entropy-weighted VIKOR (EW-VIKOR) can be computed as

$$w_j = \frac{1 + (1/\ln n) \sum_i^n e_{ij}}{\sum_{j=1}^m (1 + (1/\ln n) \sum_i^n e_{ij})}, \quad (11)$$

where e_{ij} is the information entropy of j th indicator for the i th intersection; n is the number of analyzed intersections.

The e_{ij} can be computed as

$$e_{ij} = \frac{x_{ij}}{X_j} \ln \left(\frac{x_{ij}}{X_j} \right), \quad (12)$$

$$X_j = \sum_{i=1}^n x_{ij}.$$

The utility and regret measures for all intersections can be computed as

$$U_i = \sum_{j=1}^m w_j \frac{(x_j^* - x_{ij})}{(x_j^* - x_j^-)}, \quad (13)$$

$$R_i = \max_j [w_j (x_j^* - x_{ij}) (x_j^* - x_j^-)],$$

where U_i is the utility measure; R_i is the regret measure; and x_j^* is the ideal solution, $x_j^* = \max_i x_{ij}$; x_j^- is the negative solution, and $x_j^- = \min_i x_{ij}$.

Let $U^* = \min_i U_i$, $U^- = \max_i U_i$, $R^* = \min_i R_i$, and $R^- = \max_i R_i$, the EW-VIKOR index of importance of the i th intersection can be computed as follows:

$$P_i = 1 - \alpha \frac{(U_i - U^*)}{(U^- - U^*)} + (1 - \alpha) \frac{(R_i - R^*)}{(R^- - R^*)}, \quad (14)$$

where α is the weight for the strategy of maximum group utility, whereas $1 - \alpha$ is the weight of the individual regret, here $\alpha = 0.5$.

The greater the P_i is, the more important the analyzed intersection is. The analyzed intersections can be sorted by the value of P_i . If $P_i = 0$, the intersection is the least important and some maintenance methods should be taken into account to ensure that the interaction condition stays at a certain level. If $P_i = 1$, the intersection is the most important and more resources of traffic safety improvements should be assigned and implemented.

In the research, to fully address the issues of combining the indicators of traffic safety assessment and node importance, four strategies have been proposed under the framework of intersection traffic safety screening and the MEW-VIKOR methods are developed, as shown in Figure 1:

- (1) Strategy 1 is using the EW-VIKOR method to compute the ranking results based on the indicators of traffic safety assessment. The results of traffic safety assessment will be incorporated into the process of computing the node importance as an impact factor, and the EW-VIKOR method will be running for one more time.
- (2) Strategy 2 is using the EW-VIKOR method to compute the ranking results based on the indicators of node importance. The results of node importance will be incorporated into the process of traffic safety assessment as an impact factor and the EW-VIKOR method will be running for one more time.
- (3) Strategy 3 treated all the traffic safety assessment and node importance indicators equally, and the EW-VIKOR will be used to compute the ranking results based on all the indicator set of traffic safety assessment and node importance.
- (4) Strategy 4 is a MEW-VIKOR method. The first layer computes the ranking results based on the indicators of traffic safety assessment and node importance, respectively. The second layer computes the ranking results based on the results of first layer, which includes the ranking results of traffic safety assessment and node importance. The third layer is the final ranking results, which comprehensively account for

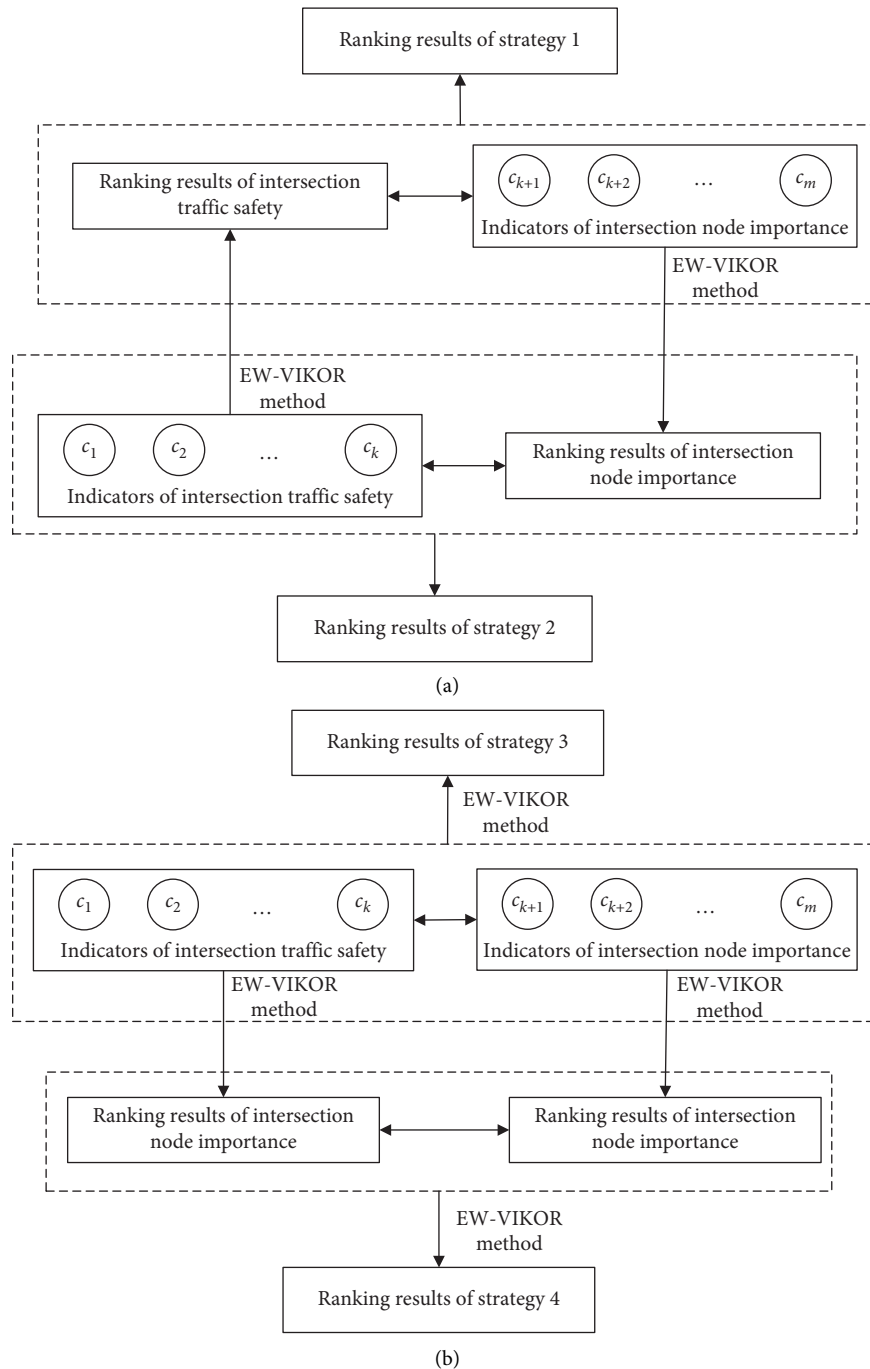


FIGURE 1: Flow chart of the proposed framework with four strategies: (a) strategies 1 and 2 and (b) strategies 3 and 4.

the effects of traffic safety assessment and node importance.

4. Data

In the research, six indicators have been developed from the perspectives of node importance and traffic safety, which demonstrate the complex interactions among the human factors, vehicle characteristics, roadway design features, and traffic flow movement. Based on the developed indicators, a framework with four strategies has been proposed for

intersection traffic safety screening. To examine the effectiveness of the proposed indicators and verify the efficiency of the proposed framework with four strategies, a roadway network of an old town in Futian District, Shenzhen City, China, has been adopted, which includes 26 intersections and 52 roadway segments, as shown in Figure 2(a).

To compute the indicators of node importance, the topology of the roadway network needs to be extracted. The intersections are treated as the network nodes, and the roadway segment between the intersections are treated as the network edges. The topology of the roadway network of an

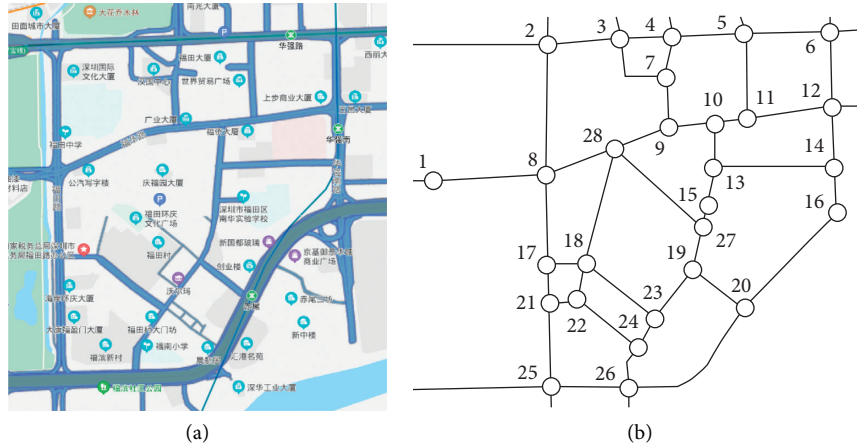


FIGURE 2: Roadway network of an old town in Futian District, Shenzhen City, China: (a) a map of research zone and (b) the topology of roadway network.

old town in Futian District is shown in Figure 2(b). The traffic flow of an individual segment in the roadway network can be considered as the weighting factors. The lengths of the roadway segments are measured to compute the shortest path between intersections i and j . The Dijkstra algorithm is employed to compute the shortest path between i and j . The statistics of all the shortest paths from i to j ($j \neq i$) are shown in Table 1.

Other than the data of segment length and the length of the shortest path, the information of the traffic flow is needed to compute the indicators of the node importance. In the research, instead of the annual average daily traffic (AADT), the capacity is used to measure the traffic flow of the shortest path because the AADT data are not available. The capacity of the individual segment is computed as the product of the number of through lanes and the capacity of the through lane. The capacity of the through lane is equal to 1700 pcu per lane. The statistics of the traffic flow of the shortest path are shown in Table 1. The range of the traffic flow of the shortest path is from 13,852 to 37,526.

Regarding the indicators of traffic safety, to obtain Y_i , the y_{ip} in equation (4) is computed by using the negative binomial (NB) regression model. The factors of speed limit, percent of trucks, and important measures of roadway design features, such as lane widths, median types, and shoulder widths are employed as the explanatory variables since they have shown significant impacts on the crash frequencies [31]. The study period of y_{ip} and y_{io} is 5 years, and the weight factor ω_i is equal to 0.5. The indicators of MMTC (i) and d_i are obtained from the video record with the recoding time of 30 min. The calculation results are shown in Table 2.

5. Modeling Results

Based on the indicators of traffic safety and node importance, the ranking results could be obtained by using the proposed MEW-VIKOR method. Using the three indicators of traffic safety, Y_i , MMTC (i), and d_i , the intersection ranking results have been obtained with the focus of conventional traffic safety evaluation. Using the three indicators

TABLE 1: Statistics of the shortest path and traffic flow.

ID	Length of the shortest path				Traffic flow of the shortest path			
	Min	Max	Mean	SD	Min	Max	Mean	SD
1	0.40	1.77	1.13	0.32	6800	51000	27704	9966
2	0.27	1.64	1.01	0.35	10200	78200	33370	15752
3	0.17	1.61	0.95	0.40	3400	61200	28333	14456
4	0.13	1.50	0.85	0.40	3400	57800	25815	12519
5	0.26	1.66	0.89	0.41	3400	54400	27200	11433
6	0.28	1.92	1.07	0.47	10200	68000	37526	14254
7	0.13	1.37	0.76	0.35	3400	37400	19393	8837
8	0.26	1.37	0.75	0.29	6800	44200	21156	9493
9	0.16	1.18	0.65	0.29	3400	30600	16748	7657
10	0.11	1.24	0.63	0.30	3400	44200	16622	8812
11	0.11	1.36	0.70	0.33	3400	54400	22919	12024
12	0.20	1.64	0.90	0.41	6800	78200	30600	16442
13	0.13	1.18	0.65	0.30	3400	40800	16874	9117
14	0.18	1.59	0.94	0.42	3400	68000	22793	15082
15	0.09	1.18	0.66	0.29	3400	37400	15867	8745
16	0.18	1.77	1.00	0.39	6800	61200	28711	13413
17	0.13	1.61	0.82	0.40	3400	44200	19393	9927
18	0.12	1.48	0.75	0.37	3400	40800	15489	9539
19	0.14	1.31	0.69	0.33	3400	37400	16244	9446
20	0.21	1.52	0.83	0.33	3400	44200	20400	10458
21	0.11	1.71	0.87	0.44	3400	47600	21659	12082
22	0.11	1.60	0.81	0.41	3400	44200	18763	10931
23	0.11	1.41	0.75	0.38	3400	40800	17630	10836
24	0.11	1.53	0.82	0.43	3400	44200	20904	12175
25	0.26	1.92	1.03	0.47	10200	68000	37022	16369
26	0.14	1.66	0.93	0.45	3400	47600	25311	13280
27	0.09	1.17	0.65	0.29	3400	34000	15111	8293
28	0.21	1.12	0.65	0.24	3400	37400	13852	8271

of node importance, CC (i), BC (i), and DC (i), the intersection ranking results with the focus of roadway network function and traffic flow have been obtained. Using the six indicators and the proposed framework, the intersection ranking results have been obtained with four strategies. The intersection ranking results of the proposed approaches with the different focuses are shown in Table 3. The comparison results are shown in Figure 3.

TABLE 2: Indicators of intersection node importance and traffic safety.

ID	Indicators of node importance			Indicators of traffic safety			
	CC (<i>i</i>)	BC (<i>i</i>)	DC (<i>i</i>)	Y_i	MMTC (<i>i</i>)	d_i	
1	0.88	0.00	0.04	6	0.32	6.84	
2	0.99	0.03	0.07	6	0.60	6.77	
3	1.05	0.06	0.11	7	1.14	6.42	
4	1.18	0.05	0.11	8	1.24	6.18	
5	1.13	0.06	0.11	4	0.74	6.26	
6	0.93	0.04	0.07	0	0.45	6.18	
7	1.32	0.21	0.11	7	0.52	6.96	
8	1.33	0.22	0.15	5	1.22	7.05	
9	1.55	0.53	0.11	0	0.35	6.20	
10	1.59	0.63	0.11	0	0.66	6.67	
11	1.43	0.28	0.11	0	0.63	6.90	
12	1.11	0.14	0.11	0	0.80	6.28	
13	1.53	0.50	0.11	5	1.03	6.09	
14	1.07	0.10	0.11	0	1.05	6.67	
15	1.52	0.41	0.07	0	0.56	6.83	
16	1.00	0.03	0.07	0	0.65	6.38	
17	1.22	0.12	0.11	8	1.12	6.34	
18	1.34	0.24	0.15	0	0.26	7.02	
19	1.46	0.47	0.11	7	0.70	6.47	
20	1.20	0.06	0.11	0	0.61	6.67	
21	1.15	0.12	0.11	6	0.36	6.49	
22	1.23	0.20	0.11	7	0.62	6.62	
23	1.34	0.35	0.11	5	0.50	6.40	
24	1.23	0.25	0.11	7	1.05	6.40	
25	0.98	0.00	0.07	0	0.41	6.36	
26	1.08	0.07	0.11	5	0.35	6.15	
27	1.53	0.46	0.11	0	0.35	6.50	
28	1.54	0.37	0.15	8	1.09	6.21	

TABLE 3: The results of intersection ranking.

Intersection ID	Results of traffic safety	Results of node importance	Strategy 1	Strategy 2	Strategy 3	Strategy 4
1	0.20	0.00	0.00	0.15	0.00	0.00
2	0.44	0.14	0.62	0.28	0.56	0.21
3	0.94	0.23	0.79	0.39	0.61	0.46
4	1.00	0.36	0.87	0.56	0.65	0.60
5	0.51	0.32	0.70	0.41	0.64	0.40
6	0.15	0.08	0.51	0.05	0.29	0.05
7	0.40	0.54	0.76	0.74	0.76	0.52
8	0.92	0.57	0.91	0.72	0.77	0.78
9	0.06	0.92	0.75	0.64	0.95	0.33
10	0.36	1.00	0.84	0.68	1.00	0.64
11	0.34	0.66	0.79	0.54	0.83	0.50
12	0.45	0.32	0.67	0.31	0.65	0.39
13	0.79	0.88	0.95	0.95	0.94	0.99
14	0.56	0.26	0.69	0.25	0.62	0.36
15	0.27	0.79	0.81	0.59	0.90	0.49
16	0.34	0.15	0.60	0.13	0.56	0.18
17	0.95	0.43	0.87	0.65	0.69	0.65
18	0.00	0.59	0.66	0.51	0.79	0.18
19	0.55	0.82	0.85	0.99	0.90	0.75
20	0.31	0.37	0.69	0.37	0.66	0.38
21	0.20	0.35	0.62	0.50	0.66	0.27
22	0.48	0.47	0.74	0.66	0.72	0.54
23	0.30	0.64	0.73	0.78	0.81	0.46
24	0.87	0.49	0.84	0.69	0.74	0.68
25	0.11	0.11	0.52	0.09	0.52	0.07
26	0.16	0.26	0.58	0.37	0.62	0.20
27	0.07	0.84	0.75	0.61	0.92	0.32
28	0.92	0.78	1.00	1.00	0.91	0.99

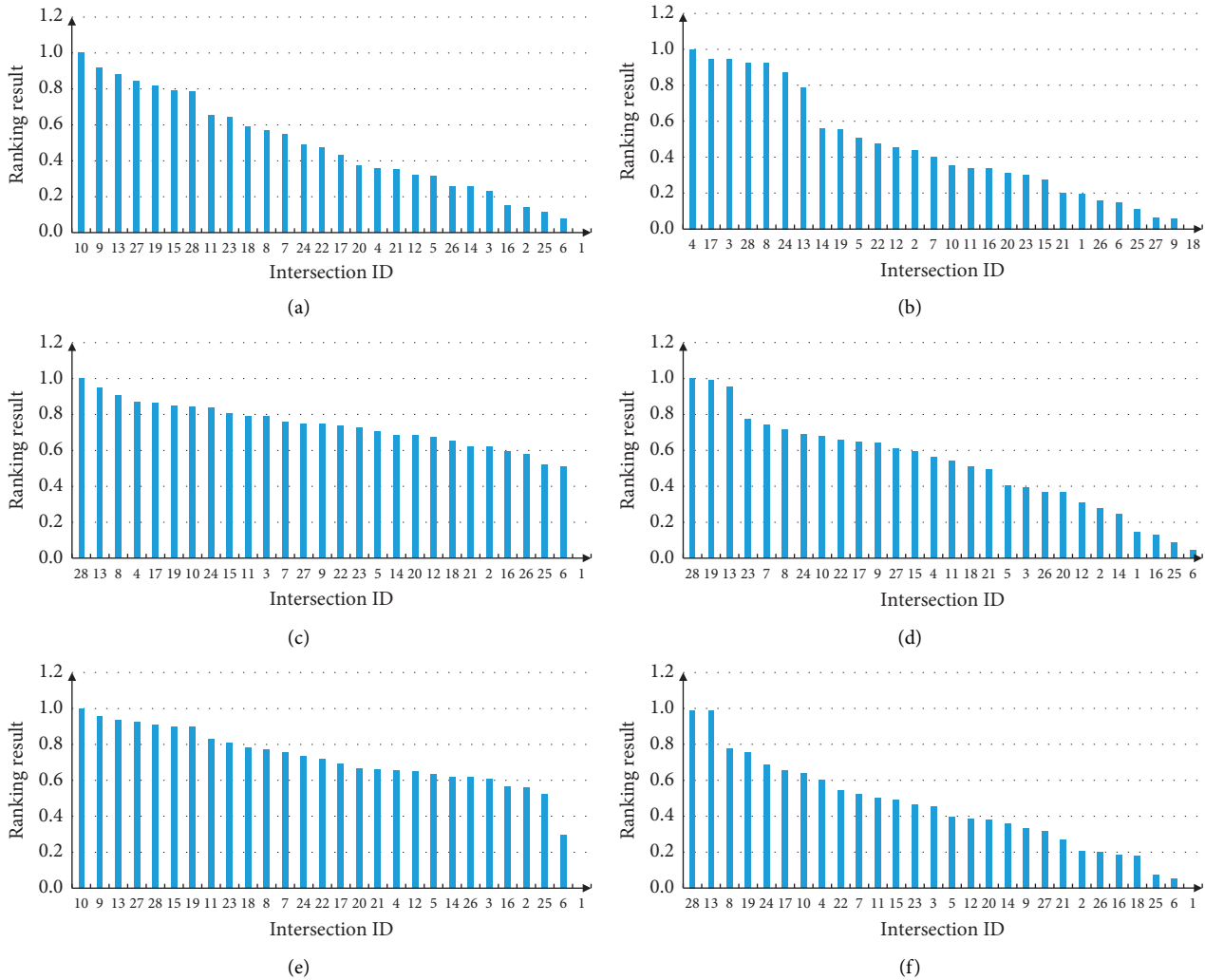


FIGURE 3: Comparison of the ranking results with analyzed intersections: (a) ranking results of node importance, (b) ranking results of traffic safety, (c) ranking results of strategy 1, (d) ranking results of strategy 2, (e) ranking results of strategy 3, and (f) ranking results of strategy 4.

From the comparison, the results indicate that strategies 1 and 3 have the similar pattern and changing trend, which is different compared to the results of node importance and traffic safety. The strategies 2 and 4 have the similar pattern and changing trend, which is a compromise solution of the node importance and traffic safety. In other words, strategies 2 and 4 represent the ranking result features of node importance and traffic safety simultaneously.

To further verify the performance of the proposed methods, the consistency test has been applied. With the ranking results of two methods, the consistency test analyzed consistency rate, which is a ratio of the intersections with same ranking order in total intersections, and the results are shown in Figure 4. The results demonstrated that the consistency rate between the ranking results of strategy 3 and node importance is 78.57%, which is significantly greater than the others. The ranking results of strategy 3 represent more roadway network function and traffic flow characteristics compared with other strategies.

The consistency rate between the ranking results of traffic safety and strategies 1, 2, and 3 is 0. The consistency rate between the ranking results of traffic safety and strategy 4 is 7.14%. The findings indicate that ranking results of strategy 4 represent more traffic safety assessment features compared with the other strategies. In addition, the consistency rate between the ranking results of strategy 4 and the node importance is 14.29%, which is greater than the consistency rate between strategy 4 and the traffic safety. Though strategy 4 represents more node importance features compared with the traffic safety, strategy 4 represents the superior balance between roadway network function and traffic safety assessment.

The results of the consistency test between the four strategies are shown in Figure 4(b). The results show that strategies 1 and 4 have the greatest similarity, and the consistency rate of the ranking results is 32.14%. The consistency rate between the strategies 1 and 3 is 17.86%, and between the strategies 3 and 4 is 14.29%. The consistency rate of the rest of strategy combinations is 7.14%. The findings

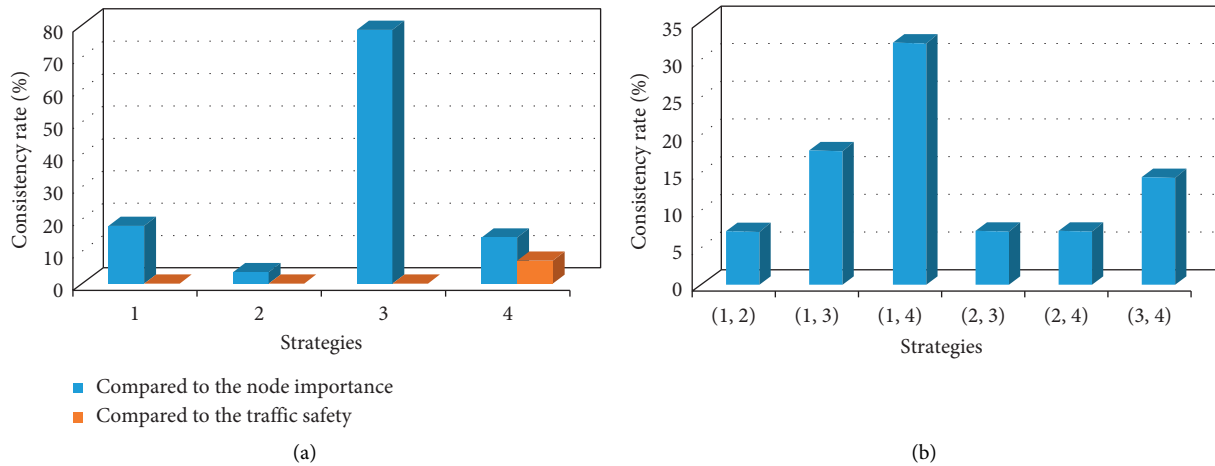


FIGURE 4: Consistency test results of the proposed methods: (a) the proposed four strategies compared the node importance and traffic safety and (b) comparison between the four strategies.

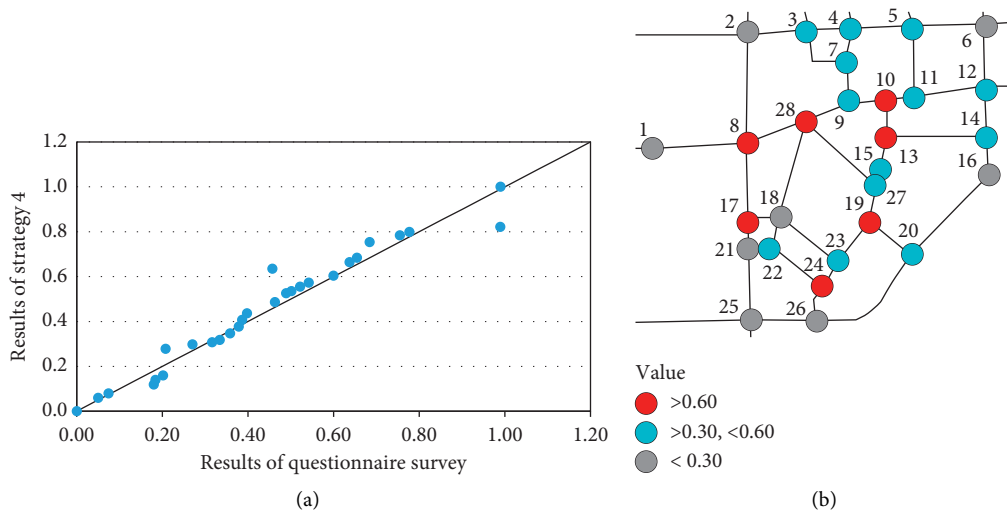


FIGURE 5: Comparison between the results of questionnaire survey and the proposed framework with strategy 4: (a) compared to the questionnaire survey and (b) differences with ranking value.

indicate that the strategies 1 and 4 could provide consistency results that cover both perspectives of traffic safety and node importance. Combined the comparison results and the consistency test, the proposed framework with strategy 4 is recommended for intersection traffic safety screening, since it has both merits of node importance and traffic safety.

To verify the effectiveness of the proposed method with strategy 4, a questionnaire survey has been conducted. In total, 42 people who are from the government office, research institute, and public have participated the survey. Each participant ranked the 28 intersections according to their own expertise and experience. The ranking results of the poll have been analyzed and compared with the proposed framework with strategy 4, which are shown in Figure 5(a). The results of the proposed framework with strategy 4 are closely approximate to the results of the questionnaire survey. The consistency rate between the survey results and the proposed framework with strategy 4 is 85.71. The

findings indicate the ranking results could represent the attitude and expectation of the public and agencies.

The proposed framework could be used as the method of BSID with an appropriate threshold setting. The ranking results with the values that are greater than the threshold could be the intersections that are the black spots. In the research, for the proposed framework with strategy 4, when the threshold is setting to 0.60, the intersection of 8, 10, 13, 17, 19, 24, and 28 have been identified as the black spots, as shown in Figure 5(b). The results are consistent with the intersection safety investigation, and the rate of the false-positive cases and false-negative cases is 0. The false-positive case is an intersection involved in safety investigation while it is not needed, and a false-negative case is not involving a site in safety investigation while it is needed. The rates of false-positive and false-negative cases in identifying black spots are the assessing standards in justifying the performance of the traffic safety screening method. The findings

show that the proposed framework with strategy 4 contributes significantly to the reduction of false-positive and false-negative cases in identifying the black spot intersections.

6. Conclusions

In the research, a framework with the indicators that are from the perspectives of complex network and traffic safety is proposed for the intersection traffic safety screening. By incorporating the traffic flow and the characteristics of roadway network topology, three indicators have been developed to measure the node importance. The observed and estimated crash frequencies, modified time-to-collision, and a distance that describes the nonlane-based movements at intersection have been proposed from the perspective of traffic safety assessment. A MEW-VIKOR approach is proposed to compute the ranking results, and four strategies have been developed to account for the effects of the six indicators simultaneously. To verify the effectiveness of the proposed framework for intersection traffic safety screening, a roadway network with 28 intersections in Shenzhen has been adopted.

The ranking results of the proposed framework with two layers could represent the features of traffic safety and the characteristics of node importance and satisfy the expectation from the public, government, and research institutes. With an appropriate threshold setting, the ranking results are consistent with the intersection safety investigation and contribute significantly to the reduction of false-positive and false-negative cases in identifying the black spot intersections.

The inappropriate designs at intersection can cause safety problems and impact the operation efficiency of neighboring zones and even the overall network. The screening, ranking, and identification of black spots are the first steps of the traffic safety management process. Errors and bias in black spot identification might result in the inefficient use of resources for traffic safety improvements and impact the effectiveness of the traffic safety management. The proposed framework could be used as a guideline to develop traffic management policies, enhance the level of traffic management, and reduce the impacts of traffic crashes and congestion.

Data Availability

The data will be available upon request to the corresponding author.

Conflicts of Interest

The authors declare that there are no conflicts of interest.

Acknowledgments

This research was supported by funding provided by the National Key R&D Program of China (Grant number: 2019YFF0301400).

References

- [1] C. Dong, D. B. Clarke, S. H. Richards, and B. Huang, "Differences in passenger car and large truck involved crash frequencies at urban signalized intersections: an exploratory analysis," *Accident Analysis & Prevention*, vol. 62, pp. 87–94, 2014.
- [2] C. Dong, S. H. Richards, D. B. Clarke, X. Zhou, and Z. Ma, "Examining signalized intersection crash frequency using multivariate zero-inflated Poisson regression," *Safety Science*, vol. 70, pp. 63–69, 2014.
- [3] N. Levine, "Houston, Texas, metropolitan traffic safety planning program," *Transportation Research Record: Journal of the Transportation Research Board*, vol. 1969, no. 1, pp. 92–100, 2006.
- [4] X. Qin, M. A. Sultana, M. V. Chitturi, and D. A. Noyce, "Developing truck corridor crash severity index," *Transportation Research Record: Journal of the Transportation Research Board*, vol. 2386, no. 1, pp. 103–111, 2013.
- [5] ITT Corporation, *Study Analyst User's Manual*, Colorado Springs, CO, USA, 2011.
- [6] M. H. Rahman, M. Abdel-Aty, J. Lee, and M. S. Rahman, "Enhancing traffic safety at school zones by operation and engineering countermeasures: a microscopic simulation approach," *Simulation Modelling Practice and Theory*, vol. 94, pp. 334–348, 2019.
- [7] L. B. Meuleners, D. Hendrie, A. H. Lee, and M. Legge, "Effectiveness of the black spot programs in western Australia," *Accident Analysis & Prevention*, vol. 40, no. 3, pp. 1211–1216, 2008.
- [8] F. Yakar, "Identification of accident-prone road sections by using relative frequency method," *PROMET—Traffic & Transportation*, vol. 27, no. 6, pp. 539–547, 2015.
- [9] A. Borsos, S. Cafiso, C. D'Agostino, and D. Miletics, "Comparison of Italian and Hungarian black spot ranking," *Transportation Research Procedia*, vol. 14, pp. 2148–2157, 2016.
- [10] W. Cheng and S. P. Washington, "Experimental evaluation of hotspot identification methods," *Accident Analysis & Prevention*, vol. 37, no. 5, pp. 870–881, 2005.
- [11] W. Cheng and S. Washington, "New criteria for evaluating methods of identifying hot spots," *Transportation Research Record: Journal of the Transportation Research Board*, vol. 2083, no. 1, pp. 76–85, 2008.
- [12] E. De Pauw, S. Daniels, T. Brijs, E. Hermans, and G. Wets, "Safety effects of an extensive black spot treatment programme in Flanders-Belgium," *Accident Analysis and Prevention*, vol. 66, pp. 72–79, 2014.
- [13] N. Veeramisti, A. Paz, and J. Baker, "A framework for corridor-level traffic safety network screening and its implementation using Business Intelligence," *Safety Science*, vol. 121, pp. 100–110, 2020.
- [14] A. Montella, "Safety reviews of existing roads," *Transportation Research Record: Journal of the Transportation Research Board*, vol. 1922, no. 1, pp. 62–72, 2005.
- [15] Z. Fan, C. Liu, D. Cai, and S. Yue, "Research on black spot identification of safety in urban traffic accidents based on machine learning method," *Safety Science*, vol. 118, pp. 607–616, 2019.
- [16] S. Cafiso and G. Di Silvestro, "Performance of safety indicators in identification of black spots on two-lane rural roads," *Transportation Research Record: Journal of the Transportation Research Board*, vol. 2237, no. 1, pp. 78–87, 2011.

- [17] K. Geurts, G. Wets, T. Brijs, and K. Vanhoof, "Identification and ranking of black spots: sensitivity analysis," *Transportation Research Record: Journal of the Transportation Research Board*, vol. 1897, no. 1, pp. 34–42, 2004.
- [18] A. Montella, "A comparative analysis of hotspot identification methods," *Accident Analysis & Prevention*, vol. 42, no. 2, pp. 571–581, 2010.
- [19] M. Ghadi and Áö Török, "A comparative analysis of black spot identification methods and road accident segmentation methods," *Accident Analysis & Prevention*, vol. 128, pp. 1–7, 2019.
- [20] Y. Yang, L. Yu, X. Wang et al., "A novel method to evaluate node importance in complex networks," *Physica A: Statistical Mechanics and Its Applications*, vol. 526, Article ID 121118, 2019.
- [21] L. C. Freeman, "Centrality in social networks conceptual clarification," *Social Networks*, vol. 1, no. 3, pp. 215–239, 1978.
- [22] M. E. J. Newman, "A measure of betweenness centrality based on random walks," *Social Networks*, vol. 27, no. 1, pp. 39–54, 2005.
- [23] A. Charly and T. V. Mathew, "Estimation of traffic conflicts using precise lateral position and width of vehicles for safety assessment," *Accident Analysis & Prevention*, vol. 132, Article ID 105264, 2019.
- [24] J. Wu, H. Xu, Y. Zheng, and Z. Tian, "A novel method of vehicle-pedestrian near-crash identification with roadside LiDAR data," *Accident Analysis & Prevention*, vol. 121, pp. 238–249, 2018.
- [25] T. Fu, L. Miranda-moreno, and N. Saunier, "A novel framework to evaluate pedestrian safety at non-signalized locations," *Accident Analysis & Prevention*, vol. 111, pp. 23–33, 2018.
- [26] H. Behbahani, N. Nadimi, and S. S. Naseralavi, "New time-based surrogate safety measure to assess crash risk in car-following scenarios," *Transportation Letters*, vol. 7, no. 4, pp. 229–238, 2015.
- [27] K. Ozbay, H. Yang, B. Bartin, and S. Mudigonda, "Derivation and validation of new simulation-based surrogate safety measure," *Transportation Research Record: Journal of the Transportation Research Board*, vol. 2083, no. 1, pp. 105–113, 2008.
- [28] S. Opricovic and G.-H. Tzeng, "Compromise solution by MCDM methods: a comparative analysis of VIKOR and TOPSIS," *European Journal of Operational Research*, vol. 156, no. 2, pp. 445–455, 2004.
- [29] Z. Liu, C. Jiang, J. Wang, and H. Yu, "The node importance in actual complex networks based on a multi-attribute ranking method," *Knowledge-Based Systems*, vol. 84, pp. 56–66, 2015.
- [30] N. Ploskas and J. Papathanasiou, "A decision support system for multiple criteria alternative ranking using TOPSIS and VIKOR in fuzzy and nonfuzzy environments," *Fuzzy Sets and Systems*, vol. 377, pp. 1–30, 2019.
- [31] C. Dong, C. Shao, D. B. Clarke, and S. S. Nambisan, "An innovative approach for traffic crash estimation and prediction on accommodating unobserved heterogeneities," *Transportation Research Part B: Methodological*, vol. 118, pp. 407–428, 2018.